



**Paired Impulse Response Function and Layer-
Peeling Method for Anomaly Detection and
Condition Assessment of Pipelines**

Wei Zeng

B.Eng., M.Eng.

Thesis submitted in fulfilment of the requirements for the degree
of Doctor of Philosophy

The University of Adelaide

Faculty of Engineering, Computer and Mathematical Sciences

School of Civil, Environmental and Mining Engineering

Copyright© 2020

Abstract

Water transmission and distribution pipeline systems are one of society's most important infrastructure assets. They consist of buried pipes that are often old and deteriorating and their condition is extremely difficult and expensive to determine. This PhD thesis focuses on developing non-invasive and cost-effective methods to both detect anomalies in water pipelines and to assess the condition of pipelines that will allow for predictive repair. The first stage of the research is to identify and localize anomalies in the pipelines. The second stage is to assess the detailed condition of the pipe wall or the size of a blockage if the anomalies in the pipeline are deteriorated sections or blockages.

In the thesis, a novel paired impulse response function (termed paired-IRF) technique has been developed for anomaly detection in pressurised pipelines. This is the first time that a transient-based method has been experimentally validated to be able to fully eliminate the effects from background pressure fluctuations and noise. The technique has a high spatial resolution by transferring the anomaly-induced wave reflections into sharp spikes. It has a high detectability by making use of a continuous signal as the injected wave. The continuous wave injection leads to continuous wave reflections and thus provides a large amount of information for signal analysing. The technique can be applied in pipe networks with arbitrary configurations and achieves a wide detection range. The advantages listed above make the technique potentially attractive for field applications.

A layer-peeling method has also been developed for condition assessment in pressurised pipelines. The layer-peeling method, which has previously been applied to the inspection of musical instruments and the design of optical fibers, has in this thesis for the first time been applied to water pipelines. It considers the frequency-dependent dissipation and dispersion of the transient waves in the pipeline and enables a bi-directional reconstruction of pipelines with

branches. To compensate the cumulative errors which can occur in the layer-peeling method, a fast inverse transient method is developed. To improve the spatial resolution and the tolerance to background pressure fluctuations and noise, the paired-IRF technique has been combined with the layer-peeling method in the thesis.

To assist in applying the techniques in the field, a voice-coil-based transient generation system has been developed to generate transient waves and a customized in-pipe optical fiber sensor array has been used for transient pressure measurement. The transient generation and measurement system has been applied in the laboratory and will be used to validate the proposed techniques in the field in the future.

Statement of Originality

I certify that this work contains no material which has been accepted for the award of any other degree or diploma in my name, in any university or other tertiary institution and, to the best of my knowledge and belief, contains no material previously published or written by another person, except where due reference has been made in the text. In addition, I certify that no part of this work will, in the future, be used in a submission in my name, for any other degree or diploma in any university or other tertiary institution without the prior approval of the University of Adelaide and where applicable, any partner institution responsible for the joint-award of this degree.

I acknowledge that copyright of published works contained within this thesis resides with the copyright holder(s) of those works.

I also give permission for the digital version of my thesis to be made available on the web, via the University's digital research repository, the Library Search and also through web search engines, unless permission has been granted by the University to restrict access for a period of time.

Signed:Date:

This page is intentionally blank.

Acknowledgements

I express my gratitude and thanks to my supervisors Prof. Martin Lambert, Prof. Angus Simpson, Prof. Benjamin Cazzolato, Dr Aaron Zecchin and Dr Jinzhe Gong. Thanks to Martin for providing fantastic research ideas and taking care of me in life. Thanks to Angus for his unwavering attention to detail. Thanks to Benjamin for his professional guidance during my PhD program. Thanks to Aaron for his great support on mathematical problems that emerged during my PhD program. Thanks to Jinzhe for his substantial professional suggestions and guidance on my papers.

I gratefully acknowledge the support from technicians Mr Brenton Howie, Mr Simon Golding and Mr Stan Woithe in the Robin Hydraulics Laboratory at the University of Adelaide. They provided support throughout my laboratory experiments.

I would like to thank the postgraduate students within the School for their companionship and friendship. I also thank the staff in the School for their support to make my PhD program organised.

I would like to thank my parents, my brother and sister for their love and support. I have been missing my family in China and their encouragement and love from thousands of kilometres away make me feel close to them.

Last, but not least, I express my deep gratitude to my fiancée Ziying Zhang who has been always willing to listen to me about my research even without understanding what I was saying.

This page is intentionally blank

Table of Contents

Abstract	iii
Statement of Originality	v
Acknowledgements	vii
Table of Contents.....	ix
Publications Arising from This Thesis	xv
Journal Papers.....	xv
Conference Papers	xvi
List of Tables.....	xvii
List of Figures	xix
1. Introduction	1
1.1 Research Background	1
1.1.1 Significance of anomaly detection and condition assessment for water pipelines	1
1.1.2 Limitations of traditional technologies.....	2
1.1.3 Anomaly detection and condition assessment in pipelines using fluid transient waves	4
1.2 Research Aims	10
1.3 Organisation of the Thesis	11
2. Synopsis of Publications.....	13
2.1 Paper 1: Paired Impulse Response Function Technique (Chapter 3) ..	13
2.2 Paper 2: Characterization of Different Anomalies (Chapter 4)	17
2.3 Paper 3: Layer-Peeling Method (Chapter 5).....	18
2.4 Paper 4: Bidirectional Layer-Peeling Method (Chapter 6)	20
2.5 Paper 5: Fast Inverse Transient Method (Chapter 7)	21
2.6 Paper 6: Layer-Peeling Method with Paired-IRF (Chapter 8).....	22

2.7 Paper 7: Voice-Coil Transient Generator and In-Pipe Sensors (Chapter 9) 23

3. Paired-IRF method for Leakage Detection of Pipes in a Network (Journal Publication 1) 25

Statement of Authorship 27

3.1 Introduction 30

3.2 Leak Detection using Conventional Methods 33

 3.2.1 Example system details 33

 3.2.2 The wave reflection using a sharp signal input with a short duration 34

 3.2.3 IRF extraction with a continuous signal input 35

3.3 Leak Detection using a Paired-IRF Method 38

 3.3.1 Paired-IRF method applied to a reservoir-pipeline-valve system 39

 3.3.2 Paired-IRF method applied in pipe networks 41

3.4 Numerical Case Studies 42

 3.4.1 Case 1: Reservoir-pipeline-valve system 43

 3.4.2 Case 2: Pipe network 44

3.5 Experimental Verification 46

 3.5.1 Experimental setup 46

 3.5.2 Experimental analysis 47

3.6 Conclusions 53

3.7 Appendix 54

 3.7.1 Derivation of equation (3-7) 54

 3.7.2 Derivation of equation (3-16) 55

4. Characterization and Detection of Multiple Types of Anomalies in Pipe Networks using a Paired Impulse Response Function Approach (Journal Publication 2) 57

Statement of Authorship 59

4.1 Introduction 62

4.2 Methodology: The Proposed Paired-IRF Method 65

4.3 Paired-IRFs for Different Anomalies 68

4.3.1	System configuration and anomalies.....	68
4.3.2	Discrete anomalies (leak, junction and closed in-line valve).....	70
4.3.3	Extended anomalies with uniform properties (section with an impedance change).....	73
4.3.4	Extended anomalies examples with non-uniformly distributed properties.....	76
4.3.5	Summary on the anomaly-induced features in the paired-IRF trace	78
4.4	Case Study in a Pipe Network	79
4.4.1	Pipe system configuration	79
4.4.2	Detection of anomalies in the pipe network	80
4.4.3	Detection of anomalies with contaminated pressures	82
4.5	Discussion on Field Application.....	84
4.6	Conclusions.....	85
5.	Condition Assessment of Water Pipelines using a Modified Layer Peeling Method (Journal Publication 3).....	87
	Statement of Authorship.....	89
5.1	Introduction.....	92
5.2	The Layer Peeling Method for Pipeline Condition Assessment.....	95
5.2.1	Impulse response function (IRF).....	96
5.2.2	Wave dissipation and dispersion	99
5.2.3	Wave transmission and reflection	103
5.2.4	Procedures of the modified layer peeling method.....	106
5.3	Numerical Verification	107
5.3.1	Case 1: Frictionless pipe.....	108
5.3.2	Case 2: Effects of unsteady friction	110
5.3.3	Case 3: Effect of viscoelasticity	112
5.4	Experimental Verification.....	114
5.4.1	Experimental pipeline layout.....	114
5.4.2	Experimental data.....	115
5.4.3	Reconstruction of the pipeline.....	116
5.5	Discussion.....	118
5.5.1	Resolution.....	118

5.5.2	Location of the generator	119
5.5.3	Wave dissipation and dispersion.....	119
5.6	Conclusions	119
6.	Condition Assessment of Pipelines using a Bi-directional Layer-Peeling Method and a Dual-sensor Configuration (Journal Publication 4).....	121
	Statement of Authorship	123
6.1	Introduction	126
6.2	Problem Formulation and Framework of the New Method	129
6.2.1	Problem formulation	129
6.2.2	The framework of the bi-directional layer-peeling method.....	131
6.3	Mathematic Processes of the Bi-directional Layer-Peeling Method .	134
6.3.1	Pre-processing of transient pressure data.....	134
6.3.2	Wave reflection and transmission modelling.....	136
6.3.3	The circulation process of the bi-directional layer-peeling algorithm.....	140
6.4	Numerical Simulations	141
6.4.1	System layout and parameters	141
6.4.2	Data pre-processing	142
6.4.3	Pipeline reconstruction using the proposed method	145
6.5	Experimental Verification	147
6.5.1	System layout.....	147
6.5.2	Experimental data analysis	148
6.5.3	Bi-directional reconstruction of the pipeline	150
6.6	Conclusions	151
7.	Inverse Wave Reflectometry Method for Hydraulic Transient-Based Pipeline Condition Assessment (Journal Publication 5).....	153
	Statement of Authorship	155
7.1	Introduction	158
7.2	Forward Modelling - Wave Reflectometry Method.....	161
7.2.1	Hydraulic transient wave propagation	161

7.2.2	Wave transmission with simplification of the modeling of steady friction	163
7.2.3	Wave reflection with an impedance change	165
7.2.4	Procedure of the wave reflectometry method.....	166
7.3	Formulation of the Optimization Problem – Inverse Wave Reflectometry Method	167
7.3.1	Optimization process	168
7.3.2	Decision variables and constraints	169
7.3.3	Multiple-stage optimization	169
7.3.4	Objective function	170
7.3.5	Optimization process	170
7.4	Numerical Case Studies	171
7.4.1	Case 1: Uniform deterioration	171
7.4.2	Case 2: Non-uniform deterioration.....	174
7.4.3	Case 3: Multiple deteriorations	176
7.5	Experimental Verification.....	178
7.5.1	Pipeline layout and experimental data.....	178
7.5.2	Estimation of the wall thickness change and wave speed reduction using the inverse wave reflectometry method	179
7.6	Conclusions.....	181
8.	Pipeline Reconstruction using a Pseudo Random Binary Sequence Excitation with the Layer Peeling Method (Journal Publication 6)	183
	Statement of Authorship.....	185
8.1	Introduction.....	188
8.2	Problem Formulation and Framework of the New Technique	191
8.3	Wave Excitation and Signal Pre-processing	195
8.3.1	Pseudo random binary sequence (PRBS) excitation	195
8.3.2	Least squares deconvolution	196
8.3.3	Wave separation	198
8.4	IRFs with a First-order Accuracy and the First Pipeline Reconstruction	199
8.4.1	IRF equations	199
8.4.2	IRFs with a first-order accuracy	202

8.4.3	First (initial) pipe impedance reconstruction	203
8.5	IRFs with a Second-order Accuracy and the Second Pipe Impedance Reconstruction.....	206
8.5.1	IRFs with a second-order accuracy.....	207
8.5.2	Second pipe impedance reconstruction.....	209
8.6	Experimental Verification	210
8.6.1	Experimental data and IRF determination	210
8.6.2	Reconstruction of the pipe impedance	212
8.7	Conclusions	214
8.8	Appendix	215
8.8.1	Derivation of equation (8-15).....	215
8.8.2	Derivation of equation (8-17).....	215
9.	Leak Detection for Pipelines using In-Pipe Optical Fiber Pressure Sensors and a Paired-IRF Technique (Journal Publication 7)	217
	Statement of Authorship	219
9.1	Introduction	222
9.2	Experimental Setup	224
9.2.1	In-pipe optical fiber pressure sensor array.....	225
9.2.2	Voice-coil-based transient pressure wave generation system...	226
9.2.3	Experimental pipeline system	227
9.3	Transient Tests using Step Waves and a Conventional Pressure Transducer	228
9.4	Leak Detection using the In-Pipe Optical fiber Sensors	230
9.4.1	Detection method	230
9.4.2	Data analysis and results	231
9.5	Conclusions	233
10.	Conclusions	235
10.1	Research Contributions	235
10.2	Scope of Future Work	237
11.	References	241

Publications Arising from This Thesis

Journal Papers

The following peer-reviewed journal papers are the major outcomes of this research and they form the main body of this thesis.

1. Zeng, W., Gong, J., Simpson, A. R., Cazzolato, B. S., Zecchin, A. C., Lambert, M. F. (Forthcoming). "Paired-IRF method for leakage detection of pipes in a network." *Journal of Water Resources Planning and Management*, DOI: 10.1061/(ASCE)WR.1943-5452.0001193. (Accepted on 29-Oct-2019).
2. Zeng, W., Zecchin, A. C., Gong, J., Cazzolato, B. S., Lambert, M. F., Simpson, A. R. (2019). "Characterization and detection of multiple types of anomalies in pipe networks using a paired impulse response function approach." *Urban Water Journal* (Submitted).
3. Zeng, W., Gong, J. Z., Zecchin, A. C., Lambert, M. F., Simpson, A. R., Cazzolato, B. S. (2018). "Condition assessment of water pipelines using a modified layer-peeling method." *Journal of Hydraulic Engineering*, 144(12), 04018076. DOI: 10.1061/(ASCE)HY.1943-7900.0001547.
4. Zeng, W., Gong, J., Cazzolato, B. S., Zecchin, A. C., Lambert, M. F., Simpson, A. R. (2019). "Condition assessment of pipelines using a bi-directional layer-peeling method and a dual-sensor configuration." *Journal of Sound and Vibration*, 457(9), 181-196. DOI: 10.1016/j.jsv.2019.05.054.

5. Zeng, W., Zecchin, A. C., Gong, J., Lambert, M. F., Simpson, A. R., Cazzolato, B. S. (2019). "Inverse wave reflectometry method for hydraulic transient-based pipeline condition assessment." *Journal of Hydraulic Engineering* (Submitted).
6. Zeng, W., Gong, J., Lambert, M. F., Cazzolato, B. S., Simpson, A. R., Zecchin, A. C. (2019). "Pipeline reconstruction using a pseudo random binary sequence excitation with the layer peeling method." *Mechanical System and Signal Processing* (To be submitted).
7. Zeng, W., Gong, J., Cook, P. R., Arkwright, J. W., Simpson, A. R., Cazzolato, B. S., Zecchin, A. C., Lambert, M. F. (2019). "Leak detection for pipelines using in-pipe optical fiber pressure sensors and a paired-IRF technique." *IEEE Sensors Journal* (Submitted).

Conference Papers

The following conference papers are also outcomes of this research.

1. Zeng, W., Gong, J., Lambert, M. F., Simpson, A. R., Cazzolato, B. S., Zecchin, A. C. (2018). Detection of extended blockages in pressurised pipelines using hydraulic transients with a layer-peeling method. *29th IAHR Symposium on Hydraulic Machinery and Systems*, Kyoto, Japan.
2. Zeng, W., Zecchin, A. C., Gong, J., Simpson, A. R., Cazzolato, B. S., Lambert, M. F. (2019). Detection of multiple anomalies in pipe networks using a paired-IRF technique. *17th International Computing & Control for the Water Industry Conference*, Exeter, UK.

List of Tables

Table 3.1 Accuracy analysis of the detection result.....	50
Table 4.1 Characteristics of the discrete anomalies and uniform anomalies. .	71
Table 4.2 Anomaly-induced features in the paired-IRF trace.	79
Table 4.3 Tracking of the visible high-order wave reflections.	82
Table 5.1 Viscoelastic parameters used in the numerical case.....	112
Table 6.1 Tracking of the wave reflections.	143
Table 6.2 Physical details of the pipeline system used in the laboratory experiments.	148
Table 7.1 Comparison between the estimated results with different levels of noise and the real values.....	173
Table 8.1 Physical details of the copper pipeline system.....	193

This page is intentionally blank.

List of Figures

Figure 1.1 Framework of the PhD thesis.....	12
Figure 2.1 Generator and sensor configuration for the paired-IRF technique.	14
Figure 2.2 Schematic of the experimental pipe network.....	15
Figure 2.3 Measured pressure waves on the experimental pipe network at (a) P_1 and (b) P_2	16
Figure 2.4 Paired-IRF extracted for the experimental pipe network.....	16
Figure 2.5 (a) leak; (b) junction; (c) partially closed in-line valve or discrete blockage; (d) section with diameter change or extended blockage with a uniform diameter; (e) section with material change or deterioration with a uniform wave speed; (f) extended blockage with non-uniformly distributed diameters; and (g) wall deteriorated section with non-uniformly distributed wave speeds.	17
Figure 2.6 Schematic diagram of the testing systems for (a) a musical instrument and (b) a water pipe.	19
Figure 2.7 Pipeline configuration for the layer-peeling method.	19
Figure 2.8 Wave speed reconstructed from the modified layer-peeling method for the frictionless pipe. (The two plots are virtually coincident)..	20
Figure 2.9 Schematic of the testing configuration for the bi-directional layer-peeling method.	20
Figure 2.10 Optimization process of the fast inverse transient method (where NG is the maximum number of generations).	22
Figure 2.11 Schematic of the voice-coil based transient generation system...	23

Figure 2.12 Photograph of the in-pipe optical fiber sensor array. 24

Figure 2.13 Schematic of the installation of the generator and sensors in the field. 24

Figure 3.1 Pipeline configuration for Case 1. 34

Figure 3.2 Simulated pressure wave with a pulse valve excitation at P_1 35

Figure 3.3 Normalized valve opening in the numerical case with a PRBS valve excitation; (a) 0.4 s period, and (b) enlarged figure. 37

Figure 3.4 Simulated pressure waves with a PRBS valve excitation for Case 1 at (a) P_1 and (b) P_2 38

Figure 3.5 Least squares deconvolution (p_1 to τ) for Case 1 with a PRBS excitation. 38

Figure 3.6 Schematic of a pipe section in a pipe network. 41

Figure 3.7 Paired-IRF extracted for Case 1 with a PRBS valve excitation. ... 43

Figure 3.8 Schematic and configuration of the pipe network (Case 2). 45

Figure 3.9 Simulated pressure waves with a PRBS valve excitation for Case 2 at (a) P_1 and (b) P_2 45

Figure 3.10 Paired-IRF extracted for Case 2 with a PRBS valve excitation. . 45

Figure 3.11 Schematic of the experimental pipeline system. 47

Figure 3.12 Measured data with a step valve excitation for the experimental case: (a) valve opening τ and (b) pressure at P_1 48

Figure 3.13 Normalized valve opening perturbation in the experiment in (a) a 2 s period; and (b) a 0.1 s period. 49

Figure 3.14 Measured pressure waves with a PRBS valve excitation for the experimental case at (a) P_1 and (b) P_2 50

Figure 3.15 Paired-IRF extracted for the experimental case with a PRBS valve excitation.50

Figure 3.16 Measured background pressure fluctuations and noise in the field pipe: (a) P_{b1} and (b) P_{b2}51

Figure 3.17 Paired-IRF extracted for the experimental case with a PRBS valve excitation with pressure waves contaminated by realistic background pressure fluctuations and noise.....52

Figure 3.18 Measured pressure waves with the generator valve partially opened for the experimental case at (a) P_1 and (b) P_253

Figure 3.19 Paired-IRF extracted for the experimental case with the valve partially opened.53

Figure 4.1 System configuration of the Paired-IRF method.65

Figure 4.2 Block diagram describing the wave propagation process.....65

Figure 4.3 Pipeline configuration for Case 1.69

Figure 4.4 Anomaly types in Case 1: (a) leak; (b) junction; (c) partially closed in-line valve or discrete blockage; (d) section with an increased impedance; (e) section with a decreased impedance; (f) extended blockage with non-uniformly distributed diameters; and (g) wall deteriorated section with non-uniformly distributed wave speeds. 70

Figure 4.5 Normalized valve opening in the numerical case with a random valve excitation..... 70

Figure 4.6 Simulated pressure waves for Case 1 with a leak.71

Figure 4.7 Paired-IRF for Case 1 with a discrete anomaly; (a) leak, (b) junction and (c) partially closed in-line valve.72

Figure 4.8 Paired-IRF for Case 1 with; (a) a section with an increased impedance and (b) a section with a decreased impedance.74

Figure 4.9 Effects of the length of the section with a diameter change on the paired spikes: (a) $2L_d/a_d < L_P/a$; (b) $2L_d/a_d = L_P/a$; (c) $L_d/a_d = L_P/a$; (d) $L_d/a_d > L_P/a$; (e) $L_d/a_d = 2L_P/a$; (f) $L_d/a_d > 2L_P/a$ 75

Figure 4.10 Blockage profile for Case 1 with a blocked section. 76

Figure 4.11 Paired-IRF for Case 1 with a blocked section. 77

Figure 4.12 Wave speed profile for Case 1 with a deteriorated section; (a) $L_g = 0.496$ m and (b) $L_g = 1.800$ m..... 77

Figure 4.13 Paired-IRF for Case 1 with a deteriorated section; (a) $L_g = 0.496$ m and (b) $L_g = 1.800$ m. 78

Figure 4.14 Schematic and configuration of the pipe network (Case 2). 80

Figure 4.15 Simulated pressure waves for Case 2 with simulated pressure at: (a) P_1 and (b) P_2 81

Figure 4.16 Paired-IRF extracted for Case 2 with simulated pressures..... 82

Figure 4.17 Measured background pressure fluctuations and noise in the field: (a) P_{B1} and (b) P_{B2} 83

Figure 4.18 Paired-IRF extracted for Case 2 with contaminated pressures.... 83

Figure 4.19 Averaged paired-IRF from 20 tests for Case 2 with contaminated pressures..... 84

Figure 4.20 Schematic of the installation of the generator and sensors in the field. 85

Figure 5.1 Block diagram describing the wave transmission and reflection process in a pipeline..... 95

Figure 5.2 Schematic diagram of the testing systems; (a) musical instrument, and (b) water pipeline. 98

Figure 5.3 Wave transmission and reflection at a junction..... 105

Figure 5.4 Space-time diagram of the wave propagation.....	106
Figure 5.5 Main steps of the modified layer peeling method for pipeline condition assessment.	107
Figure 5.6 Pipeline configuration 1.....	109
Figure 5.7 Input and reflected signals.	109
Figure 5.8 Wave speed reconstructed from the modified layer peeling method for the frictionless pipe without measurement noise. (The two plots are virtually coincident).....	109
Figure 5.9 Reflection with noise and IRF.	110
Figure 5.10 Wave speed reconstructed from the modified layer peeling method for the frictionless pipe with measurement noise.....	110
Figure 5.11 Pipeline configuration 2.....	111
Figure 5.12 Wave speed reconstructed from the modified layer peeling method for the unsteady friction case.....	112
Figure 5.13 Pipeline configuration 3.....	113
Figure 5.14 Wave speed reconstructed from the modified layer peeling method for the viscoelastic case (Model 2 - with viscoelasticity and frequency-independent wave reflections and transmissions; Model 3- with viscoelasticity and frequency-dependent wave reflections and transmissions).	113
Figure 5.15 System layout of the experimental pipeline system.....	115
Figure 5.16 Experimental pressure traces.	115
Figure 5.17 Individual IRFs and averaged IRF.	116
Figure 5.18 Reconstruction using individual IRFs: (a) reconstructed wall thickness distribution compared with the theoretical values; and (b)	

reconstructed wave speed distribution compared with the theoretical values.	117
Figure 5.19 Reconstruction using the averaged IRF: (a) reconstructed wall thickness distribution compared with the theoretical values; and (b) reconstructed wave speed distribution compared with the theoretical values.	117
Figure 5.20 An enlarged view of Figure 5.19.	118
Figure 6.1 Schematic diagram of the testing system for the single-sided layer-peeling method (both generator and pressure transducer are located close to the dead end).	130
Figure 6.2 Schematic diagram of a pipeline network (each of the five hydrants may be used to locate the wave generator and the dual-pressure transducer).	130
Figure 6.3 Schematic diagram of the testing configuration for the bi-directional layer-peeling-based pipeline condition assessment technique.	131
Figure 6.4 Main steps of the bi-directional layer-peeling method for pipeline condition assessment (numbers in the brackets represent the steps).	133
Figure 6.5 Block diagram describing the wave propagation process in a pipeline along two directions (both upstream and downstream).	133
Figure 6.6 Wave propagation in the i_{th} pipe section.	137
Figure 6.7 Wave propagation process with (a) an impedance change; and (b) a bifurcation or junction node.	140
Figure 6.8 Pipeline configuration of the numerical case study.	142
Figure 6.9 (a) Input signal; and (b) reflected signals in the numerical case study.	144

Figure 6.10 (a) Forward wave reflections; and (b) backward wave reflections
in the numerical case study. 144

Figure 6.11 (a) Forward IRF; and (b) backward IRF for the numerical case
study. 145

Figure 6.12 Wave speed reconstruction for Case A when neglecting the
bifurcation node (a) left side, (b) right side. 146

Figure 6.13 Wave speed reconstruction of the right side of the pipeline when
setting the impedance unchanged at the position of the bifurcation
or junction node (Case B). 146

Figure 6.14 Wave speed reconstruction of the right side of the pipeline when
incorporating the scattering equation of the bifurcation or junction
node (Case C). 147

Figure 6.15 System layout of the experimental pipeline system. 148

Figure 6.16 Experimental pressure traces at the two close proximity
transducers. 149

Figure 6.17 (a) Forward wave reflections; and (b) backward wave reflections
in the experimental case before and after application of a Savitzky-
Golay filter. 149

Figure 6.18 (a) Forward IRF; and (b) backward IRF in the experimental case.
..... 150

Figure 6.19 Reconstruction using the averaged IRF (the upstream side is set
as the positive direction). 151

Figure 7.1 Wave propagation in the pipeline. 163

Figure 7.2 Optimization process of the IWRM (NG is the maximum number
of generations). 168

Figure 7.3 Main stages of the EDA. 170

Figure 7.4 Pipeline configuration for Case 1.	172
Figure 7.5 Simulated pressure traces for Case 1; (a) input wave, and (b) reflected wave.	172
Figure 7.6 Wave reflections combined with three Gaussian noise level for Case 1; (a) SNR = 5 dB, (b) SNR = 0 dB and (c) SNR = -5 dB..	173
Figure 7.7 Reflected wave combined with noise for Case 2.....	174
Figure 7.8 Averaged objective values versus N for Case 2.	175
Figure 7.9 Wave speed estimation from the IWRM for Case 2.....	175
Figure 7.10 Objective values versus generation for $N = 5$ for Case 2.	176
Figure 7.11 Pipeline configuration for Case 3.	177
Figure 7.12 Simulated wave reflections for Case 3; (a) without noise, and (b) combined with noise.	177
Figure 7.13 Wave speed estimation from the multi-stage IWRM for Case 3.	177
Figure 7.14 Experimental pipeline configuration.	178
Figure 7.15 Pressure waves in the experimental case: (a) measured input wave; and (b) measured and predicted reflected waves with $N = 6$	179
Figure 7.16 Pipe wall thickness and wave speed estimation from the IWRM with $N = 2$ for the experimental case.	180
Figure 7.17 Wave speed estimation from the IWRM for the experimental case with (a) $N = 4$, and (b) $N = 6$	181
Figure 8.1 Layout of the pipeline system used in the numerical and laboratory studies.	193
Figure 8.2 The structure and procedures of the proposed technique.	194

Figure 8.3 Normalized inverse repeat PRBS valve opening (τ) perturbation
(numerical case study)..... 195

Figure 8.4 Simulated pressure head traces at (a) P₁; (b) P₂ and (c) P₃. 196

Figure 8.5 Results of the least squares deconvolution (a) p_{2_1} ; and (b) p_{3_1}
(numerical case study)..... 197

Figure 8.6 Directional deconvolutions at P₂: (a) forward; and (b) backward.
..... 199

Figure 8.7 Block diagram describing the wave propagation process in (a) a
lumped pipeline with one section and (b) a lumped pipeline with
two sections. 200

Figure 8.8 First-order IRFs of (a) the left side of the pipeline; and (b) right
side of the pipeline. 203

Figure 8.9 Space-time diagram of the wave propagation..... 204

Figure 8.10 First (initial) pipeline reconstruction of the impedance
distribution in the numerical case study compared with the
theoretical values. 206

Figure 8.11 First (initial) pipeline reconstruction in the numerical case study
compared with the theoretical values: (a) wall thickness
distribution; and (b) wave speed distribution. 206

Figure 8.12 Secord-order terms in the IRF equations. 208

Figure 8.13 IRFs with a second-order accuracy of (a) the pipe section on the
left of P₂; and (b) the pipe section on the right side of P₂. 209

Figure 8.14 Second pipe impedance reconstruction in the numerical case
study compared with the theoretical values: (a) wall thickness
distribution; and (b) wave speed distribution. 210

Figure 8.15 Normalized τ perturbation (Experiment)..... 211

Figure 8.16 Experimental pressure perturbations at (a) P_1 ; (b) P_2 and (c) P_3 .
..... 211

Figure 8.17 Least squares deconvolution (a) p_{2_1} ; and (b) p_{3_1}
(Experiment). 212

Figure 8.18 IRFs with a first-order and a second-order accuracy for (a) the
pipe section on the left side of P_2 ; and (b) the pipe section on the
right side of P_2 (Experiment). 212

Figure 8.19 First and second reconstruction using the extracted IRFs: (a)
reconstructed wall thickness distribution compared with the
theoretical values; and (b) reconstructed wave speed distribution
compared with the theoretical values..... 213

Figure 9.1 Photograph of the new generation in-pipe optical fiber sensor array.
..... 226

Figure 9.2 Schematic of the FBG pressure sensors. 226

Figure 9.3 Schematic of the voice-coil based transient generation system. . 227

Figure 9.4 Schematic of the experimental pipeline system. 228

Figure 9.5 Pressure traces measured by the flush-mounted pressure transducer
 T_1 229

Figure 9.6 Measured pressure waves with a PRBS valve excitation for the
experimental case at (a) P_1 and (b) P_2 232

Figure 9.7 Paired-IRF extracted for the experimental case with a PRBS valve
excitation..... 232

Chapter 1

Introduction

1.1 Research Background

1.1.1 Significance of anomaly detection and condition assessment for water pipelines

Water transmission and distribution pipeline systems (WTDPSs) are critical infrastructure for every city all around the world. However, some of the current WTDPSs are wasteful and inefficient, with the pipelines suffering blockage, corrosion, deterioration and leakage. Detecting these anomalies and assessing the pipeline condition is a significant challenge due to the fact that most of the pipelines are buried underground and are long in length. Successful and accurate assessments enable targeted maintenance and rehabilitation of the pipelines to conserve valuable water resources, reduce operating costs and prevent potential pipe faults. Overall, anomaly detection and condition assessment in water pipelines are essential to the cost-effective management of the WTDPSs.

Leakage in WTDPSs is the major reason for water loss and contributes to significant economic cost and associated energy consumption. According to an estimate by the World Bank, the worldwide water-loss volume amounts to 48.6 billion m³ per year (Cataldo et al. 2012). The transported water can also be contaminated due to backflow through leak openings along the pipe during low-pressure events (Fox et al. 2016).

Pipe wall deterioration is common in aged WTDPSs and can be caused by internal or external corrosion (Swietlik et al. 2012) and the spalling of cement mortar lining (Stephens et al. 2008). These wall deteriorated sections in the system usually reduce water transmission efficiency (Tran et al. 2010), creates water quality problems (Vreeburg and Boxall 2007), and may also develop into more serious blockages or bursts over time (Zamanzadeh et al. 2007).

Blockages also commonly exist in WTDPSs and they can be caused by physical and/or chemical processes such as material deposition. By increasing the roughness of pipe walls and reducing the flow area, blockages in a WTDPS reduce the system efficiency and cause a waste of energy associated with water transmission. In addition, they increase the potential for water contamination.

The maintenance of WTDPSs can be very expensive and the maintenance cost is expected to increase with the ageing of the infrastructure. In the US, more than US\$1 trillion will be required between 2011 to 2035 to replace ageing water mains and address projected growth (AWWA 2012). Given the considerable costs and the significant social importance, strategically targeted maintenance, replacement and rehabilitation are imperative to ensure the reliability and integrity of these critical WTDPSs. However, due to the sheer size of the WTDPSs and the fact that much of the system is buried underground, non-invasive and cost-effective anomaly detection and condition assessment of these pipes are very challenging.

1.1.2 Limitations of traditional technologies

To detect the anomalies in pipelines, a number of commercial detection techniques are available. Ground-penetrating radar (Eiswirth and Burn 2001) and electromagnetic techniques (Atherton et al. 2000; Roubal 2002) have been applied to detect leaks. However, these methods are only capable of detecting leaks within a small range of the WTDPSs. Thus, detecting leaks along the pipelines given the large size of WTDPSs is labour intensive and not cost-effective. Surface penetrating radar (Donazzolo and Yelf 2010) and magnetic flux leakage have been used to determine the structure of the pipe wall, but they

are only suitable for localized inspection and are inefficient and costly for long-range applications. Closed-circuit television (CCTV) inspection (Tran et al. 2009) captures images of the inner surface of a pipe using a camera on a carrier that travels within the pipeline. However, this method is intrusive, costly and not reliable for identifying the severity of deterioration (e.g. the depth of a crack) (Hao et al. 2012).

Acoustic-based leak detection techniques have been developed over three decades, and they are commercially used in WTDPSs (Fuchs and Riehle 1991; Tafuri 2000). One such technique uses the cross-correlation of measured active leak signals at two locations to determine the location of the leak (Gao et al. 2004). The cross-correlation method was theoretically developed and further improvement was made by adding weighting functions in the correlators (Gao et al. 2017). Despite its successful commercial applications, such techniques can only achieve passive leak detection, which means only leaks which are generating sufficient noise can be detected. Blockages and wall corruptions which have a high potential to further develop into leaks cannot be found using such methods.

With increasing investments in water distribution systems in many cities, an increasing number of pressure transducers and accelerometers are permanently installed in the pipeline network system to monitor the system (Stephens et al. 2018). This makes a large amount of data accessible and thus enables the training of artificial neural network models, which are designed to detect leaks and bursts (Mounce et al. 2010; Romano et al. 2014). However, the reliability of the detection heavily relies on a large amount of useful data, which may take a long time to obtain even with sufficient sensors. Similar to the acoustic-based leak detection techniques, such data-driven detection methods are also passive and only capable of detecting leaks and bursts.

1.1.3 Anomaly detection and condition assessment in pipelines using fluid transient waves

Among the anomaly detection and condition assessment technologies that are being developed, fluid transient analysis based methods have shown considerable potential due to the advantages of cost-effectiveness and non-invasiveness. Hydraulic transient pressure waves are injected into a pipeline through a generator and wave reflections will be generated if the incident wave encounters an anomaly such as a leakage or a blockage. By analysing these reflections using appropriate algorithms, the anomalies in the pipeline and the condition of the pipeline can be determined. This process is akin to the use of sonar waves to detect remote objects within marine environments.

The transient wave generator and sensors can be installed at existing connection ports, such as hydrants, air valves and scour valves. The transient tests do not require any excavation and do not disrupt the water supply service. Transient waves can propagate along the pipeline over a long distance in a short time (few seconds) due to the fast transient wave speed (typically 300 m/s to 1400 m/s for pipelines depending on the material and relative wall thickness). The inherent health information of the pipeline (anomalies in the pipeline and the pipeline condition) is carried by the transient waves and thus the detection range can be very large. Overall, transient based methods are cost-effective and non-invasive.

Over the last two and half decades, intensive simplified numerical simulations, some elaborately controlled laboratory experiments and some field tests have been conducted with the aim of developing transient-based anomaly detection and condition assessment techniques (Stephens 2008; Colombo et al. 2009; Puust et al. 2010; Stephens et al. 2013). However, many challenges have impeded the implementation of these techniques in real WTDPSs. As a result, further research has to be conducted to advance the transient-based techniques to make them practical in field applications.

(a) Anomaly detection

The time-domain reflectometry method is the most straightforward transient-based anomaly detection method in the time domain. By directly analyzing the reflected pressure wave, the location of the anomaly, such as a leak, can be determined based on the time series and the wave speed of the pipe (Brunone 1999). The detectability of this method is discussed with experiments taken with different leak sizes by Ferrante et al. (2014).

The transient pressure waves can be also transferred to the frequency domain to generate the frequency response diagram (FRD) of the pipeline. The FRD of a pipe is the plot of the frequency response function which describes the magnitude of the system response to each oscillatory excitation at a specific frequency (Chaudhry 2014). The location range of a leak was determined by Lee et al. (2005a) based on the sequence of the resonance peaks in the FRD. Blockages were also localized based on the shift of the resonance peaks in the FRD (Mohapatra et al. 2006a). To get a high resolution of the detection, a large number of FRD harmonics need to be measured in these methods to provide sufficient information of the anomaly. Although Gong et al. (2013a) only used the first three resonant frequencies to determine the leak location, it is difficult to accurately get the FRD in the field and such FRD-based methods are heavily dependent on the system configuration. Thus, the FRD-based methods can only be applied to single pipelines or simple systems with only one type of anomaly (such as leaks) existing in the pipeline. Furthermore, frequency-dependent wave dissipation and dispersion caused by friction, viscoelasticity and fluid-structure interaction may distort the FRD and further impede the anomaly detection.

Another transient-based detection method is to calculate the impulse response function (IRF) of the pipeline which can improve the spatial resolution of the detection (Vítkovský et al. 2003b). The IRF of a pipeline is the pressure response of the pipeline when an impulse pressure signal is injected into the pipeline. The wave reflection in the IRF trace is much sharper than the original

wave reflection, and thus the spatial resolution which is determined by the duration of the wave reflection can be highly improved.

Since sharp signals with a short duration (such as a pulse signal) are not tolerant to system pressure fluctuations and other sources of interference, continuous signals such as the pseudo-random binary sequence (PRBS) were adopted by Liou (1998) in a numerical study to extract the IRF to determine leak locations. Experimental studies were conducted by Nguyen et al. (2018) with a valve connected to a pipeline operated following a PRBS pattern. However, the measurement of the dynamic valve opening in the experiments involves errors which largely reduce the accuracy of the extracted IRF. Other factors such as experimental uncertainties, measurement error, systematic error and hydraulic noise may lead to numerical artifacts in the IRF trace, which are difficult to be distinguished with the anomaly-induced wave reflections.

Detailed reviews on anomaly detection techniques that are relevant to the research in this thesis can be found in the *Introduction* sections in Chapters 3 and 4. Except for several papers on field tests, all the research on transient-based anomaly detection has been conducted numerically or in controlled laboratory conditions. The system background pressure fluctuations and noise are a significant obstacle for the transient-based methods to be applied in the field (**Research Gap 1**). Many transient based methods, especially the FRD-based methods, are limited to applications to single pipes or simple pipe systems. The IRF-based methods are validated in single pipes in the laboratory but not in complicated pipe networks (**Research Gap 2**). Due to the factors such as experimental uncertainties, measurement error, systematic error and hydraulic noise in the transient tests, the detectability of the current transient-based methods is relatively low and only large anomalies can be detected (**Research Gap 3**).

(b) Pipeline condition assessment

In terms of the transient-based methods, most of them focus on detecting discrete elements, such as leaks (Brunone 1999; Vítkovský et al. 2007; Ferrante

et al. 2009; Shamloo and Haghghi 2009; Duan et al. 2011) and discrete blockages (Wang et al. 2005; Lee et al. 2008b; Sattar et al. 2008; Meniconi et al. 2011a). In ageing WTDPs, extended blockages caused by tuberculation and extended sections of pipe wall degradation caused by spalling of the cement mortar lining and widespread corrosion are common. Some research considers an extended blockage with a uniform diameter (Duan et al. 2012) or a deteriorated section with a uniform wave speed (Gong et al. 2013c); however, the properties of blockages and deteriorated sections in the real WTDPs are normally non-uniformly distributed.

To assess the detailed conditions of these extended anomalies, such as the shape of the blockage and the severity of the deterioration at different locations, pipe wall thickness (or diameter) distribution and the wave speed distribution needs to be reconstructed in order to achieve a spatially continuous condition assessment. Two spatially continuous pipe condition assessment methods are available in the hydraulic transient field and they are inverse transient analysis (ITA) (Stephens et al. 2013) and the reconstructive method of characteristics (RMOC) (Gong et al. 2014a).

The ITA which was first proposed by Liggett and Chen (1994) for detecting leaks was applied to pipeline condition assessment by Stephens et al. (2008; 2013). It involves an optimization process to minimize the error between numerical results by the method of characteristics (MOC) with assumed parameters (e.g. wave speeds) and experimental values. In this way, the assumed parameters can be calibrated and used to interpret the condition of the real pipeline. To improve the computational efficiency of ITA, a head-based MOC model with a flexible computational grid (Zhang et al. 2018a) and a multi-stage parameter-constraining ITA (Zhang et al. 2018b) were developed. However, an accurate transient simulation of real WTDPs, on which the ITA heavily relies, is challenging due to pipeline parameter uncertainties. Wave dissipation and dispersion of the transient waves which are ignored in the current ITA will affect the identifiability performance of the technique (Vítkovský et al. 2007). The background pressure fluctuations and noise which

exist in the WTDPSSs may also reduce the reliability of the results obtained by the ITA.

The reconstructive MOC analysis assesses the condition of a pipeline, section by section, by inverting the conventional MOC calculation (Gong et al. 2014a). The method removes the iterative optimizer-driven model calibration process, which makes the method computationally efficient. An extension was made by (Zhang et al. 2019) to relax the requirement of a dead-end boundary. But the application of the method is still restricted to simple pipe systems. The reconstructive MOC can only consider steady friction in the transient flow, while the unsteady friction and the pipe wall viscoelasticity, which can cause large wave dissipation and dispersion, are not considered. Ignoring these factors may lead to overestimating the size of the blockage or the severity of deterioration.

In other research fields, the layer-peeling method was developed and applied in the reconstruction of the geometry of short air ducts with varying cross-sections (Amir and Shimony 1995a, b). The method was applied to the inspection of musical wind instruments (Sharp and Campbell 1997) and the design of optical fibers (Wang and Erdogan 2001). In these applications, the IRF of the system is extracted and then utilized to reconstruct the bore of the musical instruments or the long-period optical fibre grating section by section. The capacity of the layer-peeling method was improved in the musical field by increasing the length of reconstruction (Sharp 1998), enhancing the robustness (Forbes et al. 2003), increasing the axial resolution (Li et al. 2005) and coupling the higher mode acoustic waves in the method (Hendrie 2007). The layer-peeling method is a powerful tool in these fields, but there is no application of the layer-peeling concept to pipeline condition assessment using hydraulic transients.

Detailed reviews on pipeline condition assessment that are relevant to the research in this thesis can be found in the *Introduction* sections in Chapters 5 to 8. Based on the review of different transient-based methods, it can be found that the current transient-based techniques for spatially continuous pipe condition assessment do not consider wave dissipation and dispersion which may be

significant in the field (**Research Gap 4**). The applications of these methods are limited to single pipelines (**Research Gap 5**).

(c) Transient tests

Incident pressure waves in water pipelines are usually generated by conventional valve movements. Discrete step waves can be achieved by closing a side-discharge solenoid valve sharply (Gong et al. 2013c) and pulse pressure waves can be achieved using a close-open-close valve movement. Another method to generate a sharper pressure wave is to use an underwater electrical spark-based generator (Gong et al. 2018a). The generator can result in significantly sharper wavefronts and wider signal bandwidths. As the generator is submerged in water, an electrical spark induced by a high instantaneous voltage across two electrodes vaporizes the intermediate fluid causing the development of a localized vapour cavity. An extremely sharp and strong pressure pulse can be generated due to the collapse of the cavity. These generators can generate transient waves with a short duration, less than 0.1 milliseconds for the spark-based generator and several milliseconds for the solenoid valve in the laboratory. However, generating continuous signals which can be controlled are challenging for the transient generators in existence. Although continuous pseudo random binary sequences have been generated by using two solenoids (Gong et al. 2016a), the generated signal is difficult to control.

Pressure transducers are normally used to collect the transient pressures in transient tests for anomaly detection and condition assessment. However, there are often simultaneous waves travelling in opposite directions. In the acoustics research field, two microphones have been used to measure the acoustic waves in ducts in order to separate the directional waves (Seybert and Ross 1977; Chung and Blaser 1980). Similar research in transient research field was conducted by (Shi et al. 2017) using a pair of pressure transducers in close proximity. However, two access ports in close proximity used to install pressure transducers are rarely available on a field pipeline.

Overall, to make the anomaly detection and the condition assessment methods more practical, it requires persistent transient wave generation that can be controlled and pressure measurement at multiple locations in close proximity (**Research Gap 6**).

1.2 Research Aims

The overall aim of the thesis is to develop practical transient-based techniques for anomaly detection and condition assessment in water pipelines. In order to fulfil the overall aim of this research, three main research aims have been proposed, with a number of specific sub-aims, as listed below.

Aim 1: To develop practical transient-based anomaly detection technologies for pressurised water pipelines using multiple sensors.

Aim 1.1: To develop a practical leak detection technique with high detectability, high spatial resolution, high tolerance to background pressure fluctuations and noise and high practicability in pipe networks.

Aim 1.2: To extend the technique to detect different kinds of anomalies, such as blockages and deteriorated sections.

Aim 2: To develop efficient and effective transient-based pipeline condition assessment technologies for pressurised water pipelines.

Aim 2.1: To develop a modified layer-peeling method for pipeline condition assessment considering wave dissipation and dispersion.

Aim 2.2: To extend the new approach to complicated pipeline systems.

Aim 2.3: To develop other transient-based methods based on the layer-peeling method for long pipelines.

Aim 2.4: To combine the layer-peeling method with the paired-IRF technique.

Aim 3: To develop new transient generation and measurement systems and verify the developed new techniques by experiments.

It should be noted that Aim 1 is to identify and localize anomalies in pipe systems and Aim 2 is to further obtain detailed conditions of these anomalies, such as the diameter profile of a blockage or the distribution of wall thickness of a deteriorated section.

1.3 Organisation of the Thesis

This thesis has ten chapters in total. The main body (Chapters 3 to 9) of this thesis is presented as a collection of the seven journal publications arising from the research undertaken. The framework of the thesis is shown in Figure 1.1. The journal paper manuscripts have been reformatted in accordance with University guidelines, and sections have been renumbered for inclusion within this thesis.

Chapter 2 gives a synopsis of Chapters 3 to 9 corresponding to the journal publications. A brief summary is given on each journal publication with the innovations highlighted. Some selected results and extension work beyond the publications are also shown in this chapter.

Chapters 3 to 4 focus on the development of anomaly detection techniques for pressurized pipelines. **Chapter 3** (Journal paper 1, Aim 1.1) proposes a novel paired-IRF technique with experimental validation on leak detection. **Chapter 4** (Journal paper 2, Aim 1.2) extends the technique to detect different kinds of anomalies and further improves its detection range and the tolerance to background pressure fluctuations and noise.

Chapters 5 to 7 focus on the development of pipeline condition assessment technologies for pressurised water pipelines. **Chapter 5** (Journal paper 3, Aim 2.1) proposes a novel layer-peeling method for pipeline condition assessment. **Chapter 6** (Journal paper 4, Aim 2.1) extends the new approach to applications to complicated pipeline configurations. **Chapter 7** (Journal paper 5, Aim 2.3)

proposes a fast inverse transient method by incorporating a reversed layer-peeling method.

Chapters 8 (Journal paper 6, Aim 2.4) combines the layer-peeling method (**Chapters 3 to 4**) with the paired-IRF method (**Chapters 5 to 7**) to achieve robust pipeline condition assessment.

Chapters 9 (Journal paper 7, Aim 3) develops a voice-coil based generator and a new generation in-pipe optical fiber sensor array which can facilitate the transient tests in **Chapters 3-8**.

Chapter 10 summarises the major contributions of this research with discussions on the scope of future work.

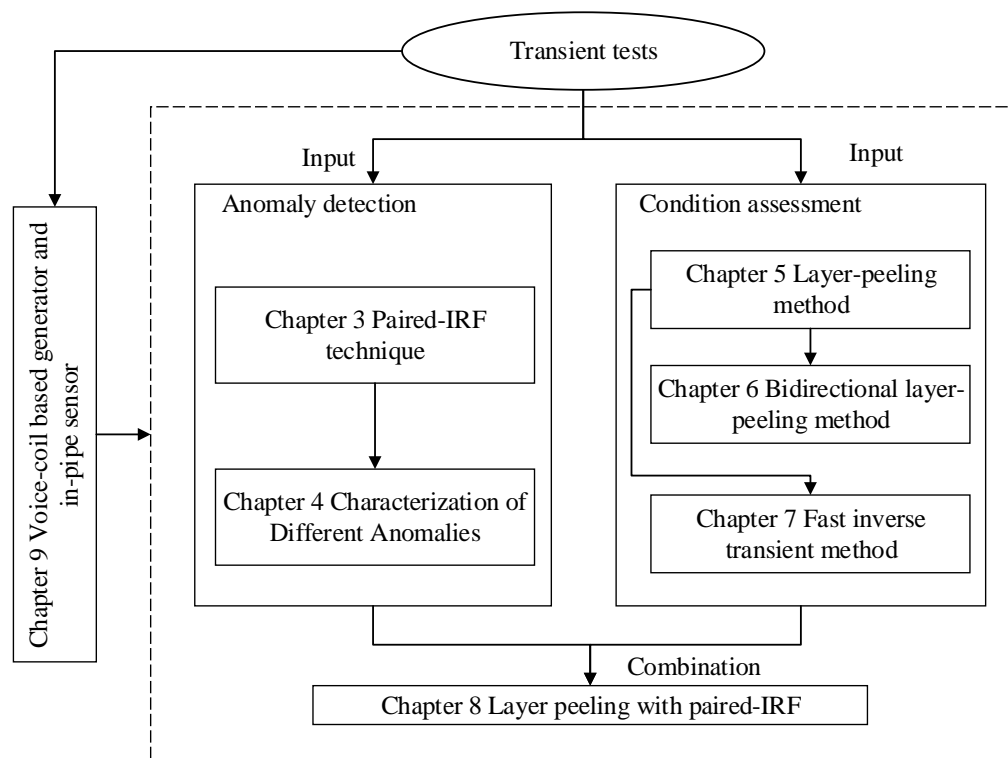


Figure 1.1 Framework of the PhD thesis.

Chapter 2

Synopsis of Publications

This chapter provides a brief summary for Chapters 3 to 9, corresponding to the seven journal publications as given in the *Publications arising from this thesis*. The background, methodologies and innovations are briefly presented for each paper. The latest experiment designed and conducted by the candidate for Chapter 3 is supplemented in Chapter 2 to show the capacity of the paired-IRF technique. A numerical case included in Chapter 5 is briefly presented in Chapter 2 to show the accuracy of the layer-peeling method. Detailed methodologies and case studies can be found in Chapters 3 to 9.

2.1 Paper 1: Paired Impulse Response Function Technique (Chapter 3)

For the hydraulic transient-based detection methods, there are some key factors impeding application in the field. 1) Background pressure fluctuations and noise in the pipe network always exist and they will contaminate the transient pressure waves measured. 2) Many methods are restricted to pipe systems with a simple configuration. 3) The detectability of these methods is not high enough to detect anomalies that only induce small wave reflections.

In Chapter 3, continuous transient waves were sent into the pipeline with pressure responses measured by two transducers (separated by a distance). The generator (G) and sensor (P_1 and P_2) configuration is shown in Figure 2.1. Given this set-up, a signal analysis methodology with high-order (the order is defined based on the number of times that the incident pressure wave is reflected by

discontinuities within the pipeline) wave reflections neglected has been theoretically derived to extract the major components of the deconvolution between these two measured pressure traces P_2 and P_1 (after being transferred into the frequency domain), as shown by

$$\frac{P_2}{P_1} = H + \underbrace{R_R \left(\frac{1}{H} - H \right)}_{\text{order} = 1} \quad (2-1)$$

where R_R after transforming to the time domain is the impulse response function (IRF) of the pipeline at the right side of the generator and H is the transfer function of the section between the transducers. The term $1/H$ in the brackets physically means transferring the IRF forward in time by Δt , while $-H$ in the brackets means reversing the sign of the IRF after delaying it by Δt . The term Δt is the wave propagation time in section $P_1 - P_2$. Thus, the deconvolution consists of a pair of IRFs of the pipeline with opposite signs and a time shift associated with the distance between the transducers. Hereon, they are referred to as a *paired-IRF*. A leak is shown to induce a pair of spikes in the paired-IRF trace. With the paired-IRF obtained, the leak can be localized by analyzing the occurrence times of the leak-induced paired-spikes.

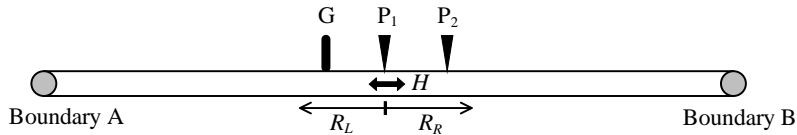


Figure 2.1 Generator and sensor configuration for the paired-IRF technique.

According to numerical and experimental validations, it shows the novel paired-IRF method 1) has a high tolerance to realistic background pressure fluctuations and noise in real pipe networks, 2) is able to be applied in pipe networks with arbitrary configurations, 3) has a very high detectability because powerful continuous signal is used and the leak-induced features (a pair of spiked pulses with opposite signs and a fixed time interval) can be easily differentiated from other noise in the paired-IRF trace.

An experimental case (not included in Chapter 3) is given below to show the capacity of the new method. Figure 2.2 shows the layout of the experimental pipe system. A pipeline that is 37.46 m in length with an internal diameter of 22.14 mm was connected with the water main through a copper pipe and a hose pipe. The water main is connected with the Adelaide Central Business District (CBD) pipe network. A discharge orifice connected with a T-junction was used to simulate the leak (L_1 in Figure 2.2). The diameter of the orifice was calibrated to be 0.93 mm. Joint J_2 is composed of a brass block and a Swagelok pipe fitting. An opened side discharge valve (G) was connected to the pipe to discharge water and hydraulic noise (transient wave) was generated by the turbulence of the flow around and through the valve. Two pressure transducers (P_1 and P_2) were installed close to G with a separation distance of 0.8 m. All the joints of the pipeline and other installed transducers are shown in the schematic.

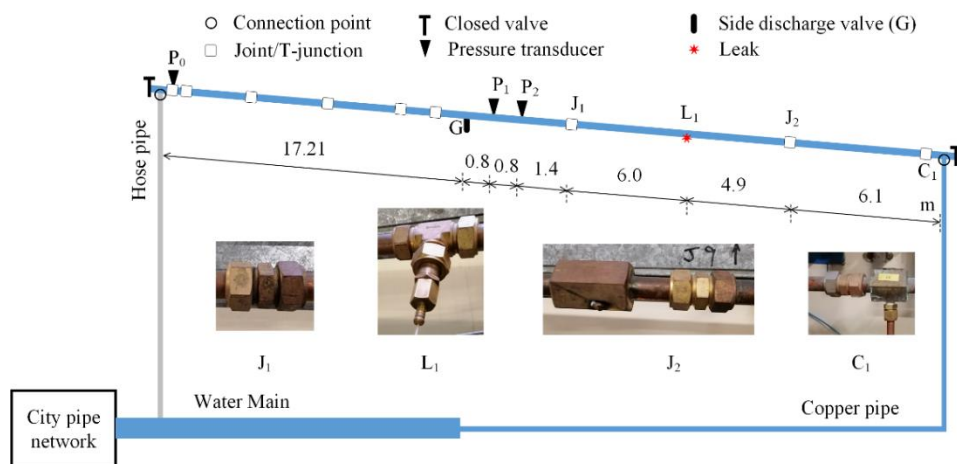


Figure 2.2 Schematic of the experimental pipe network.

The transient pressure waves caused by the turbulent flow through the valve are shown in Figure 2.3. They are contaminated with the background pressure fluctuations and noise from the CBD pipe network. The paired-IRF trace obtained from the measured pressures is shown in Figure 2.4. The simulated leak, as well as the joint J_2 , can be clearly identified by the paired spikes shown in the paired-IRF trace.

To the author’s knowledge, this is the first time that a transient-based method has been experimentally validated to be able to fully eliminate the effects from background pressure fluctuations and noise from a real pipe network in anomaly detection. Different transient-based methods have been developed and validated on the same laboratory pipe in the past years (Wang et al. 2002; Lee et al. 2007b; Gong et al. 2016a; Nguyen et al. 2018), and it is the first time that a joint inducing small (1%) wave reflections has been clearly identified even with the background pressure fluctuations and noise.

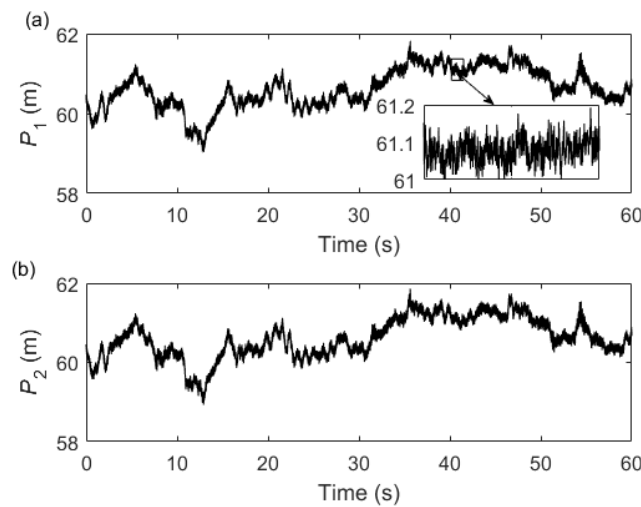


Figure 2.3 Measured pressure waves on the experimental pipe network at (a) P_1 and (b) P_2 .

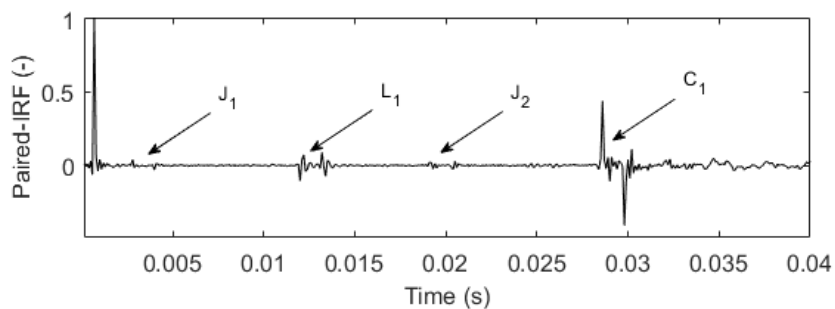


Figure 2.4 Paired-IRF extracted for the experimental pipe network.

2.2 Paper 2: Characterization of Different Anomalies (Chapter 4)

Chapter 4 makes some further extensions of the paired-IRF technique proposed in Chapter 3. With the paired-IRF technique developed in Chapter 3, different anomalies including leaks, blockage, deteriorated section, etc., in pipe systems can be detected, but they are difficult to be distinguished from one another. In Chapter 4, these anomalies as shown in Figure 2.5 have been characterized based on the features of the spikes they induced in the paired-IRF trace in order to distinguish them.

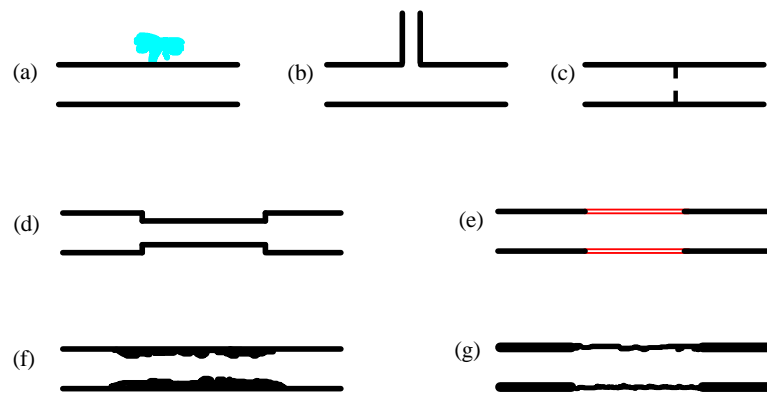


Figure 2.5 (a) leak; (b) junction; (c) partially closed in-line valve or discrete blockage; (d) section with diameter change or extended blockage with a uniform diameter; (e) section with material change or deterioration with a uniform wave speed; (f) extended blockage with non-uniformly distributed diameters; and (g) wall deteriorated section with non-uniformly distributed wave speeds.

In Chapter 3, only first-order wave reflections are considered in the analysis. However, in Chapter 4, the paired-IRF technique has been extended to incorporate all high-order wave reflections. If the detection range extends from the pipe on which the pressure transducers are installed to other pipes in the network, high-order wave reflections will emerge in the paired-IRF trace. These reflections will be incorrectly treated as spikes induced by some extra

anomalies using the first-order paired-IRF technique proposed in Chapter 3 and can be corrected with the high-order paired-IRF technique.

Further improvement of the tolerance of the method to background pressure fluctuations and noise has been achieved using an averaging process. The extracted paired-IRF traces from individual transient tests/simulations can be averaged to diminish the noise in the averaged paired-IRF trace.

After the extensions, the paired-IRF technique 1) can be used to detect different types of anomalies in pipe networks and 2) has a wider detection range and 3) higher tolerance to realistic background pressure fluctuations and noise.

2.3 Paper 3: Layer-Peeling Method (Chapter 5)

The paired-IRF technique is able to identify and localize blockages and deteriorated sections in pipe systems and generally estimate their sizes. To obtain detailed conditions of these anomalies, such as the diameter profile of a blockage or the distribution of wall thickness of a deteriorated section, another technique – the layer-peeling method has been developed and presented in Chapter 5. In the method, a pipe has been discretised to many sections and the details of the pipe can be reconstructed section by section. The process is similar to peeling the pipe layer by layer to get the detailed information of the pipe step by step, and thus the method is defined as layer-peeling method.

The layer-peeling method has been applied previously in the acoustics research field to reconstruct the internal profile of tubular music instruments, as shown in Figure 2.6 (a). In Chapter 5, the original layer-peeling method has been further developed for application to water transmission pipelines by 1) modifying the end boundary from being an acoustic source tube to a closed valve; 2) incorporating the effects of unsteady friction and pipe wall viscoelasticity into the layer-peeling algorithm; and 3) incorporating frequency-dependent wave reflections and transmissions. Using the impulse response function (IRF) as the input of the modified layer-peeling method, the diameter, the wall thickness and the wave speed of the pipeline can be reconstructed

section by section. It is the first time that the layer-peeling method has been applied to water pipelines.

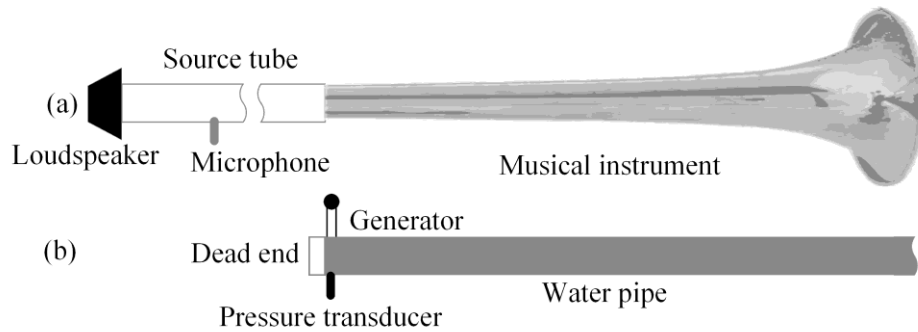


Figure 2.6 Schematic diagram of the testing systems for (a) a musical instrument and (b) a water pipe.

A case study on a frictionless metallic pipeline as shown in Figure 2.7 is given below with details included in Chapter 5. Two deteriorated sections exist in the pipe with its wave speed distribution shown by the solid line in Figure 2.8. A pressure pulse wave was injected into the pipeline at the upstream face of the closed valve, and the wave reflections were simulated using the method of characteristics. The proposed layer-peeling method applied to the simulated pressure accurately yields reconstructed wave speed distributions that are almost identical to the theoretical values (as shown in Figure 2.8). More case studies with incorporating the effects of unsteady friction and pipe wall viscoelasticity can be found in Chapter 5.

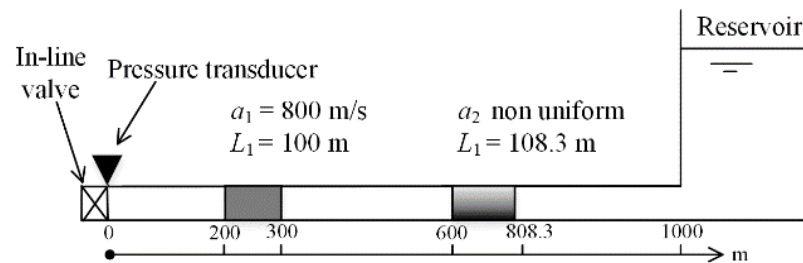


Figure 2.7 Pipeline configuration for the layer-peeling method.

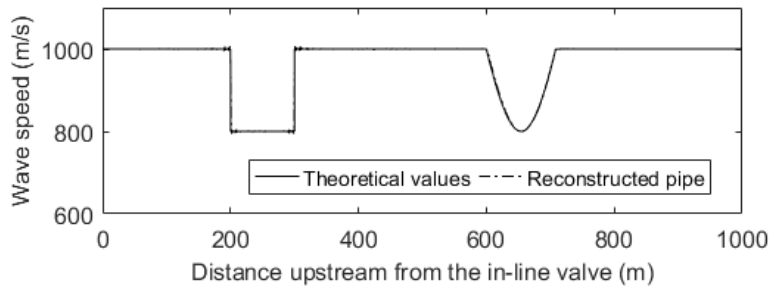


Figure 2.8 Wave speed reconstructed from the modified layer-peeling method for the frictionless pipe. (The two plots are virtually coincident).

2.4 Paper 4: Bidirectional Layer-Peeling Method (Chapter 6)

Chapter 6 makes further extensions of the layer-peeling method proposed in Chapter 5. Some limitations exist in the first-generation layer-peeling method and have impeded the application to pipelines in water distribution systems. These are outlined as follows: 1) it is difficult to satisfy the requirement that both the incident transient wave is injected into the pipeline at a dead-end and that the pressure responses are measured immediately upstream of the dead-end; 2) off-takes and cross-connections in a pipeline network may also generate wave reflections and affect the wave reflections induced by the deteriorated pipe sections.

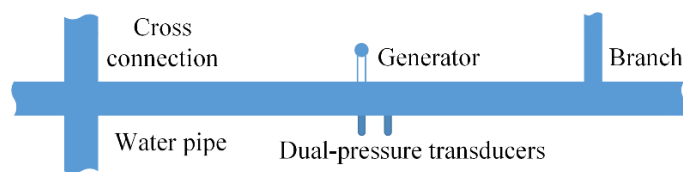


Figure 2.9 Schematic of the testing configuration for the bi-directional layer-peeling method.

By using two sensors installed at interior points along the pipeline, the new technique removes the need of a dead-end boundary condition, as shown in Figure 2.9. It enables a bi-directional reconstruction of the pipeline by

modifying the boundary of the layer-peeling algorithm. Pipelines with branches can be properly analyzed since the model of a bifurcation point is incorporated in the algorithm (providing the potential to apply the proposed methodology to pipes in water distribution systems that contain numerous junctions).

2.5 Paper 5: Fast Inverse Transient Method (Chapter 7)

For the layer-peeling methods developed in Chapters 5 and 6, any spikes in the measured pressure traces will be treated as wave reflections induced by an impedance change caused by the change of the wave speed or/and diameter. However, these spikes of small magnitude may be caused by some pipe components, such as pipe fittings, or by noise and fluid-structure interaction. The effects of these can be reduced significantly using the paired-IRF method in Chapter 3 but cannot be fully eliminated. Therefore, the reconstruction process using the layer-peeling method may suffer from cumulative errors if the pipeline is very long.

In Chapter 7, a faster inverse transient method has been developed. The layer-peeling method was reversed to create a new wave reflectometry method that can efficiently simulate the wave reflections. The layer-peeling method uses the wave reflections as the input and calculates the impedance distribution of the pipeline, while the wave reflectometry method takes the impedance distribution as the input and outputs the wave reflections. By assuming impedance information of the pipeline and then calibrating it through an evolutionary algorithm, as shown in Figure 2.10, a faster inverse transient method has been developed to compensate for the cumulative errors which may occur in the layer-peeling method in some instances.

The proposed method: 1) concentrates on the major wave reflections and minimizes the effects from the signal noise and other interferences; 2) a highly efficient wave reflectometry method has been developed by reversing the layer-

peeling method, thus significantly improving the computational efficiency of the inverse calibration process.

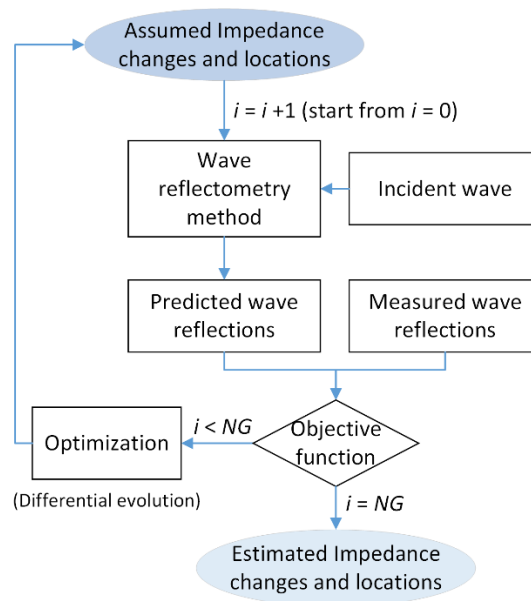


Figure 2.10 Optimization process of the fast inverse transient method (where NG is the maximum number of generations).

2.6 Paper 6: Layer-Peeling Method with Paired-IRF (Chapter 8)

The layer-peeling method takes the IRF of a pipeline as the input to reconstruct the impedance distribution of the pipeline. In the conventional methods used to calculate the IRF, the incident transient wave injected into the pipe needs to be separated from the wave reflections. Thus, discrete signal inputs, such as a pulse or step signal, are normally adopted as the injected waves (as shown in Chapters 5 and 6) since they can be visually separated from the wave reflections.. However, such discrete signals are not tolerant to background pressure fluctuations and noise. In the paired-IRF method, continuous signals have been used as the input to calculate the pipeline paired-IRF, which is the superposition of a pair of IRFs with opposite signs and a fixed time shift. The paired-IRF can be then further manipulated to obtain the IRF of the pipeline which is the input to the layer-peeling method.

In Chapter 8, a three-sensor configuration with two sections of wall deterioration is considered. The paired-IRF equations for such a specific configuration have been derived. The process to get the IRF of the pipeline was presented, followed by the pipeline impedance reconstruction using the layer-peeling method.

2.7 Paper 7: Voice-Coil Transient Generator and In-Pipe Sensors (Chapter 9)

Apart from pulse or step pressure waves, continuous transient pressure waves have been commonly used in the proposed techniques in Chapters 3 to 8. These techniques also require transient pressure measurements at two locations in close proximity in the pipe, which is often difficult to achieve for buried pipelines using conventional flush-mounted pressure transducers.

In Chapter 9, a voice-coil-based transient generation system has been developed as shown in Figure 2.11. It can be connected to a side-tapping in a pipe to provide a controlled discharge of water from the pipe. The piston of the voice-coil actuator can travel perpendicularly through the brass block and its movement is controlled by the signal generation software developed in the LabVIEW platform. If the piston oscillates persistently, a continuous flow perturbation can be excited and it in turn induces persistent transient pressure waves inside the pipe.

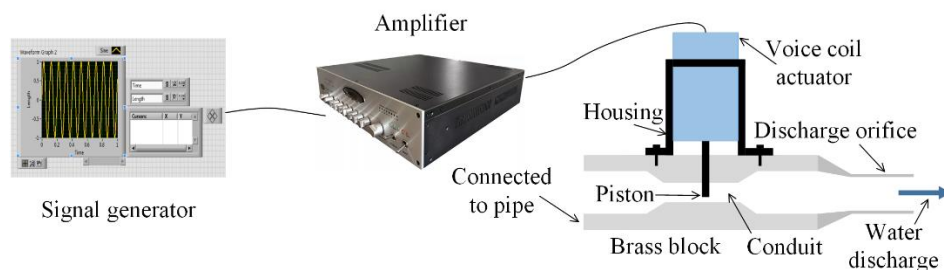


Figure 2.11 Schematic of the voice-coil based transient generation system.

A new generation in-pipe optical fiber sensor array for transient pressure measurement, as shown in Figure 2.12, was developed in this chapter. The protective cable carries two fiber-Bragg-grating (FBG)-based pressure sensors and can be deployed into pressurized pipes to measure pressures.

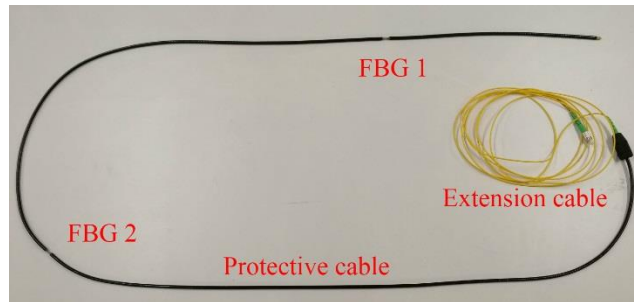


Figure 2.12 Photograph of the in-pipe optical fiber sensor array.

In the field, the voice-coil based transient generator can be installed at a fire hydrant (as shown in Figure 2.13), an air valve or some other kinds of access ports. The in-pipe sensor array can be inserted into the pipe at the same place as shown in Figure 2.13. Thus, only one access port is needed for such transient generation and measurement systems. Such merit makes the developed techniques in Chapters 3 to 8 more practical in the field. In addition, the transient pressure measurement by the in-pipe sensors is more accurate than that by the pressure transducer which measures the pressure in the stub rather than that in the pipe.

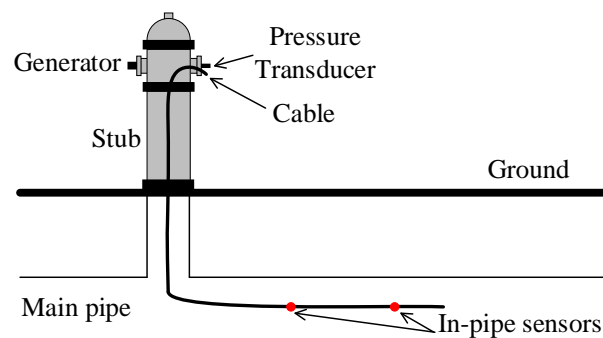


Figure 2.13 Schematic of the installation of the generator and sensors in the field.

Chapter 3

Paired-IRF method for Leakage Detection of Pipes in a Network (Journal Publication 1)

Wei Zeng¹, Jinzhe Gong¹, Angus R. Simpson¹, Benjamin S. Cazzolato², Aaron C. Zecchin¹, Martin F. Lambert¹

¹School of Civil, Environmental and Mining Engineering, the University of Adelaide, Adelaide, SA 5005 Australia

²School of Mechanical Engineering, University of Adelaide, SA 5005, Australia

Citation: Zeng, W., Gong, J., Simpson, A. R., Cazzolato, B. S., Zecchin, A. C., Lambert, M. F. (Forthcoming). "Paired-IRF method for leakage detection of pipes in a network." *Journal of Water Resources Planning and Management*, DOI: 10.1061/(ASCE)WR.1943-5452.0001193.

Statement of Authorship

Title of Paper	Paired-IRF method for leakage detection in pipe networks
Publication Status	<input type="checkbox"/> Published <input checked="" type="checkbox"/> Accepted for Publication <input type="checkbox"/> Submitted for Publication <input type="checkbox"/> Unpublished and Unsubmitted work written in manuscript style
Publication Details	Zeng, W., Gong, J., Simpson, A., Cazzolato, B., Zecchin, A., Lambert, M. (2019). Paired-IRF method for leakage detection of pipes in a network. <i>Journal of Water Resources Planning and Management</i> . (Accepted)

Principal Author

Name of Principal Author (Candidate)	Wei Zeng			
Contribution to the Paper	Conception and design of the project Analysis and interpretation of research data Draft the paper			
Overall percentage (%)	75 %			
Certification:	This paper reports on original research I conducted during the period of my Higher Degree by Research candidature and is not subject to any obligations or contractual agreements with a third party that would constrain its inclusion in this thesis. I am the primary author of this paper.			
Signature	<table border="1" style="width: 100%;"> <tr> <td style="width: 60%;"></td> <td style="width: 20%;">Date</td> <td style="width: 20%;">8/11/2019</td> </tr> </table>		Date	8/11/2019
	Date	8/11/2019		

Co-Author Contributions


By signing the Statement of Authorship, each author certifies that:


- i. the candidate's stated contribution to the publication is accurate (as detailed above);
- ii. permission is granted for the candidate to include the publication in the thesis; and
- iii. the sum of all co-author contributions is equal to 100% less the candidate's stated contribution.


Name of Co-Author	Jinzhe Gong			
Contribution to the Paper	Conception and design of the project Analysis and interpretation of research data Critically revising the paper			
Signature	<table border="1" style="width: 100%;"> <tr> <td style="width: 60%;"></td> <td style="width: 20%;">Date</td> <td style="width: 20%;">24/11/19</td> </tr> </table>		Date	24/11/19
	Date	24/11/19		

Name of Co-Author	Angus Simpson			
Contribution to the Paper	Conception and design of the project Analysis and interpretation of research data Critically revising the paper			
Signature	<table border="1" style="width: 100%;"> <tr> <td style="width: 60%;"></td> <td style="width: 20%;">Date</td> <td style="width: 20%;">4 Nov. 2019</td> </tr> </table>		Date	4 Nov. 2019
	Date	4 Nov. 2019		

Please cut and paste additional co-author panels here as required.

Name of Co-Author	Benjamin Cazzolato		
Contribution to the Paper	Conception and design of the project Analysis and interpretation of research data Critically revising the paper		
Signature		Date	08 Nov. 2019

Name of Co-Author	Aaron Zecchin		
Contribution to the Paper	Conception and design of the project Analysis and interpretation of research data Critically revising the paper		
Signature		Date	15/11/19

Name of Co-Author	Martin Lambert		
Contribution to the Paper	Conception and design of the project Analysis and interpretation of research data Critically revising the paper		
Signature		Date	22/11/19

Abstract

Pipeline leak detection is critical for targeted maintenance and water loss reduction within water distribution systems. This paper proposes a hydraulic-transient, impulse response function (IRF)-based, signal analysis approach for leak detection in water pipelines and networks. In the proposed approach, continuous pressure signals are sent into the pipeline, where pressure responses are measured by two transducers (separated by a distance) located close to the generator. Given this set-up, a signal analysis methodology is theoretically derived to extract the major components of the deconvolution between these two measured pressure traces. The result shows that the deconvolution consists of a pair of IRFs of the pipeline with opposite signs and a time shift associated with the distance between the transducers. Hereon, they are referred to as a paired-IRF. A leak is shown to induce a pair of pulses on the paired-IRF trace. With the paired-IRF obtained, the leak can be localized by analyzing the occurrence times of the leak-induced paired-pulses. Numerical verification is undertaken in both a single pipe and a pipe network using the pipeline pressure responses simulated by the method of characteristics. The leaks in the pipelines are successfully detected using the new approach. Experimental verification is conducted on a laboratory copper pipeline with a leak simulated by a discharge orifice. The proposed method is found to accurately localize the leak even with the pressure waves contaminated by realistic background pressure fluctuations and noise. The numerical and experimental cases demonstrate that the novel paired-IRF method is applicable to pipe networks, robust to system interference and able to deal with realistic background pressure fluctuations and noise.

3.1 Introduction

A reliable supply of potable water is an essential resource, particularly in water scarce regions; however, a large amount of water is lost during transmission within water distribution systems (WDSs) for most cities worldwide. The amount of water lost during transmission often exceeds 50% in some undeveloped countries or regions (Mutikanga et al. 2009). According to the investigation by International Water Association (Lambert 2002) and the Asian Development Bank (McIntosh and Yniguez 1997), the non-revenue water (NRW) or unaccounted for water (UFW) is between 20 - 40% for most countries or cities that have been studied. The leakage of WDSs contributes to significant economic cost, associated energy consumption and water contamination (Fox et al. 2016), and is ascribed as the major reason for the NRW (Nixon and Ghidaoui 2006; Colombo et al. 2009).

Growing attention has been given to developing non-invasive leak detection methods which enable predictive repair and strategically targeted pipe maintenance of the WDSs. Over the past two decades, a number of hydraulic transient-based leak detection methods have been developed (Liggett and Chen 1994; Liou 1996; Brunone 1999; Covas and Ramos 1999, 2001; Mpesha et al. 2001; Wang et al. 2002; Ferrante and Brunone 2004; Lee et al. 2005b; Lee et al. 2007b; Covas and Ramos 2010; Duan et al. 2011; Shucksmith et al. 2012; Wang and Ghidaoui 2018b, a; Wang et al. 2019). Typically, hydraulic transient waves are injected into the pipeline by a fast acting electro-mechanical valve. The transient waves will be reflected by any physical anomalies, such as a leak, and the location of the anomaly can be obtained by analyzing the transient pressure waves using frequency response diagrams (FRD) in the frequency domain (Lee et al. 2006; Lin et al. 2019). However, these frequency-domain hydraulic transient-based methods are limited to single pipelines or simple pipeline systems. Time domain methods can be also used to analyze the collected pressure waves, such as the inverse transient analysis, time-domain reflectometry method and impulse response method. These methods have been reviewed and the major gaps are identified and explained below.

The inverse transient analysis (ITA) was an early application to leak detection in pipe networks in the time domain (Liggett and Chen 1994; Nash and Karney 1999; Vítkovský et al. 2000; Kapelan et al. 2003; Covas and Ramos 2010). The transient responses of a numerical pipeline model with assumed leak locations were simulated by the MOC. Then, an optimization process was conducted to minimize the error between numerical predictions and experimental values to find the location of the leak. However, ITA is not computationally efficient, especially for pipelines of substantial length, which involve a large number of parameters to calibrate. A head-based MOC model with a flexible computational grid (Zhang et al. 2018a), and a multi-stage parameter-constraining ITA (Zhang et al. 2018b) was developed recently to significantly improve the computational efficiency of ITA. However, there are still many practical issues (e.g. wave dissipation and dispersion (Duan et al. 2010)) that affect the identifiability performance of the technique (Vítkovský et al. 2007). ITA heavily relies on an accurate forward transient simulation, which is challenging for real WDSs due to pipeline parameter uncertainties. The background pressure fluctuations which exist in the WDSs may also reduce the reliability of the results obtained by ITA.

The time-domain reflectometry method is the most straightforward transient-based leak detection method in the time domain. By directly analyzing the reflected pressure wave, the location of a leak can be determined based on the time series and the wave speed of the pipe (Brunone 1999). The size of the leakage can be determined by the wave reflection magnitude (Vítkovský et al. 2003b). The detectability of this method is discussed with experiments taken with different leak sizes (Ferrante et al. 2014).

To improve the resolution of the time-domain reflectometry method, the impulse response function (IRF) of a pipeline was utilized for leak detection (Vítkovský et al. 2003b). The IRF of a pipeline is the pressure response of the pipeline when an ideal impulse pressure signal is injected into the pipeline. An experimental study with a pulse input generated by a side discharge valve was conducted by Lee et al. (2007b) to detect leaks on an experimental pipe.

As sharp signals with a short duration (such as a pulse signal) are not robust to system pressure fluctuations and other sources of interference, continuous signals such as the pseudo-random binary sequence (PRBS) were adopted by Liou (1998) in a numerical study to extract the IRF to determine leak locations. Experimental studies were conducted by Nguyen et al. (2018) with the valve opening following a PRBS pattern. The valve opening was used as the input to extract the IRF since the incident wave and reflected wave cannot be visually separated like sharp signals with a short duration. A least squares method was applied to enhance the accuracy of the deconvolution. However, the measurement of the dynamic valve opening in the experiments involves errors which may reduce the accuracy of the extracted IRF. The non-linear relationship between the valve opening and the pressure generated will induce some fluctuations or spikes on the IRF trace, thus potentially masking the leak-induced reflections (details of the numerical case study exhibiting this limitation are illustrated in the following section). Due to the factors such as experimental uncertainties, measurement error, systematic error and hydraulic noise, the IRF trace extracted in experimental work always involves numerical artifacts (i.e. discrete spikes appearing as “noise” on the IRF), such as the experimental result shown in Nguyen et al. (2018). Distinguishing these artifacts from the real leak-induced reflections is difficult when the leak is small.

Overall, most of the transient-based methods in the time domain with a short and sharp signal input are not tolerant to system background pressure fluctuations and other interferences in field experiments. The use of continuous signals such as PRBS signal in the IRF method can suppress these side effects, but spikes not caused by leaks may be often confused with the leak-induced spikes. The use of the valve opening as the input to extract the IRF also generates additional problems.

The research presented in this paper proposes a novel paired-IRF method in the time domain which 1) is able to be applied in pipe networks, 2) can differentiate leak-induced features (a pair of spiked pulses with opposite signs and a fixed time interval) from other numerical artifact spikes on the IRF trace, 3) can avoid problems caused by using the valve opening as the input since the valve opening

is not used as the input signal but is replaced by the measured pressure, and 4) can deal with realistic background pressure fluctuations and noise.

In this paper, the conventional leak-detection methods are briefly reviewed with the practical issues discussed. A novel paired-IRF method is then theoretically derived to solve these limitations. To validate the new method, numerical case studies have been conducted on both a single pipe and a pipe network. Experiments with continuous signal inputs (including transient waves caused by a PRBS valve excitation and hydraulic noise by opening a valve) and a pair of pressure transducers on a laboratory pipeline have been conducted to further validate the proposed new leak detection method.

3.2 Leak Detection using Conventional Methods

In this section, the conventional wave reflectometry method and IRF method are briefly reviewed with a discussion of practical issues related to the use of these methods such as characterization of the valve dynamics, measurement errors and background pressure noise. To facilitate the discussion, numerical studies on a reservoir-pipeline -valve system (Case 1) as shown in Figure 3.1 are utilized.

3.2.1 Example system details

The system possesses the following properties: the internal diameter of the pipeline is assumed to be 400 mm throughout; the wave speed is 1000 m/s; the Darcy-Weisbach factor f is 0.02; a leak with $C_d A_L = 4 \times 10^{-5} \text{ m}^2$ and initial flowrate = 1.2 L/s for the initial pressure head = 50 m (C_d is the discharge efficiency and A_L is the area of the leak orifice) is located 70 m away from the dead-end; a transient generator (G) in the form of a valve with an initial flowrate = 46.9 L/s (The Reynolds number $Re \approx 1.3 \times 10^5$) and a pressure transducer P_1 are located close to the dead-end (as shown in Figure 3.1); the dimensionless valve opening τ is equal to 1 when the valve is fully opened and 0 when it is fully closed; and another transducer P_2 2 m away from P_1 is only used in the

new method. The method of characteristics (Wylie and Streeter 1993) with a time step of 0.0001 s for all the numerical cases has been applied to simulate the transient pressures with valve excitations.

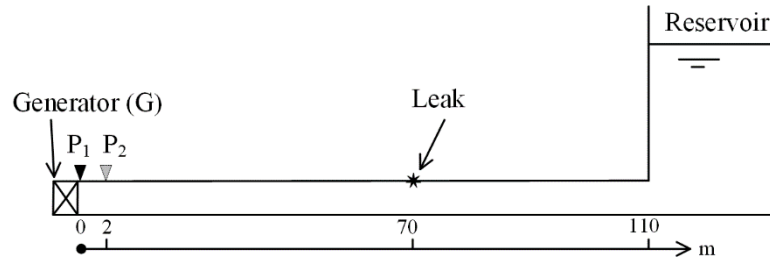


Figure 3.1 Pipeline configuration for Case 1.

3.2.2 The wave reflection using a sharp signal input with a short duration

Consider the case of a sharp pulse wave of 4 ms duration being injected into the pipe by operating the generator. At location P_1 , the simulated transient pressure p_1 is shown in Figure 3.2. The wave reflection caused by the leak is marked in the rectangle in the figure, and it is typically used to detect the leak in water pipes. However, if the background pressure fluctuations, hydraulic noise, wave dissipation, dispersion and other interferences in real WDSs are considered, the leak-induced reflection will be not sufficiently distinctive within the signal and even submerged in the noise. In addition, the generation of such a sharp signal is sometimes not allowed by the water utility as it may generate large pressure fluctuations, threatening pipes and devices in the pipe system. Another disadvantage of generating such signals is the large mechanical vibration generated by sharply operating the valve. This leads to large pressure fluctuations on the collected pressure traces and can mask the leak-induced wave reflections. Overall, signals with a small magnitude and high tolerance to noise are needed to make the transient-based leak detection methods more non-invasive and robust.

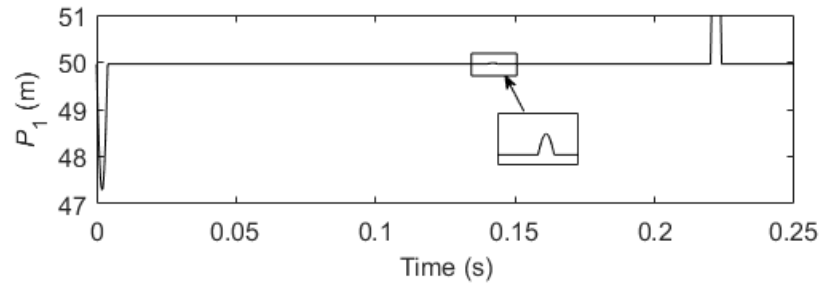


Figure 3.2 Simulated pressure wave with a pulse valve excitation at P₁.

3.2.3 IRF extraction with a continuous signal input

The pseudo random binary sequence (PRBS) signal commonly used in the electrical and electronics field consists of the summation of a series of randomly spaced steps changes. The known periodicity of the random sequences results in the high degree of noise tolerance of the signal. Thus, the signal has also been applied to detect leakages in water pipelines (Liou 1998). Details about the characteristics of the PRBS and the method to formulate it can be found in Godfrey (1993).

In this paper, an inverse repeat PRBS signal generated from a 10-stage shift register has been utilized as the valve excitation, with a clock frequency of 100 Hz. It should be noted that any other kinds of continuous signals with sufficient power and a wide bandwidth can be used to extract the IRF and the PRBS signal chosen in this paper is just a case for the purpose of the study. In the numerical cases, the downstream valve shown in Figure 3.1 follows the pattern shown in Figure 3.3 (a), with the normalized valve opening defined as $\tau^* = (\tau - \tau_0)/\tau_0$, where τ_0 is the averaged τ . Unlike the ideal PRBS signals utilized in the numerical studies in (Lee et al. 2007b; Gong et al. 2013b; Nguyen et al. 2018), the maneuverability of the valve is considered limited by its response time, as shown in Figure 3.3 (b). The value τ^* is assumed to linearly rise from the minimum position to the maximum position in 3 ms, and then linearly drop back to the minimum position in 3 ms, rather than instantaneously changing position as assumed in previous studies.

The simulated pressure perturbation at P_1 is shown in Figure 3.4. Unlike the transient pressure traces using sharp signals with a short duration (Figure 3.2), the pressure traces are highly complex and the incident waves and reflected waves cannot be separated visually. Thus, a deconvolution process is used to extract the system IRF with the normalized valve opening τ^* as the input of the deconvolution and p_1 as the output. The deconvolution process is defined as

$$R(j\omega) = Y(j\omega)/X(j\omega) \quad (3-1)$$

where $R(j\omega)$, $Y(j\omega)$ and $X(j\omega)$ are the Fourier transforms of the IRF, output and input of the deconvolution, respectively, j is the imaginary unit and ω is the angular frequency. The division is straightforward and pointwise for each frequency.

In the direct deconvolution process based on the inverse transform of Eq. (3-1), the denominator $X(j\omega)$ can tend to zero at high frequencies, leading to a singular inversion problem. To solve this issue, the least squares deconvolution in the time domain is applied as (Nguyen et al. 2018)

$$\mathbf{R} = (\mathbf{X}^T\mathbf{X} + \lambda\mathbf{I})^{-1}\mathbf{X}^T\mathbf{y} \quad (3-2)$$

where \mathbf{X} is a lower triangular matrix consisting of the input elements (in this case) and with rows being incrementally delayed vectors of the input, \mathbf{y} and \mathbf{R} are the column vectors of the output time series P_1 (in this case) and the time-domain series of the IRF coefficients, respectively, \mathbf{I} is the identity matrix, and λ is a positive constant parameter which can be adjusted to determine the suppression level of the noise (Wang et al. 2018).

The system IRF is extracted using Eq. (3-2) as shown in Figure 3.5 with the leak-induced spike marked in the ellipse. Compared with Figure 3.2, the spatial resolution is improved as the duration of the spike is much smaller than that of the wave reflection in Figure 3.2. However, some numerical artifacts in the form of spikes were found as shown in Figure 3.5. These are mainly induced by the non-linear relationship between τ and P_1 as expressed by

$$Q_{\tau} = \tau C_d A_{\tau} \sqrt{2gP_1} \quad (3-3)$$

where Q_{τ} is the flow rate from the generator, A_{τ} is the area of the valve when it is fully open and g is the acceleration of gravity. Due to the non-linear relationship between τ and the pressure at the valve, the actual wave-based shape of τ is not the same with that of the injected pressure wave. By using τ as the input of the deconvolution instead of the injected pressure wave (which is not able to be measured in the experiments), some spikes/pulses can be induced in the IRF trace to compensate for the difference between τ and the injected pressure wave.

The induced spiked pulses by the non-linear issue are of similar magnitude to the leak-induced reflection, and thus may mask the leak-induced reflections. Apart from the non-linear issue, another practical issue is that τ is difficult to be accurately measured and this may significantly reduce the accuracy and practicability of this method.

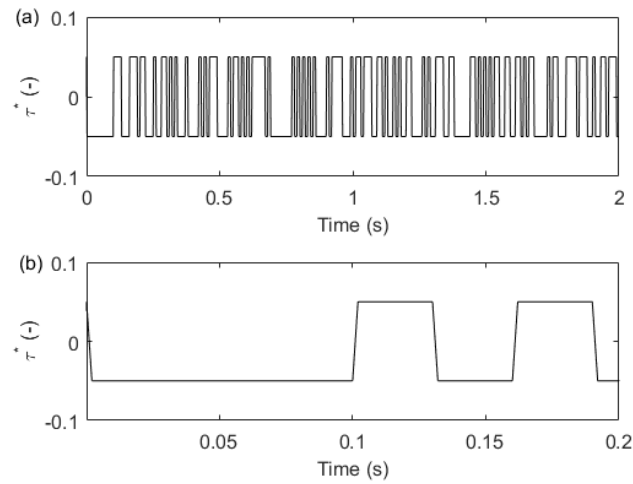


Figure 3.3 Normalized valve opening in the numerical case with a PRBS valve excitation; (a) 0.4 s period, and (b) enlarged figure.

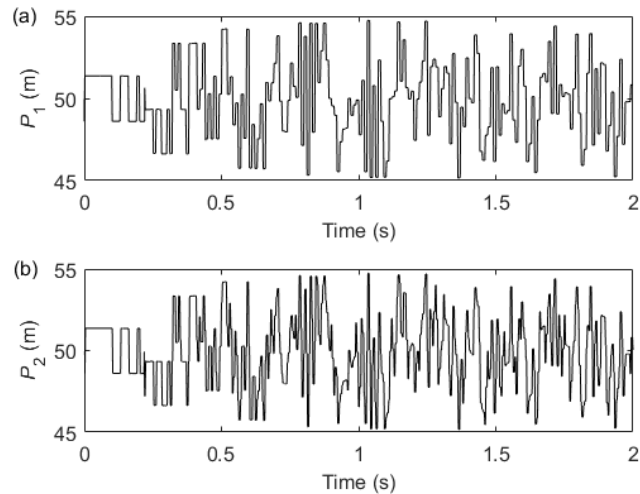


Figure 3.4 Simulated pressure waves with a PRBS valve excitation for Case 1 at (a) P_1 and (b) P_2 .

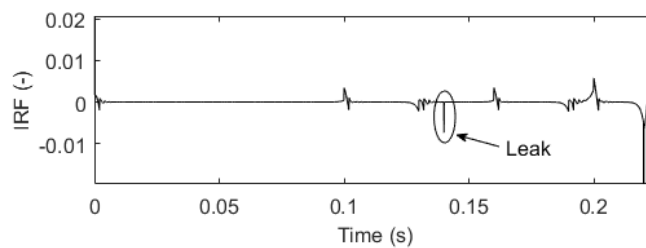


Figure 3.5 Least squares deconvolution (p_1 to τ) for Case 1 with a PRBS excitation.

3.3 Leak Detection using a Paired-IRF Method

To solve the practical issues presented in the former sections, a novel method, referred to as the *paired-IRF method*, is developed and proposed in this section. Within the following discussion, the configuration of Case 1 shown in Figure 3.1 including the pressure transducer P_2 is used. It is important to note that the proposed method only uses two sets of pressure traces without the valve opening variation.

3.3.1 Paired-IRF method applied to a reservoir-pipeline-valve system

As shown in Figure 3.1, the pipe section between the two transducers is assumed to be uniform and the transfer function for a uni-directional pressure wave propagating through this section is defined as $H(j\omega)$. The IRF on the right side of the generator (G) is defined as $R(j\omega)$, and the valve reflection ratio is $r_v(j\omega)$. $P_0(j\omega)$ is the injected pressure wave generated by the valve without any reflections from the valve and other components of the pipe system, and

$$P_v = P_0(1 + r_v) \quad (3-4)$$

is the pressure wave generated at the valve including the pressure wave reflection of P_0 by the valve.

In the following, the order of the pressure wave has been defined based on the number of times that the generated pressure wave is reflected by discontinuities within the pipeline, excluding the reservoir and valve boundaries. By neglecting higher-order (order > 1) wave reflections in the pipeline, the pressure $P_1(j\omega)$ can be written as

$$P_1 = P_v + (1 + r_v)P_vR \quad (3-5)$$

where $P_v(j\omega)$ is the incident pressure wave input to the pipeline propagating towards the reservoir (0th-order), P_vR is the 1st-order wave reflection of P_v by the pipeline, and $(1 + r_v)P_vR$ is the measured pressure response including the further reflection by the valve r_vP_vR (1st-order).

Considering the transfer function between the two pressure transducers, the pressure measurement of $P_2(j\omega)$ can be determined as

$$P_2 = H(P_v + r_vP_vR) + \frac{P_vR}{H} \quad (3-6)$$

where: $(P_v + r_v P_v R)$ is the 0th-order and 1st-order forward pressure waves propagating towards the reservoir at P_1 ; $H(P_v + r_v P_v R)$ is the pressure response after reaching P_2 ; and $P_v R/H$ is the 1st-order wave reflection at P_2 before the wave reaches P_1 . By dividing P_2 by P_1 , the following equation can be obtained

$$\frac{P_2}{P_1} = \underbrace{H}_{\text{order 0}} + \underbrace{\left(\frac{1}{H} - H\right)R}_{\text{order 1}} - \underbrace{\frac{(1/H-H)(1+r_v)R^2}{1+R+r_v R}}_{\text{order } \geq 2} \quad (3-7)$$

The detail of the derivation of (3-7) can be found in the Appendix. According to Eq. (3-7), three major terms can be found as follows: (1) 0th-order incident wave H , which represents the incident pulse δ_0 ($\delta_0 = 1$ at $t = 0$ and $\delta_0 = 0$ when $t > 0$) with a time delay by $\Delta t = L_p/a$ and a slight dissipation caused by transmission through the pipe section from P_1 to P_2 ; (2) the 1st-order wave reflections, and (3) higher ($> 1^{\text{st}}$)-order wave reflections which can be neglected within the time $t < 2L/a$, where L is the length of the pipe of interest ($L = 110$ m for Case 1).

Further explanation of the 1st-order term is given below as it consists of the leak-induced information. Within the time $t < 2L/a$, the IRF transferred from R represents spiked pulse(s) induced by leak(s) or any other defects which can generate wave reflections. The term $1/H$ in the brackets physically means transferring the spiked pulse(s) forward by Δt , while $-H$ in the brackets means reversing the sign of the spiked pulse(s) after delaying it (them) by Δt . Thus, one leak will induce a pair of spiked pulses with opposite directions and with a time interval of $2\Delta t$. The deconvolution P_2/P_1 after being transferred into the time domain consists of a superimposed pair of IRFs with opposite directions and a fixed time shift, and thus may be defined as the paired-IRF.

The round-trip travel time t_{leak} of the pressure wave from P_1 to the leak and back to P_1 can be obtained by averaging the times of the pair of leak-induced spiked pulses. Thus, the location of the leak can be determined by

$$L_{leak} = \frac{a \cdot t_{leak}}{2} \quad (3-8)$$

where L_{leak} is the distance from the leak to P_1 and a is the wave speed.

3.3.2 Paired-IRF method applied in pipe networks

A dead end is not always available in pipelines found in real WDSs. Therefore, a more general pipeline configuration is the case of a single pipe section connected to the broader network at its upstream and downstream points (i.e. arbitrary boundary conditions), as shown in Figure 3.6. The transfer function is defined as H_1 for the pipe section from the generator to the transducer G- P_1 and H_2 for the section P_1 - P_2 . The IRF of the pipe on the left side of the P_1 is defined as $R_L(j\omega)$. Analogously, $R_R(j\omega)$ is defined for the pipe at the right side of P_1 .

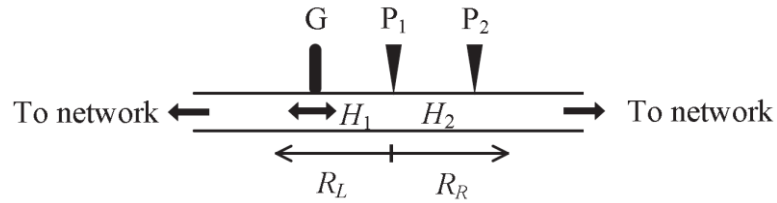


Figure 3.6 Schematic of a pipe section in a pipe network.

The relationship between the IRFs at the generation point and those at P_1 can be written as

$$R_R^G = H_1^2 \cdot R_R \quad (3-9)$$

$$R_L^G = R_L / H_1^2 \quad (3-10)$$

where the superscript G means the IRF for an input originating at the generator. By assigning the pressure wave injected through the generation point as P_0 and neglecting high-order wave reflections, pressures at G, P_1 and P_2 can be written as

$$P_G = P_0 + P_0 \cdot R_L^G + P_0 \cdot R_R^G \quad (3-11)$$

$$P_1 = P_0 H_1 + P_0 H_1 R_L^G + P_0 R_R^G / H_1 \quad (3-12)$$

$$P_2 = P_0 H_1 H_2 + P_0 H_1 H_2 R_L^G + P_0 R_R^G / H_1 / H_2 \quad (3-13)$$

Substituting Eqs. (3-9) and (3-10) into Eqs. (3-12) and (3-13) yields

$$P_1 = P_0 H_1 + P_0 R_L / H_1 + P_0 H_1 R_R \quad (3-14)$$

$$P_2 = P_0 H_1 H_2 + P_0 H_2 R_L / H_1 + P_0 H_1 R_R / H_2 \quad (3-15)$$

and a further division process between P_2 and P_1 gives

$$\frac{P_2}{P_1} = \underbrace{H_2}_{\text{order 0}} + \underbrace{\left(\frac{1}{H_2} - H_2\right) R_R}_{\text{order 1}} - \underbrace{\frac{(1/H_2 - H_2) R_R (R_L / H_1^2 + R_R)}{1 + R_L / H_1^2 + R_R}}_{\text{order } \geq 2} \quad (3-16)$$

The detail of the derivation of (3-16) can be found in the Appendix. Three major terms can be also found in Eq. (3-16) with the 0th-order and 1st-order terms identical to those in Eq. (3-7). By neglecting the higher-order terms in Eq. (3-16), the same paired-IRF equation can be obtained with Eq. (3-7). The paired-IRF can be then used to localize leaks (or any other defect) on the right side of the transducers in the pipe, while the wave reflections from the left side of pipe will not appear in the paired-IRF trace. The identification of the directional information of the wave reflections is a significant advantage. By exchanging the positions of the generator and the transducer P_2 , leaks (or any other defect) on the left side of pipe can be also detected. If the generation point is located at P_1 , which is a common case in the field, then $H_1 = 1$ and there will be no change of the 0th-order and 1st-order terms.

3.4 Numerical Case Studies

Numerical simulations have been conducted on a reservoir-pipeline-valve system and a pipe network to verify the proposed paired-IRF method for leak detection.

3.4.1 Case 1: Reservoir-pipeline-valve system

The reservoir-pipeline-valve system as shown in Figure 3.1 (Case 1) is utilized to validate the new method. The configuration of the system (Figure 3.1) and parameters of the pipe are detailed in the previous sections. The PRBS valve excitation as shown in Figure 3.3 has been applied. The simulated pressures P_1 and P_2 are shown in Figure 3.4. By applying the proposed paired-IRF method to the simulated pressures P_1 and P_2 , the IRF trace can be obtained as shown in Figure 3.7. Three major spikes can be observed in the obtained paired-IRF trace, excluding the reservoir reflections at $t \approx 0.22$ s. The first spiked pulse at $t = 0.002$ s represents the incident wave whose magnitude is close to unity (not fully displayed in the figure). The second and the third spiked pulses have the same magnitude with different signs and with a time interval of 0.004 s. This pair of spiked pulses are induced by the leak according to the theoretical analysis in the former sections (Eq. (3-7)). According to the configuration of the system, the travel time of the wave between the two transducers is $\Delta t = 0.002$ s. It is equal to the occurrence time of the incident pulse and is half of the time interval of the paired pulses induced by the leak, which validates the theoretical analysis of the paired-IRF method as anticipated by Eq. (3-7). By averaging the arrival times of the pair of leak-induced pulses ($t_1 = 0.138$ s, $t_2 = 0.142$ s), the round-trip travel time of the pressure wave t_{leak} can be obtained as 0.14 s. By using Eq. (3-8), the location of the leak can be calculated as 70 m away from the dead-end (or P_1), which is identical to the real value, and thus further validates the paired-IRF method.

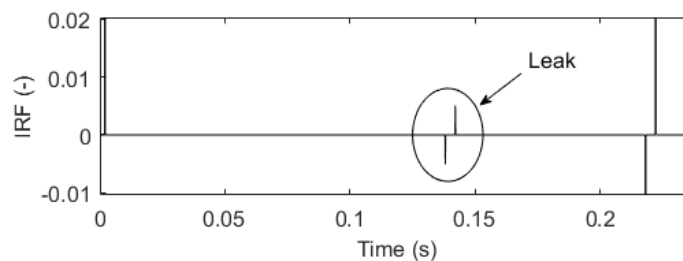


Figure 3.7 Paired-IRF extracted for Case 1 with a PRBS valve excitation.

3.4.2 Case 2: Pipe network

A pipe network connected to a reservoir as shown in Figure 3.8 is utilized in Case 2. All the pipelines in the system are uniform with the same internal diameter of 200 mm. The length of each pipe is given in Figure 3.8. The wave speed is assumed to be 1000 m/s and the Darcy-Weisbach factor f is assumed to be 0.02 for all the pipes (The Reynolds number $Re \approx 2.5 \times 10^4$ for most pipes). The transient generator (a side-discharge valve) with an initial flowrate = 2.2 L/s and the first pressure transducer P_1 are co-located in one of the pipes as shown in Figure 3.8. The second transducer is located 2 m away from the first transducer. Two leaks which are modelled using orifice emitters in the simulation are assumed to be located at the specific locations represented by the asterisks in Figure 4.14. The diameter of the leaks are 6 mm and 8 mm for the leaks L_1 and L_2 with corresponding flowrates of 0.8 L/s and 1.4 L/s, respectively,.

A PRBS signal consistent with the one shown in Figure 3.3 was emitted by the generator. The pressure waves propagate along the pipe in two directions with complex wave reflections from the pipe junctions. The simulated pressure traces at P_1 and P_2 are shown in Figure 3.9. By applying the paired-IRF method to the pressure traces, the paired-IRF can be obtained as Figure 3.10. The time interval of the pair of the spiked pulses at around 0.2 s is 4 ms which corresponds to the distance between the two transducers (2 m). The round-trip travel time t_{leak} is 0.2 s according to Figure 3.10, and thus the leak location is calculated to be 100 m away from P_1 which is identical to the leak location in the numerical model. Another set of paired pulses can be found at around 0.3 s, which corresponds to the junction J_1 as shown in Figure 3.8. The leak and all the junctions on the left side of the transducers do not affect the result of the paired-IRF trace.

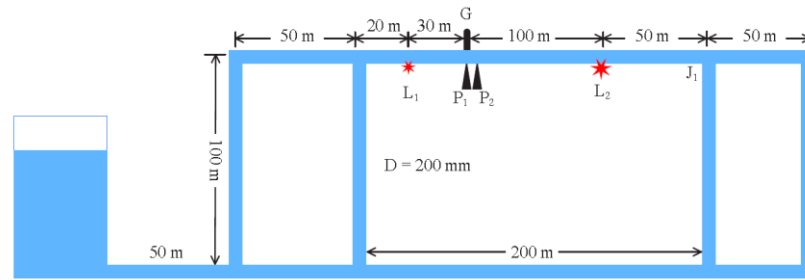


Figure 3.8 Schematic and configuration of the pipe network (Case 2).

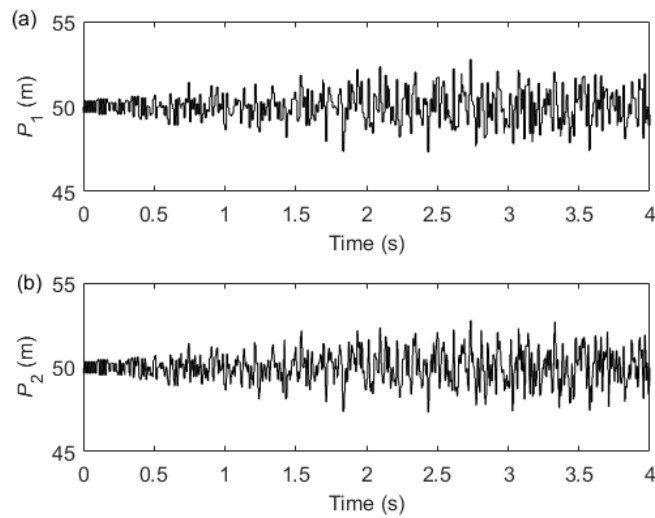


Figure 3.9 Simulated pressure waves with a PRBS valve excitation for Case 2 at (a) P₁ and (b) P₂.

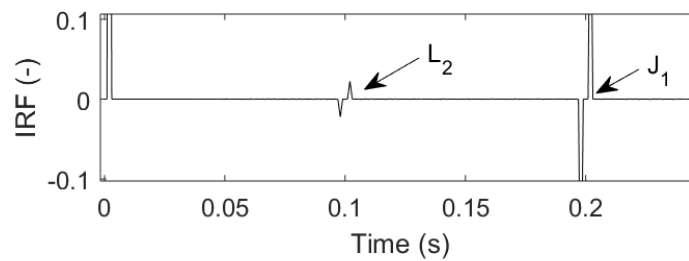


Figure 3.10 Paired-IRF extracted for Case 2 with a PRBS valve excitation.

3.5 Experimental Verification

Laboratory experiments have been conducted by the candidate on a single copper pipeline system with a leak in the Robin Hydraulics Laboratory at the University of Adelaide to validate the paired-IRF method. The pipe system has been set up in the laboratory by previous researchers and technicians and has been used continuously for more than three decades. Additional changes were made by the candidate for the purpose of this research.

3.5.1 Experimental setup

Figure 3.11 shows the layout of the experimental pipeline system. A reservoir-pipeline-valve system was made by connecting the pipeline with a pressurized tank at the upstream end and closing the in-line valve at the downstream end. The pipeline is 37.46 m in length with an internal diameter D_0 of 22.14 mm throughout the pipe. The wave speed of the pressure wave in the pipe was calculated using the theoretical formula as $a_0 = 1319$ m/s (Gong et al. 2018b). A discharge orifice connected with a T-junction was used to simulate the leak (L_1 in Figure 3.11). The flow rate out from the emulated leak is 0.0148 L/s and the diameter of the orifice is calibrated to be 0.93 mm, by assuming $C_d=0.9$. A voice-coil based transient generator (G) shown in Figure 3.11 was developed and the PRBS transient pressure signals were generated. The working principle of the voice-coil based transient generator is the same with the side-discharge valve-based transient generator presented in (Gong et al. 2016a), with the driving device being changed from two solenoids to a voice coil actuator (model: BEI_{KIMCO} LAS22-42-000A-P01). The voice coil is controlled by a control system with custom-designed signals imported. The maximum flow rate through the device, when fully open with a base pressure of 30.2 m, was measured as 0.029 L/s and the minimum flow rate was 0.009 L/s (as the generator cannot be fully sealed). The generator was connected to an interior point on the pipe as shown in Figure 3.11. The valve opening of the generator is measured by an integrated position sensor. Two pressure transducers were installed at the upstream side of G with a separation distance of 0.8 m. All the

joints of the pipeline and other installed transducers are shown in the schematic. Joint J_1 is a Swagelok pipe fitting and J_2 is composed of a brass block and a swage lock pipe fitting as shown in Figure 3.11. The sampling rate of the experiments was 10 kHz.

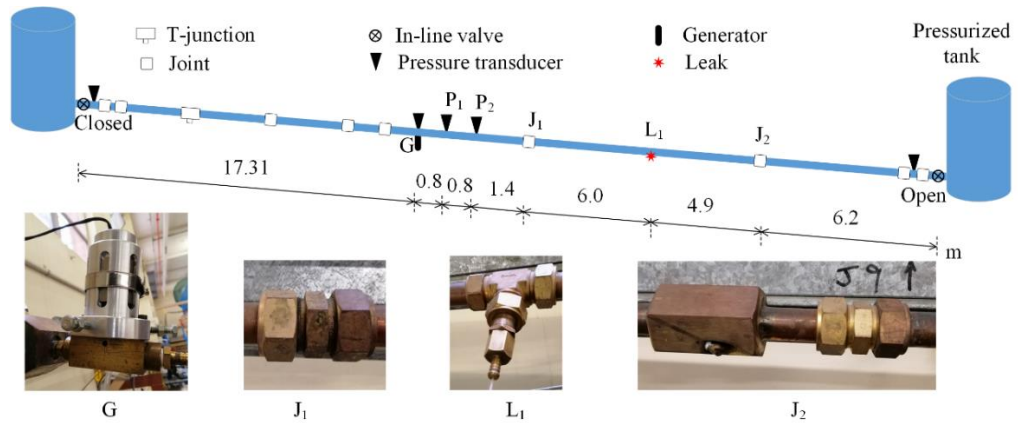


Figure 3.11 Schematic of the experimental pipeline system.

3.5.2 Experimental analysis

(a) Experimental case 1: Step valve excitation

The first test was conducted with the generator sharply closed as shown in Figure 3.12 (a). The measured pressure at P_1 is shown in Figure 3.12 (b). The pulse at $t = 0.032$ s is caused by the superposition of the wave reflection from the closed valve and that from the pressurized tank. From this data, it is clear that the leak-induced wave reflection is difficult to be observed since it is submerged in the pressure fluctuations caused by the wave reflections from other discontinuities in the pipe and hydraulic noise in the system.

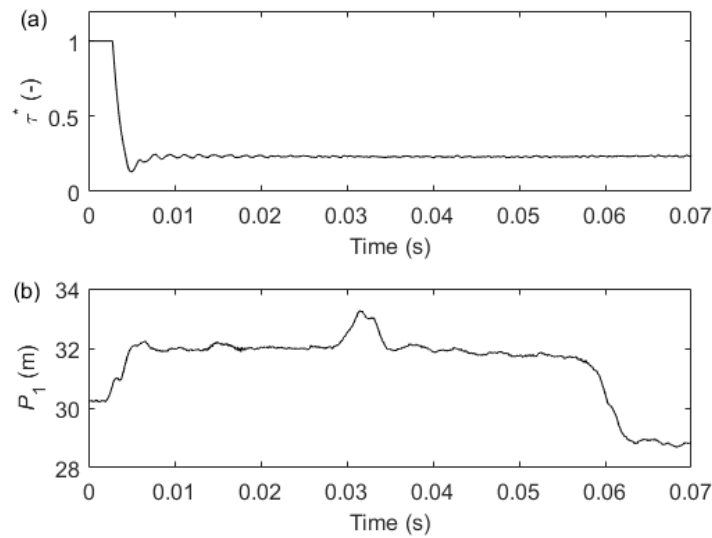


Figure 3.12 Measured data with a step valve excitation for the experimental case: (a) valve opening τ and (b) pressure at P_1 .

(b) Experimental case 2: PRBS valve excitation

The second test was conducted with the valve opening of the generator controlled by the ideal PRBS signal sent into the control system of the generator. As shown in Figure 3.13, the normalized valve opening perturbation followed the PRBS pattern, but with small tracking errors due to the maneuverability of the voice coil transient generator.

The measured pressure perturbations in a 2 s period are plotted in Figure 3.14 which shows little visible structure in the time domain. The paired-IRF was then extracted from the pressure traces and the result is shown in Figure 3.15. Three pairs of pulses (excluding the tank reflector-induced pulses) can be found on the paired-IRF in the figure. The occurrence times of these pulses, as well as the average times calculated, are listed in Table 3.1. According to the configuration of the pipeline system shown in Figure 3.11, these three pairs of pulses are attributed to be induced by the joint J_1 , the simulated leak L_1 and the joint J_2 . The corresponding distances of these pulses to P_1 were then calculated and compared with the measured values as shown in Table 3.1. High accuracy

of the detection was obtained according to the error analyses in the table, thus validating the proposed paired-IRF method.

The leak-induced pulses are not as distinctive as those in the numerical cases, but some oscillations around the two major spikes are observed. It is thought that these are caused by the way the leak was simulated which is composed of a T-junction and a discharge orifice. Pressure waves may also propagate in the T-junction and may cause other minor reflections. Some other minor fluctuations can be also observed on the paired-IRF trace, and they are mostly caused by continuous hydraulic noise induced by the leak itself, distributed anchors along the pipe (which may make the pipeline slightly uneven in effective wall thickness) and other uncertainties associated with the experiments.

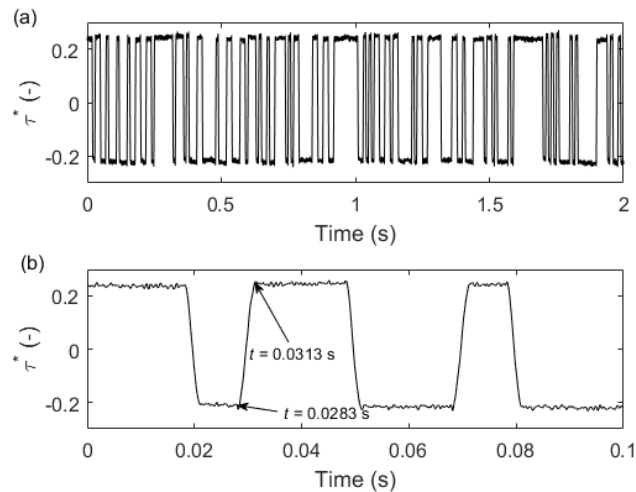


Figure 3.13 Normalized valve opening perturbation in the experiment in (a) a 2 s period; and (b) a 0.1 s period.

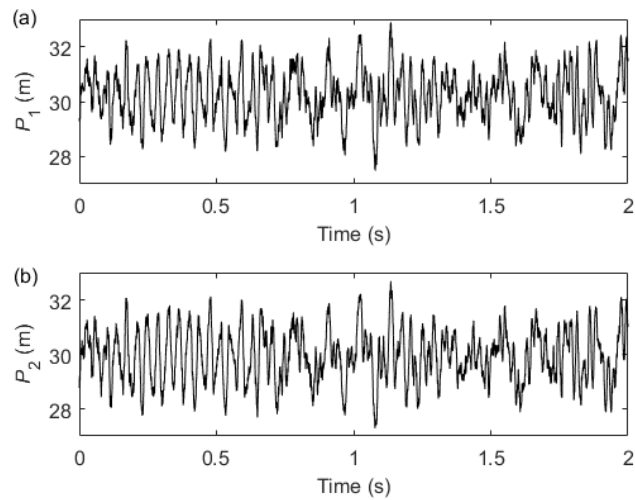


Figure 3.14 Measured pressure waves with a PRBS valve excitation for the experimental case at (a) P_1 and (b) P_2 .

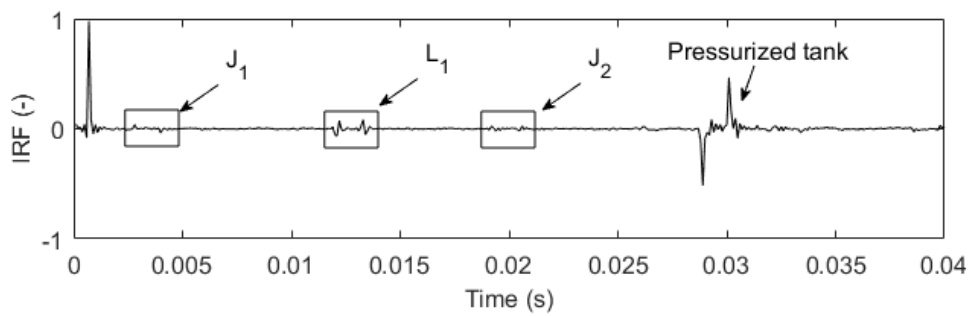


Figure 3.15 Paired-IRF extracted for the experimental case with a PRBS valve excitation.

Table 3.1 Accuracy analysis of the detection result.

Defect No.	t_1 (ms)	t_2 (ms)	t_{av} (ms)	L_c (m)	L_m (m)	Error = $(L_c - L_m) / L_m$ (%)
J ₁	2.8	4.0	3.4	2.24	2.20	1.8
L ₁	12.0	13.2	12.6	8.31	8.20	1.3
J ₂	19.2	20.4	19.8	13.06	13.10	0.3

* L_c is the calculated distance to P_1 (m), and L_m is the measured distance to P_1 (m).

(c) Experimental case 3: PRBS valve excitation with the pressure waves contaminated

To test the ability of this method to deal with realistic background pressure fluctuations and noise in real pipe networks, the paired-IRF is extracted using contaminated pressure waves in Case 3. Two pressure traces (relative to the initial pressures) measured by two pressure transducers with 1.83 m apart, on a field pipe in a city pipe network, are shown in Figure 3.16. Instead of using P_1 and P_2 in Figure 3.14, the contaminated pressures P_1+P_{b1} and P_2+P_{b2} are used to extract the paired-IRF. The result is shown in Figure 3.17, from which the leak-induced spikes, as well as the joint-induced spikes, can be clearly observed. A slight decrease in the magnitude of these spikes, including the first spike at $t = 0.6$ ms, can be found and it can be ascribed to the effect of the background pressure fluctuations and noise.

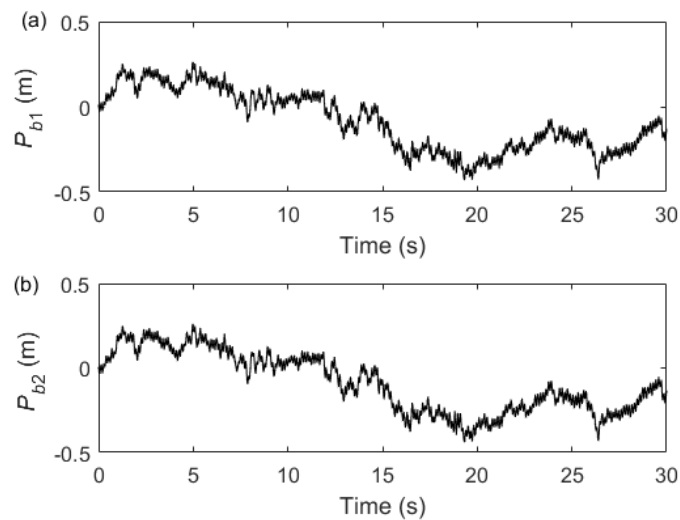


Figure 3.16 Measured background pressure fluctuations and noise in the field

pipe: (a) P_{b1} and (b) P_{b2} .

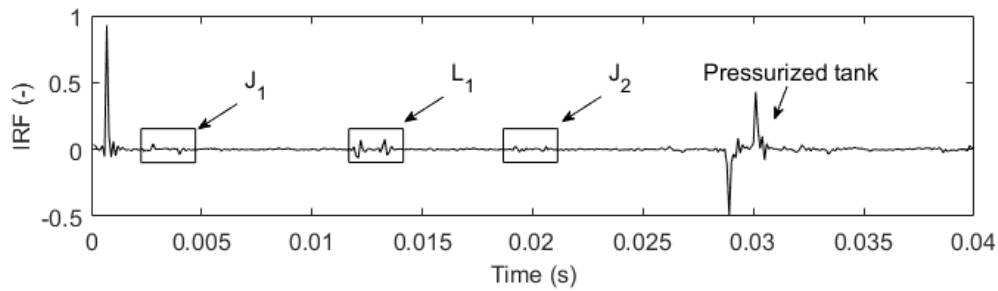


Figure 3.17 Paired-IRF extracted for the experimental case with a PRBS valve excitation with pressure waves contaminated by realistic background pressure fluctuations and noise.

(d) Experimental case 4: hydraulic noise by opening a valve

To test the method with the use of other types of signals, another experiment was conducted with the voice-coil based generator not in operation. The generator was fixed with a partial opening with the flow rate ≈ 0.027 L/s out from the generator. Hydraulic noise was generated by the turbulence of the flow around and through the valve. The induced micro-hydraulic waves (magnitude < 0.3 m of head) as shown in Figure 3.18 were used to excite the system so as to extract the paired-IRF, as shown in Figure 3.19. A critical result is that this IRF is almost identical with Figure 3.15, meaning that the condition assessment, as for the experimental case 2 can be effectively undertaken. This result illustrates that such micro-hydraulic waves were sufficient to excite the system into an active state such that the paired-IRF could be obtained under controlled laboratory conditions.

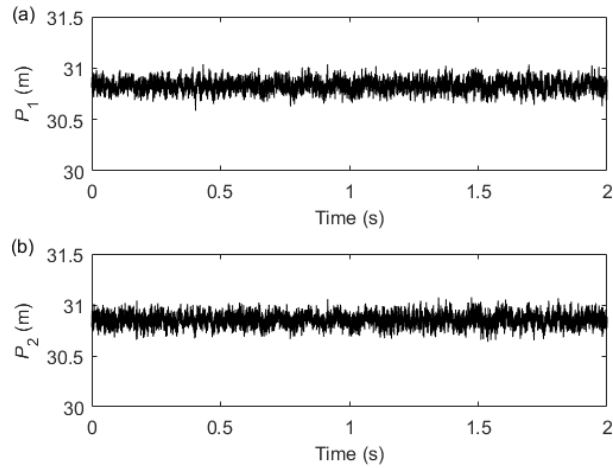


Figure 3.18 Measured pressure waves with the generator valve partially opened for the experimental case at (a) P_1 and (b) P_2 .

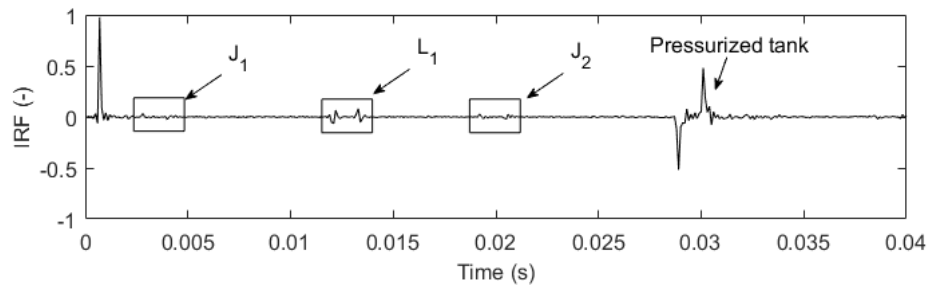


Figure 3.19 Paired-IRF extracted for the experimental case with the valve partially opened.

3.6 Conclusions

A novel paired-IRF method for leak detection in single pipelines and pipe networks has been proposed in this paper. Continuous signals such as the PRBS signal, which can reduce the impacts of hydraulic noise, background pressure fluctuations and other interferences that existed in the real WDSs, have been applied in the new method. Two pressure transducers are utilized to obtain two transient pressure traces, which are then used to extract the paired-IRF. This avoids the use of the valve perturbation profile which can introduce

linearization errors and is difficult to determine accurately in practice. A pair of spiked pulses with opposite directions and a fixed time interval is induced by a leak in the paired-IRF trace, and this feature can help to differentiate the leak-induced signals from system pressure fluctuations, hydraulic noise and other interference. The technique can be applied to pipes in complex networks and enables operators to focus on one side of the pipe at a time, which improves detectability.

Numerical simulations have been conducted on a single pipe and a pipe network and the results have provided a numerical validation of the proposed paired-IRF method. Laboratory experiments on a 1-inch copper pipe have further validated the new leak detection approach. Apart from the pair of leak-induced pulses, other joint-induced paired-pulses have also been observed. In the experiments, the leak was accurately localized as well as the joints in the pipe. Further experimental results using contaminated pressures waves demonstrate that the method is able to deal with realistic background pressure fluctuations and noise, which is a strong merit of this approach. Finally, the experimental results with the valve-induced hydraulic noise used as the injected pressure waves show that different types of signals can be used in this approach, including signals with a very small magnitude.

The paired-IRF method can be also used to detect other anomalies in pipes, such as a blockage or a deteriorated section. Future work is going to be conducted to extend the method to detect different types of anomalies with different features in the paired-IRF trace.

3.7 Appendix

3.7.1 Derivation of equation (3-7)

Equation (3-7) is derived from Eqs. (3-5) and (3-6) as follows:

Taking the ratio of (3-6) and (3-5) yields:

$$\frac{P_2}{P_1} = \frac{H(P_v + r_v P_v R + P_v R / H^2)}{P_v + P_v R + r_v P_v R} \quad (3-17)$$

Manipulating this to factor out H from the fraction yields

$$\frac{P_2}{P_1} = H + \frac{(1/H - H)R}{1 + R + r_v R} \quad (3-18)$$

which can then be expanded to yield

$$\frac{P_2}{P_1} = \underbrace{H}_{\text{order 0}} + \underbrace{\left(\frac{1}{H} - H\right)R}_{\text{order 1}} - \underbrace{\frac{(1/H - H)(1 + r_v)R^2}{1 + R + r_v R}}_{\text{order } \geq 2} \quad (3-19)$$

3.7.2 Derivation of equation (3-16)

Equation (3-16) is derived from Eqs. (3-14) and (3-15) as follows:

Taking the ratio of (3-15) and (3-14) yields:

$$\frac{P_2}{P_1} = \frac{P_0 H_1 H_2 + P_0 H_2 R_L / H_1 + P_0 H_1 R_R / H_2}{P_0 H_1 + P_0 R_L / H_1 + P_0 H_1 R_R} \quad (3-20)$$

Manipulating this to factor out H from the fraction yields

$$\frac{P_2}{P_1} = H_2 + \frac{(1/H_2 - H_2)R_R}{1 + R_L / H_1^2 + R_R} \quad (3-21)$$

which can then be expanded to yield

$$\frac{P_2}{P_1} = \underbrace{H_2}_{\text{order 0}} + \underbrace{\left(\frac{1}{H_2} - H_2\right)R_R}_{\text{order 1}} - \underbrace{\frac{(1/H_2 - H_2)R_R(R_L / H_1^2 + R_R)}{1 + R_L / H_1^2 + R_R}}_{\text{order } \geq 2} \quad (3-22)$$

Acknowledgements

The research presented in this paper has been supported by the Australian Research Council through the Discovery Project Grant DP170103715. The authors thank technicians Mr Brenton Howie and Mr Simon Golding from the School of Civil, Environmental and Mining Engineering for their support in the experimental work.

Chapter 4

Characterization and Detection of Multiple Types of Anomalies in Pipe Networks using a Paired Impulse Response Function Approach (Journal Publication 2)

Wei Zeng¹, Aaron C. Zecchin¹, Jinzhe Gong¹, Benjamin S. Cazzolato², Martin F. Lambert¹, Angus R. Simpson¹

¹School of Civil, Environmental and Mining Engineering, the University of Adelaide, Adelaide, SA 5005 Australia

²School of Mechanical Engineering, University of Adelaide, SA 5005, Australia

Citation: Zeng, W., Zecchin, A. C., Gong, J., Cazzolato, B. S., Lambert, M. F., Simpson, A. R. (2019). "Characterization and detection of multiple types of anomalies in pipe networks using a paired impulse response function approach." *Urban Water Journal* (Submitted).

Statement of Authorship

Title of Paper	Characterization and Detection of Multiple Types of Anomalies in Pipe Networks using a Generalized Paired-IRF Approach
Publication Status	<input type="checkbox"/> Published <input type="checkbox"/> Accepted for Publication <input checked="" type="checkbox"/> Submitted for Publication <input type="checkbox"/> Unpublished and Unsubmitted work written in manuscript style
Publication Details	Zeng, W., Zecchin, A., Gong, J., Cazzolato, B., Lambert, M., Simpson, A. Characterization and Detection of Multiple Types of Anomalies in Pipe Networks using a Generalized Paired-IRF Approach. Urban Water Journal (Submitted)

Principal Author

Name of Principal Author (Candidate)	Wei Zeng		
Contribution to the Paper	Conception and design of the project Analysis and interpretation of research data Draft the paper		
Overall percentage (%)	75 %		
Certification:	This paper reports on original research I conducted during the period of my Higher Degree by Research candidature and is not subject to any obligations or contractual agreements with a third party that would constrain its inclusion in this thesis. I am the primary author of this paper.		
Signature		Date	8/11/2019

Co-Author Contributions

By signing the Statement of Authorship, each author certifies that:

- i. the candidate's stated contribution to the publication is accurate (as detailed above);
- ii. permission is granted for the candidate to include the publication in the thesis; and
- iii. the sum of all co-author contributions is equal to 100% less the candidate's stated contribution.

Name of Co-Author	Aaron Zecchin		
Contribution to the Paper	Conception and design of the project Analysis and interpretation of research data Critically revising the paper		
Signature		Date	15/11/19

Name of Co-Author	Jinzhe Gong		
Contribution to the Paper	Conception and design of the project Analysis and interpretation of research data Critically revising the paper		
Signature		Date	24/11/19

Please cut and paste additional co-author panels here as required.

Name of Co-Author	Benjamin Cazzolato		
Contribution to the Paper	Conception and design of the project Analysis and interpretation of research data Critically revising the paper		
Signature		Date	8 th Nov. 2019

Name of Co-Author	Martin Lambert		
Contribution to the Paper	Conception and design of the project Analysis and interpretation of research data Critically revising the paper		
Signature		Date	22/11/19

Name of Co-Author	Angus Simpson		
Contribution to the Paper	Conception and design of the project Analysis and interpretation of research data Critically revising the paper		
Signature		Date	4 Nov 2019

Abstract

Anomaly detection in pipe networks is critical for targeted maintenance within water distribution systems. In this paper, a new generalized paired impulse response function (termed paired-IRF) technique is proposed for the detection of multiple types of anomalies (leaks, blockages and wall-deteriorated sections) simultaneously. Numerical studies on a single pipe were conducted to individually investigate the features of the response induced by different anomalies in the paired-IRF trace. With these features characterized from the case studies, the type, location and size of an anomaly can be determined using the paired-IRF trace. The new detection technique considers both principal and second-order wave reflections in pipe networks. The robustness of the method was tested on a pipe network by contaminating the simulated pressures with background pressure interference as measured in the field. The proposed technique is able to identify these anomalies and its accuracy can be further improved by an averaging process.

4.1 Introduction

Water distribution systems (WDSs) typically consist of buried pipe networks that are often deteriorating with age. Many pipe sections are blocked, deteriorated or even cracked over time, which leads to a reduction of the water transmission efficiency, an increase in pipe burst rates and a large amount of water lost through leakage. In addition, pipelines may be further hindered in their efficient operation from the in-line valves in the system that may sometimes be throttled or closed during maintenance work but are not re-opened thereafter (Stephens et al. 2004). Overall, detection and localization of these anomalies (leak, in-line valve, junction, blockage and deterioration) in pipe networks is critical for predictive repair, strategically targeted pipe maintenance, and optimal operation of WDSs.

A number of hydraulic transient-based detection methods have been developed to detect these anomalies in WDSs (Colombo et al. 2009; Xu and Karney 2017). Firstly, controlled hydraulic transient pressure waves can be injected into a pipeline. Theoretically, any physical discontinuity, such as a leak or a deteriorated section, can induce specific wave reflections which can be analyzed in the frequency domain or in the time domain. In terms of discrete anomalies (anomalies with such limited spatial extent that they can be considered as lumped elements) such as a leak, a partially closed in-line valve (equivalent to a discrete blockage in the numerical model) or a junction, the following analysis methods have been used for detection purposes: the frequency response diagrams (FRD) analysis (Lee et al. 2006; Sattar and Chaudhry 2008; Gong et al. 2013); the cepstrum analysis (Taghvaei et al. 2006; Shucksmith et al. 2012); the transient damping method (Wang et al. 2002; Wang et al. 2005); the inverse transient analysis (Liggett and Chen 1994; Vítkovský et al. 2000; Covas et al. 2001; Capponi et al. 2017); the time-domain reflectometry (TDR) methods (Brunone 1999; Ferrante and Brunone 2004; Gong et al. 2018b); and the impulse response function (IRF) analysis (Liou 1998; Vítkovský et al. 2003; Lee et al. 2007; Nguyen et al. 2018). These methods can be also used to detect extended anomalies with uniform properties

(Duan et al. 2012; Gong et al. 2012; Gong et al. 2018a), such as a section with a diameter change (this can be caused by an extended blockage with a uniform diameter) and a section with a material change (this can be caused by an extended wall deterioration with a uniform wave speed). In terms of extended anomalies with non-uniform properties, such as the blockage and wall deterioration in the field, the reconstructive method of characteristics (Gong et al. 2014; Zhang et al. 2019), inverse transient analysis (Stephens et al. 2013; Zhang et al. 2018a; Zhang et al. 2018b), the approximate inverse scattering technique (Jing et al. 2018) and the layer-peeling method (Zeng et al. 2018; Zeng et al. 2019a) can be applied to locate and estimate the size of the anomaly. In addition, the paired-IRF method (Zeng et al. 2019b) that was developed for leak detection has the potential to identify and locate all of these anomalies. These above-mentioned methods were selectively reviewed below with the paired-IRF method being highlighted.

In the TDR method, a leak existing in the pipe can be localized using the time series and the wave speed (Brunone 1999). The size of the leakage can be determined by the wave reflection magnitude (Vítkovský et al. 2003). The spatial resolution of the detection can be improved by extracting the impulse response function (IRF) of a pipeline (Lee et al. 2007), which corresponds to the pressure response of the pipeline when an impulse pressure signal is injected into the pipe. To further improve the robustness of the method, persistent signals, such as the pseudo-random binary sequence (PRBS) were adopted by Liou (1998) to extract the system IRF for leak detection on a numerical pipe. Experimental studies were conducted by Nguyen et al. (2018), and the system IRF was extracted using a least squares method. However, due to factors such as pipe parameter uncertainties, background hydraulic noise and numerical uncertainties, the experimental IRF trace typically involves numerical artifacts (i.e. discrete spikes appearing as “noise” on the IRF), such as the IRF trace extracted in Nguyen et al. (2018). Thus, it is challenging to distinguish these artifacts from the real anomaly-induced spikes which are typically of small magnitudes in the IRF trace.

To overcome the problem mentioned in the IRF method, a paired-IRF method has been proposed by Zeng et al. (2019b) for leak detection and validated with experimental results. The pressures measured by a pair of pressure transducers were used to extract the paired-IRF trace. In this case, the dynamic opening of the generator was not used as the input in the proposed method, and thus the measurement error is significantly reduced. A pair of spikes with a specific pattern is induced by a leak and has been used to differentiate the leak signal amongst the noise in the paired-IRF trace. The paired-IRF has only been used for leak detection, and the anomaly-induced features are still unknown for the other types of anomalies, such as a discrete blockage, or an extended wall deterioration. In addition, only the principal (first-order) wave reflections in the paired-IRF trace have been studied with some visible second-order reflections neglected. Without a clear explanation of these second-order reflections, they may be incorrectly treated as the spikes induced by extra anomalies, leading to inaccurate detection.

In this paper, a new-generation paired-IRF technique has been proposed by incorporating higher-order wave reflections in order to explain these reflections in the paired-IRF and thus avoid misdiagnosis. The technique has been generalized by characterizing different anomalies based on their own features of the spikes induced in the paired-IRF traces. These features can be used to distinguish the anomaly amongst other types and numerical errors. The noise level in the paired-IRF trace is significantly reduced by averaging multiple paired-IRF traces from different tests.

In the following sections, the new paired-IRF equation is given at first with all the higher-order reflections incorporated. Eight types of anomalies were investigated on a single pipe system with the focus on the first-order reflections. The anomaly-induced features in the paired-IRF trace were extracted and characterized. These features were then validated on a numerical pipe network with multiple anomalies. The second-order wave reflections observed in the paired-IRF trace in the pipe network case were explained using the new paired-IRF equation. The robustness of the method was tested with pressures contaminated by background pressure fluctuations measured from a real pipe

network. The noise in the paired-IRF trace was significantly reduced by an averaging process.

4.2 Methodology: The Proposed Paired-IRF

Method

The system configuration of the paired-IRF method is given in Figure 4.1 to illustrate the basic methodology. The corresponding block diagram is shown in Figure 4.2 which illustrates the wave propagation process in the pipe. A transient generator (G) in the form of a side-discharge valve is installed on the pipe, and a pair of pressure transducers P_1 and P_2 are installed at the right side (without loss of generality). The pipe section of interest is to the right of P_1 (P_1 -B). The generator emits pressure waves into the pipeline induced by varying the valve opening (τ), persistently. The boundaries of the pipe are assumed to be arbitrary, such as junctions in a pipe network, or a valve and a reservoir in a single pipe system. The terms H_1 and H_2 are defined as the transfer functions of the section G- P_1 and the section P_1 - P_2 , respectively. The term R represents the impulse response function in the frequency domain with the subscripts L and R referring to the pipe at the left side and right side of P_1 .

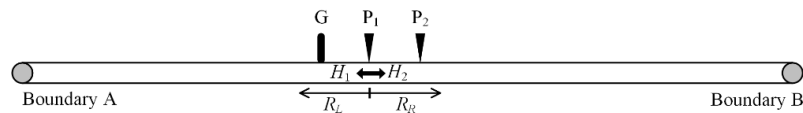


Figure 4.1 System configuration of the Paired-IRF method.

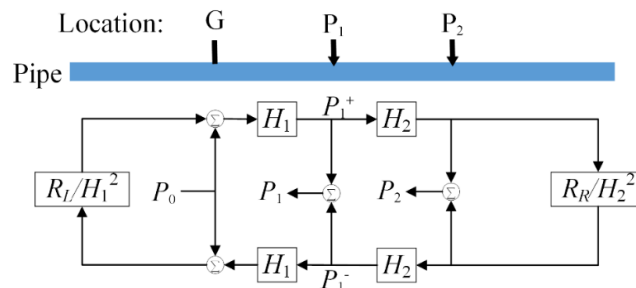


Figure 4.2 Block diagram describing the wave propagation process.

The paired-IRF method was first developed in (Zeng et al. 2019b) with only first-order wave reflections considered. In this paper, a new-generation paired-IRF method is proposed to include all the higher-order wave reflections.

According to the block diagram in Figure 4.2, the pressures P_1 and P_2 can be written as

$$P_1 = P_1^+ + P_1^- \quad (4-1)$$

$$P_2 = P_1^+ H_2 + \frac{P_1^-}{H_2} \quad (4-2)$$

in which the superscripts + and – indicate the positive direction (from P_1 to P_2) and negative direction (from P_2 to P_1), respectively. By assuming $P_0(j\omega)$ is the original pressure wave generated by the generator without any reflections and according to Figure 4.2, the directional pressure waves P_1^+ and P_1^- considering all higher-order wave reflections can be written as

$$P_1^+ = \left(1 + \frac{R_L}{H_1^2}\right) H_1 P_0 + R_L P_1^- \quad (4-3)$$

$$P_1^- = R_R P_1^+ \quad (4-4)$$

A rearrangement of Eqs. (4-3) and (4-4) gives the explicit expressions of P_1^+ and P_1^- as

$$P_1^+ = \frac{(H_1 + R_L/H_1)}{(1 - R_L R_R)} P_0 \quad (4-5)$$

$$P_1^- = \frac{R_R (H_1 + R_L/H_1)}{(1 - R_L R_R)} P_0 \quad (4-6)$$

Substituting Eqs. (4-5) and (4-6) into Eqs. (4-1) and (4-2) yields

$$P_1 = \frac{(1 + R_R)(H_1 + R_L/H_1)}{(1 - R_L R_R)} P_0 \quad (4-7)$$

$$P_2 = \frac{(H_2+R_R/H_2)(H_1+R_L/H_1)}{(1-R_LR_R)} P_0 \quad (4-8)$$

where a further division between P_2 and P_1 gives

$$\frac{P_2}{P_1} = \frac{(H_2+R_R/H_2)}{(1+R_R)} \quad (4-9)$$

To further explore the physical meaning of the equation, it is expanded using a Taylor series expansion as

$$\frac{P_2}{P_1} = H_2 + \underbrace{\left(\frac{1}{H_2} - H_2\right) R_R}_{\text{order} = 1} - \underbrace{\left(\frac{1}{H_2} - H_2\right) R_R^2}_{\text{order} = 2} + \dots + \underbrace{(-1)^{n-1} \left(\frac{1}{H_2} - H_2\right) R_R^n}_{\text{order} = n} \quad (4-10)$$

in which the first-order and all the higher (≥ 2)-order wave reflections are clearly presented. By neglecting the higher-order wave reflections, Eq. (4-10) can be simplified to

$$\frac{P_2}{P_1} = H_2 + \underbrace{\left(\frac{1}{H_2} - H_2\right) R_R}_{\text{order} = 1} \quad (4-11)$$

which is identical to the result in (Zeng et al. 2019b). By defining the one-way travel time of the transient wave in the section P₁-P₂ as Δt , the term $1/H_2$ in the brackets for a lossless system means transferring the IRF forward by Δt , while $-H_2$ in the brackets means reversing the sign of the IRF after delaying it by Δt . Thus, P_2/P_1 after transforming to the time domain consists of a pair of superimposed IRFs and hereon defined as the paired-IRF.

The first-order approximation would be accurate enough if the detection range is in a single pipe, such as the section G-B in Figure 4.1. If the detection range extends beyond the boundary of the single pipe, such as to other pipes connected with the boundary B in Figure 4.1, the second-order terms of visible magnitudes need to be considered. Thus Eq. (4-10) can be simplified to

$$\frac{P_2}{P_1} = H_2 + \underbrace{\left(\frac{1}{H_2} - H_2\right) R_R}_{\text{order} = 1} - \underbrace{\left(\frac{1}{H_2} - H_2\right) R_R^2}_{\text{order} = 2} \quad (4-12)$$

incorporating the second-order term.

Noting that Eqs. (4-11) and (4-12) give the frequency-domain transfer function of the paired-IRF, the time-domain paired-IRF P_2/P_1 from Eqs. (4-11) and (4-12) can be calculated using a least squares deconvolution (Nguyen et al. 2018) or a truncated singular value decomposition (Forbes et al. 2003).

4.3 Paired-IRFs for Different Anomalies

In this section, numerical analyses have been conducted on a reservoir-pipeline-valve system (referred to as Case 1), as shown in Figure 4.3. Since the pipe of interest is a single pipe, second-order wave reflections can be neglected. The paired-IRF technique with Eq. (4-11) was then applied to this system with different anomalies existing in the pipe. By analyzing the features of the spikes induced by different anomalies in the paired-IRF trace, these anomalies were characterized, which makes the paired-IRF technique generalized to a broader array of anomalies. Validation is conducted on a numerical pipe network with multiple anomalies in the next section.

4.3.1 System configuration and anomalies

The configuration in Figure 4.3 can be considered as a special case of the general configuration in Figure 4.1 by assuming the boundary condition at the left side of the pipe is a reservoir and that the right side is a valve. The water height in the reservoir is assumed to be 60 m from the bottom and the valve is partially closed to result in a base flow rate of $0.02 \text{ m}^3/\text{s}$ in the pipe. The first transducer P_1 is located 80 m away from the reservoir and the second one P_2 is at the right side of P_1 with the distance L_p equal to 1 m. The internal diameter of the pipeline is assumed to be 120 mm throughout, the wave speed a is 1000 m/s and the Darcy-Weisbach factor f is 0.02. The method of characteristics (Wylie and Streeter 1993) with a time step of 0.0001 s for all the numerical cases has been applied to simulate the transient pressures.

An anomaly from those shown in Figure 4.4 is assumed to exist at a distance of 50 m (measured from the left side of the anomaly if the anomaly is not discrete) downstream to P_1 . These anomalies are classified into three groups based on their characteristics. The anomalies in the first group are discrete and include leaks (Figure 4.4 (a)), junctions (Figure 4.4 (b)) and partially closed in-line valves or discrete blockages (Figure 4.4 (c)). Those in the second group are extended anomalies with uniformly distributed properties, such as a section with an increased impedance (e.g. an extended blockage with a uniform diameter or a replacement of pipe section with a smaller diameter) (Figure 4.4 (d)) and a section with a decreased impedance (e.g. a deteriorated section with uniform pipe wall thinning or a replacement of pipe section with a lower wave speed) (Figure 4.4 (e)). The third group includes extended blockages with non-uniformly distributed diameters (Figure 4.4 (f)) and pipe wall deteriorated sections with non-uniformly distributed wave speeds (Figure 4.4 (g)).

It should be noted that any type of persistent signal can be used as the injected transient wave so long as it has a wide spectrum with sufficient power. The generator was set to produce valve changes randomly (following a white noise sequence) in the cases considered in this paper. A 0.2 s period of the normalized valve opening of the generator τ^* (defined as $\tau^* = (\tau - \tau_0)/\tau_0$ with τ_0 being the initial τ) is given in Figure 4.5.

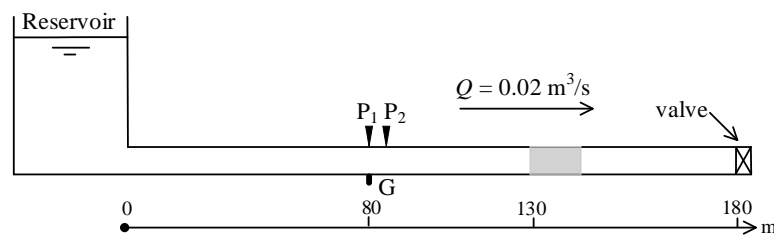


Figure 4.3 Pipeline configuration for Case 1.

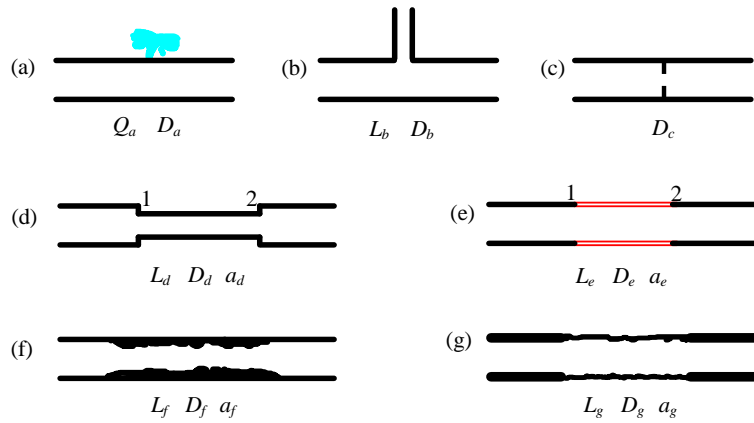


Figure 4.4 Anomaly types in Case 1: (a) leak; (b) junction; (c) partially closed in-line valve or discrete blockage; (d) section with an increased impedance; (e) section with a decreased impedance; (f) extended blockage with non-uniformly distributed diameters; and (g) wall deteriorated section with non-uniformly distributed wave speeds.

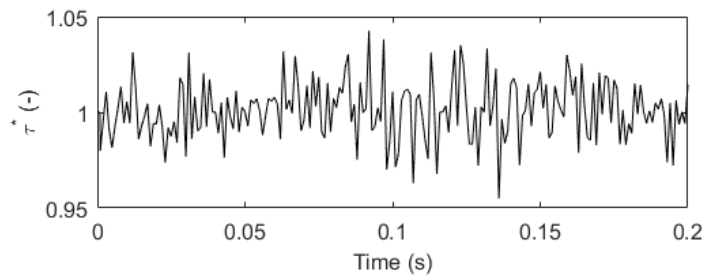


Figure 4.5 Normalized valve opening in the numerical case with a random valve excitation.

4.3.2 Discrete anomalies (leak, junction and closed in-line valve)

The anomaly in Figure 4.3 is considered to be a discrete anomaly in this subsection. The characteristics of the anomalies are given in Table 4.1. The simulated pressures at P_1 and P_2 with the leak in Table 4.1 existing in the pipe are shown in Figure 4.6. The paired-IRF P_2/P_1 can be obtained as Figure 4.7 (a).

It can be shown from the paired-IRF trace that the leak induces a pair of spikes with opposite directions (negative for the first spike) and with an occurrence time interval of $2t_p$, where $t_p = L_p/a$. If a discrete impulse signal was injected into the pipe, the leak will induce a negative spike (Lee et al. 2007). These paired spikes are a superposition of the leak-induced spike after time-shifting forward by t_p added to the same spike after reversing its sign and delaying by t_p .

Table 4.1 Characteristics of the discrete anomalies and uniform anomalies.

Anomaly type	Characteristics
Leak	The flowrate, equivalent diameter and discharge coefficient: $Q_a = 0.84$ L/s, $D_a = 6$ mm and $C_d = 0.9$
Junction	The diameter, wave speed and length of the branch pipe: $D_b = 50$ mm, $a_b = 1000$ m/s and $L_b = 60$ m
Partially closed in-line valve	The area and equivalent diameter of the in-line valve: $A_c = 0.0028$ m ² and $D_c = 60$ mm.
Section with a diameter change	The length, diameter and wave speed of this section: $L_d = 5$ m, $D_d = 100$ mm and $a_d = 1000$ m/s.
Section with a material change	The length, diameter and wave speed of this section: $L_e = 4.5$ m, $D_e = 120$ mm and $a_e = 900$ m/s.

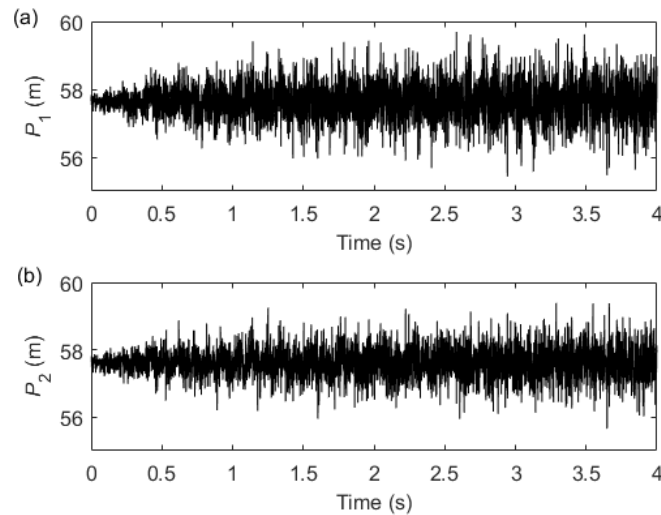


Figure 4.6 Simulated pressure waves for Case 1 with a leak.

The round-trip travel time t_a (travel from P_1 to the leak and back to P_1) of the paired spikes can be used for localization, and it can be obtained by averaging the times of the pair of spikes in the paired-IRF trace. The distance L_a between the leak and P_1 can be obtained by

$$L_a = \frac{a \cdot t_a}{2} \quad (4-13)$$

From Figure 4.7 (a), it can be observed that the round-trip travel time is $t_a = 0.1$ s, and thus the distance is then calculated as 50 m, which is consistent with the distance in the model (Figure 4.3). The spikes at 0.2 s are induced by the upstream reservoir.

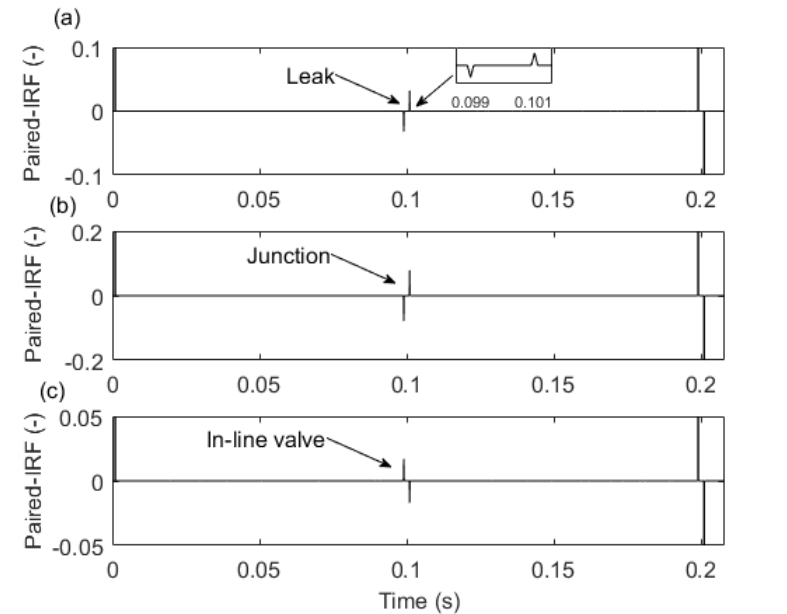


Figure 4.7 Paired-IRF for Case 1 with a discrete anomaly; (a) leak, (b) junction and (c) partially closed in-line valve.

If the junction in Table 4.1 exists in the pipe, the paired-IRF trace extracted with the same approach can be obtained as Figure 4.7 (b). It should be noted that the branch pipe is long enough to avoid any superposition of the wave reflections from the end boundary of the branch pipe with the wave reflections from the main pipe. From the paired-IRF trace generated, it is shown that the junction also induces a pair of spikes with a similar pattern to those induced by a leak. But the magnitude of the spikes induced by the junction is much higher than the leak-induced spikes due to the large wave reflection at the junction.

If the partially closed in-line valve in Table 4.1 exists in the pipe, the paired-IRF trace extracted can be obtained as Figure 4.7 (c). It should be noted that the partially closed in-line valve presented in the model can be also used to model

a discrete blockage. It shows from the paired-IRF trace that the partially closed in-line valve (or an equivalent discrete blockage) also induces a pair of spikes with similar features to the leak. But the first spike of the paired spikes is positive since a positive wave reflection will be reflected by a partially closed in-line valve (or a discrete blockage).

4.3.3 Extended anomalies with uniform properties (section with an impedance change)

Extended anomalies with uniformly distributed properties are discussed in this section.

(a) Paired-IRFs

The transient waves will be reflected at the cross-section with an impedance change (e.g. caused by a change in diameter, wall thickness or wave speed). The impedance of a pipe section is defined as $B = a/gA$ with g representing the acceleration due to gravity and A representing the internal cross section area of the pipe section. The wave reflection ratio for an incident pressure wave propagating from pipe section 1 to section 2 can be then calculated as

$$r = \frac{p_r}{p} = \frac{B_2 - B_1}{B_2 + B_1} \quad (4-14)$$

where p_r is the reflected wave, p is the incident wave and the subscripts 1 and 2 refer to pipe section 1 and pipe section 2, respectively.

The anomaly in Figure 4.3 is assumed to be a section with an increased impedance (caused by the decrease of diameter) as shown in Figure 4.4(d) with details given in Table 4.1. The paired-IRF trace was obtained as shown in Figure 4.8 (a). Two pairs of spikes can be found in the paired-IRF trace. The time interval between the spikes in each pair is $2L_p/a$, and that between these two pairs (from the first spike in the first pair to the first spike in the second pair) is $2L_D/a$. According to Eq. (4-14), for a positive incident wave, a positive reflected wave will be generated by the sudden contraction interface (Interface

1 in Figure 4.4 (d)), and thus the first spike in the first pair is positive. The first spike in the second pair is negative since a negative wave is reflected by the sudden expansion interface (Interface 2 in Figure 4.4 (d)) according to Eq. (4-14).

Similar analyses were conducted on a section with a decreased impedance (caused by the change in wall material) as shown in Figure 4.4 (e) with details given in Table 4.1. As shown from the obtained paired-IRF trace in Figure 4.8 (b), two pairs of spikes can be also found with the signs of these spikes opposite with those induced by the section with an increased impedance. This is because a negative wave will be reflected at Interface 1 in Figure 4.4 (e), and a positive wave will be reflected at Interface 2 in Figure 4.4 (e) according to Eq. (4-14).

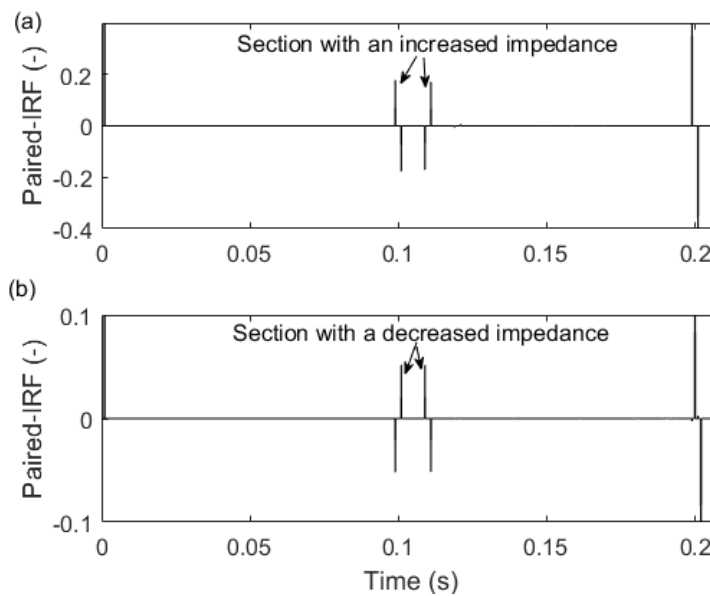


Figure 4.8 Paired-IRF for Case 1 with; (a) a section with an increased impedance and (b) a section with a decreased impedance.

(b) Sensitivity Analysis on anomaly extent

A sensitivity analysis has been conducted on the length of the extended anomaly with uniform properties to study the effects of the anomaly length. The section with a decreased diameter (an increased impedance) was taken as an example here, and similar conclusions can be obtained for sections with other changes.

When the length of the section with a diameter change L_d is set to 0.2 m, 0.5 m, 1.0 m, 1.5 m 2.0 m and 5.0 m, the paired spikes as obtained are shown in Figure 4.9 (a) to (f), respectively. The orders of these two pairs are labelled in the figures with (1) and (2) representing the first and second pair, respectively. If $2L_d/a_d < L_P/a$ (L_P is the sensor spacing), as the case shown in Figure 4.9 (a), the two pairs of spikes are superimposed. With $2L_d/a_d = L_P/a$, as the case shown in Figure 4.9 (b), the time interval for any two adjacent spikes are both L_P/a . If $L_d/a_d = L_P/a$, as the case shown in Figure 4.9 (c), the negative spikes in the first and second pairs are overlapped and thus only three spikes can be observed. By further increasing L_d to $L_d/a_d > L_P/a$, as the case shown in Figure 4.9 (d), the superposed pairs can be separated. Once $L_d/a_d = 2L_P/a$, as the case shown in Figure 4.9 (e), the time interval for any two adjacent spikes becomes the same with a larger time interval of $2L_P/a$. If $L_d/a_d > 2L_P/a$, as the case shown in Figure 4.9 (f), these two pairs become distinctly separated.

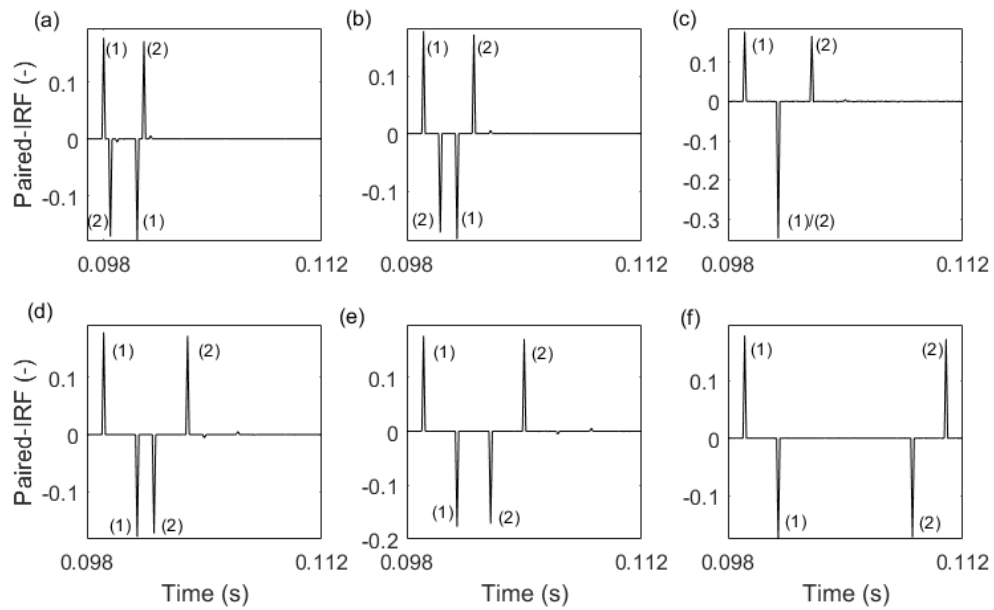


Figure 4.9 Effects of the length of the section with a diameter change on the paired spikes: (a) $2L_d/a_d < L_P/a$; (b) $2L_d/a_d = L_P/a$; (c) $L_d/a_d = L_P/a$; (d) $L_d/a_d > L_P/a$; (e) $L_d/a_d = 2L_P/a$; (f) $L_d/a_d > 2L_P/a$.

According to the patterns of the paired spikes for the section with a diameter change with different lengths, it can be concluded that the round-trip travel time of the wave in the section T_d (from one end of the section to the other end and

back to the first end) is equal to the time interval between the first and second spikes if the duration of the spiked region (defined as the region from the first spike to the last spike induced by the same anomaly in the paired-IRF trace) $T_s \leq 4L_p/a$. If $T_s > 4L_p/a$, then T_d is equal to the time interval between the first and the third spikes. The length of the section with a diameter change can be then estimated as $L_d = aT_d/2$.

4.3.4 Extended anomalies examples with non-uniformly distributed properties

In the real world, extended blockages and wall deteriorated sections in the pipe are normally spatially non-uniform, and these anomalies with non-uniformly distributed properties are investigated in this section. A blockage with non-uniformly distributed diameters as shown in Figure 4.10 was studied. The length of the blockage L_f is 0.6 m and the wave speed a_f is assumed to be 1000 m/s throughout the blocked section. The induced spikes in the paired-IRF trace are shown in Figure 4.11. Since L_f/a_f is smaller than L_p/a , two groups of spikes can be visually separated with opposite signs and a fixed time interval of $2L_p/a$. Due to the decrease of the diameter at the beginning of the blockage as shown in Figure 4.10, the spikes at the beginning of the first group of spikes are mainly positive according to Eq. (4-14). According to Eq. (4-10), the second group of spikes were obtained by flipping the anomaly-induced spikes upside down after delaying them. Thus, positive spikes can be also found at the end of the second group of spikes due to the increase of the diameter at the end of the blockage. Overall, mainly positive spikes can be found at both edges of the spiked region.

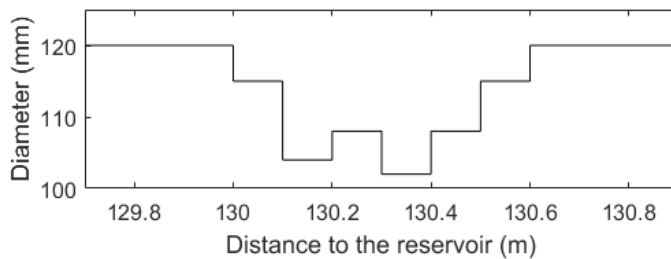


Figure 4.10 Blockage profile for Case 1 with a blocked section.

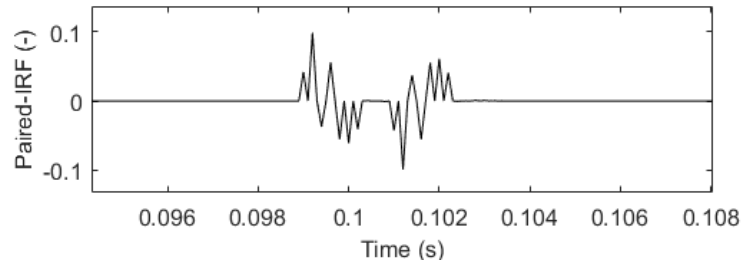


Figure 4.11 Paired-IRF for Case 1 with a blocked section.

A wall deteriorated section with non-uniformly distributed wave speeds $a_{g,i}$ shown in Figure 4.12 (a) was also studied. The deteriorated section contains N segments and the subscript i presents the number of the segment. The length of the deteriorated section is assumed to be 0.496 m and the diameter is assumed to be 120 mm. Two groups of spikes can be also found in the paired-IRF trace as shown in Figure 4.13 (a). In contrast to the spikes induced by the blockage (Figure 4.11), negative spikes can be found at both sides of the spiked region.

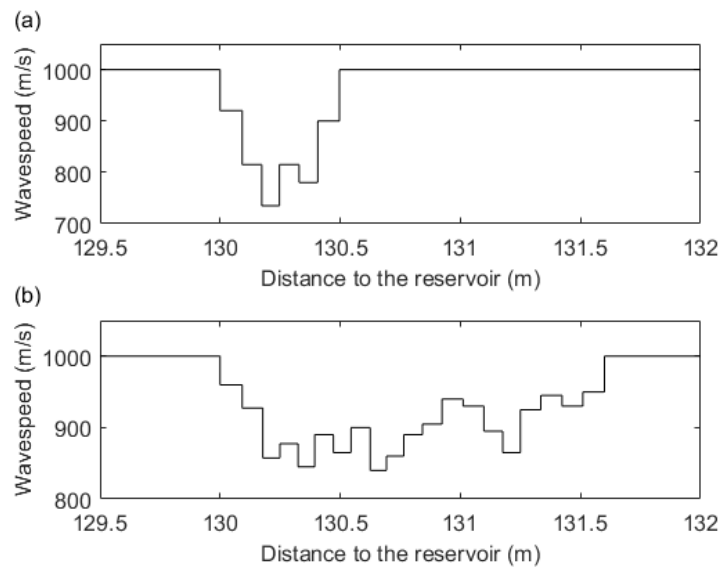


Figure 4.12 Wave speed profile for Case 1 with a deteriorated section; (a) $L_g = 0.496$ m and (b) $L_g = 1.800$ m.

Another longer deteriorated section with the same diameter and the wave speed distribution shown in Figure 4.12 (b) was also studied. The length of the deteriorated section is 1.800 m. Since $\sum_{i=1}^N L_{g,i}/a_{g,i} > L_P/a$, the two groups of

spikes are superposed and cannot be visually separated, as shown in Figure 4.13 (b). But the spikes at both edges of the spiked region are still found to be mainly negative.

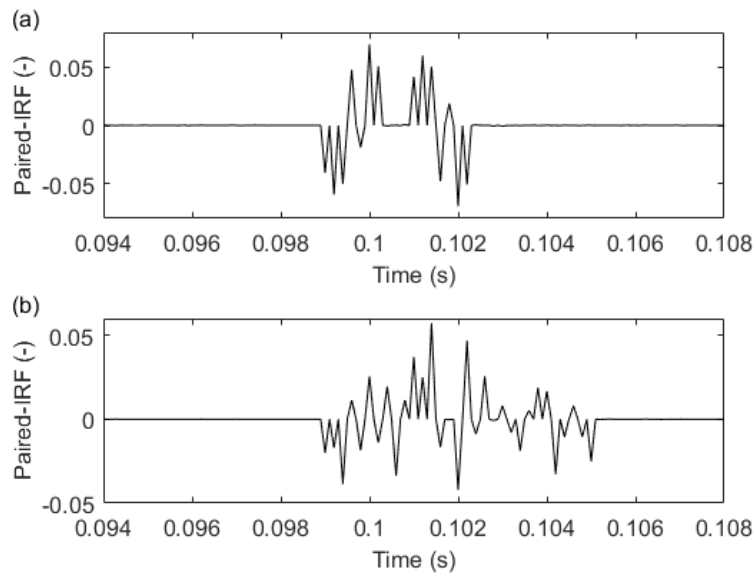


Figure 4.13 Paired-IRF for Case 1 with a deteriorated section; (a) $L_g = 0.496$ m and (b) $L_g = 1.800$ m.

4.3.5 Summary on the anomaly-induced features in the paired-IRF trace

Based on the studies in the previous sections above, a summary as shown in Table 4.2 has been made on the features that different anomalies induced in the paired-IRF trace. These features can be used to identify and localize the anomaly and calculate the length of the anomaly if the anomaly is not discrete.

Table 4.2 Anomaly-induced features in the paired-IRF trace.

Group	Anomaly	Common Features in this Group	Individual Features
Discrete	Leak		The first spike is negative.
	Junction	A pair of spikes; with opposite signs; and the time interval of $2t_p$.	The first spike is negative; The magnitude of spikes is large.
	Partially closed in-line valve (Discrete blockage)		The first spike is positive.
Extended with uniform properties	Section with an increased impedance	Two pairs of spikes; with opposite signs for spikes in each pair; the time interval = $2t_p$ for spikes in each pair;	The first and last spikes are positive.
	Section with a decreased impedance	and the time interval between the two pairs = $2L_d/a_d$ or $2L_e/a_e$.	The first and last spikes are negative.
Extended with non-uniform properties	Extended Blockage (Non-uniform)	Multiple spikes grouped together;	Mainly positive spikes are found at both sides of the spiked region.
	Extended Deterioration (Non-uniform)	Two pairs are superposed if $L_f/a_f (L_g/a_g) < L_p/a$.	Mainly negative spikes are found at both sides of the spiked region.

4.4 Case Study in a Pipe Network

In this section, a case study is considered involving a numerical pipe network with multiple types of anomalies. The characteristics summarized in the above section were applied in this case to identify and locate these anomalies. The extended paired-IRF equation (Eq. (4-12)) was applied to this case to explain the second-order wave reflections in the paired-IRF trace. The sensitivity of the method to noise was tested by using contaminated pressures.

4.4.1 Pipe system configuration

A pipe network connected to a reservoir with the water level equal to 60 m as shown in Figure 4.14 is utilized in this case study (referred to Case 2). The Darcy-Weisbach factor f is 0.02 for all pipes. The length of each pipe is given in Figure 4.14, and the diameter for the pipes are 200 mm excluding one pipe of which the diameter is shown in the figure as 150 mm. An extended blockage (B_1) in this branch pipe with a length $L_B = 0.2$ m is represented by decreasing the corresponding pipe diameter to 130 mm. The wave speed of all the pipes is 1000 m/s excluding the extended wall-deteriorated section D_1 as shown in

Figure 4.14. The wave speed profile in this section is the same as the one shown in Figure 4.12 (b). Two T-junctions are labelled as J_1 and J_2 in the schematic. Two leaks are labelled as L_1 and L_2 with the corresponding locations shown in the schematic. The locations of the transient generator and pressure transducers can be found in Figure 4.14. The generator is excited randomly (following a white noise sequence) similar to that shown in Figure 4.5.

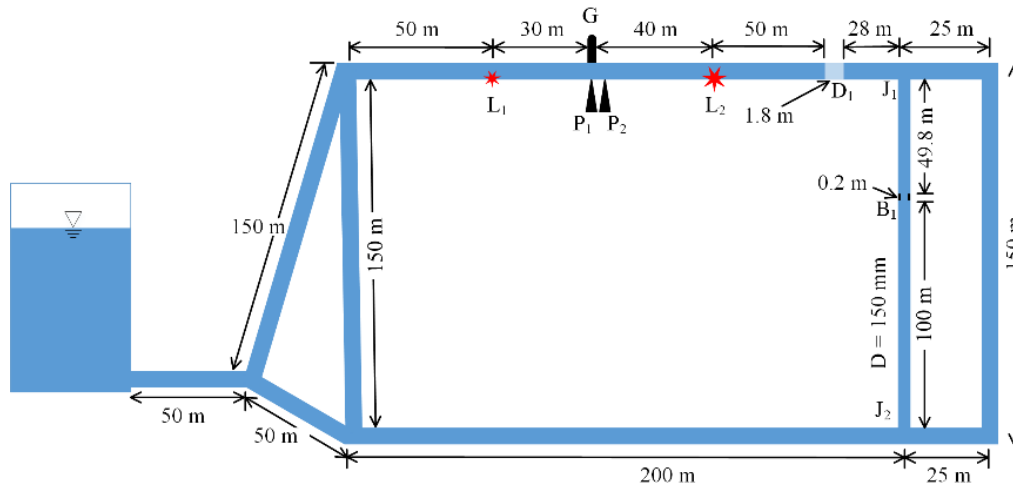


Figure 4.14 Schematic and configuration of the pipe network (Case 2).

4.4.2 Detection of anomalies in the pipe network

The simulated pressure perturbations in a 4 s period are plotted in Figure 4.15. The paired-IRF has been extracted from the pressure traces and the result is shown in Figure 4.16. Some paired spikes and grouped spikes can be observed in the paired-IRF trace. According to the features summarized in Table 4.2, the paired spikes at 0.08 s correspond to a leak (L_2) with a distance of 40 m from P_1 considering the first spike is negative and the spikes are of small magnitude. The grouped spikes at around 0.18 s indicate a wall-deteriorated section (D_1) with a distance of 90 m from P_1 considering the spikes at the edge of the spiked region are mainly negative. The paired spikes at 0.24 s and at 0.54 s indicate two junctions (J_1 and J_2) since the spikes are of large magnitude with the first spike in the pair being negative. The two pairs of spikes at around 0.34 s are induced by an extended blockage with a uniform diameter (B_1) since the first spike is positive.

If the pipe section G-J₁ is of interest, only the first-order wave reflections are visible in the paired-IRF trace within the corresponding time period 0 s - 0.24 s. However, with a further extension of the detection range to other pipes, some other spikes apart from the first-order components can be also found in the trace. These spikes may be incorrectly treated as reflections induced by extra anomalies if only the first-order paired-IRF equation is used. Thus, a clear explanation of them by using the new paired-IRF equation (Eq. (4-12)) is essential to avoid misinterpretation of the paired-IRF trace. The physical meaning of R_R^2 in Eq. (4-12) is the second-order reflections of the anomaly-induced wave reflections entering the same pipe sections again. For example, the wave reflection induced by the junction J₁ will enter into the same pipe (G-J₁) again and be reflected by L₂, D₁ and J₁ by the second time, and these second-order wave reflections are coded as L₂/J₁, D₁/J₁ and J₁/J₁, respectively, as shown in Table 4.3. Similarly, the wave reflections induced by L₂ and D₁ will enter into the same pipe (G- J₁) and be reflected by J₁ by the second time, and they are coded as L₂/J₁ and D₁/J₁, respectively. Other second-order wave reflections without being reflected by a junction are too small to be visually observed in the paired-IRF trace. The wave paths of these second-order wave reflections are shown in Table 4.3.

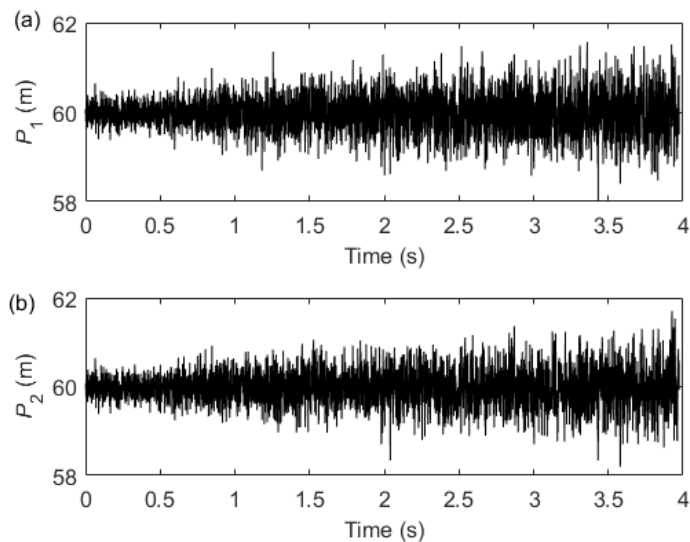


Figure 4.15 Simulated pressure waves for Case 2 with simulated pressure at:
(a) P₁ and (b) P₂.

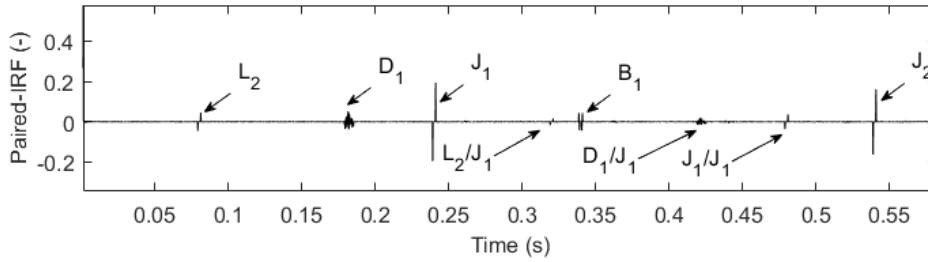


Figure 4.16 Paired-IRF extracted for Case 2 with simulated pressures.

Table 4.3 Tracking of the visible high-order wave reflections.

Code in Figure 4.16	Wave paths
L_2/J_1	G - L_2 - G - J_1 - G
	G - J_1 - G - L_2 - G
D_1/J_1	G - D_1 - G - J_1 - G
	G - J_1 - G - D_1 - G
J_1/J_1	G - J_1 - G - J_1 - G

4.4.3 Detection of anomalies with contaminated pressures

To examine the robustness of the detection method to background pressure interference, the simulated pressures were additively mixed with two measured pressure traces (P_{B1} and P_{B2} as shown in Figure 4.17), respectively, which contain the system background pressure fluctuations and noise. That is, the simulated pressures were superimposed onto realistic pressure traces, measured in the field, in order to synthetically create realistic noise conditions. The background pressures were measured at two locations with a spacing of 1.8 m on a pipe section in a real pipe network in the field.

By using the contaminated pressures, the paired-IRF was obtained and is shown in Figure 4.18. To focus on the first-order reflections, the paired-IRF trace is shown from 0 s to 0.3 s. Compared with the result shown in Figure 4.16, some noise consisting of small spikes can be observed in the trace and can be ascribed to the effects by the pressure interference.

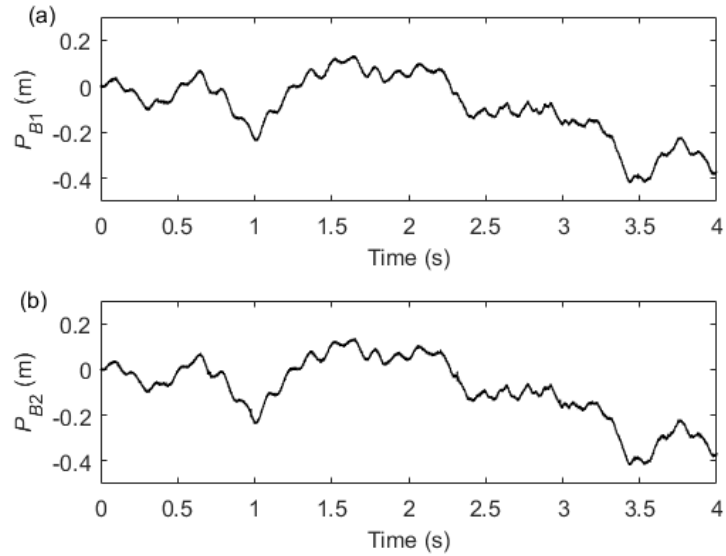


Figure 4.17 Measured background pressure fluctuations and noise in the field:
 (a) P_{B1} and (b) P_{B2} .

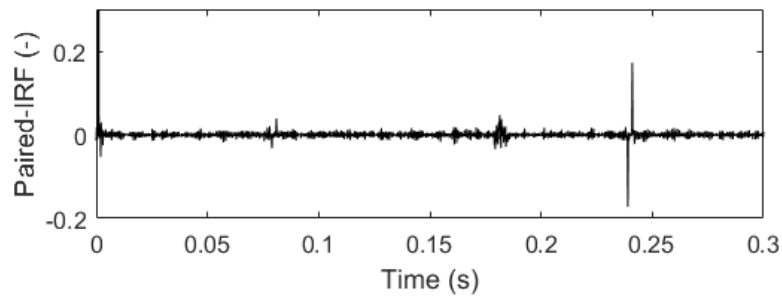


Figure 4.18 Paired-IRF extracted for Case 2 with contaminated pressures.

To improve the tolerance of the method to noise, multiple transient tests can be conducted. The extracted paired-IRF traces from individual tests can be averaged to diminish the noise in the averaged paired-IRF trace. In this simulation case, transient simulations were conducted 20 times with random valve excitations and the simulated pressures were contaminated with different periods of the measured pressure fluctuation and noise. The averaged paired-IRF trace from these 20 individual paired-IRF traces is shown in Figure 4.19. It shows that the noise level in the averaged paired-IRF trace has been significantly reduced by the averaging process. Some extra spikes can be still

found in the averaged trace, such as those at $t = 0.16$ s as shown in the zoomed plot in Figure 4.19. However, these spikes are small in amplitude, not paired or grouped with other spikes, and thus can be differentiated from the anomaly-induced spikes.

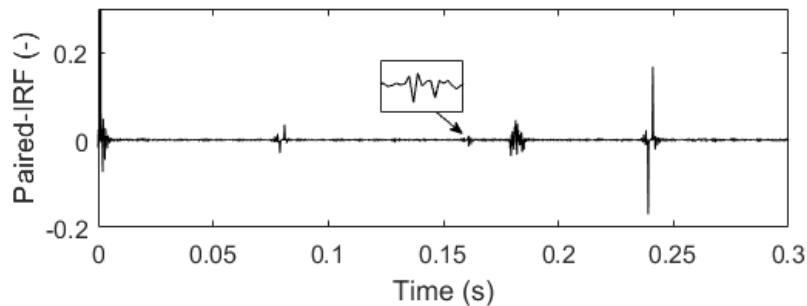


Figure 4.19 Averaged paired-IRF from 20 tests for Case 2 with contaminated pressures.

4.5 Discussion on Field Application

As presented in the methodology of the paired-IRF method, two pressure transducers are necessary to be installed on the pipe at two different locations within a short distance. In field tests, the pressure transducers and the generator are normally connected with the pipe through fire hydrants (as shown in Figure 4.20), air valves or other kinds of fittings. However, two ports in close proximity are often unavailable in the field. Another issue in the field is the effect of the connection stubs on the pressure measurement, such as the fire hydrant shown in Figure 4.20. The transient pressure waves will oscillate in the connection stub, and thus the pressure trace measured at the upside of the connection stub (such as the pressure transducer in Figure 4.20) is different than the real pressure trace in the pipe. The diameter and the length of the stub have a very close relationship with the deviation between the measured pressure trace by the transducer with the real pressure trace in the pipe (Liu and Simpson 2018). To address the issues discussed, the in-pipe fibre optic sensors, which have already been applied to leak detection (Gong et al. 2018c) and wave separation (Shi et al. 2019) in the laboratory, may be utilized to obtain reliable

transient pressure traces in a field pipe. It is envisaged that a cable carrying multiple fibre optic sensors (as shown in Figure 4.20) can be inserted into the pipe at one connection port at which the transient generator can be also installed.

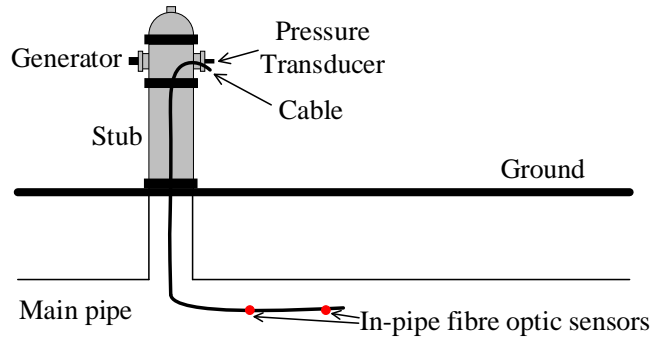


Figure 4.20 Schematic of the installation of the generator and sensors in the field.

4.6 Conclusions

In this paper, the paired-IRF approach has been extended to improve its reliability by incorporating all the high-order wave reflections and by taking an averaging process to improve its capability of detecting different anomalies in pipes. By analyzing the features of the anomaly-induced spikes in the paired-IRF traces, eight kinds of anomalies classified into three groups were characterized as follows.

1) A discrete anomaly can induce a pair of spikes with opposite signs and a fixed time interval which is determined by the distance of the two pressure transducers. The first spike for a leak or a junction is negative, and that for a partially closed in-line valve (or a discrete blockage) is positive. The spikes induced by a junction are normally of high magnitude.

2) An extended anomaly with uniform properties can induce two pairs of spikes. The time interval between the spikes in each pair is determined by the distance of the pressure transducers and the interval between these two pairs is determined by the length of the anomaly. The signs of the spikes are different

for sections with an increased impedance (e.g. extended blockages) and sections with a decreased impedance (e.g. sections with uniform pipe wall thinning).

3) An extended anomaly with non-uniform properties can induce multiple spikes that are grouped together. The signs of the spikes at the edges of the spiked region are different for blockages and wall deteriorated sections.

With the characterization of these anomalies, the generalized paired-IRF technique is capable of detecting multiple types of anomalies in pipes. A validation case study was conducted on a numerical pipe network with multiple anomalies. The anomalies were successfully detected and localized. With the detection range extended to other pipes in the network, some second-order wave reflections were observed in the trace, and they were successfully explained by the new paired-IRF equation. The anomalies were successfully detected even though the simulated pressures were contaminated with background pressure fluctuations and noise measured in a real pipe network. An averaging process of the paired-IRF traces from multiple tests has also been proposed and it significantly enhanced the tolerance of the method to background pressure fluctuations and noise.

Acknowledgements

The research presented in this paper has been supported by the Australian Research Council through the Discovery Project Grant DP190102484.

Chapter 5

Condition Assessment of Water Pipelines using a Modified Layer Peeling Method (Journal Publication 3)

Wei Zeng¹, Jinzhe Gong¹, Aaron C. Zecchin¹, Martin F. Lambert¹ Angus R. Simpson¹, Benjamin S. Cazzolato²

¹School of Civil, Environmental and Mining Engineering, the University of Adelaide, Adelaide, SA 5005 Australia

²School of Mechanical Engineering, University of Adelaide, SA 5005, Australia

Citation: Zeng, W., Gong, J. Z., Zecchin, A. C., Lambert, M. F., Simpson, A. R., Cazzolato, B. S. (2018). "Condition assessment of water pipelines using a modified layer-peeling method." *Journal of Hydraulic Engineering*, 144(12), 04018076. DOI: 10.1061/(ASCE)HY.1943-7900.0001547.

Statement of Authorship

Title of Paper	Condition assessment of water pipelines using a modified layer peeling method	
Publication Status	<input checked="" type="checkbox"/> Published	<input type="checkbox"/> Accepted for Publication
	<input type="checkbox"/> Submitted for Publication	<input type="checkbox"/> Unpublished and Unsubmitted work written in manuscript style
Publication Details	Zeng, W., Gong, J., Zecchin, A., Lambert, M., Simpson, A., Cazzolato, B. (2018). Condition assessment of water pipelines using a modified layer peeling method. Journal of Hydraulic Engineering, 144(12)	

Principal Author

Name of Principal Author (Candidate)	Wei Zeng	
Contribution to the Paper	Conception and design of the project Analysis and interpretation of research data Draft the paper	
Overall percentage (%)	75 %	
Certification:	This paper reports on original research I conducted during the period of my Higher Degree by Research candidature and is not subject to any obligations or contractual agreements with a third party that would constrain its inclusion in this thesis. I am the primary author of this paper.	
Signature		Date 8/11/2019

Co-Author Contributions

By signing the Statement of Authorship, each author certifies that:

- i. the candidate's stated contribution to the publication is accurate (as detailed above);
- ii. permission is granted for the candidate to include the publication in the thesis; and
- iii. the sum of all co-author contributions is equal to 100% less the candidate's stated contribution.

Name of Co-Author	Jinzhe Gong	
Contribution to the Paper	Conception and design of the project Analysis and interpretation of research data Critically revising the paper	
Signature		Date 24/11/19

Name of Co-Author	Aaron Zecchin	
Contribution to the Paper	Conception and design of the project Analysis and interpretation of research data Critically revising the paper	
Signature		Date 15/11/19

Please cut and paste additional co-author panels here as required.

Name of Co-Author	Martin Lambert		
Contribution to the Paper	Conception and design of the project Analysis and interpretation of research data Critically revising the paper		
Signature		Date	22/11/19

Name of Co-Author	Angus Simpson		
Contribution to the Paper	Conception and design of the project Analysis and interpretation of research data Critically revising the paper		
Signature		Date	4 Nov. 2019

Name of Co-Author	Benjamin Cazzolato		
Contribution to the Paper	Conception and design of the project Analysis and interpretation of research data Critically revising the paper		
Signature		Date	8 th Nov. 2019

Abstract

Pipe wall condition assessment is critical for the targeted maintenance and for failure prevention in water distribution systems. This paper proposes a novel approach for condition assessment of water pipelines by adapting the layer peeling method. This method was previously developed for, and applied to, tubular musical instruments. In the proposed approach, the impulse response function (IRF) of a pipeline is obtained using measured pressure traces resulting from transient events. The original layer peeling method is further developed for application to water transmission pipelines by 1) modifying the end boundary from being an acoustic source tube to a closed valve; 2) incorporating the effects of unsteady friction and pipe wall viscoelasticity into the layer peeling algorithm; and 3) incorporating frequency-dependent wave reflections and transmissions. Using the IRF and the modified layer peeling method, the impedance of a pipeline can be estimated section by section from downstream (the dead-end) to upstream of the pipeline. The distribution of wave speeds and wall thickness can then be determined. In this study, numerical verifications were conducted using the pipeline pressure responses simulated by the method of characteristics (MOC). The deteriorated pipe sections (sections with changes in impedance) were accurately detected using the new approach. Experimental verification of the result was conducted on a laboratory copper pipeline. A short section of pipe with a thinner wall thickness was successfully detected.

5.1 Introduction

Water distribution systems (WDS) are important infrastructure assets. They normally consist of buried pipeline networks that are massive in scale, and often old and deteriorated. However, the condition of these pipes is extremely difficult and expensive to determine. Over the past two decades, a number of non-invasive, hydraulic, transient-based methods have been developed for fault detection in water pipelines (Chaudhry 2014). Hydraulic transient-based fault detection in a pipeline system is conducted with a transient disturbance, typically a pulse or a step pressure wave introduced by abruptly operating a valve. The resulting transient waves propagate along the pipeline, and any physical changes or anomalies such as leaks or blockages may result in specific wave reflections (Lee et al. 2007a). Anomalies in the pipes are located by analyzing time series and wave speed (Brunone 1999). The size of a leak or a blockage can be determined by examining the magnitude of the wave reflection.

Most of the transient-based methods focus on the detection of discrete elements, such as leaks (Brunone 1999; Vítkovský et al. 2007; Ferrante et al. 2009; Shamloo and Haghghi 2009; Duan et al. 2011; Gong et al. 2014b) and blockages (Wang et al. 2005; Lee et al. 2008b; Sattar et al. 2008; Meniconi et al. 2011a; Meniconi et al. 2016). In addition to discrete faults, extended blockages caused by tuberculation (Meniconi et al. 2012a; Duan et al. 2013; Duan et al. 2014; Duan 2016) and extended sections of pipe degradation caused by spalling of the cement mortar lining and widespread corrosion are common in ageing WDS; however, research on transient-based pipe wall condition assessment is limited. Distributed pipe deterioration may reduce the water transmission efficiency (Tran et al. 2010), create water quality problems (Clark and Haught 2005) and may develop into bursts or severe blockages over time (Zamanzadeh et al. 2007). Thus, developing cost-effective techniques for pipeline condition assessment is essential in enabling strategically targeted pipe maintenance, replacement and rehabilitation.

The inverse transient analysis (ITA) (Stephens et al. 2013) and the reconstructive method of characteristics (MOC) analysis (Gong et al. 2014a) are two available, transient-based techniques for continuous pipe-wall condition assessment. The inverse transient method (ITA) was first proposed by Liggett and Chen (1994) for detecting leaks in a pipe network. It was further developed by Vítkovský et al (2000; 2007) and Covas et al.(2010) and was first applied to pipeline condition assessment by Stephens et al. (2008; 2013).

In ITA, the transient responses of a numerical pipeline model with assumed parameters (e.g. wave speeds) are simulated by the MOC. Then, an optimization process is conducted to minimize error between numerical and experimental values. By iteratively modifying the parameters in the model, the best possible match of the numerical pressure traces with the traces measured from a real pipe can be obtained. The numerical pipe model that provides the best match is used to interpret the condition of the real pipeline. However, ITA is not computationally efficient, especially for pipelines of substantial length which involves a large number of parameters to calibrate. A head-based MOC model with a flexible computational grid (Zhang et al. 2018a), a multi-stage parameter-constraining ITA (Zhang et al. 2018b) and a combined analysis of the pressure signal to pre-localize anomalies (Meniconi et al. 2015) could be used to improve the computational efficiency. There are also many practical issues (e.g. wave dissipation and dispersion(Duan et al. 2010)) that affect the identifiability of the technique (Vítkovský et al. 2007).

The reconstructive MOC analysis assesses the condition of a pipeline section by section by inverting the conventional MOC calculation (Gong et al. 2014a). The method is computationally efficient, because the pipeline properties are calculated analytically instead of through an iterative, optimizer-driven model calibration process. However, when the pipeline configuration is either complex, or wave dissipation is significant or dispersion needs to be considered, it would be impossible to handle these situations using the reconstructive MOC algorithm.

A technique that shares a similar principle to the reconstructive MOC analysis is the layer peeling method, which was developed in the acoustics research field. An early technique named acoustic pulse reflectometry was proposed by Ware and Aki (1969) as a seismological technique for observing stratifications in the earth's crust. The layer peeling method was built on this, and applied reconstructions of the geometry of short air ducts with varying cross sections (Amir and Shimony 1995a, b). It was then applied to bore reconstruction of musical wind instruments in order to inspect their qualities (Sharp and Campbell 1997). In these applications, an acoustic source tube with properties designed to prevent or control wave reflections is attached to one end of the duct/instrument to extract the impulse response function (IRF) of the system. The IRF is then analyzed to determine the acoustic impedance and reflection coefficients moving section by section away from the acoustic source. Further research has been conducted into 1) increasing the length of the tubular objects that can be reconstructed (Sharp 1998), 2) enhancing the robustness (Forbes et al. 2003), 3) increasing the axial resolution (Li et al. 2005), and 4) coupling the higher mode acoustic waves in the method (Hendrie 2007). However, there is no application of the layer peeling concept to pipeline condition assessment using hydraulic transients to date.

The research reported in this paper develops a novel pipeline condition assessment approach that uses the IRF of a pipeline and a modified layer peeling algorithm. The key innovations include: the use of a dead-end boundary condition instead of an acoustic tube and the determination of the directional IRF at the dead-end; the incorporation of wave dissipation and dispersion induced by unsteady friction and pipe wall viscoelasticity; and the incorporation of the frequency-dependent wave reflection and transmission at cross-sections with an impedance change.

The new technique enables the distribution of pipeline impedance to be determined, from which wall thickness and wave speed along the pipe can be reconstructed. Compared with the ITA method (Stephens et al. 2013), the proposed approach is more efficient, because it does not need a time-consuming, iterative, forward-modelling and optimization process. Compared

with the reconstructive MOC analysis, the proposed approach is more accurate, because it can conveniently incorporate frequency-dependent effects, such as wave dissipation and dispersion.

To validate the new layer-peeling-based approach, extensive numerical simulations have been conducted for pipes with and without both friction or viscoelasticity; with uniformly and non-uniformly distributed deteriorations; and with and without measurement noise. For all the numerical cases, the distribution of the wave speed along the pipe was accurately reconstructed. Experimental verification was also conducted on a copper pipeline in the laboratory. A pipe section with a thinner wall thickness was clearly identifiable in the reconstructed pipe impedance. Towards the end of this paper, a discussion of the limitations and practical challenges of the new method is presented. Finally conclusions are made.

5.2 The Layer Peeling Method for Pipeline Condition Assessment

The principle of the new approach is illustrated in Figure 5.1, which is a block diagram describing the wave propagation and reflection process in a pipeline. In the figure, the superscripts (+ and -) illustrate forward and backward directions respectively, the subscripts 1, 2, and i represent the number of the pipe section, and the subscripts l and r represent the left side and right side of the section.

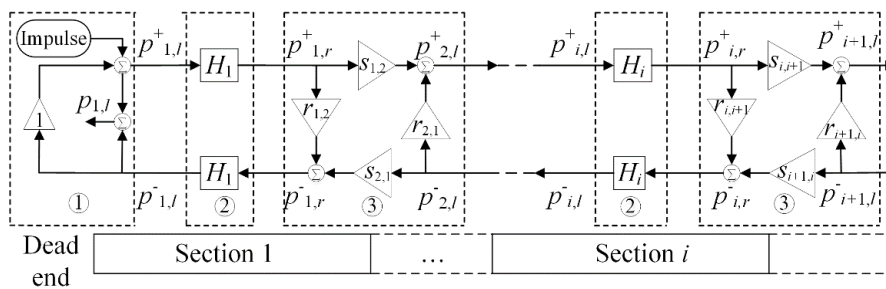


Figure 5.1 Block diagram describing the wave transmission and reflection process in a pipeline.

The method includes the four following main steps. First, the IRF of a pipeline system ($p_{1,l}$), which is the input to the modified layer peeling algorithm, is determined through transient analysis, and pre-processed to yield the directional IRF ($p_{1,l}^+$ and $p_{1,l}^-$). Second, the dissipation, and the dispersion of pressure waves during the propagation in each pipe section, is formulized as a transfer function (H_i). Thirdly, the wave transmission and reflection at the interface between pipe sections is represented using reflection ratios ($r_{i,i+1}$ and $r_{i+1,i}$) and transmission ratios ($s_{i,i+1}$ and $s_{i+1,i}$). Finally, a recursive procedure is applied to reconstruct the reflection and transmission ratios section by section, using the IRF and the propagation functions. These four components are discussed in detail in subsequent sections.

5.2.1 Impulse response function (IRF)

This section illustrates the two steps to get the directional IRF that is the input of the layer peeling method. First, a singular value decomposition is used to obtain the IRF of the pipeline system. The formulae to transfer the system IRF to the directional IRF are then given.

(a) Methods for obtaining the system IRF

The IRF $z(t)$ is defined as the response measured at the output when an ideal impulse input is injected into a system. In a linear transmission system, a real signal input $x(t)$ with N data samples, such as a pulse, can be treated as N scaled impulses with different starting times. Each scaled impulse generates a scaled response that starts at the same time as the input impulse. Thus, the overall response of the system $y(t)$ is the sum of these scaled responses, which may be written as (Smith 1999)

$$y(n) = \sum_{m=-\infty}^{\infty} x(n-m)z(m) \quad (5-1)$$

The method used to obtain the IRF in this research is based on deconvolution in the time domain using the singular value decomposition (Agulló et al. 1995). Equation (5-1) can be rewritten in the matrix form $\mathbf{y} = \mathbf{Xz}$, in which \mathbf{X} is a

triangular matrix of $x_{ij} = x_{i-j+1}$ for $j \leq i$ and $x_{ij} = 0$ for $j > i$, and \mathbf{y} is the column vector of the wave reflections. Applying the singular value decomposition to \mathbf{X} gives $\mathbf{X} = \mathbf{P}\mathbf{\Lambda}\mathbf{Q}^T$, where \mathbf{P} , \mathbf{Q} are orthonormal matrices composed of column vectors \mathbf{p}_i and \mathbf{q}_i , respectively, and $\mathbf{\Lambda}$ is a diagonal matrix composed of the singular values λ_i sorted in descending order of size. Then \mathbf{X} can be written as $\mathbf{X} = \sum_{i=1}^N \lambda_i \mathbf{q}_i \mathbf{p}_i^T$ and the IRF $\mathbf{z} = \mathbf{X}^{-1}\mathbf{y}$ can be written as (Agulló et al. 1995)

$$\mathbf{z} = \left(\sum_{i=1}^N \lambda_i^{-1} \mathbf{p}_i \mathbf{q}_i^T \right) \mathbf{y} \quad (5-2)$$

However, a small value of λ_i when i approaches N makes a significant contribution to \mathbf{X}^{-1} , which results in distorted deconvolution. A combination of a *truncation regularization* and a *Tikhonov's regularization* gives (Forbes et al. 2003)

$$\mathbf{z} = \left(\sum_{i=1}^J \frac{\lambda_i}{\lambda_i^2 + \alpha_c} \mathbf{p}_i \mathbf{q}_i^T \right) \mathbf{y} \quad (5-3)$$

where J is the truncation point and $J < N$, α_c is an regularization parameter. A smaller J or a larger α_c results in a smoother but less sharp IRF. The two parameters can be determined by trial and error until satisfactory results are achieved (Forbes et al. 2003). The algorithm in Eq. (5-3) is used in this paper.

(b) From the system IRF to the directional IRF

In the conventional layer peeling method, which has previously been applied to musical instruments (Sharp 1996), a long, uniform, source tube, which is two times longer than the musical instrument, was attached to one end of the instrument, as shown in Figure 5.2 (a). The source tube enables the identification and separation of the forward signal input and the backward wave reflections. Thus, the IRF calculated from the system response is directional. It represents the impulse reflections from the instrument only (i.e. no impact from the source tube).

In a water transmission line systems, it is not feasible to connect a long source tube to a water pipeline. Instead, a dead-end boundary condition is considered by closing an inline valve, as shown in Figure 5.2 (b). A pressure wave generator and a transducer are installed close to the dead-end.

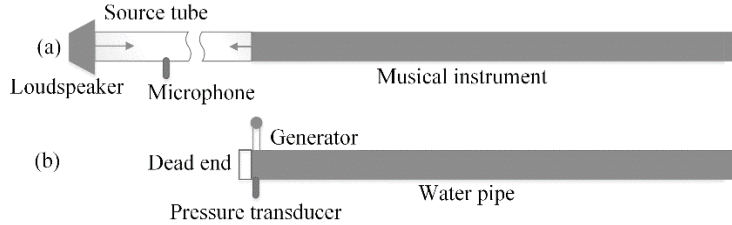


Figure 5.2 Schematic diagram of the testing systems; (a) musical instrument, and (b) water pipeline.

Due to the dead end, the directional impulse reflection $p_{1,l}^-$ would be further reflected by the end boundary, and will again enter into the pipeline system, as shown in the first dashed box in Figure 5.1. Neglecting any loss in the reflection at the dead-end, i.e. the reflection coefficient is unity, the magnitude of the system IRF at the dead end [$p_{1,l}$, may be directly determined from Eq. (5-3)] is effectively two times that of the directional impulse reflections from the pipe discontinuities (backward propagating wave, $p_{1,l}^-$), i.e.

$$p_{1,l} = 2p_{1,l}^- \quad (5-4)$$

As shown in Figure 5.1 (a), the forward propagating wave into the pipeline is described as

$$p_{1,l}^+ = \delta_0 + p_{1,l}^- \quad (5-5)$$

where δ_0 refers to a pulse signal with $\delta_0 = 1$ at $t = 0$ and $\delta_0 = 0$ when $t \neq 0$.

The two directional IRF signals, which represent the impulse reflections from the pipe discontinuities and the forward-propagating wave into the pipeline respectively, can be obtained through Eqs. (5-4) and (5-5), and written as

$$p_{1,l}^- = 0.5p_{1,l} \quad (5-6)$$

$$p_{1,l}^+ = \delta_0 + 0.5p_{1,l} \quad (5-7)$$

5.2.2 Wave dissipation and dispersion

For a fluid-filled pipe, the wave speed (a) in the fluid depends on the properties of the fluid and the pipe wall. For deteriorated sections of a metallic pipeline, the change in wall thickness affects the wave speed governed by the following formula (Wylie and Streeter 1993),

$$a = \sqrt{\frac{K/\rho}{1+(K/E)(D/e)c_1}} \quad (5-8)$$

where K represents the bulk modulus of the water; ρ is the density of water; E is the Young's modulus of elasticity of the pipe wall; D is the pipe's inner diameter; e is the wall thickness of the pipe; and c_1 is the pipeline restraint factor. The value of c_1 depends on whether the pipe is thin walled ($D/e > 25$) or thick walled ($D/e \leq 25$) (Wylie and Streeter 1993). For a structurally degraded, viscoelastic pipeline, the wave speed may also change due to the degradation of the pipe elasticity.

Pressure waves in pipelines experience frequency-dependent dissipation and dispersion due to friction and viscoelasticity from the pipe wall (Gong et al. 2016c). The wave dissipation and dispersion in the i th pipe section (within which the properties are assumed uniform) can be described by a transfer function H_i such that

$$P_{i,r}^+ = P_{i,l}^+ H_i \quad (5-9)$$

$$P_{i,r}^- = P_{i,l}^- / H_i \quad (5-10)$$

where P is the Fourier transformation of p .

The following part of this section illustrates the processes used to obtain the analytical expression of the transfer function.

The one-dimensional (1D) momentum equation for transient fluid flow (Wylie and Streeter 1993) is given as

$$\frac{1}{gA} \frac{\partial q}{\partial t} + \frac{\partial h}{\partial x} + h_{fT} = 0 \quad (5-11)$$

in which h represents the piezometric head, q represents the volumetric flow rate, g is acceleration due to gravity, A is the internal cross-section area of the section, and the head loss h_{fT} , which is the sum of a steady-state component h_{fS} and an unsteady-state component h_{fU} .

The continuity equation for the 1D transient flow incorporating the viscoelastic behavior of the pipe wall is given as (Covas et al. 2005)

$$\frac{gA}{a^2} \frac{\partial h}{\partial t} + \frac{\partial q}{\partial x} + 2A \frac{\partial \varepsilon_r}{\partial t} = 0 \quad (5-12)$$

where ε_r is the retarded circumferential strain in the pipe wall.

Using the concept of steady-oscillatory flow with h^* , q^* and ε_r^* representing the time varying oscillatory components of head, flow and retarded strain, Eq. (5-11) and Eq. (5-12) can be transformed into the frequency domain (Gong et al. 2016c) as

$$\frac{1}{gA} j\omega q^* + \frac{\partial h^*}{\partial x} + Rq^* = 0 \quad (5-13)$$

$$\frac{gA}{a^2} j\omega h^* + \frac{\partial q^*}{\partial x} + 2Ai\omega \varepsilon_r^*(j\omega) = 0 \quad (5-14)$$

Where j is the imaginary unit, R is the linearized resistance per unit length, and can be described by a summation of the steady friction part R_s and unsteady friction part R_u , i.e.

$$R = R_s + R_u \quad (5-15)$$

where $R_s = fQ_0/(gDA^2)$, with f representing the Darcy-Weisbach friction factor. The expression of R_u depends on the selection of the unsteady friction model in the time domain. If the Vardy and Brown unsteady friction model for smooth-pipe turbulent flow (Vardy and Brown 1995) is chosen, the expression of R_u can be written based on the derivation by Vítkovský et al. (2003a) as

$$R_u = \frac{2j\omega}{gA} \left(\frac{j\omega D^2}{4\nu} + \frac{1}{C^*} \right)^{-1/2} \quad (5-16)$$

where ν is kinematic viscosity of fluid and C^* is the shear decay coefficient. $C^* = 0.00476$ for laminar flows and $C^* = 7.41/Re^k$ for smooth pipe turbulent flow with $k = \log_{10}(14.3/Re^{0.05})$ and Re representing the Reynolds number.

With the multi-element Kelvin-Voigt model (Covas et al. 2005) for viscoelastic effects, and the corresponding frequency domain transformation (Gong et al. 2016c), $\varepsilon_r^*(i\omega)$ in Eq.(5-14) can be written as

$$\varepsilon_r^*(j\omega) = Ch \sum_{k=1}^N \frac{J_k}{j\omega\tau_k+1} \quad (5-17)$$

where $C = c_1 D \rho g / 2e$, J_k is the creep-compliance of the k_{th} Kelvin-Voigt element and τ_k is the retardation time of the dashpot of the k_{th} Kelvin-Voigt element.

Combining Eqs. (5-13), (5-14) and (5-17) yields

$$\frac{\partial^2 h^*}{\partial x^2} + (\omega^2 - gARj\omega) \left(\frac{2C}{g} \sum_{k=1}^N \frac{J_k}{j\omega\tau_k+1} + \frac{1}{a^2} \right) h^* = 0 \quad (5-18)$$

The equation can be also written as

$$\frac{\partial^2 h^*}{\partial x^2} + \frac{\omega^2}{a_c^2} h^* = 0 \quad (5-19)$$

Therefore, the pressure wave after propagating a distance of Δx can be written as

$$h^*(x + \Delta x) = h^*(x)e^{-j\omega\Delta x/a_c} \quad (5-20)$$

in which a_c is the complex wave speed described by

$$a_c = \sqrt{\frac{\omega^2}{(\omega^2 - gARj\omega) \left(\frac{2C}{g} \sum_{k=1}^N \frac{J_k}{j\omega\tau_{k+1}} + \frac{1}{a^2} \right)}} \quad (5-21)$$

If friction is neglected (Gong et al. 2016c) and then $R = 0$, then

$$a_c = \sqrt{\frac{1}{\left(\frac{2C}{g} \sum_{k=1}^N \frac{J_k}{j\omega\tau_{k+1}} + \frac{1}{a^2} \right)}} \quad (5-22)$$

If viscoelastic behavior of the pipe wall is neglected, then the expression for the complex wave speed simplifies to

$$a_c = a \sqrt{\frac{1}{(1 - gARj/\omega)}} \quad (5-23)$$

If both the friction and the viscoelastic effects of the pipe wall are neglected, the expression of the complex wave speed a_c collapses to the elastic wave speed a .

The complex wave speed a_c can be also treated in the following form $a_c = a_r + ja_j$ (Suo and Wylie 1990) such that a_e and μ_e in Eq.(5-24) can represent the equivalent wave speed and frequency dependent attenuation respectively with the following expressions:

$$a_e = \frac{|a_c|^2}{a_r} \quad \text{and} \quad \mu_e = \frac{\omega a_j}{|a_c|^2} \quad (5-24)$$

For a pressure wave propagating from the left boundary to the right boundary of the i th pipe section, the following equation can be obtained through Eqs. (5-20) and (5-24).

$$P_{i,r}^+ = P_{i,l}^+ \cdot e^{-\mu_e \Delta x_i} e^{-j\omega \Delta x_i / a_{e,i}} \quad (5-25)$$

in which $T/2$ is the time needed for the wave to pass through the i th section, Δx_i is the length of the section, $e^{-\mu_e \Delta x_i}$ represents the wave dissipation and $e^{-j\omega \Delta x_i / a_{e,i}}$ represents the wave dispersion. The transfer function in Eqs. (5-9) and (5-10) is given by

$$H_i = e^{-\mu_e \Delta x_i} e^{-j\omega \Delta x_i / a_{e,i}} \quad (5-26)$$

The transfer function H_i represents the wave dissipation and dispersion, and will be used in the reconstruction process outlined in the following section 2.4.

5.2.3 Wave transmission and reflection

If an incident pressure wave P (in the frequency domain) meets a discontinuity in the pipe (an interface with an impedance change), a reflected wave P_r will be generated. The incident wave will change to P_s after passing the discontinuity. The reflection coefficient r (the ratio of the reflected wave to the incident wave) and the transmission coefficient s (the ratio of the transmitted wave to the incident wave) are determined by the pipeline characteristic impedance B . They can be calculated using the formulae (Chaudhry 2014)

$$r_{i,i+1} = \frac{P_r}{P} = \frac{B_{i+1} - B_i}{B_{i+1} + B_i} \quad (5-27)$$

$$s_{i,i+1} = \frac{P_s}{P} = \frac{2B_{i+1}}{B_{i+1} + B_i} = 1 + r_{i,i+1} \quad (5-28)$$

in which

$$B = a_c / gA \quad (5-29)$$

is the complex characteristic impedance. According to Eq. (5-22), it can be seen that $r_{i,i+1}$ and $s_{i,i+1}$ are frequency-dependent for the viscoelastic model. For the unsteady friction model, the complex wave speed a_c is proportional to the elastic wave speed a if A is assumed to be constant in Eq. (5-23). Thus, $r_{i,i+1}$ and $s_{i,i+1}$ are frequency-independent for the unsteady friction model when Eq. (5-23) is substituted into Eqs. (5-27) and (5-28).

If the incident wave propagates in the opposite direction, then the reflection coefficient and the transmission coefficient can be calculated as:

$$r_{i+1,i} = -r_{i,i+1} \quad (5-30)$$

$$s_{i+1,i} = 1 - r_{i,i+1} \quad (5-31)$$

At the interface of two sections as shown in Figure 5.4, the transmitted waves and reflected waves are represented by the dot-dashed arrows and dashed arrows, respectively. According to the directions of the arrows, it follows that the forward-propagating wave $P_{i+1,l}^+$ travelling into section $i+1$ is the sum of the transmitted wave of $P_{i,r}^+$ and the reflected wave of $P_{i+1,l}^-$. The backward-propagating wave $P_{i,r}^-$ travelling into section i is the sum of the reflected wave of $P_{i,r}^+$ and the transmitted wave of $P_{i+1,l}^-$. Combining Eqs. (5-27) to (5-31), the following formulae can be written based on the analysis above:

$$P_{i+1,l}^+ = P_{i+1,l}^-(-r_{i,i+1}) + P_{i,r}^+(1 + r_{i,i+1}) \quad (5-32)$$

$$P_{i,r}^- = P_{i,r}^+(r_{i,i+1}) + P_{i+1,l}^-(1 - r_{i,i+1}) \quad (5-33)$$

The relationship of the wave transmission and reflection can also be represented by the third dashed box in Figure 5.1. By rearranging the two formulae, the relationship between the travelling waves at either side of a section interface can be summarized as (Amir and Shimony 1995a)

$$\begin{bmatrix} P_{i+1,l}^+ \\ P_{i+1,l}^- \end{bmatrix} = \frac{1}{1-r_{i,i+1}} \begin{bmatrix} 1 & -r_{i,i+1} \\ -r_{i,i+1} & 1 \end{bmatrix} \begin{bmatrix} P_{i,r}^+ \\ P_{i,r}^- \end{bmatrix} \quad (5-34)$$

In the time domain, the space-time diagram of the wave reflection and transmission are shown in Figure 5.4 for a pipeline discretized into sections. The forward-propagating waves along the diagonal in the diagram are defined as the main transmitted waves $p_{i,r}^+(iT/2)$ (thick solid lines). The backward propagating waves, at the same time and position as the main transmitted waves, are defined as the initial reflected waves $p_{i,r}^-(iT/2)$ (dashed lines). If the frequency-dependent characteristics of the wave reflection and transmission are neglected in the time domain, the initial reflected waves are only caused by the reflection of the main transmitted waves, as shown in Figure 5.4, which means

$$r_{i,i+1}^t = \frac{p_{i,r}^-(iT/2)}{p_{i,r}^+(iT/2)} \quad (5-35)$$

in which $r_{i,i+1}^t$ is the elastic wave reflection ratio in the time domain. If the elastic characteristic impedance $B_i^t = a_i/gA_i$ is known, the real characteristic impedance B_{i+1}^t can be estimated according to Eq. (5-27) as

$$B_{i+1}^t = \frac{1+r_{i,i+1}^t}{1-r_{i,i+1}^t} B_i^t \quad (5-36)$$

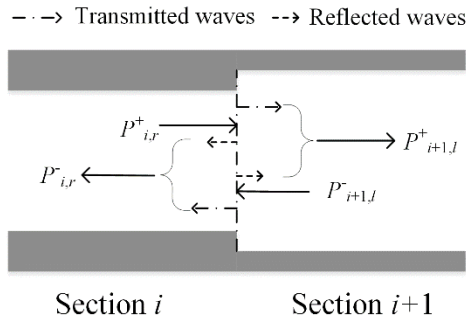


Figure 5.3 Wave transmission and reflection at a junction.

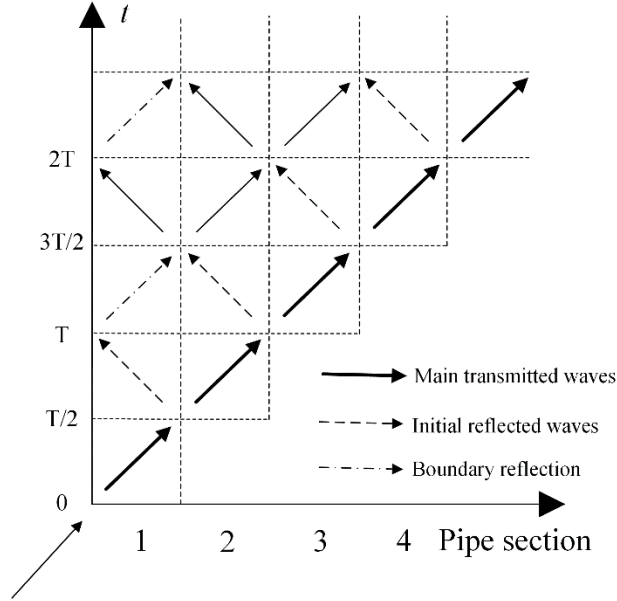


Figure 5.4 Space-time diagram of the wave propagation.

5.2.4 Procedures of the modified layer peeling method

The steps for reconstructing a pipeline with N sections using the modified layer peeling method are shown in Figure 5.5 (Note B_1 is obtained as in Gong et al. (2014a)) and described as follows.

Step 1: Use experimental data to calculate the system IRF through Eq. (5-3).

Step 2: Use the system IRF to calculate the directional IRF $p_{1,l}^-$ and forward-propagating wave $p_{1,l}^+$ through Eqs. (5-6) and (5-7).

Step 3: Use the waves at the left side of the i_{th} ($i=1$ for the first step) section $P_{i,l}^+$ and $P_{i,l}^-$ to calculate the waves at the right side of the i_{th} section $P_{i,r}^+$ and $P_{i,r}^-$ through Eqs. (5-9) and (5-10).

Step 4: Use the waves at the right side of the i_{th} section $p_{i,r}^+$ and $p_{i,r}^-$ (transferred to the time domain) to calculate the elastic reflection ratio $r_{i,i+1}^t$ through Eq. (5-35), and then obtain the elastic characteristic impedance of the next section

B_{i+1}^t through Eq. (5-36), as well as the complex characteristic impedance B_{i+1} through Eqs.(5-21) and (5-29).

Step 5: Use the complex B_i and B_{i+1} to calculate the frequency-dependent wave reflection ratio $r_{i,i+1}$. Then, use the waves at the right side of the i^{th} section $P_{i,r}^+, P_{i,r}^-$ and $r_{i,i+1}$ to calculate the waves at the left side of the $(i+1)^{\text{th}}$ section $P_{i+1,l}^+$ and $P_{i+1,l}^-$ through Eq. (5-34).

Step 6: Repeat steps 3 to 5 for $i = 2, \dots, N-1$ to calculate the characteristic impedances, wave speeds and wall thicknesses for the remaining sections.

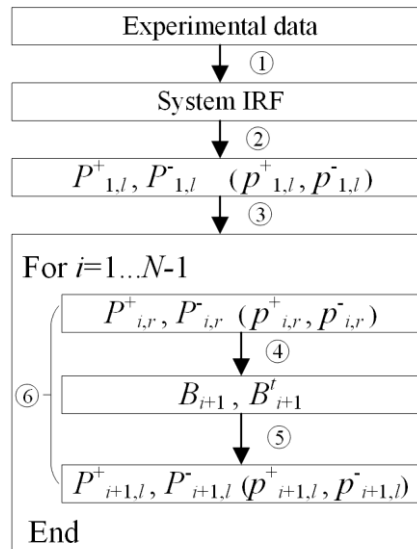


Figure 5.5 Main steps of the modified layer peeling method for pipeline condition assessment.

5.3 Numerical Verification

Numerical simulations were conducted on several reservoir-pipeline-valve systems to verify the proposed approach for pipeline condition assessment. The MOC (Wylie and Streeter 1993) has been used to obtain the transient pressure responses induced by a flow fluctuation. For large pipes with a constant outer diameter, a small change in wall thickness slightly alters the inner diameter, but can cause large change in the wave speed according to Eq.(5-8). Thus, only the

wave speed varies along the pipeline to simulate extended deterioration, and the inner diameter stays constant in the numerical cases.

5.3.1 Case 1: Frictionless pipe

The first case study was conducted for a frictionless metallic pipeline with a uniformly deteriorated section and a non-uniformly deteriorated section. The inner diameter of the frictionless pipeline is assumed to be 600 mm throughout, and the wave speed in the normal sections of the pipeline is 1000 m/s. The pipeline configuration and the properties of the deteriorated sections are given in Figure 5.6. The wave speed in the uniformly deteriorated section is 800 m/s. The wave speed in the non-uniformly deteriorated section has a gradual change from 1000 m/s to 800 m/s and back to 1000 m/s following one period of a cosine pattern of degradation over a length of 108.3 m. A pressure pulse wave, shown in Figure 5.7 (a), induced by a flow pulse was injected into the pipeline at the upstream face of the closed valve, and the wave reflections were simulated using a frictionless MOC model (time step = 0.001 s for all the numerical cases) that was given in Figure 5.7 (b). The primary reflections marked in the figure were directly induced by the deteriorated sections, and the other much smaller reflections were caused by high-order reflections. Note that reflections from the closed valve (dead-end) contributed to the signals seen in Figure 5.7 (b).

The proposed layer-peeling-based technique applied to the signals in Figure 5.7 accurately yields reconstructed wave speed distributions that are almost identical to the theoretical values (as shown in Figure 5.8). To determine how robust the proposed method is against measurement noise, the reflection signal was contaminated with white Gaussian noise, with a signal-to-noise ratio of 10. The mixed signal shown in Figure 5.9 (a) was then used to calculate the system IRF [Figure 5.9 (b)] of the pipeline using Eq. (5-3). The modified layer peeling method, without considering any wave dissipation or dispersion, was then applied to reconstruct the pipeline. The outcome shown in Figure 5.10 demonstrates that the proposed technique can reconstruct the pipeline condition (wave speed in this case) for both uniformly and non-uniformly deteriorated sections, even when measurement noise is present.

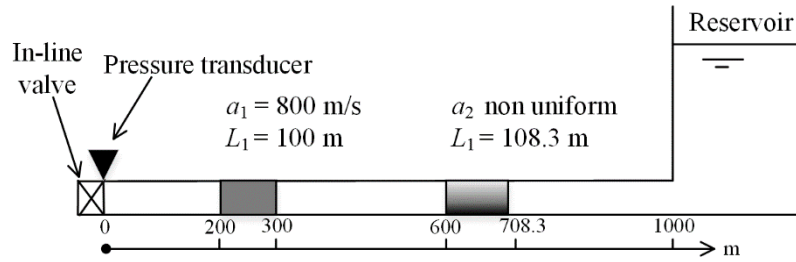


Figure 5.6 Pipeline configuration 1.

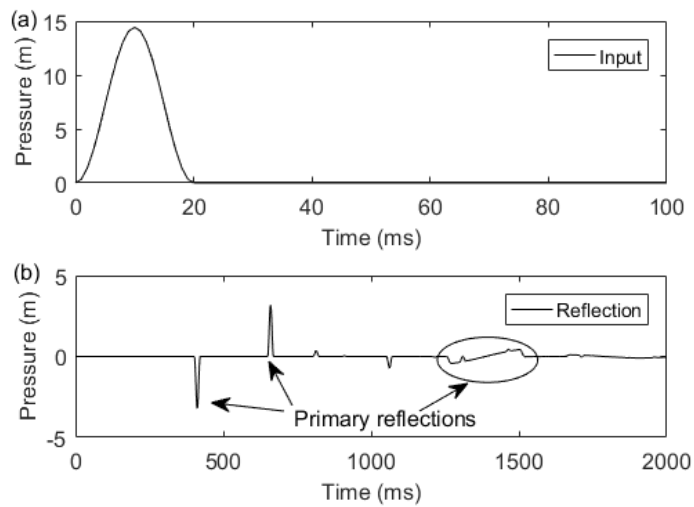


Figure 5.7 Input and reflected signals.

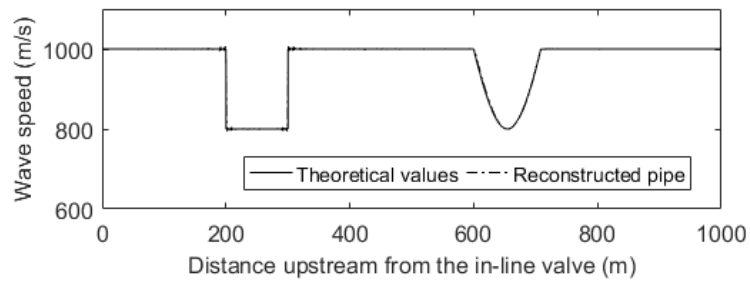


Figure 5.8 Wave speed reconstructed from the modified layer peeling method for the frictionless pipe without measurement noise. (The two plots are virtually coincident)

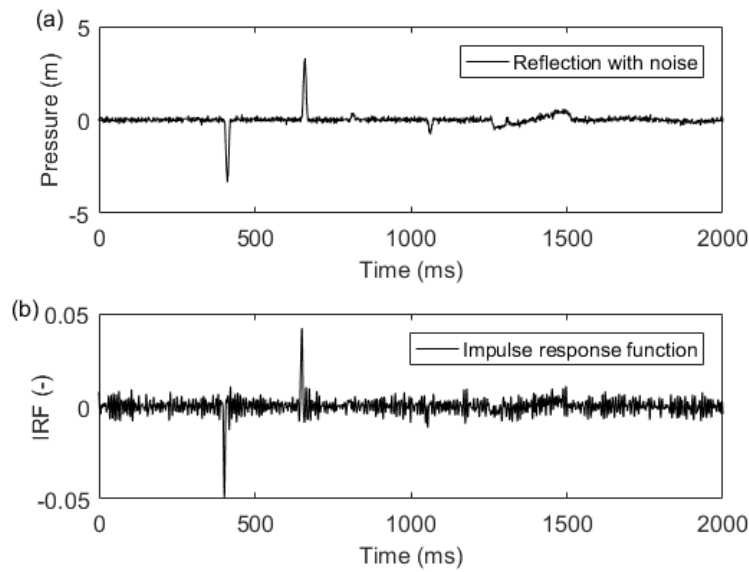


Figure 5.9 Reflection with noise and IRF.

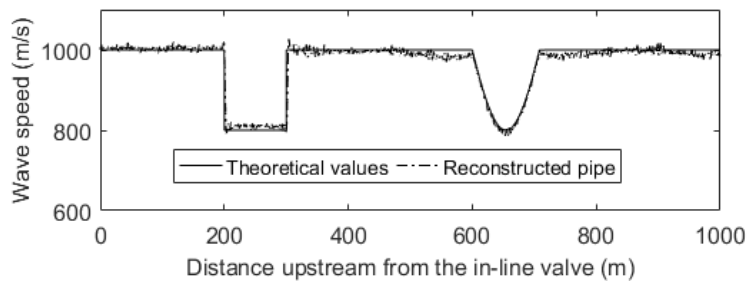


Figure 5.10 Wave speed reconstructed from the modified layer peeling method for the frictionless pipe with measurement noise.

5.3.2 Case 2: Effects of unsteady friction

A reservoir-pipeline, closed-valve system with one uniformly deteriorated section (shown in Figure 5.11) was considered to analyze the effect of the unsteady friction. The inner diameter of the pipeline is 50.6 mm and the wave speed of a normal pipeline is 1000 m/s. The steady-state flow rate Q_0 is 0.1 L/s ($V = 0.05\text{m/s}$) and the Darcy-Weisbach factor f is 0.02. A smaller-sized pipe (compared to the pipe in Figure 5.6) was chosen to highlight the effect of unsteady friction [unsteady friction effects are insignificant and typically negligible for the primary reflections in large pipes (Stephens et al. 2013)]. A

pulse wave with the same duration and waveform as case 1 was injected into the pipeline just upstream of the closed valve, and the pressure wave reflections at the same point were simulated using an unsteady friction MOC model (Vardy and Brown 1995).

The pipeline was initially reconstructed using the modified layer peeling method which is used in the frictionless case, without considering any signal dissipation or dispersion (thus ignoring unsteady friction), and the result is plotted as the dashed line in Figure 5.12. Obvious errors are shown between 200 m to 350 m.

Another reconstruction was conducted using the modified layer peeling method incorporating the transfer function that describes the unsteady friction using Eq. (5-23), (5-24) and (5-26). It needs to be emphasized that the transfer function was renewed in every step using the wave speed (and wall thickness in the experimental case), calculated in the previous time step. The result shown as the dot-dashed line in Figure 5.12 illustrates that the error was eliminated along the pipeline except at points where the impedance changed sharply (200 m and 300 m). The error at the impedance change interfaces was induced by the ripples of the IRF when transformed from the wave reflections.

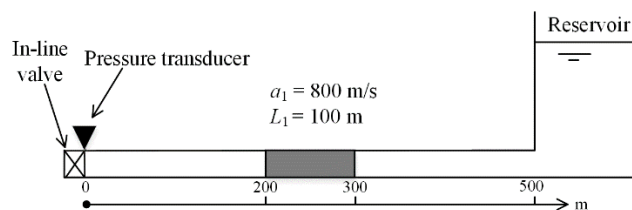


Figure 5.11 Pipeline configuration 2.

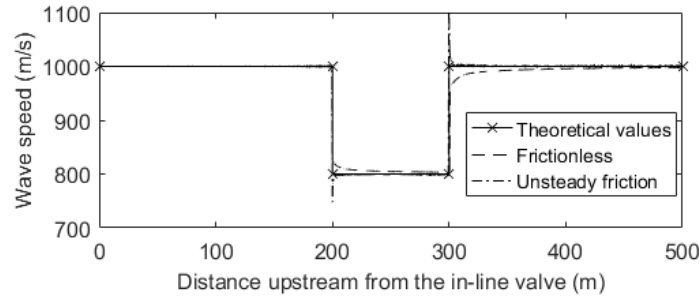


Figure 5.12 Wave speed reconstructed from the modified layer peeling method for the unsteady friction case.

5.3.3 Case 3: Effect of viscoelasticity

The pipeline system shown in Figure 5.13 was used to analyze the viscoelastic effects of the pipe wall. Friction was not considered, so that the viscoelastic effects would be highlighted. The inner diameter of the pipeline was 50.6 mm and the wave speed of a normal pipeline is 393 m/s. The physical details of the pipeline are adapted from the experimental pipeline at Imperial College as reported in Covas et al. (2005), and the viscoelastic parameters used are listed in Table 5.1. A pulse wave with the same duration and waveform as case 1 was injected into the pipeline, and the pressure wave reflections were simulated using a four-element Kelvin-Voigt viscoelastic MOC model (Covas et al. 2005).

Table 5.1 Viscoelastic parameters used in the numerical case.

Retardation time τ_k (s)	Creep coefficients J_k (Pa ⁻¹)
0.005	1.048E-10
0.5	1.029E-10
1.5	1.134E-10
5	8.083E-12

The pipeline was initially reconstructed using the modified layer peeling method, without considering any signal dissipation or dispersion (Model 1) (thus ignoring viscoelasticity). The reconstructed results plotted as the solid line in Figure 5.14 include significant errors at the deteriorated section. Another reconstruction was then conducted using the model incorporating the viscoelastic effects using Eqs. (5-22), (5-24) and (5-26), but excluding the

frequency-dependent wave reflection and transmission (Model 2). This means that the complex characteristic impedances in Eq. (5-27) were replaced by the real characteristic impedances in this model. The results shown as the dashed line in Figure 5.14 illustrate that the error was reduced but still distinct. The third reconstruction was conducted by further considering the frequency-dependent wave reflection and transmission by using complex characteristic impedances in Eq. (5-27) (Model 3). A high correlation was achieved between the reconstructed result (the dot-dashed line) and the theoretical values in Figure 5.14. A small error remains in the part of the pipeline close to the reservoir. This error was caused by neglecting the frequency-dependent characteristics of the wave reflection and transmission in Eqs. (5-35) and (5-36) in the time domain.

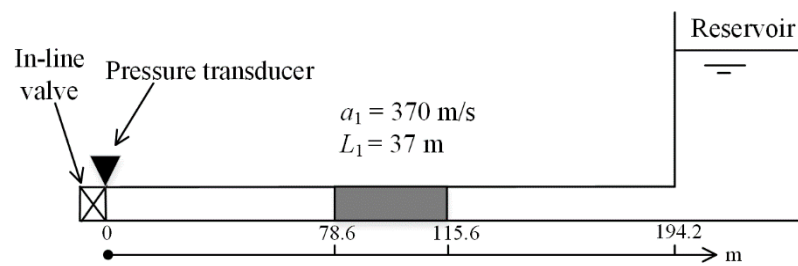


Figure 5.13 Pipeline configuration 3.

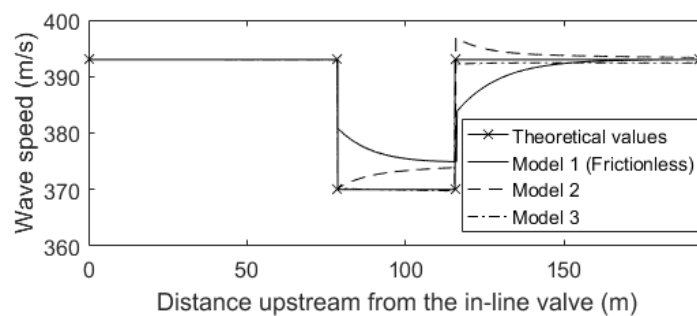


Figure 5.14 Wave speed reconstructed from the modified layer peeling method for the viscoelastic case (Model 2 - with viscoelasticity and frequency-independent wave reflections and transmissions; Model 3- with viscoelasticity and frequency-dependent wave reflections and transmissions).

5.4 Experimental Verification

Laboratory experiments have been conducted in (Gong et al. 2013c) on a single copper pipeline system in the Robin Hydraulics Laboratory at the University of Adelaide to verify the proposed technique for pipeline condition assessment. The experimental results will be used to verify the layer-peeling method proposed in this thesis.

5.4.1 Experimental pipeline layout

The layout of the experimental pipeline system is given in Figure 5.15. The pipeline was connected to a pressurized tank at the upstream side, and a dead-end was created by closure of the in-line valve at the downstream side. The basic geometry parameters are: length $L = 37.46$ m, internal diameter $D_0 = 22.14$ mm and wall thickness $e_0 = 1.63$ mm ($D/e = 13.6$). A pipe section with a thinner pipe wall with $L_1 = 1.649$ m, $D_1 = 22.96$ mm, $e_1 = 1.22$ mm ($D/e = 18.8$) and same material with the original pipeline was placed 17.805 m upstream from the in-line valve. It represents a pipe section with a uniform wall thickness reduction due to internal corrosion. A side-discharge solenoid valve was located 144 mm upstream from the closed in-line valve, for the generation of transient waves.

The wave speed of the pipeline can be calculated using Eq. (5-8) with the following parameters: $E = 124.1$ GPa, $K = 2.149$ GPa, $\rho = 999.1$ kg/m³ and $c_1 = 1.006$ which is assumed to be uniform for a thick-walled pipe. The theoretical wave speed calculated using Eq. (5-8) for the intact pipeline was $a_0 = 1319$ m/s and $a_1 = 1273$ m/s for the thinner-walled section.

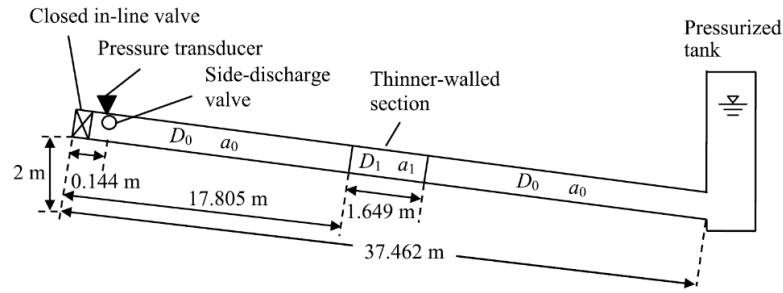


Figure 5.15 System layout of the experimental pipeline system.

5.4.2 Experimental data

A transient wave was generated by sharply closing the side-discharge solenoid valve, which was adjacent to the closed in-line valve. The pressure traces were collected by a Druck PDCR 810 pressure transducer with a 2 kHz sampling rate. Three experiments were conducted using the same configuration, with the pressure traces shown in Figure 5.16.

The pressure trace in the first 6 ms, as shown in Figure 5.16, covered the full wave front and was defined as the input signal to the system. The reflection signal could then be obtained by subtracting the input signal from the original pressure trace. With the input and reflection signals of each experiment, the system IRF of each experiment was obtained using Eq. (5-3), represented as the dash-dotted lines in Figure 5.17. To reduce the background noise, an averaged IRF (represented as the solid line in Figure 5.17) was obtained by averaging these three sets of IRF traces.

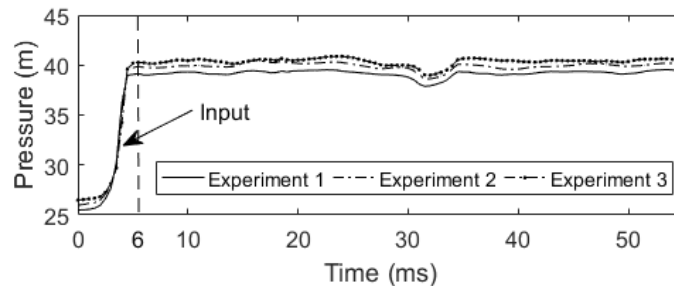


Figure 5.16 Experimental pressure traces.

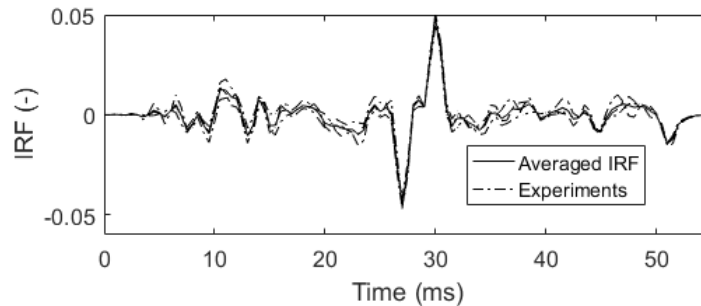


Figure 5.17 Individual IRFs and averaged IRF.

5.4.3 Reconstruction of the pipeline

The pipeline was reconstructed using the proposed approach, with the individual and averaged IRFs. The reconstructed pipelines using the individual IRFs, with the model incorporating the unsteady friction, are plotted in Figure 5.18. A reconstruction using the averaged IRF, using both frictionless and unsteady friction models, is shown in Figure 5.19. A clear dip in the reconstructed wall thickness, and a clear dip in the reconstructed wave speed, which matches well with the theoretical values, can be observed.

Perturbations in the estimated wall thickness and wave speed of the reconstructed pipelines are also illustrated in Figure 5.18 and Figure 5.19. They are caused by the joints in the pipeline, natural variations in the pipeline parameter, fluid-structure interactions, and other uncertainties associated with the experiments.

Slight differences can be seen in Figure 5.20, in which the reconstructed results using the frictionless model and the unsteady friction model are compared. The figure illustrates that the frictionless model gives a conservative result. As the base flow in the pipeline is zero (after the closure of the side-discharge valve), and the pipeline is short in length, the effect of the unsteady friction is marginal in this experimental case. Overall, the experimental results have validated the effectiveness of the proposed layer-peeling-based pipeline condition assessment technique.

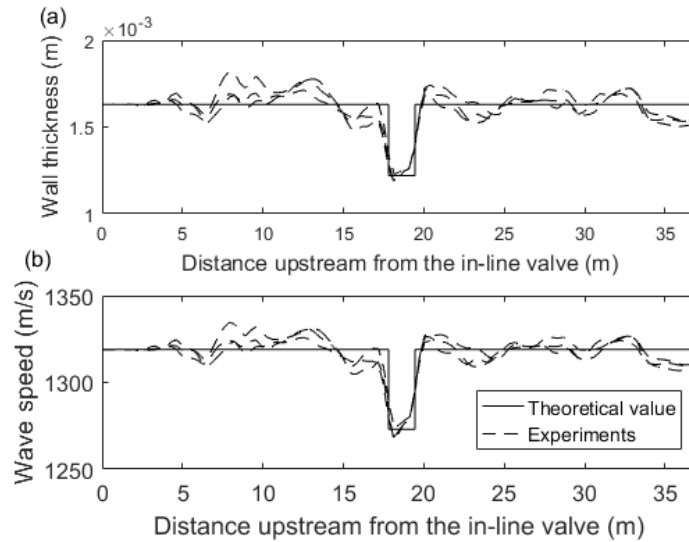


Figure 5.18 Reconstruction using individual IRFs: (a) reconstructed wall thickness distribution compared with the theoretical values; and (b) reconstructed wave speed distribution compared with the theoretical values.

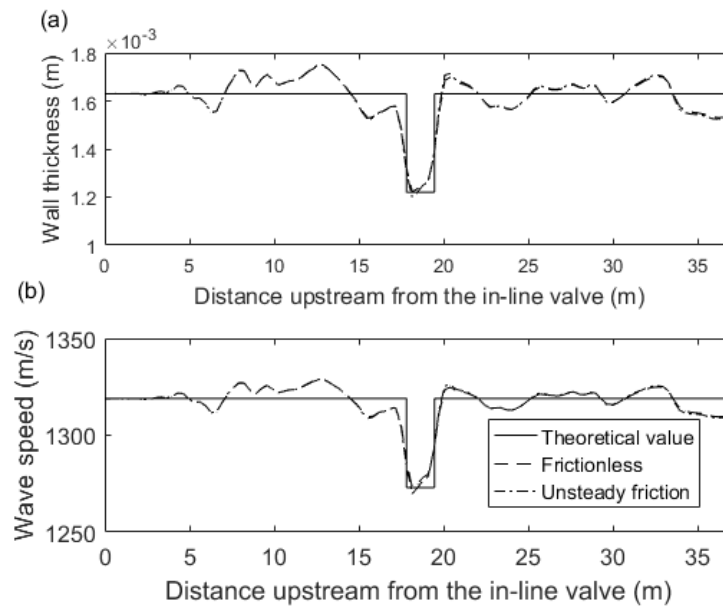


Figure 5.19 Reconstruction using the averaged IRF: (a) reconstructed wall thickness distribution compared with the theoretical values; and (b) reconstructed wave speed distribution compared with the theoretical values.

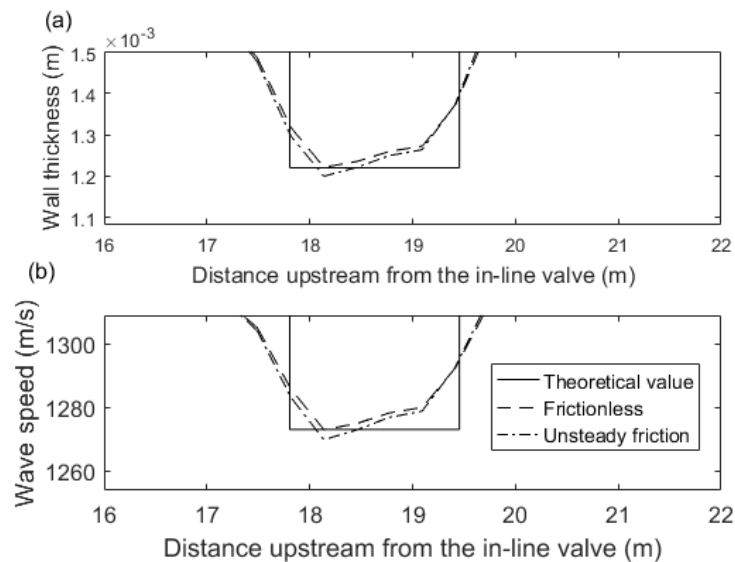


Figure 5.20 An enlarged view of Figure 5.19.

5.5 Discussion

In this section, some practical issues when applying this new approach to field pipelines are discussed. Strategies to refine this approach to enhance its practicality are also included.

5.5.1 Resolution

The proposed technique enables continuous reconstruction of pipeline conditions, which is an advantage over conventional time-domain reflectometry-based techniques that only focus on major reflections and major deteriorations (Gong et al. 2013c; Gong et al. 2015). The spatial resolution of the proposed method is limited by the effective bandwidth of the incident waves, which is determined by the sharpness of the wave front. Theoretically, one can accurately diagnose a deteriorated section with a length longer than $T_p c/2$, where T_p is the duration of the pulse. The duration of the pulse, generated by a side-discharge valve, is typically several milliseconds in the laboratory and tens of milliseconds in the field due to limitations in the maneuverability of the valve. Pressure generators that can generate high-frequency pressure waves, such as

the prototype spark-transient generator (Gong et al. 2018a), will be helpful in increasing the resolution.

5.5.2 Location of the generator

For the approach proposed in this paper, and for some other existing transient-based methods for pipeline condition assessment, the pressure generator and transducer are required to be installed close to the dead-end of the pipe. The dead-end can be achieved by closing an in-line valve, but the installation of a generator and a transducer is not always convenient. Further research will be conducted to extend the new approach to other testing configurations that do not require a dead end.

5.5.3 Wave dissipation and dispersion

This research has demonstrated that errors are likely to occur if the wave dissipation and dispersion are not properly considered in the algorithm. In field pipelines, there are uncertainties and variations in the wave dissipation and dispersion, and they are difficult to predict using theoretical models. Further research is needed to enable the *in-situ* calibration of the wave dissipation and dispersion.

5.6 Conclusions

This paper has proposed a novel approach for pipeline condition assessment. The layer peeling method previously applied to tubular musical instruments has been modified to accommodate the differences between musical instruments and water pipelines. The long source tube, which was used in the original method, has been eliminated. Unsteady friction of the transient flow, and the viscoelastic effects of the pipe wall, have been incorporated into the new method. Frequency dependent wave reflections and transmissions were also incorporated into the method. This research has demonstrated that the wall condition of water pipelines can be assessed using the reconstructed results, using the modified layer peeling method.

Numerical simulations conducted in this research have demonstrated that 1) the proposed approach can deal with multiple, deteriorated sections including non-uniformly distributed deteriorations; 2) reasonably accurate results can be achieved even when the signal is contaminated by moderate background noise; 3) wave dissipation and dispersion can be accounted for using a transfer function that is constructed to consider the unsteady friction of the transient flow and the viscoelastic effects of the pipe wall; and 4) frequency-dependent wave reflection and transmission can be incorporated in the frequency domain, and that this is important for viscoelastic pipes.

The experimental results further validated the new pipeline condition assessment approach. Three sets of experimental data were used to obtain the averaged IRF, which is the input for the modified layer peeling algorithm. The pipeline with a thinner-walled section was successfully reconstructed both with and without the unsteady friction of transient flow.

The proposed layer-peeling pipeline condition assessment technique is a promising alternative to other existing methods because of both its computational efficiency and its ability to assess a long pipe section continuously. The method is capable of conveniently incorporating wave dissipation and dispersion, and frequency-dependent reflection and transmission. Thus, it has the potential to allow engineers to conduct reliable condition assessments for real pipelines, including viscoelastic pipes.

Acknowledgements

The research presented in this paper has been supported by the Australian Research Council through the Discovery Project Grant DP170103715. The author would like to acknowledge Leticia Mooney for her editorial assistance as this paper was finalized.

Chapter 6

Condition Assessment of Pipelines using a Bi-directional Layer-Peeling Method and a Dual-sensor Configuration (Journal Publication 4)

Wei Zeng¹, Jinzhe Gong¹, Benjamin S. Cazzolato², Aaron C. Zecchin¹, Martin F. Lambert¹ Angus R. Simpson¹

¹School of Civil, Environmental and Mining Engineering, the University of Adelaide, Adelaide, SA 5005 Australia

²School of Mechanical Engineering, University of Adelaide, SA 5005, Australia

Citation: Zeng, W., Gong, J., Cazzolato, B. S., Zecchin, A. C., Lambert, M. F., Simpson, A. R. (2019). "Condition assessment of pipelines using a bi-directional layer-peeling method and a dual-sensor configuration." *Journal of Sound and Vibration*, 457(9), 181-196. DOI: 10.1016/j.jsv.2019.05.054.

Statement of Authorship

Title of Paper	Condition assessment of pipelines using a bi-directional layer-peeling method and a dual-sensor configuration
Publication Status	<input checked="" type="checkbox"/> Published <input type="checkbox"/> Accepted for Publication <input type="checkbox"/> Submitted for Publication <input type="checkbox"/> Unpublished and Unsubmitted work written in manuscript style
Publication Details	Zeng, W., Gong, J., Cazzolato, B., Zecchin, A., Lambert, M., Simpson, A. (2019). Condition assessment of pipelines using a bi-directional layer-peeling method and a dual-sensor configuration. Journal of Sound and Vibration, 457(9)

Principal Author

Name of Principal Author (Candidate)	Wei Zeng		
Contribution to the Paper	Conception and design of the project Analysis and interpretation of research data Draft the paper		
Overall percentage (%)	75 %		
Certification:	This paper reports on original research I conducted during the period of my Higher Degree by Research candidature and is not subject to any obligations or contractual agreements with a third party that would constrain its inclusion in this thesis. I am the primary author of this paper.		
Signature		Date	8/11/2019

Co-Author Contributions

By signing the Statement of Authorship, each author certifies that:

- i. the candidate's stated contribution to the publication is accurate (as detailed above);
- ii. permission is granted for the candidate to include the publication in the thesis; and
- iii. the sum of all co-author contributions is equal to 100% less the candidate's stated contribution.

Name of Co-Author	Jinzhe Gong		
Contribution to the Paper	Conception and design of the project Analysis and interpretation of research data Critically revising the paper		
Signature		Date	24/11/19

Name of Co-Author	Benjamin Cazzolato		
Contribution to the Paper	Conception and design of the project Analysis and interpretation of research data Critically revising the paper		
Signature		Date	8th Nov. 2019

Please cut and paste additional co-author panels here as required.

Name of Co-Author	Aaron Zecchin		
Contribution to the Paper	Conception and design of the project Analysis and interpretation of research data Critically revising the paper		
Signature		Date	15/11/19

Name of Co-Author	Martin Lambert		
Contribution to the Paper	Conception and design of the project Analysis and interpretation of research data Critically revising the paper		
Signature		Date	22/11/19

Name of Co-Author	Angus Simpson		
Contribution to the Paper	Conception and design of the project Analysis and interpretation of research data Critically revising the paper		
Signature		Date	4 Nov. 2019

Abstract

Over the past two and a half decades, hydraulic transients have been proposed and also used to assess the condition of pipeline systems through detection of anomalies such as extended pipe wall corrosion and blockages. This paper proposes a new bi-directional layer-peeling method which is capable of reconstructing estimates of the spatial distribution of the pipe wall thickness section by section both in the upstream and the downstream direction from the measurement site. Effects of branched pipes connected to the main pipe are also incorporated into the developed approach. A dual-sensor (a pair of closely placed pressure transducers at one measurement site), instead of a single pressure transducer, is used to both measure the pressure traces and to separate the directional hydraulic transient waves. The layer-peeling method originally developed in the acoustics field has been adapted and further developed to allow bi-directional reconstruction for pressurized water pipes. Numerical verifications are performed on a pipeline with three deteriorated sections and a uniform branch. The deteriorated sections in the pipeline are successfully detected using the pressure traces simulated by the method of characteristics (MOC). Experimental verification is also conducted on a laboratory copper pipeline, and two sections of pipe with thinner wall thicknesses, located on both sides of the dual-sensor, are successfully detected.

6.1 Introduction

Ageing water distribution systems normally consist of pipes that are old and deteriorating. Pipes buried underground are not easily observable. Thus, their condition is difficult and expensive to determine. Over the past two decades, a number of noninvasive hydraulic transient-based methods (Colombo et al. 2009; Xu and Karney 2017) have been developed for detecting discrete pipeline faults, such as leaks (Brunone and Ferrante 2001; Lee et al. 2005b; Colombo et al. 2009; Covas and Ramos 2010; Duan et al. 2011; Capponi et al. 2017) and discrete blockages (Wang et al. 2005; Lee et al. 2008b; Meniconi et al. 2011b). Over the past 15 years, increasing attention has focused on the assessment of pipe wall condition and the detection of distributed deterioration, such as extended wall thickness reduction which may be caused by either internal or external widespread corrosion of the metallic pipe wall and/or spalling of cement mortar lining of the pipe (Stephens et al. 2013; Gong et al. 2015), and extended blockages (Duan et al. 2012; Louati et al. 2017; Jing et al. 2018; Louati and Ghidaoui 2018) that may be caused by tuberculation. Distributed deterioration may reduce the water transmission efficiency (Tran et al. 2010), create water quality problems (Vreeburg and Boxall 2007) and may develop into bursts or severe blockages over time (Zamanzadeh et al. 2007). Thus, cost-effective pipe wall condition assessment approaches are needed to allow strategically targeted pipe maintenance, replacement and rehabilitation.

The transient-based pipe wall condition assessment techniques that have been validated in the field typically use a transient wave generator and multiple pressure transducers located sparsely along a pipeline (e.g. hundreds of meters apart in the field). By operating a generator connected with the pipe, such as aside-discharge valve, a portable pressure wave maker (Brunone et al. 2008; Meniconi et al. 2010), a spark generator (Gong et al. 2018a) or a piezoelectric wave generator (Lee et al. 2017), transient pressure waves can be excited. The incident wave propagates along both in the upstream and downstream directions of the pipeline, and induces specific wave reflections when encountering physical changes, such as a pipe section with a different wall thickness. The

measured pressure responses can be analyzed by inverse transient analysis (ITA) to provide a high spatial resolution wall thickness assessment (Stephens et al. 2008; 2013). The ITA approach was originally developed for leak detection in pipe networks (Liggett and Chen 1994; Vítkovský et al. 2000; 2007; Covas and Ramos 2010). It involves an iterative optimization process to find the numerical pipeline model whose pressure responses best match the real measurements. However, ITA does has disadvantages. It is computationally expensive since thousands to millions of numerical transient behavior simulations using the MOC are needed. A computationally efficient alternative is the direct wave reflection analysis approach, which directly calculates the impedance of the anomalous pipe sections from the size of the major wave reflections and finds the location from the arrival time of the reflection (Gong et al. 2015; Gong et al. 2016b); however, only major deteriorated sections can be identified and the technique is difficult to apply if the pipe condition is complex.

Other pipe wall condition assessment techniques typically require a dead-end with a transient generator and a pressure transducer in close proximity. The incident pressure wave only propagates towards one end of the pipe and wave reflections as measured are all from one direction. This simplifies the data analysis and several techniques have been proposed, including direct wave reflection analysis (Gong et al. 2013c), frequency response analysis (Duan et al. 2012) and the reconstructive MOC technique (Gong et al. 2014a).

Detection methods have also been developed in the acoustics field with applications to the detection of blockages in acoustic ducts. Wu and Fricke (1989) used the eigenfrequency shifts caused by a blockage to determine its position and dimensions, and reconstructed the cross-sectional area of the duct (Wu and Fricke 1990). Further improvements make the reconstruction more practical and operable for acoustic ducts (De Salis and Oldham 1999, 2001; Bilotta et al. 2016). However, wall thickness changes in water pipelines will only induce very limited shifts in the resonant frequencies, which are difficult to measure (Lee et al. 2008b). Another acoustic method is the layer peeling method which was proposed to reconstruct tubular acoustic systems with varying cross sections by analysing the impulse response function (Amir and

Shimony 1995a, b). Further applications and developments of the method were made by Sharp and Campbell (1997) to reconstruct the interior shape of musical wind instruments. Improvements of the method were also achieved by increasing the length of the objects that can be reconstructed (Sharp 1998) and reducing the ripples of the reconstructed results (Forbes et al. 2003).

The layer-peeling method has been modified to allow pipeline condition assessment for the first time in (Zeng et al. 2018). In this first-generation technique, the wave reflections are recorded then transferred to an impulse response function (IRF) and fed into a modified layer-peeling algorithm. The wave dissipation and dispersion caused by the unsteady friction effects of the transient flow (Vardy and Brown 2003) and the viscoelastic behaviour of the pipe wall are incorporated into the modified algorithm in the frequency domain. The normalized wave reflection induced from the interface of two pipe reaches with different properties is used to determine the impedance change of the pipeline in the time domain. This hybrid frequency-time domain approach can accurately reconstruct the impedance along a pipeline, and thus assess its wall condition. However, some limitations exist in this first-generation layer-peeling method (as well as in the other methods reviewed in above) and have impeded the application to pipelines in water distribution systems (WDSs). These are outlined as follows: 1) it is difficult to satisfy the requirement that both the incident transient wave is injected into the pipeline at a dead-end and that the pressure responses are measured immediately upstream of the dead-end; 2) off-takes and cross-connections in a pipeline network may also generate wave reflections and affect the wave reflections induced by the deteriorated pipe sections.

The research reported in the current paper makes substantial new developments in the layer-peeling algorithm to solve the above limitations. The new technique enables a bi-directional reconstruction of the impedance distribution along a pipeline with branches. To apply the bi-directional layer-peeling algorithm for pipe condition assessment, two signal processing techniques are used: 1) a wave separation technique using two transducers in close proximity (referred as a dual-sensor), which was developed in acoustics research field (Seybert and

Ross 1977; Chung and Blaser 1980) and recently adapted into the hydraulic transient research field (Shi et al. 2017); and 2) a singular value decomposition technique (Forbes et al. 2003) to obtain the IRF of the pipeline system. The key innovations of this new technique include: 1) the transient generation and measurement can be conducted at interior points along the pipeline (removing the need of a dead-end boundary condition); 2) the impedance reconstruction and condition assessment can be conducted in both the upstream and downstream directions along the pipeline from the measurement station (yielding high efficiency); and 3) pipelines with branches can be properly analyzed since the effect of wave reflection and transmission at the bifurcation point is incorporated in the algorithm (providing the potential to apply the proposed methodology to pipes in WDSs that contain numerous junctions).

To validate the proposed technique developed in this paper, a pipeline with three deteriorated sections (indicated by lower wave speeds) and including a uniform branch connection is analyzed numerically. A pulse incident wave is injected into the system at an interior point near the middle of the pipeline, and the pressure responses at two locations in close proximity are simulated using the MOC and used as the pressure trace “measurement”. The wave speed distribution of the pipeline is reconstructed using the bi-directional layer-peeling technique, and the reconstructed results are consistent with the actual theoretical values. Experimental verification is then conducted on a copper pipeline with two deteriorated sections (thinner-walled pipe sections). The two pipe sections with thinner wall thicknesses are clearly identified in the reconstructed result using the proposed bi-directional layer peeling method.

6.2 Problem Formulation and Framework of the New Method

6.2.1 Problem formulation

In the first-generation layer-peeling-based pipeline condition assessment technique that was previously developed (Zeng et al. 2018), a transient pressure

wave generator and a pressure transducer were installed close to a dead-end as shown in Figure 6.1. In a WDS, such as a simple pipe network shown in Figure 6.2, wave generators and pressure transducers can be only connected to the pipeline through specific fittings such as fire hydrants and air valves. For the pipe sections in the dashed box 1 in Figure 6.2, transient waves injected through the hydrant will propagate in both the upstream and the downstream directions of the pipeline. Even if a hydrant in the vicinity of a dead-end can be found (such as the dashed box 2), branches connected to the pipe section of interest will cause wave reflections and the existing data analysis techniques developed for single pipelines will be difficult to apply. A more common situation is that shown in dashed box 3 in Figure 6.2, where the transient wave can only be injected into the pipeline at an interior point and branch pipes are connected to the main pipeline under assessment.

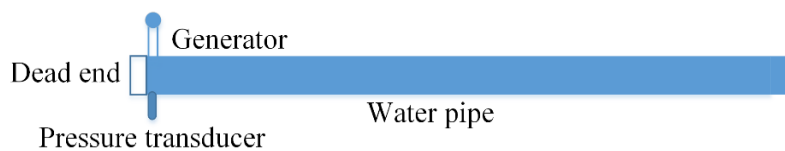


Figure 6.1 Schematic diagram of the testing system for the single-sided layer-peeling method (both generator and pressure transducer are located close to the dead end).

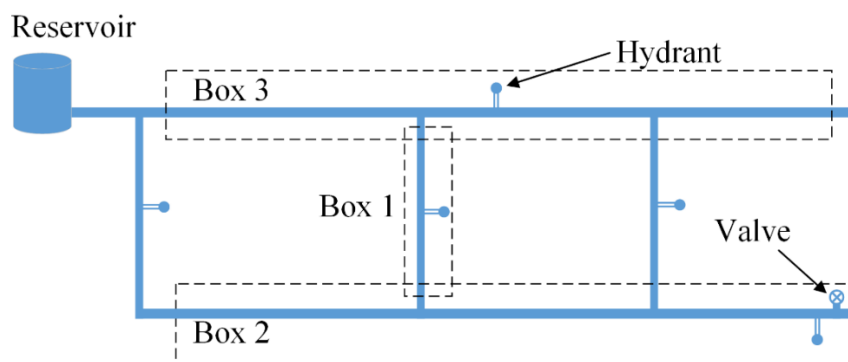


Figure 6.2 Schematic diagram of a pipeline network (each of the five hydrants may be used to locate the wave generator and the dual-pressure transducer).

To make the layer-peeling-based pipeline condition assessment technique applicable to pipe sections in a network, a system configuration shown in Figure 6.3 is considered in this paper. The wave generator (a side-discharge valve) which is located close to the dead-end in (Zeng et al. 2018) is moved to an interior point in the pipeline (such as a fire hydrant or air valve). A pair of pressure transducers in close proximity (approximately 1 m apart), which is referred to as a dual-sensor hereon, is used to separate the transient waves and thus obtain directional wave reflections. The pipe section between the pressure transducers in close proximity is assumed to be uniform.

The branch pipe in this study is assumed to have spatially uniform in properties, such that only the effect of the bifurcation node is considered. This assumption is valid when the reflections induced by the impedance change along the branch pipe are insignificant. Otherwise, the the range of the assessment on the corresponding side should be limited to the section from the generator to the branch pipe. The branch pipe is also assumed to be longer than the main pipe section that is at the right hand side of the bifurcation node, such that the boundary reflection from the branch pipe will not combine with the wave reflections from the main pipe. Otherwise, the boundary reflection needs to be accounted for based on the length of the branch pipe.

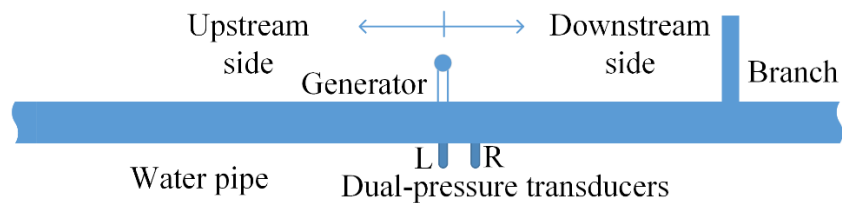


Figure 6.3 Schematic diagram of the testing configuration for the bi-directional layer-peeling-based pipeline condition assessment technique.

6.2.2 The framework of the bi-directional layer-peeling method

The pipeline in Figure 6.3 is divided into $2N$ sections with N sections in each side. The section number between the two sensors L and R is assumed to M .

This sub-section details the framework of the bi-directional layer-peeling technique (Figure 6.4), which is closely linked with the wave propagation process as shown in Figure 6.5. In Figure 6.5, H_i represents the wave dissipation and dispersion in the time domain, r and s are the wave reflection and transmission ratios, the superscripts (+ and –) illustrate forward and backward directions respectively, the subscripts l and r represent the left side and right side of the pipe section (note that these points are internal within the pipe section), The characters P (frequency domain) and p (time domain) represent the impulse response and B is the pipeline impedance. The left sensor (indicated by L) from Figure 6.3 corresponds to Box ① in Figure 6.5, while the right sensor is not shown in Figure 6.5.

The reconstruction procedures are the same for both the upstream and downstream sides of the pipe except for the wave propagation direction. Therefore, without loss of generality, only the approach for the downstream side of the pipe is illustrated to simplify the notation and description. As shown in Figure 6.4 and Figure 6.5, the experimental data measured by the sensors at L and R in Figure 6.3 were first processed [Step (1) and (2) in Figure 6.4 and Box ① in Figure 6.5]. Directional pressure waves at the generator were obtained by using a wave separation technique and then transferred to directional IRFs. The impulse responses at the left side of the first pipe section ($p_{1,l}^+$ and $p_{1,l}^-$) were then obtained using the calculated directional IRFs and imported into the bi-directional layer-peeling algorithm. By formulating the wave propagating process along a pipe section with the transfer function H_i , the impulse responses at the right side ($p_{1,r}^+$ and $p_{1,r}^-$) can be calculated [Step (3) in Figure 6.4 and Box ② in Figure 6.5]. They can be used to get the wave reflection ratio between two conjoint pipe sections [Step (4) in Figure 6.4] and then get the pipeline impedance of the next pipe section [Step (5) in Figure 6.4] based on the reflection ratio. By formulating the wave transmission and reflection at cross-sections or at branch connections, the impulse responses at the left side of pipe section 2 can be calculated [Step (6) in Figure 6.4 and Box ③ in Figure 6.5], and the above procedures can be circulated to calculate the pipeline impedance of the remaining pipe sections [Step (7) in Figure 6.4].

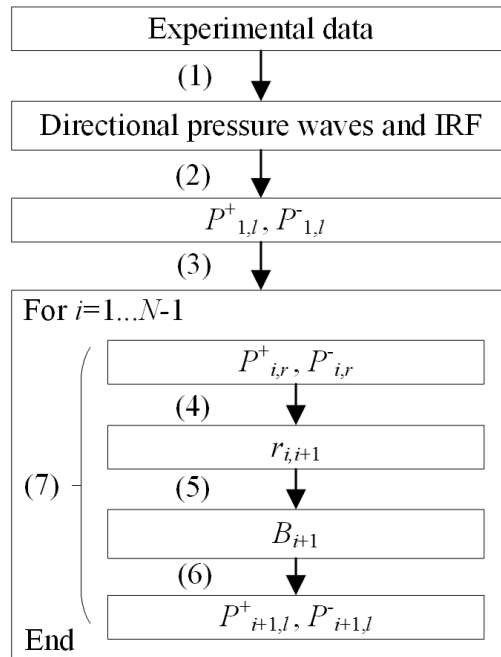


Figure 6.4 Main steps of the bi-directional layer-peeling method for pipeline condition assessment (numbers in the brackets represent the steps).

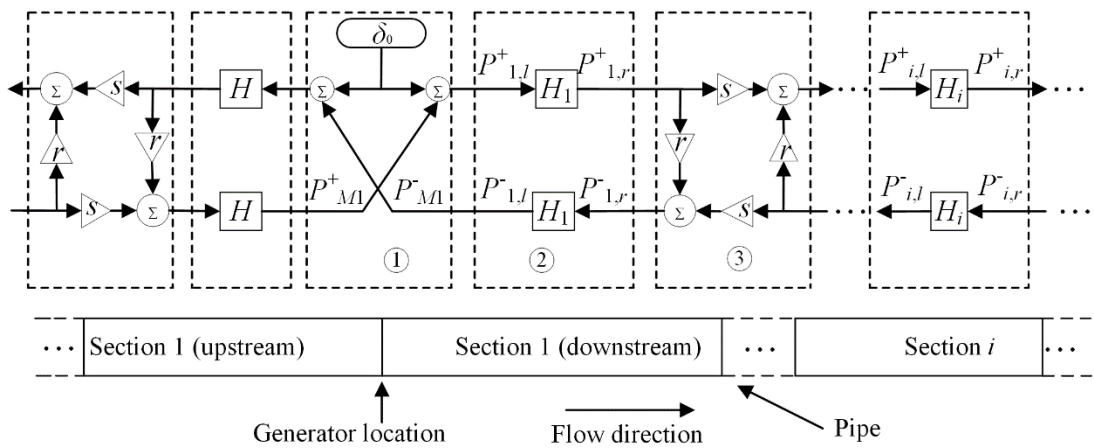


Figure 6.5 Block diagram describing the wave propagation process in a pipeline along two directions (both upstream and downstream).

6.3 Mathematic Processes of the Bi-directional Layer-Peeling Method

Corresponding to the major steps described in the previous section, the mathematic processes of the bi-directional layer-peeling method are given in this section.

6.3.1 Pre-processing of transient pressure data

(a) Wave separation

As shown in Figure 6.3, the measured pressure at sensor L at each time step is the sum of the forward and the backward waves. In the frequency-domain, the pressure measurement at sensor L (excluding the wave input $\hat{p}_l(t)$ which can be separated from the measured pressure traces) can be described as

$$\hat{P}_{M1}(j\omega) = \hat{P}_{M1}^+(j\omega) + \hat{P}_{M1}^-(j\omega) \quad (6-1)$$

where j represents the imaginary unit, and ω represents the angular frequency. The capitalised character \hat{P} with the hat represents the measured pressure in the frequency domain. The forward wave at L will reach R and the backward wave at R will reach L after passing M sections (the distance between the two sensors), thus the pressure at R is

$$\hat{P}_{M2}(j\omega) = \hat{P}_{M1}^+(j\omega)H^M(j\omega) + \hat{P}_{M1}^-(j\omega)/H^M(j\omega) \quad (6-2)$$

where $H^M(j\omega)$ represents the wave propagation transfer function of these M sections. A rearrangement of Eqs. (6-1) and (6-2) gives

$$\hat{P}_{M1}^+(j\omega) = \frac{\hat{P}_{M1}(j\omega) - \hat{P}_{M2}(j\omega)H^M(j\omega)}{1 - H^{2M}(j\omega)} \quad (6-3)$$

$$\hat{P}_{M1}^-(j\omega) = \frac{\hat{P}_{M2}(j\omega)H^M(j\omega) - \hat{P}_{M1}(j\omega)H^{2M}(j\omega)}{1 - H^{2M}(j\omega)} \quad (6-4)$$

Eqs. (6-3) and (6-4) can be used to obtain the directional pressure waves (\hat{P}_{M1}^+ and \hat{P}_{M1}^-) from the original pressure measurements by following the wave separation technique described in (Shi et al. 2017).

(b) Directional IRF

Considering directional pressure waves, the relationship between the injected wave $\mathbf{x} = [\hat{p}_I(0), \hat{p}_I(1) \cdots \hat{p}_I(N-1)]$ and the directional wave reflections $\mathbf{y} = [\hat{p}_{M1}^+(0), \hat{p}_{M1}^+(1) \cdots \hat{p}_{M1}^+(N-1)]$ or $[\hat{p}_{M1}^-(0), \hat{p}_{M1}^-(1) \cdots \hat{p}_{M1}^-(N-1)]$ can be defined using matrix notation as

$$\mathbf{y} = \mathbf{Xz} \quad (6-5)$$

where \mathbf{z} is the directional IRF that represents the response of one side of the pipe system to an ideal impulse input, and \mathbf{X} is a lower triangular matrix of $x_{ij} = x_{i-j+1}$ for $j \leq i$ and $x_{ij} = 0$ for $j > i$. A singular value decomposition of \mathbf{X} gives $\mathbf{X} = \mathbf{U}\mathbf{\Lambda}\mathbf{V}^T$, where \mathbf{U} , \mathbf{V} are orthonormal matrices composed of column vectors \mathbf{u}_i and \mathbf{v}_i , respectively, and $\mathbf{\Lambda}$ is a diagonal matrix composed of singular values λ_i sorted in descending order of size. Using a combination of a *truncation regularization* and a *Tikhonov's regularization*, the directional IRF can be obtained as (Forbes et al. 2003)

$$\mathbf{z} = \left(\sum_{i=1}^J \frac{\lambda_i}{\lambda_i^2 + \alpha_c} \mathbf{u}_i \mathbf{v}_i^T \right) \mathbf{y} \quad (6-6)$$

where $J < N$ is the truncation point and α_c is the *Tikhonov* regularization parameter. A smoother but less sharp IRF can be obtained by using a smaller J or a larger α_c . These two parameters were determined by trial and error until satisfactory results were achieved in the cases investigated in this paper (Forbes et al. 2003). Advanced methods, such as the Generalized Cross Validation and L-curve (Wang et al. 2018) can be used to obtain the optimal parameters.

By applying Eq. (6-6) to $\hat{p}_{M1}^+(t)$ and $\hat{p}_{M1}^-(t)$ with the wave input $\hat{p}_I(t)$, the directional IRFs at point L can be obtained.

(c) Input to the bi-directional layer-peeling algorithm

Apart from the forward impulse signal δ_0 as shown in Figure 6.5, the reflections of the backward impulse signal p_{M1}^+ will eventually enter into the right side of the pipeline. Therefore, the input to the right side of the pipeline is

$$p_{1,l}^+ = \delta_0 + p_{M1}^+ \quad (6-7)$$

where δ_0 is a pulse signal with $\delta_0 = 1$ at $t = 0$ and $\delta_0 = 0$ when $t \neq 0$. The corresponding output is

$$p_{1,l}^- = p_{M1}^- \quad (6-8)$$

$p_{1,l}^+$ and $p_{1,l}^-$ calculated from Eqs. (6-7) and (6-8) will be then used as the input to the bi-directional layer-peeling algorithm.

6.3.2 Wave reflection and transmission modelling

(a) Wave propagation in a uniform section

Using the concept of steady-oscillatory flow with P^* representing an oscillatory pressure wave, the transient flow in a pressurized pipeline is governed by (Chaudhry 2014)

$$\frac{\partial^2 P^*}{\partial x^2} + \frac{\omega^2}{a_c^2} P^* = 0 \quad (6-9)$$

where a_c is the complex wave speed (Suo and Wylie 1990). If only the steady friction of the transient flow is considered (neglecting unsteady friction and viscoelastic effects of the pipe wall), the complex wave speed can be described by

$$a_c = a \sqrt{\frac{1}{(1-gAR_s j/\omega)}} \quad (6-10)$$

where $R_s = fQ_0/(gDA^2)$; f is the Darcy-Weisbach friction factor; g is the acceleration of gravity; Q_0 is the base flow in the pipeline, D is internal diameter of the pipe; A is the internal cross-sectional area and a is the wave speed that depends on the properties of the fluid and the pipe wall and can be calculated from (Wylie and Streeter 1993)

$$a = \sqrt{\frac{K/\rho}{1+(K/E)(D/e)c_1}} \quad (6-11)$$

where K represents the bulk modulus of elasticity; ρ is the density of water; E is the Young's modulus of elasticity; e is the wall thickness and c_1 is the pipeline restraint factor.

The pressure wave, after propagating for a distance of Δx can be written as

$$P^*(x + \Delta x) = P^*(x)e^{-j\omega\Delta x/a_c} \quad (6-12)$$

According to the wave propagation process in the i th pipe section as shown in Figure 6.6, the incident and reflected waves at two sides of the i th pipe section can be written as

$$P_{i,r}^+ = P_{i,l}^+ H_i \quad (6-13)$$

$$P_{i,r}^- = P_{i,l}^- / H_i \quad (6-14)$$

where $H_i = e^{-j\omega\Delta x_i/a_{c,i}}$ which represents the wave dissipation and dispersion in the i th pipe section.

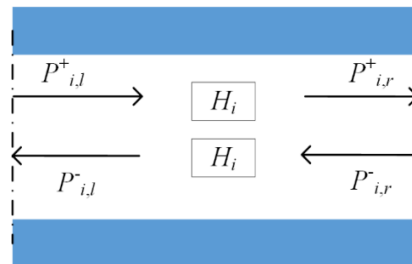


Figure 6.6 Wave propagation in the i th pipe section.

(b) Reflection and transmission ratios and scattering equations at discontinuities

If an incident pressure wave meets a discontinuity (impedance change) in the pipe from the i^{th} section to the $(i+1)^{\text{th}}$ section as shown in Figure 6.7 (a), the reflection coefficient r and the transmission coefficient s can be calculated using the formulae (Chaudhry 2014)

$$r_{i,i+1} = \frac{B_{i+1} - B_i}{B_{i+1} + B_i} \quad (6-15)$$

$$s_{i,i+1} = \frac{2B_{i+1}}{B_{i+1} + B_i} = 1 + r_{i,i+1} \quad (6-16)$$

in which $B_i = a_i/gA_i$ and the subscript $i, i + 1$ represents the wave propagating from the i^{th} section to the $(i+1)^{\text{th}}$ section. If unsteady friction of the transient flow or the viscoelastic effects of the pipe wall are considered, the characteristic impedance $B_i = a_{c,i}/gA_i$ will be complex and the approach of the layer-peeling method will be more complicated. Details of incorporating unsteady friction and viscoelasticity are comprehensively discussed in other papers and are not presented here.

If the incident wave propagates in the opposite direction (i.e., approaching the interface from the $(i+1)^{\text{th}}$ section), then the reflection coefficient and the transmission coefficient can be calculated as:

$$r_{i+1,i} = -r_{i,i+1}, \quad (6-17)$$

$$s_{i+1,i} = 1 - r_{i,i+1}. \quad (6-18)$$

If an incident pressure wave meets a bifurcation or junction node in the pipe as shown in Figure 6.7 (b), the reflection coefficient r and the transmission coefficient s from section i to section $i+1$ can be calculated using the formulae (Chaudhry 2014)

$$r_{i,i+1} = \frac{-B_i}{2B_0+B_i} \quad (6-19)$$

$$s_{i,i+1} = \frac{2B_0}{2B_0+B_i} = 1 + r_{i,i+1} \quad (6-20)$$

where $B_{i+1} = B_i$, and B_0 is the impedance of the branch. The reflection coefficient and the transmission coefficient will not change if the incident wave propagates in an opposite direction, thus

$$r_{i+1,i} = r_{i,i+1}, \quad (6-21)$$

$$s_{i+1,i} = 1 + r_{i+1,i}. \quad (6-22)$$

The reflection ratio can be also determined by the ratio of the magnitude of the wave reflection to that of the incident wave. Since the initial reflected waves $p_{i,r}^-(iT/2)$ are only caused by the main transmitted wave $p_{i,r}^+(iT/2)$. Thus

$$r_{i,i+1} = \frac{p_{i,r}^-(iT/2)}{p_{i,r}^+(iT/2)}. \quad (6-23)$$

As shown in Figure 6.7, the forward propagating wave $p_{i+1,l}^+$ into section $i+1$ is the sum of the transmitted wave from $p_{i,r}^+$ and the reflected wave induced by $p_{i+1,l}^-$, and the backward propagating wave $p_{i,r}^-$ into section i is the sum of the reflected wave induced by $p_{i,r}^+$ and the transmitted wave from $p_{i+1,l}^-$. Combining Eqs. (6-15) to (6-18), the following scattering equation (Amir and Shimony 1995a) to calculate the directional waves after passing a impedance change can be written as

$$\begin{bmatrix} p_{i+1,l}^+ \\ p_{i+1,l}^- \end{bmatrix} = \frac{1}{1-r_{i,i+1}} \begin{bmatrix} 1 & -r_{i,i+1} \\ -r_{i,i+1} & 1 \end{bmatrix} \begin{bmatrix} p_{i,r}^+ \\ p_{i,r}^- \end{bmatrix} \quad (6-24)$$

Combining Eqs. (6-19) to (6-22), the scattering equation to calculate the directional waves after passing a bifurcation or junction node can be written as

$$\begin{bmatrix} p_{i+1,l}^+ \\ p_{i+1,l}^- \end{bmatrix} = \frac{1}{1+r_{i,i+1}} \begin{bmatrix} 2r_{i,i+1} + 1 & r_{i,i+1} \\ -r_{i,i+1} & 1 \end{bmatrix} \begin{bmatrix} p_{i,r}^+ \\ p_{i,r}^- \end{bmatrix} \quad (6-25)$$

This new scattering equation is incorporated into the new bi-directional layer-peeling method described in the next section.

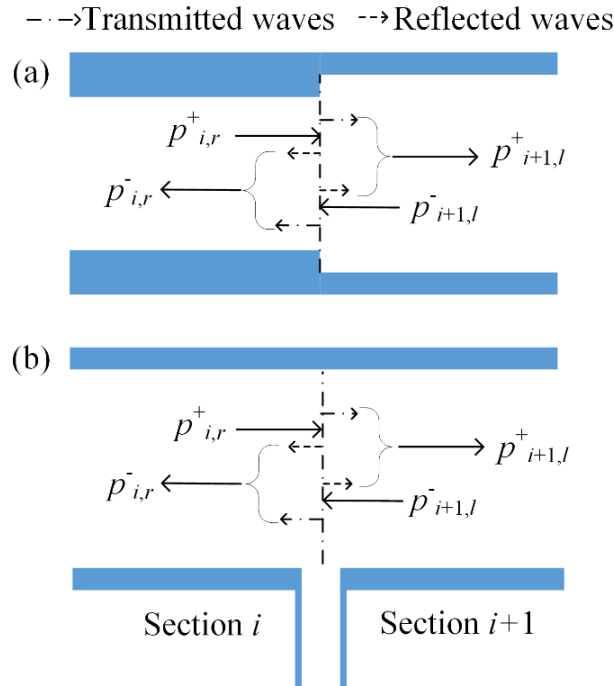


Figure 6.7 Wave propagation process with (a) an impedance change; and (b) a bifurcation or junction node.

6.3.3 The circulation process of the bi-directional layer-peeling algorithm

The major steps of the bi-directional layer-peeling method are summarized with corresponding equations used in each step to facilitate readers to replicate the simulation.

Step 1: Extract the directional pressure waves from measured experimental data using a wave separation approach (based on Eqs. (6-3) and (6-4)), and calculate the directional IRFs through Eq. (6-6).

Step 2: Calculate the input to the layer-peeling algorithm through Eqs. (6-7) and (6-8).

Step 3: (Wave propagation in a uniform section) Calculate the waves at the right side of the i^{th} ($i=1$ for the first step) section $P_{i,r}^+$ and $P_{i,r}^-$ through Eqs. (6-13) and (6-14) using the waves at the left side of the i^{th} section $P_{i,l}^+$ and $P_{i,l}^-$.

Step 4: Use $P_{i,r}^+$ and $P_{i,r}^-$ to calculate the reflection ratio $r_{i,i+1}$ through Eq.(6-23).

Step 5: Calculate the characteristic impedance of the next section B_{i+1} through Eq. (6-15) for an impedance change or setting $B_{i+1} = B_i$ for a bifurcation or junction node (note that the location of the bifurcation or junction node is known *a priori*).

Step 6: Use $P_{i,r}^+$ and $P_{i,r}^-$ and $r_{i,i+1}$ to calculate the waves at the left side of the $(i+1)^{\text{th}}$ section $P_{i+1,l}^+$ and $P_{i+1,l}^-$ through Eq. (6-24) for an impedance change or Eq.(6-25) for a bifurcation or junction node.

Step 7: Iterate steps 4 to 6 for $i=2\dots N-1$ to calculate the characteristic impedances, wave speeds and wall thicknesses for the remaining sections. Now the reconstruction of the pipeline has been completed for the section to the right hand side of the generator in Figure 6.3.

Step 8: Reverse the pipeline direction and repeat steps 2 to 6 for the original left side of the pipeline section in Figure 6.3 to reconstruct the characteristic impedances, wave speeds and wall thicknesses.

6.4 Numerical Simulations

6.4.1 System layout and parameters

Numerical simulations have been conducted on a reservoir-pipeline-valve system. The method of characteristics (Wylie and Streeter 1993) has been used

to simulate the transient wave propagation. In the numerical cases, only the wave speed varies along the pipeline and the inner diameter remains constant, the time step has been set as 0.0001 s and only steady friction is considered.

The case study has been conducted for a metallic pipeline with three uniformly distributed deteriorated sections and a uniform branch with details as shown in Figure 6.8. The boundary conditions of the main pipe and the branch do not affect the reconstruction result, and can be reservoirs, valves, dead-ends or junctions. The internal diameter of the main pipeline is 500 mm throughout and the wave speed of the normal pipeline sections is assumed to be 1000 m/s. The Darcy-Weisbach friction factor of $f = 0.02$ is assigned to the entire pipe system. The base flow in the main pipeline is set to be $0.2 \text{ m}^3/\text{s}$ from left to right, and the branch pipe is assumed to have zero base flow. A pulse wave as shown in Figure 6.9 (a) is injected into the system at the middle of the main pipeline at G. The simulated pressure responses at the two measurement points are shown in Figure 6.9 (b).

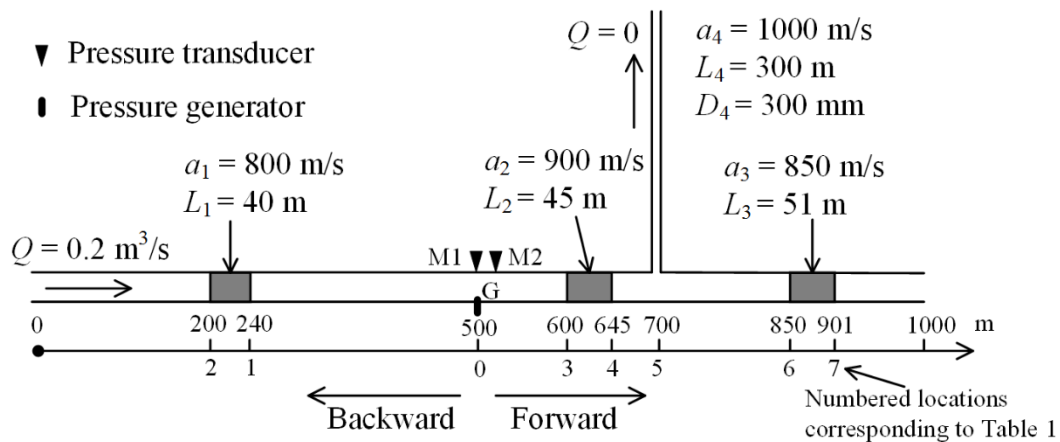


Figure 6.8 Pipeline configuration of the numerical case study.

6.4.2 Data pre-processing

With the simulated pressure traces at L and R the directional wave reflections from two sides of the pipeline can be separated using Eqs. (6-3) and (6-4). The

forward and backward wave reflections are shown in Figure 6.10, through which eleven distinctive wave reflections (with labels) can be observed.

An analysis of the paths of these wave reflections is given in Table 6.1 to illustrate the path and source (labelled as S1, S2, S3, etc. in Figure 6.10) of these wave reflections. Only the first order and second order wave reflections are discussed in detail in Table 6.1 to illustrate the wave paths. Higher order reflections are included in the results shown in Figure 6.9, but they are too small to be observed. Note that the reconstructive algorithms developed in this research take into account all the higher order reflections. It can be seen from Table 6.1 some of the wave reflections contain second-order reflections induced by the bifurcation node or the deteriorated sections from the other side of the pipeline. Taking the forward wave S4 listed in Table 6.1 as an example, the wave is caused by the re-reflection of the backward waves S6 and S7. Another case is given for the backward wave S9, which is composed of a reflected wave by the third deteriorated section and a re-reflection of the forward wave S1. In terms of the wave components propagating along the path 0-6-0, the bifurcation node will diminish the wave once the wave passes through it. The bifurcation node also generates wave reflections, such as the backward wave S8 and the component of the backward wave S11 travelling along the path 0-1-5-0.

Table 6.1 Tracking of the wave reflections.

Forward waves	Wave paths	Backward waves	Wave paths
S1	0-1-0	S6	0-3-0
S2	0-2-0	S7	0-4-0
S3	0-3-1-0	S8	0-5-0
S4	0-3-2-0 / 0-4-1-0	S9	0-6-0 / 0-1-3-0
S5	0-5-1-0 / 0-4-2-0	S10	0-7-0 / 0-1-4-0 / 0-2-3-0
		S11	0-1-5-0 / 0-2-4-0

- 1) The wave path numbering corresponds to the numbered locations in Figure 6.10;
- 2) In the case where multiple paths are used, this corresponds to coincident arrival time.

The directional wave reflections are then transformed into IRFs using Eq. (6-6). Some ripples of the IRFs as shown in Figure 6.11 are caused by the small error associated with the wave separation process and IRF calculation using Eq. (6-6).

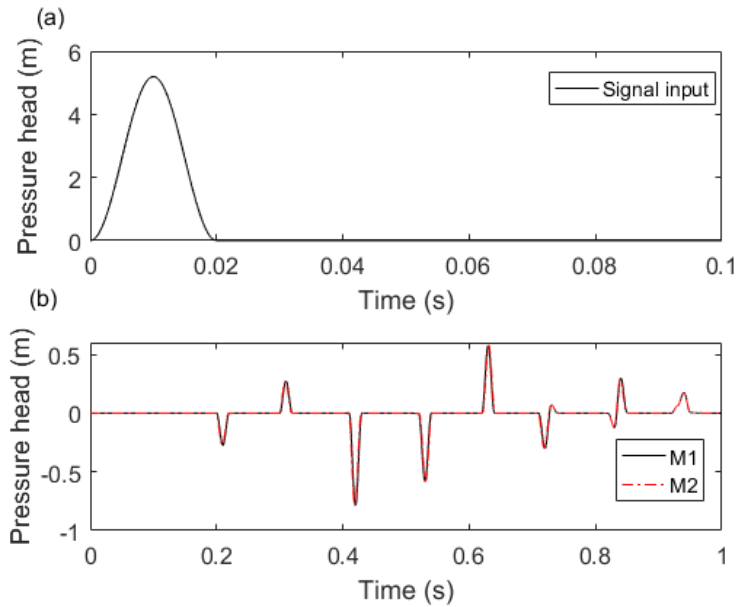


Figure 6.9 (a) Input signal; and (b) reflected signals in the numerical case study.

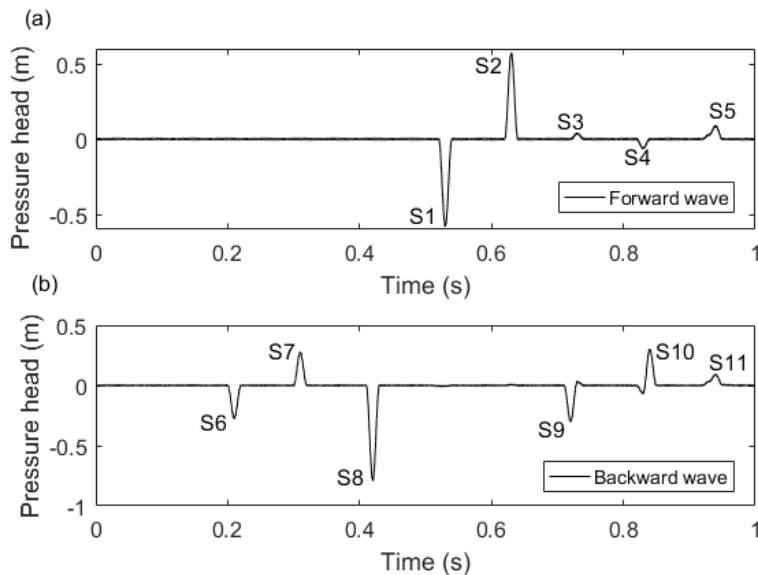


Figure 6.10 (a) Forward wave reflections; and (b) backward wave reflections in the numerical case study.

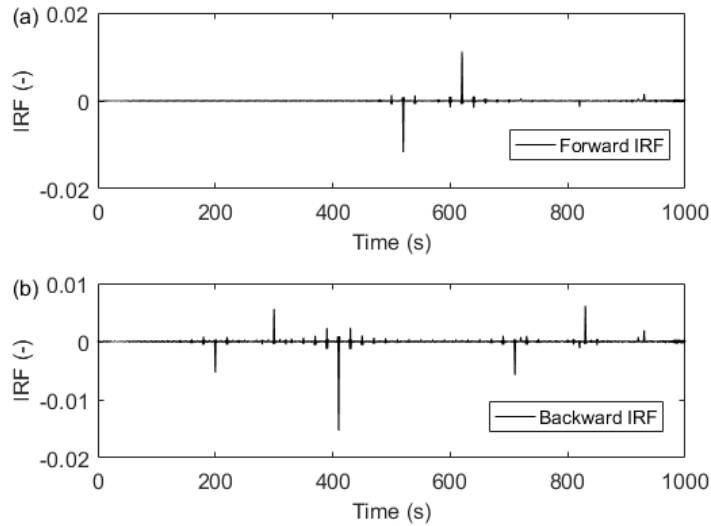


Figure 6.11 (a) Forward IRF; and (b) backward IRF for the numerical case study.

6.4.3 Pipeline reconstruction using the proposed method

To illustrate the effects of the bifurcation node on the reconstruction, the pipeline is reconstructed using three different approaches. In the first approach (Case A), the model of the bifurcation or junction node is not incorporated in Steps 5 and 6 in Figure 6.4, and thus all the wave reflections are assumed to be induced by impedance changes of the pipeline. In the second reconstruction of the right side of the pipeline (Case B), the impedance (and wave speed) is set to be unchanged at the bifurcation node in Step 5 in Figure 6.4, but the scattering equation (6-24) was used for the whole pipeline without incorporating the new scattering equation (6-25) for the bifurcation or junction node in Step 6. The third approach for reconstruction (Case C) is conducted on the right side of the pipeline by considering the bifurcation node in both Step 5 (by assuming the impedance unchanged) and Step 6 (by incorporating Eq.(6-25)). The reconstructed results using the first approach as shown in Figure 6.12 show significant errors at the location of the bifurcation node, because the significant wave reflection generated by the bifurcation node is treated as being generated by impedance changes. Even though the impedance is assumed to be unchanged in the second approach, a distinctive error can be observed at the third (from

left to right in Figure 6.8) deteriorated section in Figure 6.13. This is because the reflected waves induced by the deteriorated section will be diminished when passing the bifurcation node, and this process described by Eq.(6-25) is not incorporated into the approach. The reconstructed result as shown in Figure 6.14 matches the theoretical values as the bifurcation node is fully modelled in the third approach. Some high frequency errors observed from the figure result from the ripples of the IRFs as shown in Figure 6.11.

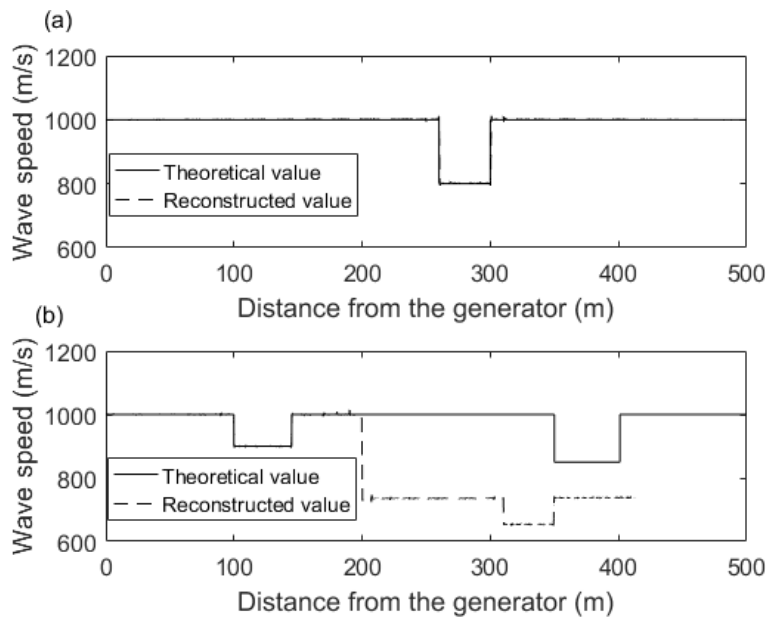


Figure 6.12 Wave speed reconstruction for Case A when neglecting the bifurcation node (a) left side, (b) right side.

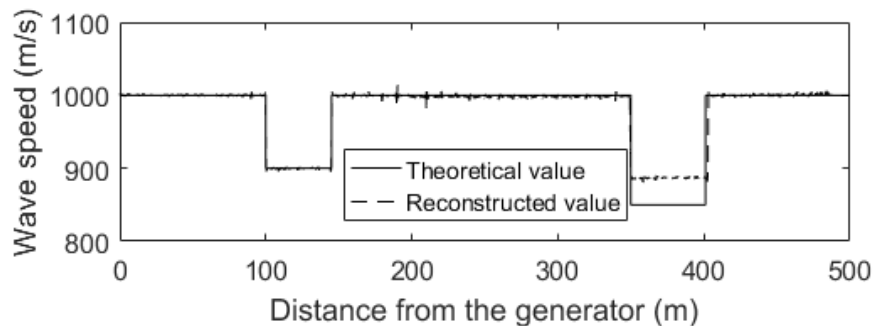


Figure 6.13 Wave speed reconstruction of the right side of the pipeline when setting the impedance unchanged at the position of the bifurcation or junction node (Case B).

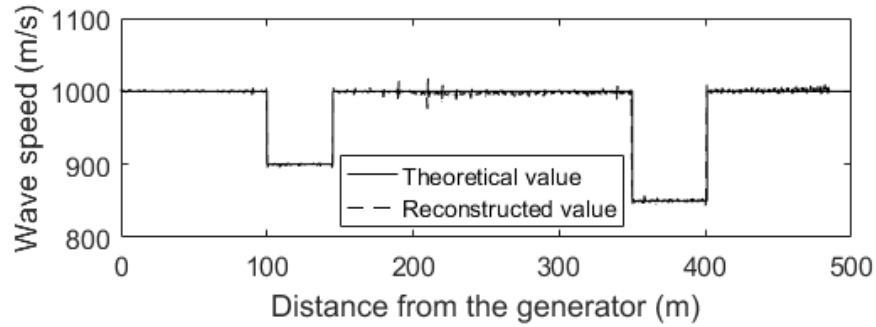


Figure 6.14 Wave speed reconstruction of the right side of the pipeline when incorporating the scattering equation of the bifurcation or junction node (Case C).

6.5 Experimental Verification

Laboratory experiments which have been conducted in (Shi et al. 2017) on the single copper pipeline system in the Robin Hydraulics Laboratory at the University of Adelaide were used to verify the proposed new bi-directional layer-peeling technique.

6.5.1 System layout

The layout of the experimental pipeline system is given in Figure 6.15. Branches were not able to be easily included in the experimental study due to space limitations in the laboratory. The pipeline is 37.43 m in length and connected to a pressurized tank at the upstream end. A dead-end was created by closing the in-line valve at the downstream end during the experiments. A solenoid side-discharge valve was installed close to the middle of the pipe as the wave generator (G). A pressure sensor (T1) was placed at the same location as the generator, and the other pressure sensor (T2) was located 0.99 m upstream (to the left) of T1. Two thinner-walled sections using Class B and Class C copper pipes were placed on the two sides of the generator. They represent pipe sections with uniform wall thickness reduction (i.e. a simulation of internal corrosion). The remainder of the pipeline was Class A copper. The physical details of the pipeline are given in Table 6.2. The wave speeds of these

pipeline sections have been calculated using Eq. (6-11) with the following parameters: $E = 124.1\text{GPa}$, $c_1 = 1.006$ (a thick-walled pipe), $K = 2.149\text{ GPa}$ and $\rho = 999.1\text{ kg/m}^3$.

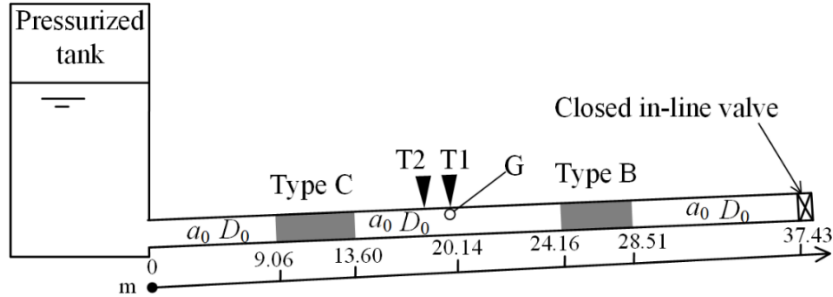


Figure 6.15 System layout of the experimental pipeline system.

Table 6.2 Physical details of the pipeline system used in the laboratory experiments.

Copper Pipe Class	Internal diameter (mm)	Wall thickness (mm)	Wave speed (m/s)
A	$D_0 = 22.14$	$e_0 = 1.63$	$a_0 = 1319$
B	$D_1 = 22.96$	$e_1 = 1.22$	$a_1 = 1273$
C	$D_2 = 23.58$	$e_2 = 0.91$	$a_2 = 1217$

6.5.2 Experimental data analysis

A step pressure wave was generated by sharply closing the side-discharge solenoid valve at G in Figure 6.15. The pressure traces were collected by the two sensors with a 20 kHz sampling rate. The pressure traces within a selected period are shown in Figure 6.16.

The first 5 ms of the pressure trace at T1 as shown in Figure 6.16 covers the full wavefront and is defined as the input signal to the pipeline system. The wave reflections at T1 and T2 can be then obtained by subtracting the input signal from the original pressure traces P_1 and P_2 , respectively. With two sets of the pressure traces, the forward and backward waves can be separated using Eqs. (6-3) and (6-4). As the separated results show some periodic fluctuations as shown in the dash-dot curves in Figure 6.17, a 3rd-order Savitzky-Golay filter (Zeng et al. 2017) with frame length equal to 51 (time length is 2.5 ms) was

applied to the separated results to obtain smoothed waves as shown in Figure 6.17. The frame length was selected by trial and error until the periodic fluctuations were eliminated in the filtered results.

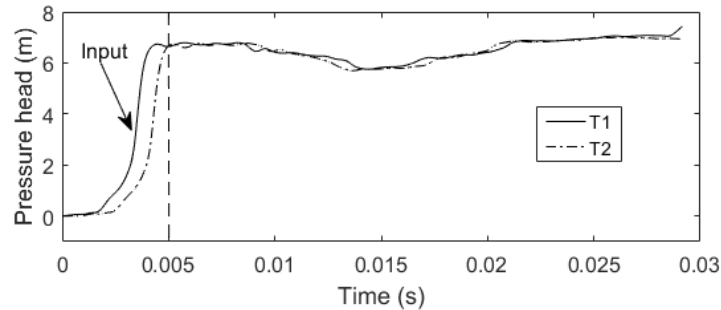


Figure 6.16 Experimental pressure traces at the two close proximity transducers.

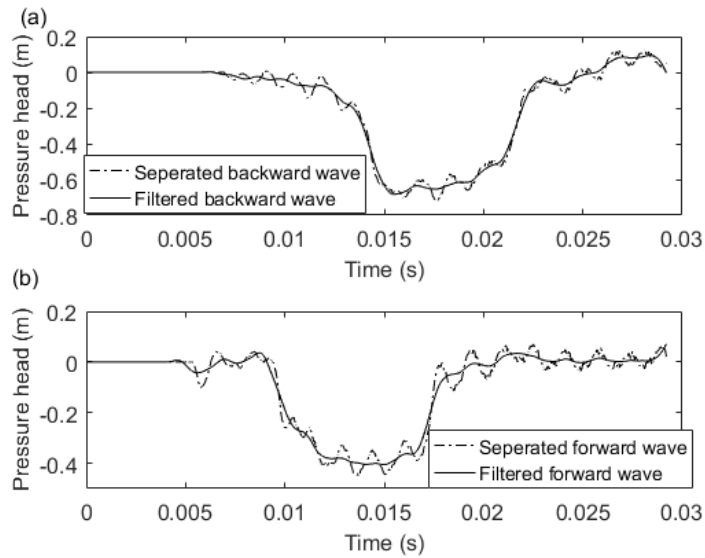


Figure 6.17 (a) Forward wave reflections; and (b) backward wave reflections in the experimental case before and after application of a Savitzky-Golay filter.

With the input and separated reflection waves, the directional IRFs of each side of the pipeline can be obtained using Eq. (6-6) as plotted in Figure 6.18.

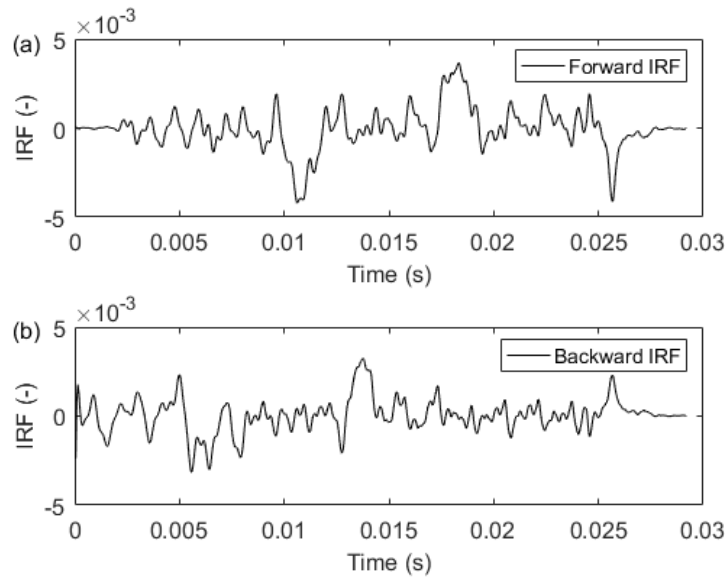


Figure 6.18 (a) Forward IRF; and (b) backward IRF in the experimental case.

6.5.3 Bi-directional reconstruction of the pipeline

Bi-directional reconstruction of the pipeline has been performed using the proposed approach with the directional IRFs (Figure 6.18). The reconstructed wall thickness and wave speed along the pipeline is plotted in Figure 6.19 and compared with the theoretical values. Two clear dips of the reconstructed wall thickness and two dips of the reconstructed wave speed can be observed in Figure 6.19 (a) and (b), respectively, and match well with the theoretical values. The amplitudes of the reductions of the pipe wall thickness and wave speed were identified.

Small perturbations in the reconstructed wall thickness and wave speed of the pipeline are also observed in Figure 6.19. They are related to the joints on the pipeline, natural variations of the pipeline properties, fluid-structure interactions, errors induced by the wave separation process and other uncertainties in experiments. Overall, the experimental results indicate that the proposed approach is effective in the controlled laboratory conditions.

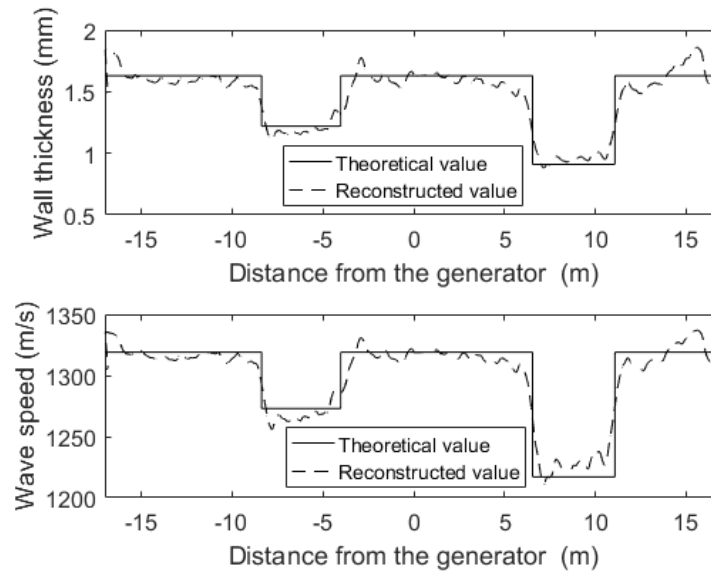


Figure 6.19 Reconstruction using the averaged IRF (the upstream side is set as the positive direction).

6.6 Conclusions

This research has proposed a new hydraulic transient-based technique for efficient pipeline condition assessment using a bi-directional layer-peeling approach and a dual-sensor configuration. A wave generator and a dual-sensor are installed at interior points of the pipeline, which is much more practical to access in real water distribution systems than a dead-end (as required by prior versions of the layer-peeling method). A discrete incident wave (e.g. pulse or step wave) is generated by the side-valve transient generator. Wave reflections from the two pipe segments on the two sides of the generator are extracted using the dual-sensor and a wave separation algorithm, resulting in two sets of directional reflected waves. Each set of the directional reflected waves, together with the original incident wave produced by the transient generator, are considered as the input to the pipe segment where the waves are entering. The scattering equation of a bifurcation or junction node representing the characteristics of wave transmission and reflection is derived and incorporated into the layer-peeling method. A bi-directional reconstruction of pipeline wall thickness and wave speed is eventually achieved using the proposed approach.

The proposed bi-directional pipeline property reconstruction technique has been verified by both numerical simulations and laboratory experiments. The numerical case study for a pipeline with three deteriorated sections and a branch pipe has demonstrated that 1) the wave reflections contain complex high order reflections from the bifurcation node connecting the branch and the deteriorated sections; 2) the new technique developed in this paper can properly incorporate these higher-order reflections into the analysis and achieve bi-directional pipeline parameter reconstruction.

In the experimental verification, two pressure traces collected by two close-proximity placed pressure sensors have been used to obtain the directional wave reflections through a wave separation technique. The directional IRFs calculated using the separated waves were taken as the inputs for the bi-directional layer-peeling method. Two deteriorated sections in the experimental copper pipeline of 22.4 mm internal diameter were then successfully identified and reconstructed, confirming the applicability of the proposed approach to real pipelines.

The proposed technique is a step further towards cost-effective pipeline condition assessment in a network environment. The layer-peeling-based algorithm is computationally efficient, and the ability to incorporate the effect of branched connections significantly advances the applicability of the technique to real pipe systems.

Acknowledgments

The research presented in this paper has been supported by the Australian Research Council through the Discovery Project Grant DP170103715.

Chapter 7

Inverse Wave Reflectometry Method for Hydraulic Transient-Based Pipeline Condition Assessment (Journal Publication 5)

Wei Zeng¹, Aaron C. Zecchin¹, Jinzhe Gong¹, Martin F. Lambert¹ Angus R. Simpson¹, Benjamin S. Cazzolato²

¹School of Civil, Environmental and Mining Engineering, the University of Adelaide, Adelaide, SA 5005 Australia

²School of Mechanical Engineering, University of Adelaide, SA 5005, Australia

Citation: Zeng, W., Zecchin, A. C., Gong, J., Lambert, M. F., Simpson, A. R., Cazzolato, B. S. (2019). "Inverse wave reflectometry method for hydraulic transient-based pipeline condition assessment." *Journal of Hydraulic Engineering* (Submitted).

Statement of Authorship

Title of Paper	Inverse wave reflectometry method for hydraulic transient-based pipeline condition assessment
Publication Status	<input type="checkbox"/> Published <input type="checkbox"/> Accepted for Publication <input checked="" type="checkbox"/> Submitted for Publication <input type="checkbox"/> Unpublished and Unsubmitted work written in manuscript style
Publication Details	Zeng, W., Zecchin, A., Gong, J., Lambert, M., Simpson, A., Cazzolato, B. (2019). Inverse wave reflectometry method for hydraulic transient-based pipeline condition assessment. Journal of Hydraulic Engineering. (Submitted)

Principal Author

Name of Principal Author (Candidate)	Wei Zeng
Contribution to the Paper	Conception and design of the project Analysis and interpretation of research data Draft the paper
Overall percentage (%)	75 %
Certification:	This paper reports on original research I conducted during the period of my Higher Degree by Research candidature and is not subject to any obligations or contractual agreements with a third party that would constrain its inclusion in this thesis. I am the primary author of this paper.
Signature	_____ Date 8/11/2019

Co-Author Contributions

By signing the Statement of Authorship, each author certifies that:

- i. the candidate's stated contribution to the publication is accurate (as detailed above);
- ii. permission is granted for the candidate to include the publication in the thesis; and
- iii. the sum of all co-author contributions is equal to 100% less the candidate's stated contribution.

Name of Co-Author	Aaron Zecchin
Contribution to the Paper	Conception and design of the project Analysis and interpretation of research data Critically revising the paper
Signature	_____ Date 15/11/19

Name of Co-Author	Jinzhe Gong
Contribution to the Paper	Conception and design of the project Analysis and interpretation of research data Critically revising the paper
Signature	_____ Date 24/11/19

Please cut and paste additional co-author panels here as required.

Name of Co-Author	Martin Lambert		
Contribution to the Paper	Conception and design of the project Analysis and interpretation of research data Critically revising the paper		
Signature		Date	22/11/19

Name of Co-Author	Angus Simpson		
Contribution to the Paper	Conception and design of the project Analysis and interpretation of research data Critically revising the paper		
Signature		Date	4 Nov. 2019

Name of Co-Author	Benjamin Cazzolato		
Contribution to the Paper	Conception and design of the project Analysis and interpretation of research data Critically revising the paper		
Signature		Date	8 th Nov. 2019

✓

Abstract

Established water distribution systems (WDSs) typically consist of pipelines buried underground that are ageing and deteriorating, and as such, it is difficult to assess their condition for the purposes of maintenance and replacement. This paper proposes a novel hydraulic transient-based inverse wave reflectometry method (IWRM) for condition assessment of water pipelines in WDSs. Instead of using the method of characteristics (MOC) for the transient modelling, a computationally high-efficiency wave reflectometry method (WRM) has been developed to simulate the transient response of a pipe system. Further efficiency improvement has been made by simplifying the friction term in the WRM. An IWRM has then been developed by combining the WRM with a differential evolution algorithm to calibrate the locations and magnitudes of the pipeline impedance changes (wall thickness changes and wave speed changes) caused by deterioration. The IWRM is able to concentrate on the major wave reflections caused by pipe impedance changes and minimize the effects from the background noise and other interferences. The proposed method has a high efficiency due to its fast WRM simulation and a small number of optimization variables. Extensive numerical verifications have been conducted on reservoir-pipeline-valve systems with a uniform deteriorated pipe section, a non-uniform deteriorated section and multiple deteriorated sections. The deteriorated sections in these case studies were all well detected even though the pressure signals were contaminated with strong noise. Experimental verification has also been conducted on a laboratory copper pipeline with one thinner-walled pipe section successfully identified.

7.1 Introduction

Condition assessment of pipelines in water distribution systems (WDSs) is of critical importance for asset management. Given that pipelines are normally buried underground and long in length (i.e. in the order of kilometers), it is often difficult to assess their condition using localized techniques, such as ultrasonic sounding and the magnetic flux detection method (Liu and Kleiner 2013). An alternative method is to use non-invasive transient-based methods which utilize hydraulic transient waves injected into the pipelines. As the hydraulic transient wave can propagate along the pipe for a long distance, transient-based techniques can enable condition assessment of a significant length of pipeline (Stephens et al. 2013).

In the past two decades, a number of transient-based techniques have been developed by analyzing the transient pressure traces both in the frequency and time domain. These methods focus on detection of discrete anomalies, such as leaks (Brunone 1999; Vítkovský et al. 2007; Ferrante et al. 2009; Shamloo and Haghighi 2009; Duan et al. 2011; Gong et al. 2014b) and discrete blockages (Wang et al. 2005; Lee et al. 2008b; Sattar et al. 2008; Meniconi et al. 2011a; Meniconi et al. 2016). Increasing attention has also been given to extended blockages (Meniconi et al. 2012a; Duan 2016) and extended wall deteriorations caused by extended internal and external corrosion and spalling of cement mortar lining (Stephens et al. 2013; Gong et al. 2018a; Zeng et al. 2018; Zhang et al. 2018a) recently. Distributed pipe deteriorations are common in ageing WDSs and may develop into bursts over time and cause pipe faults if they are not detected at an early stage. An estimation of the degree of deterioration is also essential to strategically manage pipeline assets by targeted pipe maintenance, rehabilitation or replacement.

The reconstructive Method of Characteristics (MOC) (Gong et al. 2014a), the layer peeling method (Zeng et al. 2018) and inverse transient analysis (ITA) (Stephens et al. 2013) are available transient-based techniques for spatially

continuous pipe-wall condition assessment. A selected literature review on these methods is given below.

The reconstructive MOC analysis is an inverse process of the conventional MOC calculation, and can reconstruct the impedance distribution of the pipeline section by section according to the measured wave reflections (Gong et al. 2014a). An extension was made by (Zhang et al. 2019) to relax the requirement of a dead-end boundary. The method is computationally efficient, but it is difficult to implement when wave dissipation and dispersion needs to be considered.

The layer peeling method, which was previously applied to the quality inspection of musical instruments (Amir and Shimony 1995a, b; Sharp 1996; Mamou-Mani et al. 2012), has been modified to allow pipeline condition assessment by Zeng et al. (2018; 2019b). This enables the reconstruction of the pipeline impedance incorporating wave dissipation and dispersion caused by the unsteady friction effects of the transient flow and the viscoelastic behaviour of the pipe wall. A further extension by Zeng et al. (2019a) allowed the method to be applied to complicated pipeline systems by realizing a bidirectional pipeline reconstruction and incorporating the effects of bifurcations at junction nodes in WDSs. However, both the layer peeling method and the reconstructive MOC method are sensitive to noise. Both these methods treat the signal noise, and other signal interferences, as wave reflections caused by impedance changes, and thus the reconstructed result may suffer from cumulative errors in highly noisy environments.

The inverse transient analysis (ITA) technique was first proposed and applied to leak detection in pipe networks by Liggett and Chen (1994), and was further developed by Vítkovský et al (2000; 2007) and Covas et al. (2010). It was first applied to pipeline wall condition assessment by Stephens et al. (2008; 2013). In ITA, the impedances (or wave speeds) of all the pipeline sections are commonly estimated using an evolutionary algorithm to minimize the error between numerical pressures simulated by the MOC and experimental values. The optimal numerical pipe model with the impedance distribution is then used

to interpret the condition of the pipeline. As all pipeline section variables are estimated simultaneously, the ITA does not suffer from cumulative error. However, ITA is not computationally efficient, especially for pipelines of substantial length which involve a large number of parameters to calibrate (Vítkovský et al. 2007). Improvements to ITA have been developed based on using a head-based MOC model with a flexible computational grid (Zhang et al. 2018a) and a multi-stage parameter-constraining process (Zhang et al. 2018b), however, the inverse calculation can still be computationally demanding for large systems. Some practical issues such as signal noise and uncertainties of the hydraulic parameters of the pipeline may also affect the identifiability of ITA approaches (Vítkovský et al. 2007).

Overall, the reconstruction methods (the layer peeling method and reconstructive MOC) may have cumulative errors while in contrast the ITA has low computational efficiency. In real WDSs, pump operations, tank level fluctuations and household water usage can all cause some interference to field experiments and generate noise in the measured pressure traces. Both of the time domain methods will be affected by noise and other sources of interferences in the pressure signals. To address the research gaps mentioned above, a novel hydraulic transient-based method – inverse wave reflectometry method (IWRM) has been developed in this paper. The proposed method: 1) concentrates on the major wave reflections and minimizes the effects from the signal noise and other interferences; 2) a high-efficiency wave reflectometry method has been developed and combined with a differential evolution algorithm (DEA), and thus significantly improving the computational efficiency of the inverse calibration process; and 3) further significant improvement on the computational efficiency has been made by simplifying the friction term in the forward model. By applying the IWRM, an appropriate estimate of the condition of the deteriorated sections in the pipeline is demonstrated in this paper.

The structure of the paper is described in the following: Section 2 presents the proposed forward modeling method – termed the wave reflectometry method (WRM), including the simplification of the friction term. By combining the

wave reflectometry method with the differential evolution algorithm, a novel IWRM is developed in Section 3. Extensive numerical case studies are considered in Section 4 by considering pipelines with singular sections of uniform deterioration, non-uniform deterioration and pipelines with multiple deteriorated sections. In Section 5, the IWRM is further validated by laboratory experiments conducted on a copper pipeline in a laboratory.

7.2 Forward Modelling - Wave Reflectometry

Method

The research studied in this paper involves a single pipe with a closed valve boundary, as shown in Figure 7.1. A generator (G) is installed at the end of the pipe to generate step or pulse waves and a pressure transducer (P) is installed close to the generator to measure the hydraulic transient pressures. In the numerical case studies in the paper, the pressures were simulated using the MOC.

In this section, a wave reflectometry method to simulate the hydraulic transient wave reflections for non-uniform pipelines is proposed. The propagation characteristics of transient waves are presented to demonstrate the processes of the forward modeling method.

7.2.1 Hydraulic transient wave propagation

Consider a pressurized pipe divided into sections of uniform cross-sectional properties (the length of these sections can be different) as shown in Figure 7.1. t_i in the figure represents the round-trip travel time of the hydraulic transient waves in the i^{th} pipe section. For an incident transient pressure wave entering into this system from the upstream side, the wave propagation process of transmission and reflection is presented using the arrows in this figure, and can be described as follows.

- (1) Wave injection [(a) in Figure 7.1]: the incident wave (normally step or pulse waves) enters the pipeline at the left side of pipe Section 1 at $t = 0$ s.
- (2) Wave transmission [(b) in Figure 7.1]: the hydraulic transient wave will pass through pipe Section 1 and reach the right side of pipe Section 1.
- (3) Wave reflection [(c) in Figure 7.1]: the hydraulic transient wave will enter into pipe Section 2, but part of the wave will be reflected at the interface between pipe Section 1 and pipe Section 2 if they have different impedances (e.g. caused by a change in the wave speed or wall thickness).
- (4) The wave transmissions and reflections will occur at each pipe section, as illustrated by the dashed and solid arrows shown in Figure 7.1.
- (5) Boundary reflection [(d) in Figure 7.1]: If the reflected wave reaches the end boundary, it will be fully reflected if the valve is fully closed, as shown in the dot-dashed arrows at the end boundary.

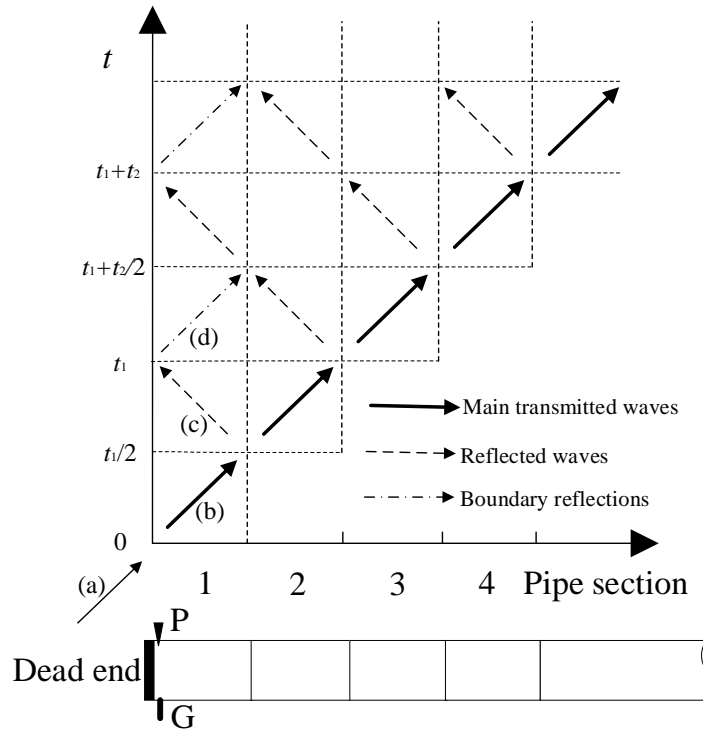


Figure 7.1 Wave propagation in the pipeline.

With the wave propagation process, the wave reflections caused by the pipeline impedance changes can be simulated by summing all the pressure waves reaching, and being reflected by, the end boundary (pressures shown as dashed and dot-dashed arrows at the left side of pipe Section 1 in Figure 7.1). The detailed steps of the proposed simulation approach are given in the following sub-sections by characterizing the wave transmission and reflection processes.

7.2.2 Wave transmission with simplification of the modeling of steady friction

For a fluid-filled pipe, the wave speed (a) of the hydraulic transient wave can be calculated from the properties of the fluid and the pipe wall as (Wylie and Streeter 1993),

$$a = \sqrt{\frac{K/\rho}{1+(K/E)(D/e)c_1}} \quad (7-1)$$

where K represents the bulk modulus of the water; ρ is the density of water; E is the Young's modulus of elasticity of the pipe wall; D is the pipe's internal diameter; e is the wall thickness of the pipe; and c_1 is the pipeline restraint factor. For deteriorated sections of a metallic pipeline, the reduction of the wall thickness reduces the wave speed.

During the wave transmission, hydraulic transient waves will dissipate because of frictional loss. The frictional loss in the i^{th} pipe section (within which the pipe properties are assumed to be uniform) can be incorporated into a transfer function H_i that can be written as (Zecchin et al. 2014)

$$H_i(j\omega) = e^{-\Gamma(j\omega)l_i} \quad (7-2)$$

where Γ is the propagation operator, l is the length of the pipe section, j represents the imaginary unit, ω represents the angular frequency, and the subscript i represents the i^{th} pipe section. If only steady friction is considered, the propagation operator can be written as

$$\Gamma(j\omega) = \frac{1}{a} \sqrt{(j\omega + R)j\omega} \quad (7-3)$$

in which R represents the resistance term, and is given by

$$R = \frac{fQ_0}{DA} \quad (7-4)$$

where f is the Darcy-Weisbach friction factor, Q_0 is the steady-state flow, D is the internal diameter of the pipe, and A is the cross-sectional area of the pipe.

The wave transmission process from the left side of i^{th} section to the right side can be then described as

$$P_{i,r}^+(j\omega) = P_{i,l}^+(j\omega)H_i(j\omega) \quad (7-5)$$

where $P(j\omega)$ is the pressure wave in the frequency domain. The superscript “+” indicates the forward direction, and the subscripts l and r represent the left side

and right side of the pipe section (note that these points are internal within the pipe section).

The wave propagation, Eq. (7-5), is in the frequency domain, which means that the incident pressure wave needs to be transformed into the frequency domain and the calculated pressure wave, after passing through the section, then needs to be inverse-transformed back into the time domain. These transformations, which are normally realized using a Fast Fourier Transform (FFT) process and an inverse Fast Fourier Transform (IFFT) process, would normally take a large amount of computational resources when implemented in the IWRM, where the forward modelling process is called on the order of thousands to millions of times. Thus, to speed up the optimization process, the modelling of the steady friction is simplified as follows.

For laboratory and field pipelines, R is a relatively small number (typically range from 0.005 to 0.1) compared with $j\omega$, excluding the extreme low frequency range and thus Eq. (7-3) can be simplified as

$$\Gamma(j\omega) \cong \frac{1}{a} \sqrt{(j\omega + R/2)^2} \quad (7-6)$$

Thus, Eq. (7-2) can be simplified to

$$H(j\omega) \cong e^{-\Delta t j\omega} e^{-\Delta t R/2} \quad (7-7)$$

in which $e^{-\Delta t j\omega}$ represents a time delay of the transient wave by $\Delta t = l/a$ seconds, and $e^{-\Delta t R/2}$ is a constant value that represents the wave attenuation caused by the steady friction within this time period. Thus, the frequency domain expression of transfer function $H(j\omega)$ can be replaced by two simple wave processing procedures in the time domain.

7.2.3 Wave reflection with an impedance change

During the wave transmission, if the transient wave p meets an interface with an impedance change, it will induce a reflected wave p_r . The original wave will

transmit to the next section by crossing the interface, and the magnitude will change to p_s . The reflection coefficient r (the ratio of the reflected wave to the incident wave) and the transmission coefficient s (the ratio of the transmitted wave to the incident wave) are determined by the pipeline characteristic impedance B as (Chaudhry 2014)

$$r_{i,i+1} = \frac{p_r}{p} = \frac{B_{i+1} - B_i}{B_{i+1} + B_i} \quad (7-8)$$

$$s_{i,i+1} = \frac{p_s}{p} = \frac{2B_{i+1}}{B_{i+1} + B_i} = 1 + r_{i,i+1} \quad (7-9)$$

in which the subscript $i, i + 1$ represents the wave propagating from the i^{th} section to the $(i+1)^{\text{th}}$ section and

$$B = a/gA \quad (7-10)$$

is the characteristic impedance. g is the acceleration due to gravity.

If the reflected wave propagating in the opposite direction [from the $(i+1)^{\text{th}}$ section to the i^{th} section] when passing the interface, the transmission coefficient can be calculated as:

$$s_{i+1,i} = 1 - r_{i,i+1} \quad (7-11)$$

7.2.4 Procedure of the wave reflectometry method

The procedure to simulate the wave reflections following a certain hydraulic transient wave injection into a pipeline with M sections can be described as follows.

- 1) Calculate the wave reflection ratios and wave transmission ratios $r_{i,i+1}$, $s_{i,i+1}$ and $s_{i+1,i}$ for $i = 1$ to $M-1$ using Eqs. (7-8), (7-9) and (7-11);
- 2) Calculate all the wave reflections reaching the wave injection point (the dead end in Figure 7.1) by

$$p_{re,i}(t + \sum_{k=1}^{k=i} t_k) = p_{In}(t) \cdot r_{i,i+1} \cdot \prod_{k=1}^{k=i} S_{k,k+1} \cdot S_{k+1,k} \cdot e^{-t_k R_k / 2} \quad (7-12)$$

in which t in the brackets is the time series of the injected wave, ranging from 0 to the length of the injected wave (T), $p_{In}(t)$ is the injected pressure wave into the pipe, $p_{re,i}$ is the wave reflection (after reaching the wave injection point) from the interface of the i^{th} pipe section to the $(i+1)^{\text{th}}$ pipe section. $p_{re,i}(0)$ to $p_{re,i}(\sum_{k=1}^{k=i} \Delta t_k)$ are equal to 0.

3) The wave reflections from the pipe will be fully reflected by the dead end boundary, and thus the boundary reflections are of the same magnitude of the wave reflections from the pipe. By summing up all the wave reflections from the pipe and the boundary reflections from $t = 0$ to $t = T$, the total wave reflection can be obtained as

$$p_{re}(t) = 2 \sum_{i=1}^{i=M-1} p_{re,i}(t) \quad (7-13)$$

It should be noted that high-order wave reflections (waves reflected by two or more pipe section interfaces) are not considered in the WRM. Generally, the absolute value of the wave reflection coefficient for deteriorated pipe sections is less than 0.1, so the value of high-order wave reflections will be typically less than 0.01, which is normally smaller than the noise and other interferences in the pressure trace.

7.3 Formulation of the Optimization Problem – Inverse Wave Reflectometry Method

In this section, the WRM is combined with an evolutionary algorithm for inverse calibration of the pipeline impedance from a measured transient pressure response. The new method - Inverse Wave Reflectometry Method (IWRM) is then developed for pipeline condition assessment.

7.3.1 Optimization process

The process of the IWRM as shown Figure 7.2 is similar to the inverse transient analysis extensively used for leak detection and pipeline condition assessment (Liggett and Chen 1994; Stephens et al. 2013). However, there are some major differences, such as the decision variables (parameters to be calibrated), definition of the objective function and the forward modelling method, which makes the IWRM computationally efficient and highly tolerant to noise. The steps for implementing IWRM are: 1) the measured incident wave is put into the WRM to simulate the wave reflections with assumed impedance changes at some assumed locations of the pipeline. 2) The simulated wave reflection is then compared with the measured wave reflection and an objective function that is defined based on the difference between the simulated wave reflection and the measured wave reflection. 3) The assumed impedance changes and locations will be calibrated until the generation during the optimization process reaches its maximum number NG .

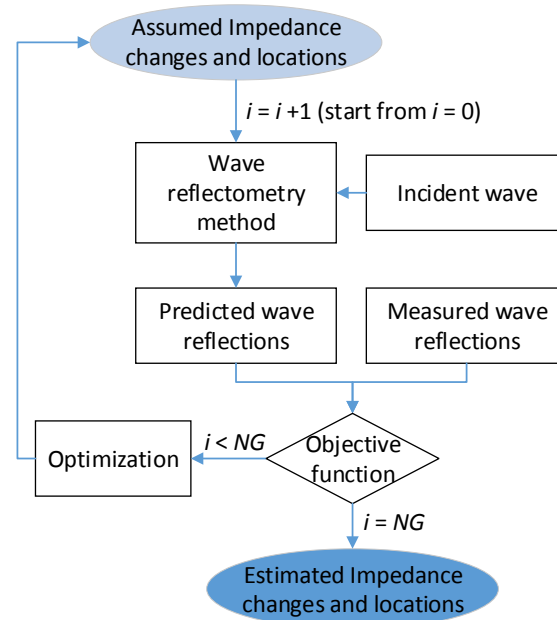


Figure 7.2 Optimization process of the IWRM (NG is the maximum number of generations).

7.3.2 Decision variables and constraints

Compared with the conventional ITA which divides the pipe into many sections and treats the impedance or wave speed of all the sections as the decision variables, the IWRM only chooses N locations L_i ($i = 1, 2, \dots, N$) and corresponding impedance changes compared with the former section ΔB_i ($i = 1, 2, \dots, N$) as the decision variables. By assuming the deterioration does not happen at the ends of the pipe, the sum of the ΔB_i ($i = 1, 2, \dots, N$) should be 0. Thus, the dimension (number of the optimized variables) is reduced to $2N-1$ by defining ΔB_N as

$$\Delta B_N = -\sum_{i=1}^{N-1} \Delta B_i \quad (7-14)$$

To determine an appropriate N , multiple trials need to be undertaken by increasing N until the optimal objective function no longer significantly decreases. For this condition, all the major reflections on the wave reflection trace have been captured in the optimization, and any further increase of N will only incorporate the small fluctuations on the wave reflection trace (mostly composed of noise and other interferences) into the optimized result.

The constraints of the optimized parameters can be defined as

$$0 < L_1 \leq L_2 \leq \dots \leq L_N < L \quad (7-15)$$

$$B_{\min} < \Delta B_1 \dots \Delta B_{N-1} < B_{\max} \quad (7-16)$$

in which L is the length of the pipe, and B_{\min} , B_{\max} are the minimum and maximum impedance changes, determined by preliminary studies.

7.3.3 Multi-stage optimization

When multiple deteriorated pipe sections exist in the pipeline, a multi-stage optimization can be conducted to assess each section step by step. Taking a pipe with 2 sections as an example, the first half of the pipe (before L_{N1}) can be

assessed using the first half of the wave reflection trace. For the second half of the pipe, the wave reflection can be calculated with assumed impedance changes and corresponding locations ranging from L_{N1} to L and the estimated impedance distribution of the first half of the pipeline. The IWRM can be then applied to obtain the impedance estimation of the second half of the pipeline.

7.3.4 Objective function

To give increased emphasis on the major reflections during the optimization, the values of the simulated wave reflections at each time step are squared, as well as those of the measured wave reflections. The objective function of the optimization is then defined as

$$f = \sum_{t=\Delta t}^{t=T} ([p_s(t)]^2 - [p_m(t)]^2)^2 \quad (7-17)$$

where p_s is the simulated wave reflection, p_m is the measured wave reflection.

Overall, the optimization problem can be defined as: minimize f subject to $0 < L_1 \leq L_2 \leq \dots \leq L_N < L$ and $B_{\min} < \Delta B_1 \dots \Delta B_{N-1} < B_{\max}$.

7.3.5 Optimization process

The differential evolution algorithm (DEA) was chosen as the optimization tool in this paper due to its convenience of application and demonstrated utility in other optimization problems (Zheng et al. 2011; Zheng et al. 2013). The four major steps involved in the process of the DEA are shown in Figure 7.3, including initialization, mutation, crossover and selection. The process of a typical DEA can be found in (Storn and Price 1997).

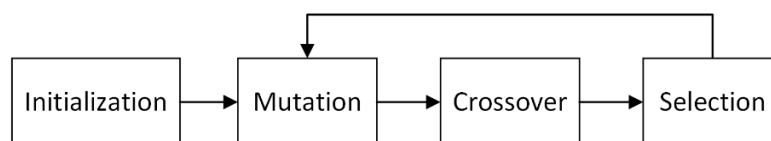


Figure 7.3 Main stages of the EDA.

In the initialization process, the dimension, population size for the evolutionary algorithm and the maximum generations of the optimization process are ND , NP and NG , respectively. The differential weight F in the mutation process is set to 0.8 and the crossover probability CR in the crossover process is set to 0.3.

Since the simulated and measured wave reflections are discrete with a certain time step, the optimized locations $L_i (i = 1, 2, \dots, N)$ are not continuous but discrete. A spatial resolution of the location $\Delta x = a\Delta t$ is obtained, and thus L_i is an integer multiple of the spatial resolution. Therefore, the continuous location values generated in the initialization and mutation processes of the DEA are converted to the nearest discrete locations.

7.4 Numerical Case Studies

Extensive numerical simulations have been conducted on reservoir-pipeline-valve systems with a uniform deterioration, with a non-uniform deterioration and with multiple deteriorations to verify the proposed IWRM for pipeline condition assessment. The transient pressure waves were generated by operating the valve following a quarter-period sine pulse pattern within 6 ms, and the pressure response in both scenarios were simulated using the MOC. The time step was set as 0.0005 s and steady friction has been incorporated in the MOC simulation.

In real WDSs, pipelines normally have an outer diameter ranging approximately from 100 to 1000 mm. A small change in pipe wall thickness may slightly alter the internal or external diameter, but can cause a large change in the wave speed. Therefore, the internal diameter of the deteriorated section is assumed to be unchanged and the impedance changes are fully ascribed to the changes of the wave speed in the numerical cases.

7.4.1 Case 1: Uniform deterioration

The first case study was conducted on a pipeline with a uniformly deteriorated section. The configuration of the pipeline system and some relevant parameters

about the pipeline is given in Figure 7.4. The internal diameter of the pipeline is assumed to be 400 mm throughout. The wave speed in the normal sections of the pipeline is 1000 m/s and drops to 960 m/s in the uniformly deteriorated section. The Darcy-Weisbach factor f is assumed to be 0.02 and the initial flow of the pipe is assumed to be 0.01 m³/s. The incident wave and wave reflections simulated using a MOC model are shown in Figure 7.5.

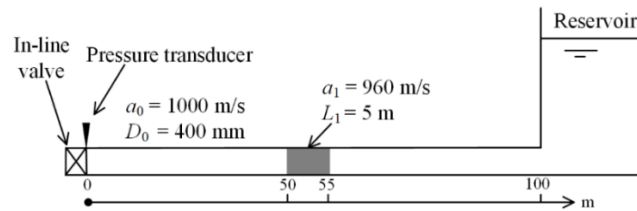


Figure 7.4 Pipeline configuration for Case 1.

By putting the pulse incident pressure wave into the WRM, a simulated wave reflection trace can be obtained as the dotted line (almost exactly coincident with the solid line) in Figure 7.5 (b). The simulation by the WRM is almost identical to the MOC result except for the tiny high-order wave reflections which are neglected in the WRM. Overall, the comparison between these two simulation results validates the WRM.

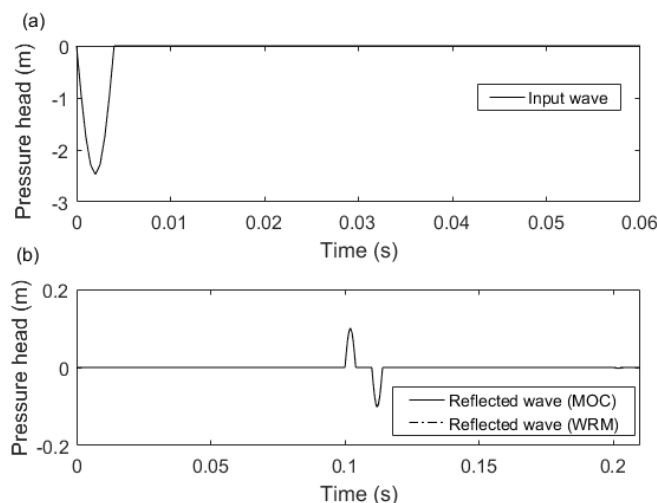


Figure 7.5 Simulated pressure traces for Case 1; (a) input wave, and (b) reflected wave.

Before the calibration process, the wave reflection signal as shown in Figure 7.5 (b) was contaminated with different levels of white noise with signal-to-noise ratios (SNRs) equal to 5, 0 and -5 dB. The mixed signals shown in Figure 7.6 were then used in the IWRM to estimate the characteristics of the deteriorated section. In this case, N , NP and NG are set to be 2, 100 and 600, respectively.

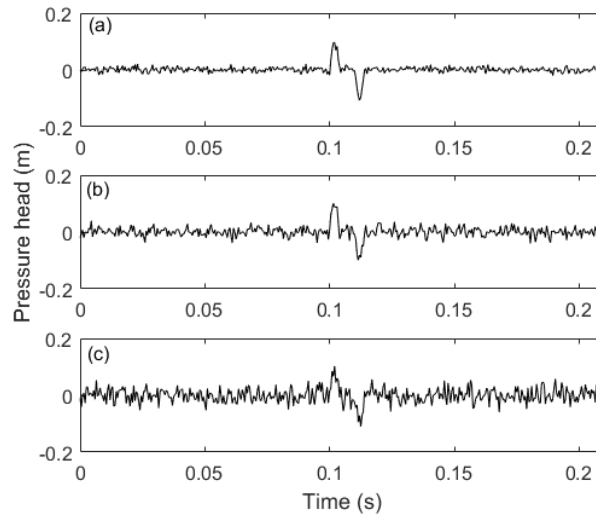


Figure 7.6 Wave reflections combined with three Gaussian noise level for Case 1; (a) SNR = 5 dB, (b) SNR = 0 dB and (c) SNR = -5 dB.

The calibrated wave speed changes Δa_i (computed from the optimized impedance changes ΔB_i) and corresponding locations L_i are listed in Table 7.1 and compared with the real values. The calibrated locations of the impedance changes are identical to the actual values for all the cases, and the calibrated wave speed changes are close to the actual values even for the case with a high level of noise. The results illustrate that the IWRM has a high tolerance to noise.

Table 7.1 Comparison between the estimated results with different levels of noise and the real values

Scenario	L_1 (m)	L_2 (m)	a_{c1} (m/s)	a_{c2} (m/s)
SNR = 5 dB	50	55	-39	+39
SBR = 0 dB	50	55	-39	+39
SNR = -5 dB	50	55	-36	+36
Real values	50	55	-40	+40

7.4.2 Case 2: Non-uniform deterioration

In real WDSs, the wave speed or the wall thickness is normally not uniformly distributed in the deteriorated pipe sections. A reconstruction process by the layer peeling method (Zeng et al. 2018) can obtain an accurate shape of the deteriorated sections, but the results rely heavily on a high SNR of the measured pressure traces. In terms of engineering applications, an estimation of the size and shape of the deteriorated sections would be enough.

The numerical pipeline system in the case study presented in the following has a similar configuration as for Case 1 as shown in Figure 7.4. The deteriorated section starts at the same position, 50 m from the valve, but the length of it is 9.3 m. The wave speed in the non-uniformly deteriorated section drops gradually from 1000 m/s to 960 m/s and then increases back to 1000 m/s, following a half period of a sine pattern. The same incident pressure pulse wave as shown in Figure 7.5 (a) was injected into the pipe, and the simulated wave reflections combined with white noise (with a SNR = 0.3 dB, where this value was selected such that the noise is significant but not so high to dominate the signal enough but the useful signal not fully submerged in the noise) are shown as the dot-dashed line in Figure 7.7.

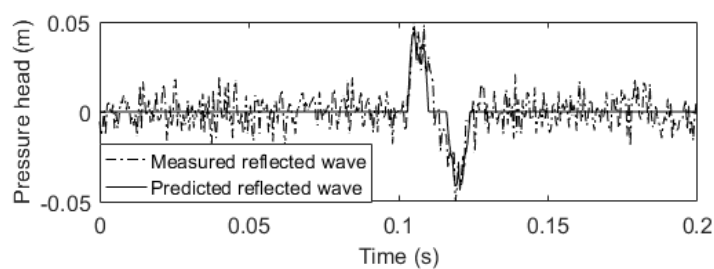


Figure 7.7 Reflected wave combined with noise for Case 2.

The NP and NG values in the IWRM are set to be 200 and 4000 in this case. With increasing N from 2 to 7, 10 trials were conducted using the pressure trace shown in Figure 7.7 for each case. The best objective values of the 10 trials for each case were then averaged and plotted in Figure 7.8. It can be seen from the

figure that the averaged objective value only decreases slightly after N reaches a value of 5. By choosing $N = 5$, the estimated results of the deteriorated section for one trial are shown in Figure 7.9, and the best objective values for different generations are shown in Figure 7.10. The comparison between the estimations and the real values illustrates the IWRM provides a satisfactory estimate of the non-uniformly distributed deterioration. Another comparison between the simulated pressure and the predicted pressure by IWRM as shown in Figure 7.7 shows that the IWRM treats the major wave reflections preferentially and thus has a high tolerance to noise which is of a relatively low magnitude.

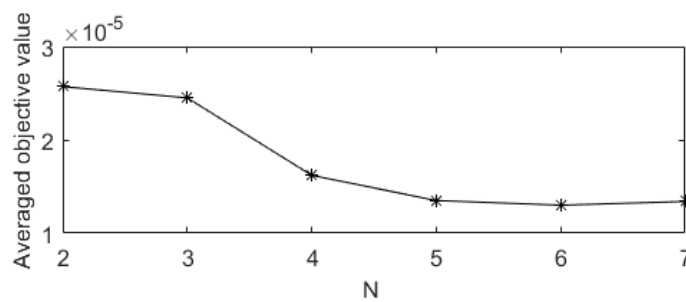


Figure 7.8 Averaged objective values versus N for Case 2.

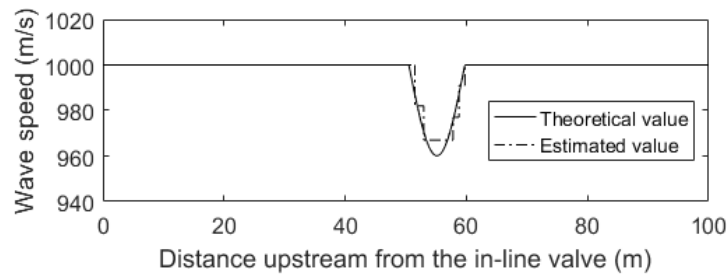


Figure 7.9 Wave speed estimation from the IWRM for Case 2.

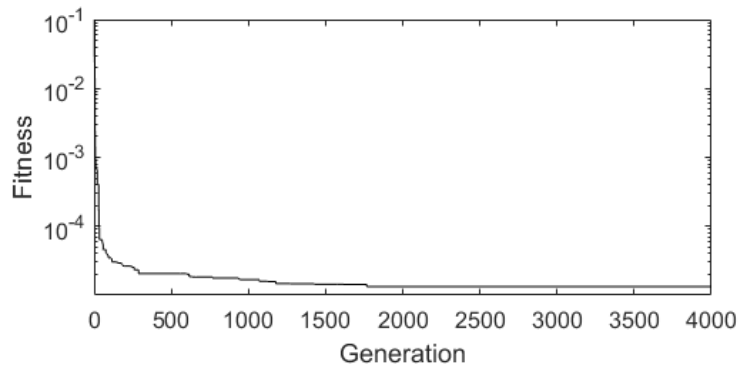


Figure 7.10 Objective values versus generation for $N = 5$ for Case 2.

7.4.3 Case 3: Multiple deteriorations

A more complex situation is considered in Case 3 by increasing the number of the deteriorated sections in the pipe to three, each with diverse shapes. The pipeline configuration is shown in Figure 7.11 with the pipeline diameter, initial flowrate equal to those of Case 1. With the same operation of the in-line valve as for Case 1, the wave reflections were simulated using the MOC as shown in Figure 7.12 (a). After manually combining the signal with noise level of SNR = 1 dB, the wave reflection trace is as shown in Figure 7.12 (b).

A multi-stage optimization was conducted to optimise the impedance values. The first pipeline section (around 0 m – 75 m) was first assessed using the wave reflection trace before 0.15 s. Then the pressure trace between 0.15 s to 0.3 s was used to estimate the second section (around 75 m – 150 m) with the previous estimation of the first section used as part of the input information. The last section (around 150 m – 225 m) was estimated with the remaining wave reflection trace. The optimization parameters N , NP and NG were set to be 5, 200 and 1000, which were sufficient to obtain an accurate estimation as shown in Figure 7.13. The locations of the deteriorated sections are accurately detected with some artefacts on the leading edge of the central section, as shown in Figure 7.13.

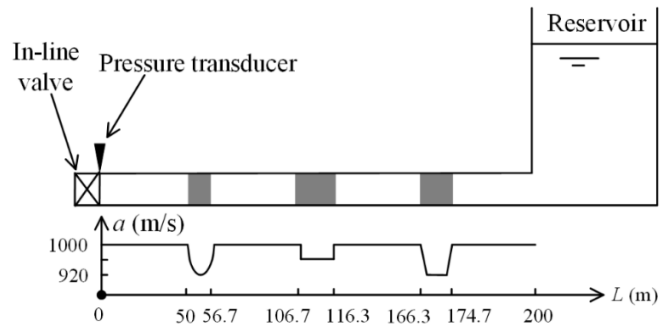


Figure 7.11 Pipeline configuration for Case 3.

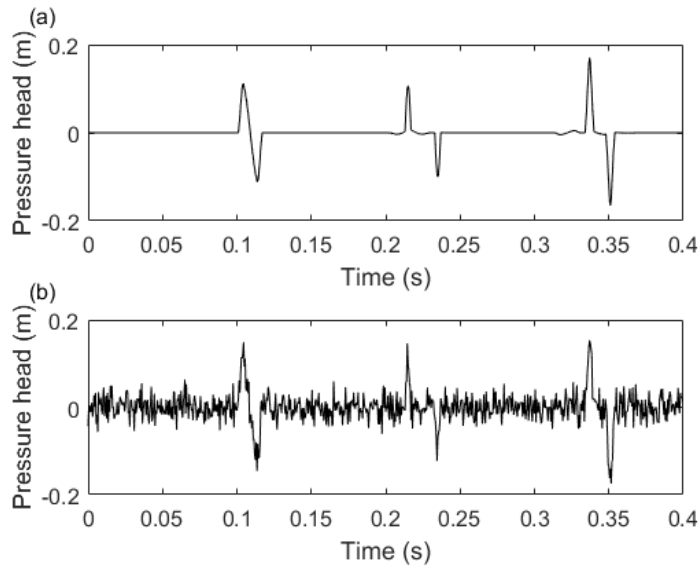


Figure 7.12 Simulated wave reflections for Case 3; (a) without noise, and (b) combined with noise.

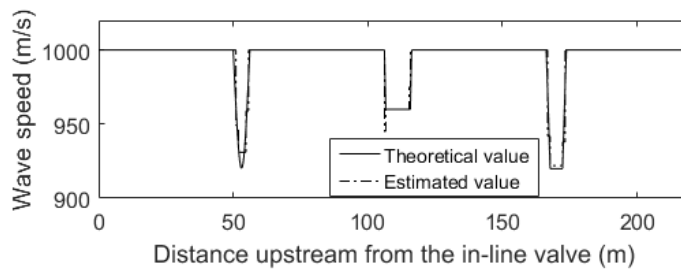


Figure 7.13 Wave speed estimation from the multi-stage IWRM for Case 3.

7.5 Experimental Verification

Laboratory experiments which have been conducted in (Gong et al. 2013c) on a single copper pipeline system in the Robin Hydraulics Laboratory at the University of Adelaide were used to verify the proposed IWRM.

7.5.1 Pipeline layout and experimental data

The pipeline as shown in Figure 7.14 was connected to a pressurized tank, and the in-line valve at the downstream side was closed. The pipe parameters for the intact pipe were length $L = 37.46$ m, internal diameter $D_0 = 22.14$ mm and wall thickness $e_0 = 1.63$ mm. A pipe section with a length L_1 of 1.649 m and a smaller wall thickness $e_1 = 1.22$ mm ($D_1 = 22.96$ mm) started at $L = 17.805$ m upstream from the fully closed in-line valve. This was used to simulate a uniform wall thickness reduction due to internal corrosion. The wave speed of the original pipeline and thinner-walled section is $a_0 = 1319$ m/s and $a_1 = 1273$ m/s, respectively.

By sharply closing the side-discharge solenoid valve located 144 mm upstream from the closed in-line valve, a transient wave was generated and injected into the pipe. The pressure trace collected by the pressure transducer (at the upstream face of the closed in-line valve) with a 2 kHz sampling rate were separated into input pressure wave and wave reflections as shown in Figure 7.15 (a) and (b), respectively.

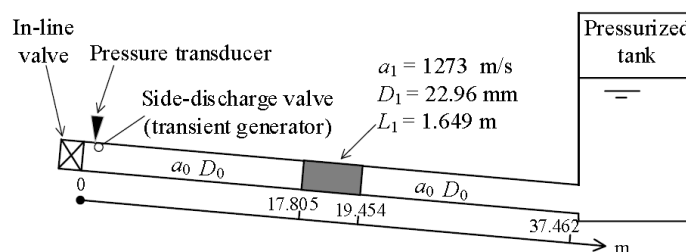


Figure 7.14 Experimental pipeline configuration.

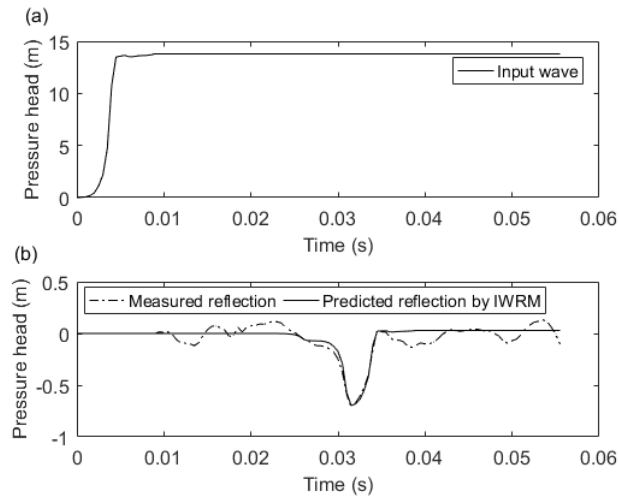


Figure 7.15 Pressure waves in the experimental case: (a) measured input wave; and (b) measured and predicted reflected waves with $N = 6$.

7.5.2 Estimation of the wall thickness change and wave speed reduction using the inverse wave reflectometry method

In this experimental case, the optimization algorithm parameters N , NP and NG were set to be 2, 100 and 600, respectively. By applying the IWRM, the impedance changes (wave speed changes and wall thickness changes) and the corresponding locations can be optimized. The optimization processes took 3.4 s to complete (wall clock time), and generated a high-accuracy solution as shown in Figure 7.16. From the comparison with the real wall thickness values and wave speed distributions, the optimized results show a good estimation of the deteriorated section. Given the spatial resolution of the optimization determined by the time step and wave speed ($\Delta x = a_1 \Delta t = 0.6365$ m), the estimation of the length of the thinner-walled section achieves the optimal solution.

By increasing N from 2 to 4 and then to 6, the best objective value decreases slightly. The estimated wave speeds for $N = 4$ and 6 are shown in Figure 7.17. The comparison between the measured reflected wave with the predicted reflected wave for $N = 6$ can be found in Figure 7.15 (b), from which it can be seen that the emphasis in the solution was given on the major wave reflections.

Three major reasons can be ascribed to the artefacts in the estimated values that occur either side of the deteriorated section, as shown in Figure 7.17: 1) the wave dispersion caused by unsteady friction, fluid-structure interaction, etc., is not included in the IWRM; 2) with a larger N used in the optimization, more noise or other interferences, such as the wave reflection by pipeline joints, will be incorporated into the optimized result; and 3) errors exist in the wave speed calculated using the theoretical equation (Eq. (7-1)). Considering the errors existing in the theoretical wave speed, the estimation of the wave speed distributions with $N = 4$ and 6 are both considered to be appropriate.

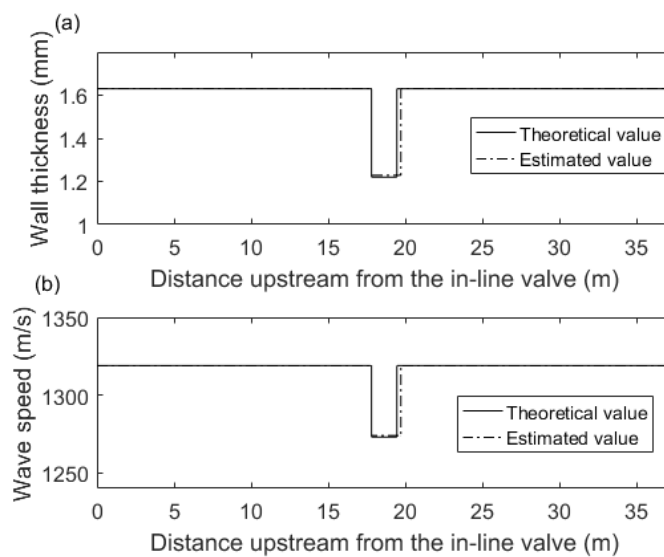


Figure 7.16 Pipe wall thickness and wave speed estimation from the IWRM with $N = 2$ for the experimental case.

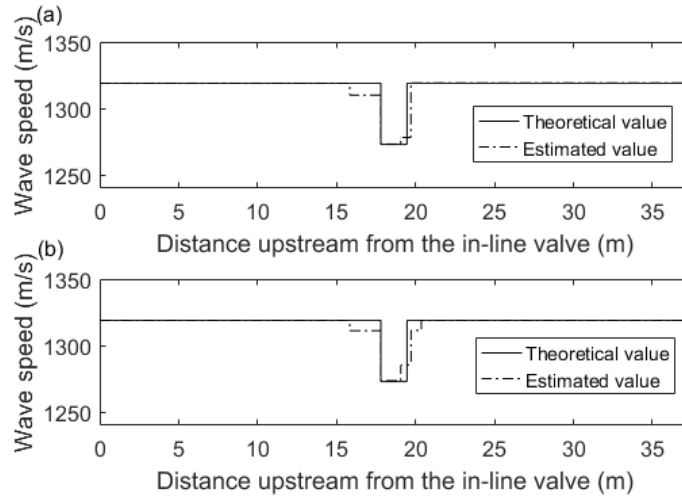


Figure 7.17 Wave speed estimation from the IWRM for the experimental case with (a) $N = 4$, and (b) $N = 6$.

7.6 Conclusions

A novel inverse wave reflectometry method (IWRM) has been developed to estimate the condition of pipelines in this paper. A computationally efficient forward modelling method, the wave reflectometry method (WRM), has been developed to simulate the wave reflections by impedance changes in a pipeline. Further simplification of the steady friction term accelerates the simulation process. By running a differential evolution algorithm with the forward model, the impedance changes and corresponding locations can be estimated. The new method focuses on the major wave reflections which are caused by the impedance changes in the pipeline. It allows the user to define the complexity of the model by choosing the number of major deteriorated sections. The tolerance of the method to noise and other interferences can be enhanced by defining a unique objective function.

Extensive numerical simulations have been conducted considering a uniform deterioration, non-uniform deterioration and multiple deteriorations. The wave reflections have been contaminated with strong noise, but the estimated results using the proposed IWRM have achieved adequate correlation with the actual values. Experimental verification has also been conducted on a 1-inch copper

pipe with a short thinner-walled pipe section. The calibration results, with different assumed numbers of deteriorated sections, have all been able to identify and localize the thinner-walled pipe section, and thus further validating the new IWRM.

The proposed IWRM is a powerful tool for pipeline condition assessment to deal with pressure signals consisting of significant contamination noise and other interferences, and thus compensates for the existing methods which normally rely heavily on the SNR of the measured pressure traces. Future work will consider more complicated pipeline configurations and incorporate wave dispersion to improve the IWRM.

Acknowledgements

The research presented in this paper has been supported by the Australian Research Council through the Discovery Project Grant DP190102484.

Chapter 8

Pipeline Reconstruction using a Pseudo Random Binary Sequence Excitation with the Layer Peeling Method (Journal Publication 6)

Wei Zeng¹, Jinzhe Gong¹, Martin F. Lambert¹, Benjamin S. Cazzolato², Angus.
R. Simpson¹, Aaron C. Zecchin¹

¹School of Civil, Environmental and Mining Engineering, the University of
Adelaide, Adelaide, SA 5005 Australia

²School of Mechanical Engineering, University of Adelaide, SA 5005,
Australia

Citation: Zeng, W., Gong, J., Lambert, M. F., Cazzolato, B. S., Simpson, A. R.,
Zecchin, A. C. (2019). "Pipeline reconstruction using a pseudo random binary
sequence excitation with the layer peeling method." *Mechanical System and
Signal Processing* (To be submitted).

Statement of Authorship

Title of Paper	Pipeline reconstruction using a pseudo random binary sequence excitation with the layer peeling method
Publication Status	<input type="checkbox"/> Published <input type="checkbox"/> Accepted for Publication <input type="checkbox"/> Submitted for Publication <input checked="" type="checkbox"/> Unpublished and Unsubmitted work written in manuscript style
Publication Details	Zeng, W., Gong, J., Lambert, M., Simpson, A., Cazzolato, B., Zecchin, A. Pipeline reconstruction using a pseudo random binary sequence excitation with the layer peeling method. Mechanical System and Signal Processing. (To be submitted)

Principal Author

Name of Principal Author (Candidate)	Wei Zeng		
Contribution to the Paper	Conception and design of the project Analysis and interpretation of research data Draft the paper		
Overall percentage (%)	75 %		
Certification:	This paper reports on original research I conducted during the period of my Higher Degree by Research candidature and is not subject to any obligations or contractual agreements with a third party that would constrain its inclusion in this thesis. I am the primary author of this paper.		
Signature		Date	8/11/2019

Co-Author Contributions

By signing the Statement of Authorship, each author certifies that:

- the candidate's stated contribution to the publication is accurate (as detailed above);
- permission is granted for the candidate to include the publication in the thesis; and
- the sum of all co-author contributions is equal to 100% less the candidate's stated contribution.

Name of Co-Author	Jinzhe Gong		
Contribution to the Paper	Conception and design of the project Analysis and interpretation of research data Critically revising the paper		
Signature		Date	24/11/19

Name of Co-Author	Martin Lambert		
Contribution to the Paper	Conception and design of the project Analysis and interpretation of research data Critically revising the paper		
Signature		Date	22/11/19

Please cut and paste additional co-author panels here as required.

Name of Co-Author	Angus Simpson		
Contribution to the Paper	Conception and design of the project Analysis and interpretation of research data Critically revising the paper		
Signature		Date	4 Nov. 2019

Name of Co-Author	Benjamin Cazzolato		
Contribution to the Paper	Conception and design of the project Analysis and interpretation of research data Critically revising the paper		
Signature		Date	8 th Nov. 2019

Name of Co-Author	Aaron Zecchin		
Contribution to the Paper	Conception and design of the project Analysis and interpretation of research data Critically revising the paper		
Signature		Date	15/11/19

Abstract

Pipe wall condition assessment is critical for targeted maintenance and failure prevention of water distribution systems. This paper proposes a spatially continuous hydraulic transient-based pipeline condition assessment technique using a layer-peeling algorithm in combination with a pseudo random binary sequence (PRBS) excitation. A three-sensor measurement configuration is used to measure the transient pressure of a pipeline system. Based on an analytical wave propagation analysis, two equations that link the measured pressures at the three locations to the impulse response functions (IRFs) of different sections of the pipeline are derived (referred to as IRF equations). A two-step pipeline impedance (related to the pipe wave speed and wall thickness) reconstruction technique is developed. In the first step, the two IRF equations are simplified to derive the first-order IRFs of the pipeline, which are then used in a layer-peeling algorithm customized for water pipelines to reconstruct the distribution of the impedance with a first-order accuracy. In the second step, the impedance distribution obtained in the first reconstruction is used to estimate the IRFs with a second-order accuracy. A second reconstruction of the impedance distribution of the pipeline is conducted using the second-order IRFs with enhanced accuracy, from which the distribution of the wave speed and wall thickness along the pipe are then determined. Both numerical and experimental verifications have been conducted on a pipeline with two thinner-walled pipe sections (simulating sections with extended corrosion). The results show that the thinner-walled sections can be successfully detected from the results of reconstruction, and the second reconstruction enhances the accuracy.

8.1 Introduction

Condition assessment of pipelines is of critical importance to allow strategically targeted pipe maintenance, replacement and rehabilitation. Given the large size of water pipeline networks in any city and town, there is a significant need in developing pipeline condition assessment techniques that are cost-effective to implement on long sections of pipe. One promising method that has been in development over the past two decades is to use controlled hydraulic transients as a tool for active detection. In this method, hydraulic transient pressure waves are injected into a pipeline through a pressure wave generator (Vítkovský et al. 2000; Brunone et al. 2008; Gong et al. 2016; Gong et al. 2018). Transient wave reflections will be generated if the incident wave encounters an anomaly such as a leakage or a blockage, and the reflected waves can be used to locate the anomaly according to the wave travel time and the wave speed. A number of techniques have been developed for detecting spatially discrete pipeline defects, such as leaks (Liggett and Chen 1994; Brunone and Ferrante 2001; Wang et al. 2002; Vítkovský et al. 2007; Gong et al. 2014; Sanz et al. 2016; Wang and Ghidaoui 2018; Wang et al. 2019) and localized blockages (Wang et al. 2005; Mohapatra et al. 2006; Lee et al. 2008b; Meniconi et al. 2012). Recent research has extended the hydraulic transient-based methods to detecting extended uniform blockages (Duan et al. 2013; Meniconi et al. 2013). Increasing attention is given on the detection of extended regions of wall thickness reduction (Shi et al. 2017; Zeng et al. 2018; Zeng et al. 2019; Zhang et al. 2019), which can be caused by internal or external widespread corrosion, and/or spalling of cement mortar lining (Gong et al. 2015b).

Short-duration and discrete pressure waves such as step and pulse signals are commonly used as the excitation in current pipeline condition assessment techniques (Colombo et al. 2009). The benefit of using such a discrete excitation is that the wave input and reflections can be visually separated in the case of long pipes containing a limited number of defects. However, a major challenge is the background pressure fluctuations and the interference in real pipe systems, which may contaminate the measured transient pressure waves.

These pressure fluctuations and interferences are difficult to be distinguished from the wave reflections induced by pipe defects (e.g. leaks), thus leading to incorrect assessment of the pipe condition (Ghazali et al. 2012). To achieve an acceptable signal-to-noise ratio, the magnitude of the discrete excitation is typically large (several meters or more in pressure head) and this can impose safety risks to the pipe system.

One approach to address the noise issue is to use persistent signals as the excitation, such as a pseudo-random binary sequence (PRBS) excitation (Lee et al. 2008a; Gong et al. 2013). The effective input signal of a persistent excitation can last for a relatively long time (typically seconds to minutes, in contrast to milliseconds for discrete step and pulse excitations), and this helps the achievement of a relatively high accumulative energy with only small pressure perturbations that do not impose safety risks for the pipeline system. In addition, the PRBS signal is very robust to system noise and other interference sources because of its auto-correlation property (Godfrey 1993). In a pipeline system, a continuous PRBS excitation can be realized using a customized side-discharge valve controlled by two solenoids with fast opening and closing actions (Gong et al. 2016).

A transient-based leak detection technique was proposed by Gong et al. (2016), and it used the PRBS excitation to extract the system frequency response diagram (FRD), which is the plot of the frequency response function (FRF) of a pipe system. For any specific pipeline system, the FRD is determined by the impedance characteristics and configuration of the pipeline. As a result, the features displayed in the FRD can be used to diagnose the condition of the pipeline. However, accurate extraction of the FRF for a broad frequency bandwidth is challenging, especially when the pipe is embedded in a complex network.

Another approach is to extract the impulse response function (IRF) of the pipeline system in the time domain. The IRF of a pipeline is the pressure response of the pipeline when an ideal impulse pressure signal is injected into the system. Signal processing techniques including the truncated singular value

decomposition, Tikhonov regularisation (Forbes et al. 2003) and the least squares deconvolution (Nguyen et al. 2018) have been developed to extract the IRF of a pipeline. However, a significant challenge in using persistent signals to extract the IRF is that the wave input and reflections cannot be visually separated. To address this problem, conventionally the valve opening variation history was recorded (e.g. using a linear voltage displacement transducer) and used this as the input instead of the injected transient wave (Lee et al. 2008a; Gong et al. 2016; Nguyen et al. 2018). Only accurately extracted IRFs are useful in real applications, since wave reflections induced by spatially continuous deteriorations are normally of small magnitude. However, the valve perturbation is difficult to measure accurately, which may significantly reduce the reliability and accuracy of the determined IRF.

To avoid the use of the valve opening perturbation, a three-pressure sensor testing configuration was firstly proposed by Nguyen et al. (2019) for pipeline condition assessment. Two sensors were installed at interior points of the pipe and one sensor was installed close to a dead-end. Instead of using the valve opening perturbation information, the three measured pressure traces were processed using a least square deconvolution approach. Some distinctive spikes were found in the deconvolution result and they were ascribed to the impedance changes along the pipeline. However, the spikes in the deconvolution results can be used only for detecting spatially discrete impedance changes, and the relationship between the deconvolution result and the IRF of the pipeline is unknown.

To enable a spatially continuous condition assessment of a pipeline, Zeng et al. (2018) adapted a layer-peeling technique originally developed for acoustic analysis in ducts (Amir and Shimony 1995a, b; Sharp 1996) to pressurized water pipelines. In Zeng et al. (2018), the layer-peeling-based pipeline condition assessment technique utilized the IRF as the algorithm input to reconstruct the impedance distribution of a pipeline from a dead end. The technique was further developed to enable a bi-directional pipe condition assessment using a pair of pressure transducers in close proximity (i.e. reconstructing the impedance of the pipe sections on both sides of the

transducer pair) (Zeng et al. 2019). However, the prerequisite to these approaches is an accurate estimate of the pipeline IRF, the accuracy of which affects the performance of the impedance reconstruction. Only discrete excitation signals (step and pulse pressure waves) were used in the previous development, which limits the ability of the approach to accurately determine the IRF for real pipe systems.

The research reported in the current paper proposes a new technique for robust and spatially continuous pipeline condition assessment by combining the persistent excitation, the three-pressure sensor measurement strategy and the layer-peeling algorithm. The key innovations and contributions of this work include: 1) the derivation of the mathematical relationship linking the measured pressure traces at three different locations with the IRFs of the corresponding pipe sections; and 2) a two-step strategy for the accurate reconstruction of the pipeline impedance distribution. The first step of the analysis is to conduct an initial pipeline impedance reconstruction using the first-order IRFs (neglecting any higher-order terms that complicate the analytic form). The second step of analysis is, firstly, to estimate the second-order terms in the IRFs and then, secondly, conduct a second pipeline impedance reconstruction with enhanced accuracy. To validate the proposed new technique, a pipeline with two deteriorated sections (pipe sections with thinner wall thicknesses) has been analyzed both numerically and experimentally. The numerical analysis is embedded in the methodology sections to clarify the procedures of the new method. The IRFs of the pipeline are determined and in which the anomaly-induced reflections are clearly shown. Successful reconstruction of the pipeline impedance, wave speed and wall thickness is achieved in both the numerical and the experimental cases.

8.2 Problem Formulation and Framework of the New Technique

A laboratory copper pipeline was used for numerical and experimental analyses in this research. The layout of the laboratory pipeline system is given in Figure

8.1. The pipeline was 37.43 m in length and connected to a pressurized tank (reservoir) at the upstream end. A dead-end was created by closing the in-line valve at the downstream end and a side-discharge PRBS generator was installed very close to the dead-end. A pressure transducer (P_1) was placed close to the PRBS generator, and another two pressure transducers (P_2 and P_3) were located in close proximity at an interior section of the pipeline. The majority of the copper pipeline was in Class A, but two sections were replaced by Class B and Class C pipes, respectively. While the copper pipe sections for different classes have different internal diameters, they share the same external diameter $D_{out} = 25.4$ mm. Other physical details are given in Table 8.1. The wave speeds are calculated by the formula (Wylie and Streeter 1993)

$$a = \sqrt{\frac{K/\rho}{1+(K/E)(D/e)c_1}} \quad (8-1)$$

where K represents the bulk modulus of the water; ρ is the density of water; E is the Young's modulus of elasticity of the pipe wall; D is the pipe's inner diameter; e is the wall thickness of the pipe; and c_1 is the pipeline restraint factor which is calculated as 1.006 based on Class A section (thick-walled pipe anchored throughout). For simplicity, this value is used for wave speed calculations for all the pipe sections. It should be noted that the formula to calculate c_1 depends on D/e and the restraint conditions with details in (Wylie and Streeter 1993). The characteristic impedance B in Table 8.1 is defined as (Wylie and Streeter 1993)

$$B = a/gA \quad (8-2)$$

with g representing the gravitational acceleration and A representing the cross-sectional area of the pipe.

The same system parameters are assigned to a numerical pipeline system on which the numerical case study is conducted and used to illustrate the procedures of the proposed method. The pressure traces at the locations of the

transducers were simulated using the method of characteristics (MOC) in the numerical case with a time step of 0.0001 s.

The pressure responses measured in the experimental case were sampled with a frequency of 10 kHz. It is assumed that the pipe section between P₂ and P₃ is uniform in properties (i.e. a wave would pass through without any reflections).

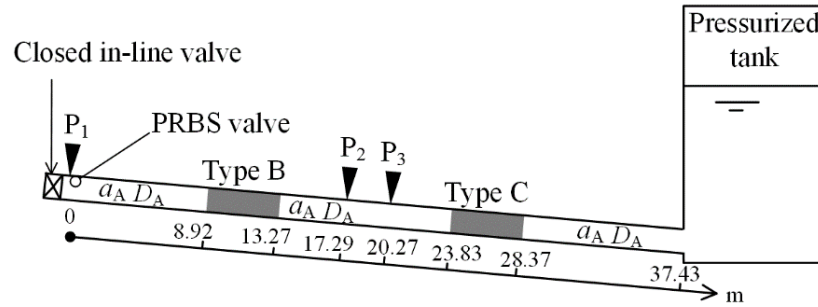


Figure 8.1 Layout of the pipeline system used in the numerical and laboratory studies.

Table 8.1 Physical details of the copper pipeline system

Pipe Class	Internal diameter (mm)	Impedance ($\times 10^5$ s/m ²)	Wall thickness (mm)	Wave speed (m/s)
A	$D_A = 22.14$	$B_A = 3.49$	$e_A = 1.63$	$a_A = 1319$
B	$D_B = 22.96$	$B_B = 3.13$	$e_B = 1.22$	$a_B = 1273$
C	$D_C = 23.58$	$B_C = 2.84$	$e_C = 0.91$	$a_C = 1217$

The structure of the proposed new technique is shown in Figure 8.2 with three major components highlighted. These three stage will be discussed in detail in following sections and are summarized as follows:

Stage 1 - Signal processing: The measured pressure head traces at P₁, P₂ and P₃ (denoted as p_1 , p_2 and p_3) are taken into a least square deconvolution (LSD) algorithm (Nguyen et al. 2018) to obtain the deconvolutions $p_{2,1} = p_2 * p_1^{-1}$ and $p_{3,1} = p_3 * p_1^{-1}$, where $*$ represents the convolution operator, and $f^1 = f^1(t)$ is taken here to mean the inverse Fourier transform of $1/F(i\omega)$ (where F is the Fourier transform of f). A wave separation (WS) technique is used to obtain the directional deconvolutions $p_{2,1}^+$ and $p_{2,1}^-$, where the superscripts + and -

represent the forward (from P_2 towards the pressurized tank – left to right in Figure 8.1) and backward directions, respectively.

Stage 2 - First-order IRFs and the initial pipeline reconstruction: A theoretical derivation is conducted to obtain two equations (defined as the IRF equations) representing the relationship between $p_{2,1}^+$, $p_{2,1}^-$, the IRFs for the pipe sections upstream and downstream of pressure transducer P_2 , the high-order wave reflections and the pipeline boundary condition. By neglecting high-order (>1) terms in the IRF equations, the first-order IRFs can be obtained. The pipeline can be then reconstructed with a first-order accuracy using the first-order IRFs and the layer-peeling method (LPM).

Stage 3 – Second-order IRFs and the second pipeline reconstruction: Second-order terms in the IRF equations can be estimated with the results from the first pipeline reconstruction. Combined with the first-order terms, the second-order IRFs can be obtained. The pipeline impedance is then reconstructed with a second-order accuracy using the second-order IRFs and the layer-peeling method.

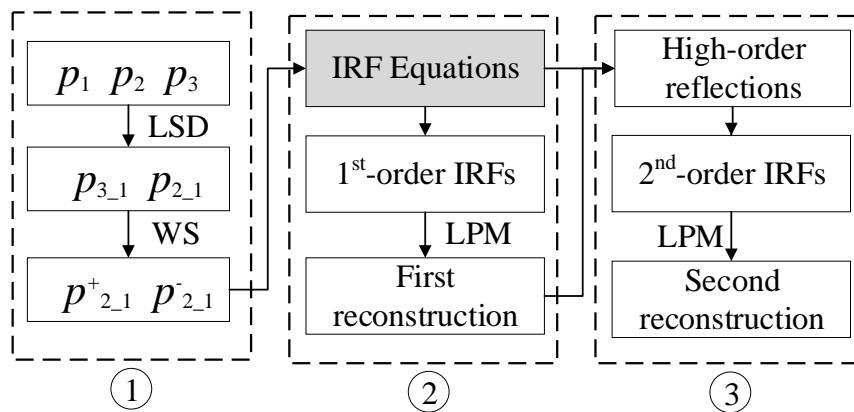


Figure 8.2 The structure and procedures of the proposed technique.

8.3 Wave Excitation and Signal Pre-processing

8.3.1 Pseudo random binary sequence (PRBS) excitation

In this work, the inverse repeat pseudo random binary sequence (IRS) (a specific type of PRBS) is used and a numerically generated section of the signal is shown in Figure 8.3. It was generated numerically from a 10-stage shift register with a clock frequency of 1000 Hz and a period of 2.046 s.

In the numerical case, the movement of the side-discharge valve (the “PRBS valve” at the end of the pipe shown in Figure 8.1) follows the wave form in Figure 8.3. The y-axis in Figure 8.3 represents the normalized valve opening perturbation. The non-dimensional valve opening τ is defined as 1 when the valve is fully open and 0 when it is fully closed. The average value of τ during valve oscillation is $\bar{\tau}$, and the normalized τ perturbation is defined as $(\tau - \bar{\tau})/\bar{\tau}$.

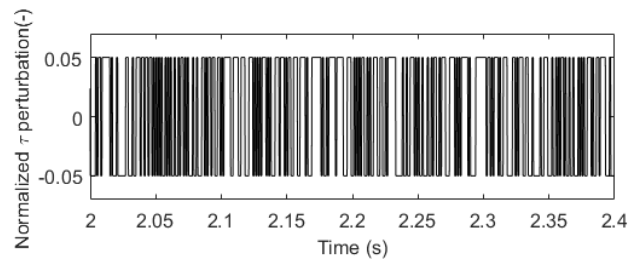


Figure 8.3 Normalized inverse repeat PRBS valve opening (τ) perturbation (numerical case study).

The simulated pressure perturbations at P_1 , P_2 and P_3 are shown in Figure 8.4. The pressure signals are highly disordered, and no distinctive wave reflections by the thinner-walled sections can be found in the original pressure signals. In the following sections, the disordered signals will be processed to uncover the hidden information about the thinner-walled sections.

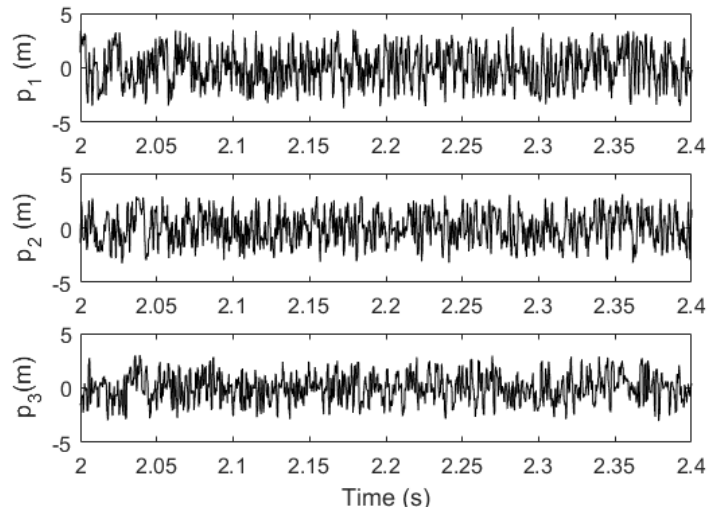


Figure 8.4 Simulated pressure head traces at (a) P₁; (b) P₂ and (c) P₃.

8.3.2 Least squares deconvolution

In the following section, division operations between two signals in the frequency domain such as

$$Z(j\omega) = Y(j\omega)/X(j\omega) \quad (8-3)$$

will be used, with j representing the imaginary unit and ω representing the angular frequency. The division is straightforward and pointwise along the frequency axis, however, the denominator $X(j\omega)$ tends to be zero (or close to zero) especially in the high-frequency range and this leads to a singularity problem. A least squares deconvolution technique (Nguyen et al. 2018) in the time domain has been applied to address this problem, and is discussed in the following.

Equation (8-3) can be rewritten in the time-domain matrix form $\mathbf{y} = \mathbf{Xz}$, in which \mathbf{X} is a lower triangular matrix consisting of the time-series of input elements and with rows being incrementally delayed vectors of the input, \mathbf{y} and \mathbf{z} are column vectors of the output time series and the time-domain series of the IRF coefficients, respectively. Given this form, the least squares estimator for

the impulse response, including regularization to reduce the effect of noise, can be written as

$$\mathbf{z} = (\mathbf{X}^T \mathbf{X} + \lambda \mathbf{I})^{-1} \mathbf{X}^T \mathbf{y} \quad (8-4)$$

where \mathbf{I} represents the identity matrix and λ is a positive constant parameter which controls the level of suppression of the noise. Details of the least squares optimization approach can be found in Nguyen et al. (2018) and approaches for choosing the suitable value of λ can be found in Wang et al. (2018).

By using Eq. (8-4), the deconvolution of p_2 and p_3 with regard to p_1 can be obtained. An example of this is shown in Figure 8.5 for the numerical case discussed above. The positive peaks with a value close to 1 in the figure are associated with the incident impulse, and the negative peaks with a value close to -1 are due to the reservoir reflections.

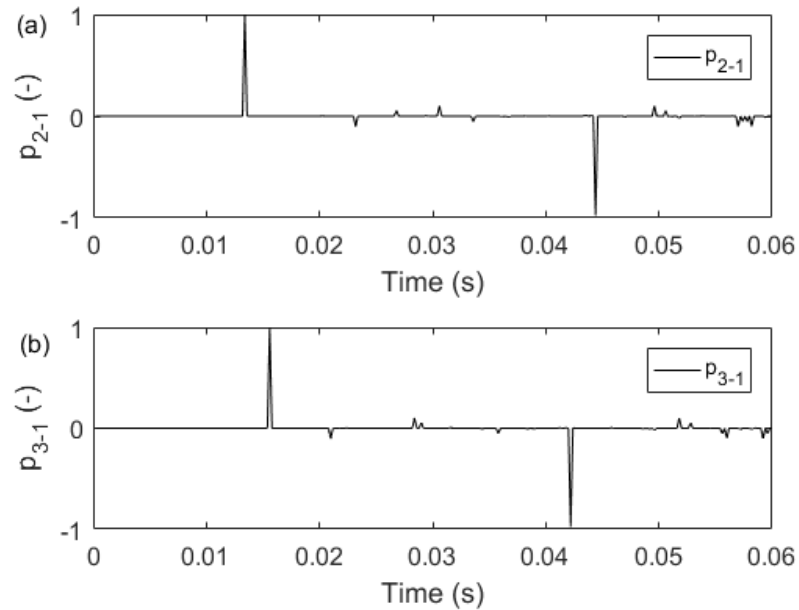


Figure 8.5 Results of the least squares deconvolution (a) p_{2-1} ; and (b) p_{3-1} (numerical case study).

8.3.3 Wave separation

The trace of the deconvolution result $p_{2,1}$ in Figure 8.5 is considered as a linear superposition of a forward travelling wave [propagating left to right towards the upstream direction (the tank)] and a backward travelling wave [propagating left to right towards the downstream direction (the closed in-line valve)], and therefore can be written as

$$P_{2,1}(j\omega) = P_{2,1}^+(j\omega) + P_{2,1}^-(j\omega) \quad (8-5)$$

where the uppercase italic P represents the pressure in the frequency-domain.

At location P_3 , the deconvolution result can be described in the frequency domain as

$$P_{3,1}(j\omega) = P_{2,1}^+(j\omega)H(j\omega) + P_{2,1}^-(j\omega)/H(j\omega) \quad (8-6)$$

where $H(j\omega)$ represents the wave propagation transfer function for the pipe section between P_2 and P_3 .

A rearrangement of Eqs. (8-5) and (8-6) gives

$$P_{2,1}^+(j\omega) = \frac{P_{2,1}(j\omega) - P_{3,1}(j\omega)H(j\omega)}{1 - H^2(j\omega)} \quad (8-7)$$

$$P_{2,1}^-(j\omega) = \frac{P_{3,1}(j\omega)H(j\omega) - P_{2,1}(j\omega)H^2(j\omega)}{1 - H^2(j\omega)} \quad (8-8)$$

Eqs. (8-7) and (8-8) can be used to obtain the directional deconvolutions ($p_{2,1}^+$ and $p_{2,1}^-$) from $p_{2,1}$ and $p_{3,1}$ following the wave separation technique and the inverse Fourier transform. The directional deconvolutions at P_2 for the numerical example case is shown in Figure 8.6.

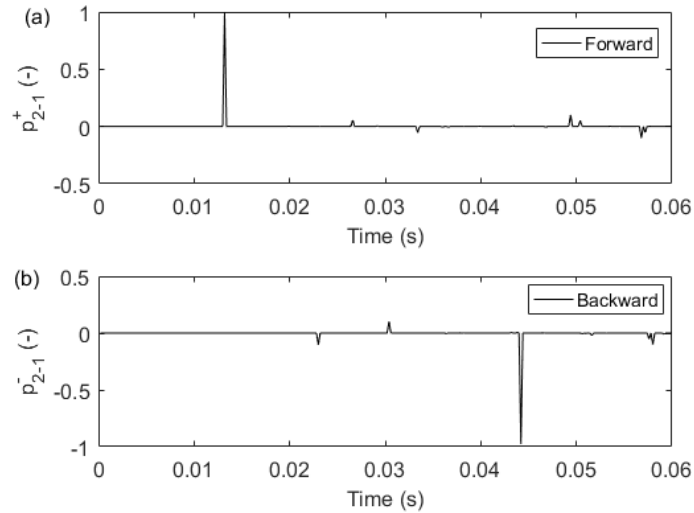


Figure 8.6 Directional deconvolutions at P_2 : (a) forward; and (b) backward.

8.4 IRFs with a First-order Accuracy and the First Pipeline Reconstruction

This section includes the analytical derivation of the IRF equations and is a key innovation and contribution of the research. The first-order IRFs for the pipe sections upstream and downstream of a transducer at an interior point (transducer P_2 in this case) can be obtained from the equations and used for the first (initial) pipeline impedance reconstruction.

8.4.1 IRF equations

By assuming an incident wave entering the pipeline (p_0 in the time domain and P_0 in the frequency domain) at location P_1 , a lumped pipeline system describing the wave propagation process is given in Figure 8.7, in which R , R_L and R_R represent the transfer functions (the frequency-domain representations of the IRFs) of the pipe system on the right (upstream) side of P_1 , the pipe section between P_1 and P_2 , and the pipe system on the right (upstream) side of P_2 (including the right-end boundary), respectively. The symbol \overleftarrow{R}_L (R_L with a backward arrow on the top) represents the IRF of the pipe section between P_1

and P_2 but excited from the right (upstream) side of P_2 . $H_{L,t}$ represents the transfer function of the pipe section between P_1 and P_2 . It can be separated into two parts including the first-order transmitted component H_L and some higher-order (≥ 2) reflections $H_L R_H$ by the discontinuities between P_1 and P_2 . In the following analysis, only first- and second-order wave reflections are considered and other higher wave reflections are ignored. The order of the wave reflections are defined by the times that the original wave has been reflected by any discontinuities.

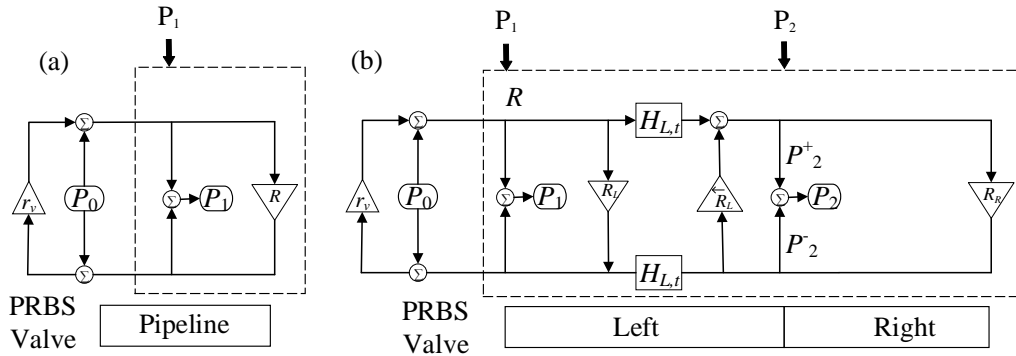


Figure 8.7 Block diagram describing the wave propagation process in (a) a lumped pipeline with one section and (b) a lumped pipeline with two sections.

According to Figure 8.7 (a), the pressure measured at P_1 , which includes the incident wave, wave reflections from the pipeline system and further reflections by the PRBS valve, can be written as

$$P_1 = (1 + r_v)P_0 + (1 + r_v)^2 P_0 R \quad (8-9)$$

where r_v represents the reflection ratio of the left boundary (the PRBS valve in this case).

The forward travelling pressure wave at P_2 consists of the result of the wave input p_0 and valve reflections, and the high-order reflections excited by the backward travelling waves. As a result, the forward travelling pressure wave at P_2 can be written as

$$P_2^+ = (1 + r_v)P_0H_{L,t} + (1 + r_v)P_0Rr_vH_{L,t} + P_2^- \cdot \overline{R_L} \quad (8-10)$$

which can be rearranged as

$$P_2^+ = (1 + r_v)P_0H_L(1 + R_H + Rr_v) + P_2^- \cdot \overline{R_L} \quad (8-11)$$

with wave reflections of the 3rd order and above neglected (i.e. the term $r_vP_0RR_H$ is neglected).

The backward travelling pressure wave at P_2 is the wave reflection from the right side of P_2 with the forward travelling pressure wave as the input. By neglecting the wave reflections of the 3rd order and above, the following simplified expression can be obtained.

$$P_2^- = (1 + r_v)P_0H_L(1 + Rr_v)R_R \quad (8-12)$$

Eq. (8-11) divided by Eq. (8-9) yields

$$P_{2,1}^+ = \frac{(1+R_H+Rr_v)H_L+P_2^-\overline{R_L}/(1+r_v)/P_0}{1+(1+r_v)\cdot R} \quad (8-13)$$

P_2^- can be replaced by Eq. (8-12), and Eq. (8-13) can be rewritten as

$$P_{2,1}^+ = H_L \frac{(1+Rr_v)(1+R_R\overline{R_L})+R_H}{1+(1+r_v)\cdot R} \quad (8-14)$$

A rearrangement of Eq. (8-14) gives

$$\begin{aligned} P_{2,1}^+ = & \underbrace{H_L(1 - R)}_{\text{order} = 1} + \underbrace{H_L(R^2 + r_vR^2 + R_H + R_R\overline{R_L})}_{\text{order} = 2} + \\ & \underbrace{H_L\left(\frac{r_vRR_R\overline{R_L} - (1+r_v)(R^3 + r_vR^3 + RR_H + RR_R\overline{R_L})}{1+R+r_v\cdot R}\right)}_{\text{order} \geq 3} \end{aligned} \quad (8-15)$$

Eq. (8-12) divided by Eq. (8-9) yields

$$P_{2,1}^- = \frac{(1+r_vR)H_LR_R}{1+(1+r_v)R} \quad (8-16)$$

A rearrangement of Eq.(8-16) gives

$$P_{2,1}^- = \underbrace{H_L R_R}_{\text{order} = 1} - \underbrace{H_L R_R R}_{\text{order} = 2} + \underbrace{\frac{(1+r_v)H_L R_R R^2}{1+(1+r_v)R}}_{\text{order} \geq 3} \quad (8-17)$$

Equations (8-15) and (8-17) illustrate the components of the directional deconvolutions and the details of the derivation of these two equations are presented in the Appendix.

8.4.2 IRFs with a first-order accuracy

The first-order IRFs can be obtained by neglecting all the high-order (>1) terms in Eqs. (8-15) and (8-17) and using a simplified H_L that considers wave dissipation but neglects dispersion. R_R in the 2nd-order term in Eq. (8-15) involves reservoir reflections which have a similar magnitude of the original wave, but the reservoir reflection appears after time t_L (round-trip wave travel time in the pipe between P_1 and P_2) in the IRF trace. Thus, the IRF corresponding to R in Eq. (8-15) obtained based on the aforementioned simplification is only valid before time t_L . Overall the first-order IRFs can be obtained from Eqs. (8-15) and (8-17) as

$$\text{IRF}_L(t) = \delta_0 - \text{IFFT}\left(\frac{P_{2,1}^+}{H_L}\right) \quad (0 \leq t \leq t_L) \quad (8-18)$$

$$\text{IRF}_R(t) = \text{IFFT}\left(\frac{P_{2,1}^-}{H_L}\right) \quad (0 \leq t \leq t_R) \quad (8-19)$$

in which IRF_L is the time-domain expression of R_L within the time period ($0 \leq t \leq t_L$) and IRF_R is the time-domain expressions of R_R within the time period ($0 \leq t \leq t_R$), $H_L = k \cdot e^{-j\omega t_L/2}$ with k representing the value of the first peak in Figure 8.5 (a) and t_R is the round-trip wave travel time in the pipe between P_2 and the tank. Terms $\text{IFFT}(P_{2,1}^+/H_L)$ and $\text{IFFT}(P_{2,1}^-/H_L)$ can be also calculated in the time domain by left shifting $p_{2,1}^+/k$ and $p_{2,1}^-/k$ by $t_L/2$ if the wave dispersion can be neglected.

With the first-order IRFs extracted as shown in Figure 8.8, the entire pipeline can be then reconstructed using the layer-peeling method described in the next section.

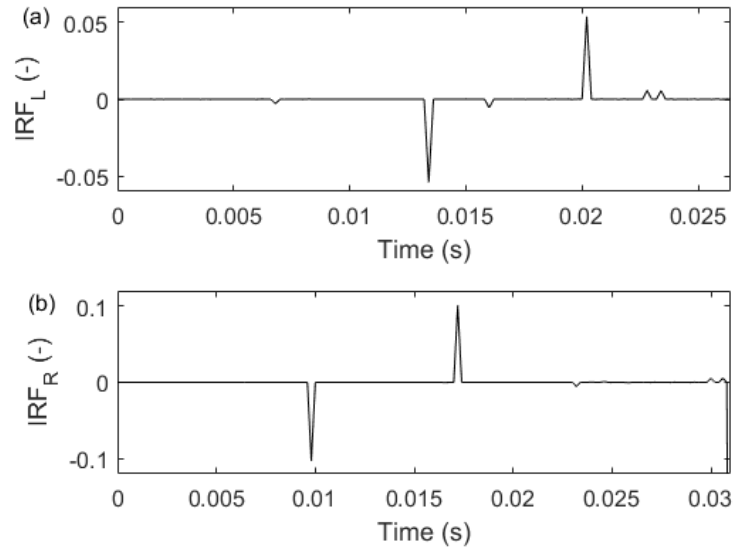


Figure 8.8 First-order IRFs of (a) the left side of the pipeline; and (b) right side of the pipeline.

8.4.3 First (initial) pipe impedance reconstruction

A brief review of the layer-peeling-based pipe impedance reconstruction technique is given below and the details of the algorithm can be found in Zeng et al. (2018). The numerical case of the pipeline system as shown in Figure 8.7 is used to illustrate the technique.

The pipe section is divided into N reaches as shown in Figure 8.9. T is the propagating time forth and back in one pipe section. The subscript i represents the i^{th} pipe reach, and subscripts l and r represent the left side and right side of a pipe reach, respectively. For the first pipe reach, $p_{1,l}^+$ is an input signal and $p_{1,r}^-$ is IRF_R . The procedures are listed as:

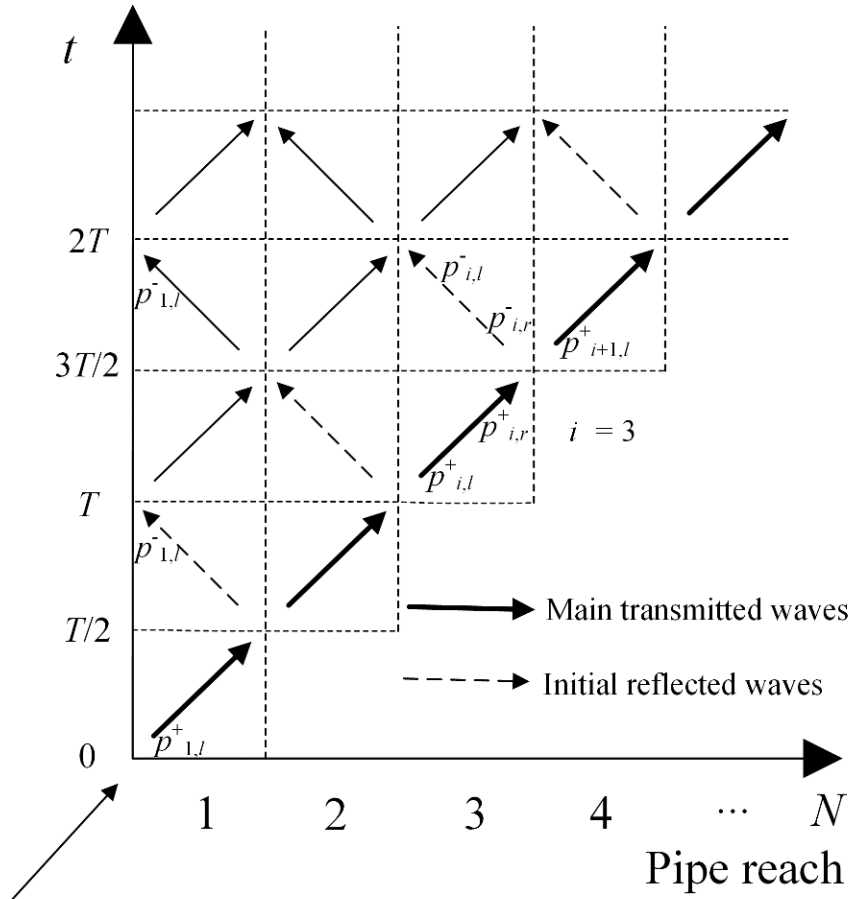


Figure 8.9 Space-time diagram of the wave propagation.

Step 1: using the waves at the left side of the i^{th} ($i=1$ for the first step) pipe reach $P_{i,l}^+$ and $P_{i,l}^-$ to calculate the waves at the right side of the i^{th} reach $P_{i,r}^+$ and $P_{i,r}^-$ through

$$P_{i,r}^+ = P_{i,l}^+ H_i \quad (8-20)$$

$$P_{i,r}^- = P_{i,l}^- / H_i \quad (8-21)$$

where H_i represents the wave transfer function (which can be used to describe wave dissipation and dispersion) in the i^{th} pipe reach.

Step 2: using the waves at the right side of the i^{th} reach $p_{i,r}^+$ and $p_{i,r}^-$ to calculate the reflection coefficient $r_{i,i+1}$ through

$$r_{i,i+1} = \frac{p_{i,r}^-(iT/2)}{p_{i,r}^+(iT/2)} \quad (8-22)$$

where $p_{i,r}^-(iT/2)$ and $p_{i,r}^+(iT/2)$ represent the initial reflected waves and main transmitted waves, respectively, as shown in Figure 8.9.

Step 3: Calculating the characteristic impedance of the next reach B_{i+1} through

$$B_{i+1} = \frac{1+r_{i,i+1}}{1-r_{i,i+1}} B_i \quad (8-23)$$

Step 4: using the waves at the right side of the i^{th} reach $p_{i,r}^+$ and $p_{i,r}^-$ together with the reflection coefficient $r_{i,i+1}$ to calculate the waves at the left side of the $(i+1)^{\text{th}}$ reach $p_{i+1,l}^+$ and $p_{i+1,l}^-$ through (Amir and Shimony 1995a)

$$\begin{bmatrix} p_{i+1,l}^+ \\ p_{i+1,l}^- \end{bmatrix} = \frac{1}{1-r_{i,i+1}} \begin{bmatrix} 1 & -r_{i,i+1} \\ -r_{i,i+1} & 1 \end{bmatrix} \begin{bmatrix} p_{i,r}^+ \\ p_{i,r}^- \end{bmatrix} \quad (8-24)$$

Step 5: Repeating Steps 1 to 4 for $i = 2 \dots N-1$ to calculate the characteristic impedance, the wave speed and the wall thickness for each of the remaining pipe reaches.

By carrying out the procedure listed above, the impedance distribution of the pipeline (the numerical case, Figure 8.7) can be reconstructed as shown in Figure 8.10. In practice, the information about the wall thickness and wave speed are more useful for pipe condition assessment. Thus they are calculated by combining Eqs. (8-1) and (8-2) with $D + 2e = D_{out}$ and the results are shown in Figure 8.11. Some errors can be observed at the first thinner-walled section and at the rear part (from 32 m to 37 m in Figure 8.10) of the pipeline. They are due to the simplification and the neglect of the high-order wave reflections.

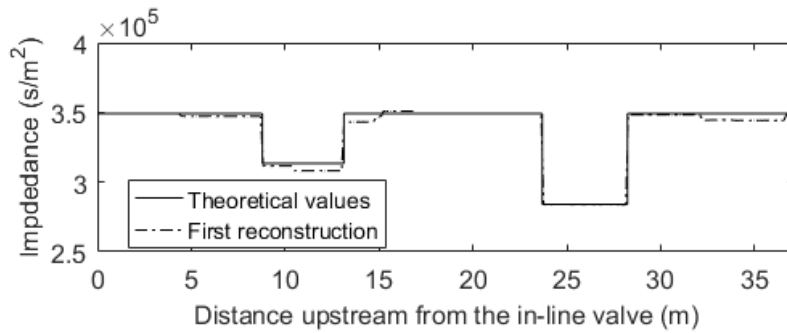


Figure 8.10 First (initial) pipeline reconstruction of the impedance distribution in the numerical case study compared with the theoretical values.

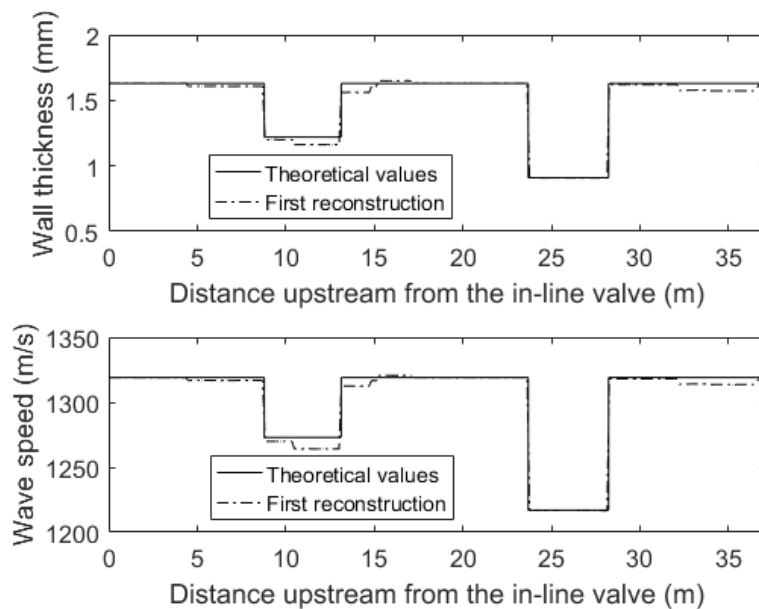


Figure 8.11 First (initial) pipeline reconstruction in the numerical case study compared with the theoretical values: (a) wall thickness distribution; and (b) wave speed distribution.

8.5 IRFs with a Second-order Accuracy and the Second Pipe Impedance Reconstruction

In this section, the second-order terms in the IRFs are calculated and the pipeline is reconstructed with a second-order accuracy.

8.5.1 IRFs with a second-order accuracy

To calculate the IRFs with a second-order accuracy, the terms with a third or higher order in Eqs. (8-15) and (8-17) are neglected. The second-order terms in the IRF equations can be calculated by using the first-order IRFs R_L and R_R . Thus, the $IRF_{L,2}$ and $IRF_{R,2}$ (the subscript 2 means they include second-order wave reflections) with a second-order accuracy can be obtained by rearranging Eqs. (8-15) and (8-17) and written as

$$IRF_{L,2} = \text{IFFT} \left[1 - \frac{P_{2,1}^+}{H_L} + (1 + r_v)R_L^2 + R_H + R_R \overleftarrow{R_L} \right] \quad (0 \leq t \leq t_L) \quad (8-25)$$

$$IRF_{R,2} = \text{IFFT} \left(\frac{P_{2,1}^-}{H_L} + R_R R_L \right) \quad (0 \leq t \leq t_R) \quad (8-26)$$

The time domain values of the three terms: R_L^2 (Term 1), $R_R R_L$ (Term 2) and $R_R \overleftarrow{R_L}$ (Term 3) in Eqs. (8-25) and (8-26) can be obtained using a convolution operation and the results are shown in Figure 8.12 (a) (b) and (c), respectively.

The term R_H can be calculated using the first-order impedance distribution of the pipeline. By assuming a pulse input $P_{1,l}^+(0) = \delta_0$ ($\delta_0 = 1$ at $t = 0$, and $\delta_0 = 0$ if $t \neq 0$) into the first reach of the pipeline, the wave propagation paths are shown in Figure 8.9. The wave at each position and each time step can be calculated following the wave propagation paths from $t = 0$ to $t = t_L$.

Step 1 ($t = T/2$): The forward travelling wave at the right side of the 1st section $P_{1,r}^+(T/2)$ can be obtained with $P_{1,l}^+(0)$ through Eq.(8-20).

Step 2 ($t = T/2$): Waves $p_{1,r}^-(T/2)$ and $p_{2,l}^+(T/2)$ can be obtained through

$$p_{i,r}^- = r_{i,i+1} \cdot p_{i,r}^+ \quad (8-27)$$

$$p_{i+1,l}^+ = (1 + r_{i,i+1}) \cdot p_{i,r}^+ \quad (8-28)$$

Step 3 ($t = T$): Waves $p_{1,l}^-(T)$ and $p_{2,r}^+(T)$ can be obtained through Eqs. (8-20) and (8-21).

Step 4 ($t = T$): Waves $p_{1,l}^+(T)$, $p_{2,r}^-(T)$ and $p_{3,l}^+(T)$ can be obtained through Eqs.(8-27) and (8-28).

Step 5: Following the wave propagation paths shown in Figure 8.9, the waves at each node and each time step can be calculated. The forward travelling wave at P_2 is r_H (time domain expression of R_H) as shown in Figure 8.12 (d).

By taking the second-order terms into Eqs. (8-25) and (8-26), the IRFs with a second-order accuracy can be obtained and as shown in Figure 8.13.

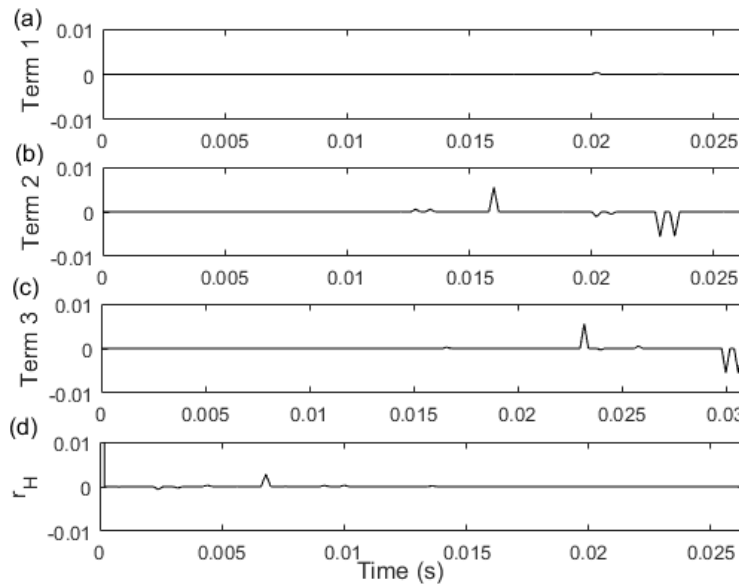


Figure 8.12 Second-order terms in the IRF equations.

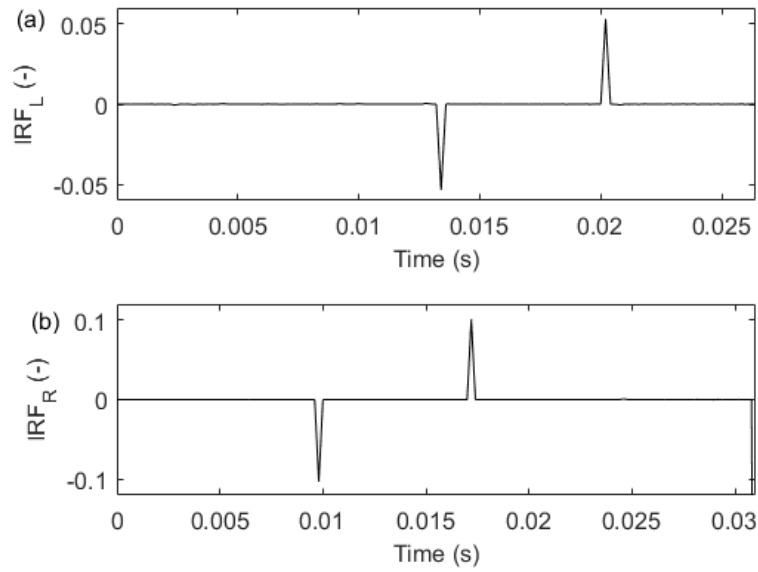


Figure 8.13 IRFs with a second-order accuracy of (a) the pipe section on the left of P_2 ; and (b) the pipe section on the right side of P_2 .

8.5.2 Second pipe impedance reconstruction

By using the IRFs with a second-order accuracy as shown in Figure 8.13, the distribution of the pipeline impedance, wall thickness and wave speed can be reconstructed with a higher accuracy. The reconstructed pipe wall thickness and wave speed results are shown in Figure 8.14, where the errors observed in the first (initial) reconstruction (Figure 8.11) have been eliminated.

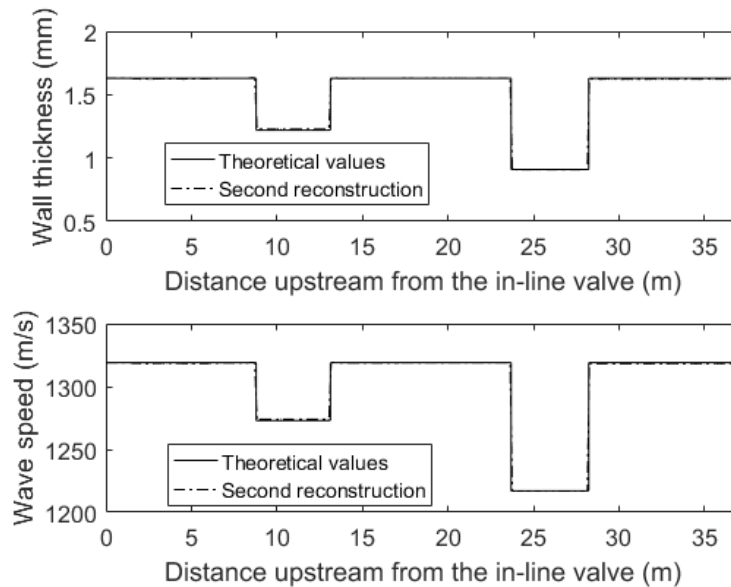


Figure 8.14 Second pipe impedance reconstruction in the numerical case study compared with the theoretical values: (a) wall thickness distribution; and (b) wave speed distribution.

8.6 Experimental Verification

Laboratory experiments have been conducted in (Nguyen et al. 2019) on a single copper pipeline system in the Robin Hydraulics Laboratory at the University of Adelaide and the results were used for validation. The layout and detailed information of the experimental pipeline system is given in Figure 8.1 and Table 8.1.

8.6.1 Experimental data and IRF determination

A customized side-discharge valve-based transient generator (Gong et al. 2015a) was used to generate PRBS transient pressure signals. The generator was connected to the pipeline at the left-hand end adjacent to the closed in-line valve as shown in Figure 8.1. The valve opening perturbation τ was measured by a linear voltage displacement transducer (LVDT). As shown in Figure 8.15, the normalized τ perturbation follows the PRBS pattern, but with small variations due to the limitation in the maneuverability of the side-discharge valve. The

PRBS signal used in the experimental case was generated from a 10-stage shift register with a clock frequency of 100 Hz and a period of 20.46 s.

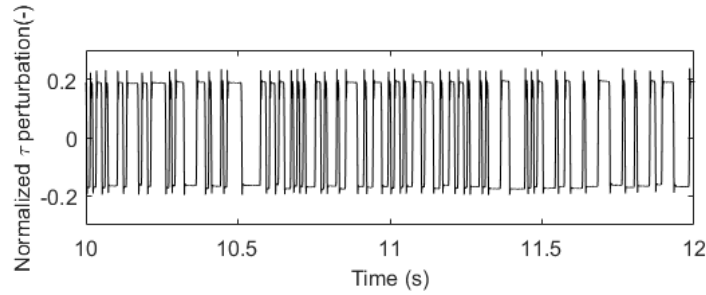


Figure 8.15 Normalized τ perturbation (Experiment).

The measured pressure perturbations in a certain period are given in Figure 8.16, which shows little visible structure. By applying Eq. (8-4), the deconvolutions can be obtained as shown in Figure 8.17. The wave separation technique and IRF equations were then applied to the deconvolutions to obtain the IRFs with a first-order accuracy shown as the solid line in Figure 8.18. Second-order terms in the IRF equations were then calculated and the IRFs with a second-order accuracy are plotted using the dot-dashed line (slightly different than the first-order IRFs) in Figure 8.18.

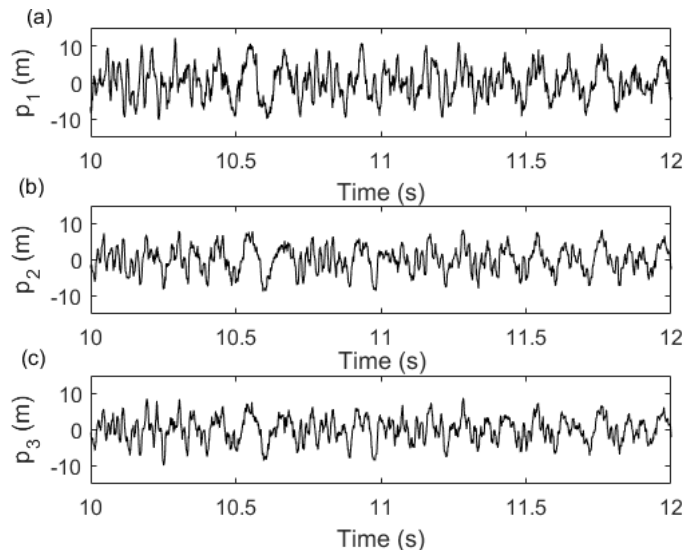


Figure 8.16 Experimental pressure perturbations at (a) P_1 ; (b) P_2 and (c) P_3 .

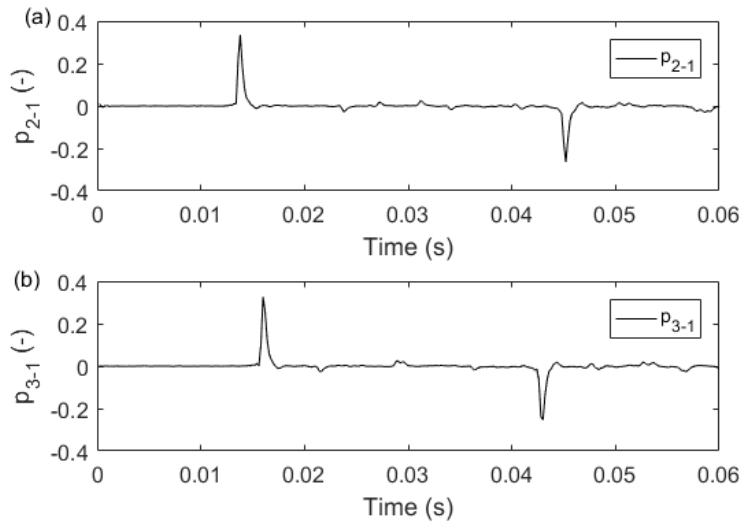


Figure 8.17 Least squares deconvolution (a) p_{2-1} ; and (b) p_{3-1} (Experiment).

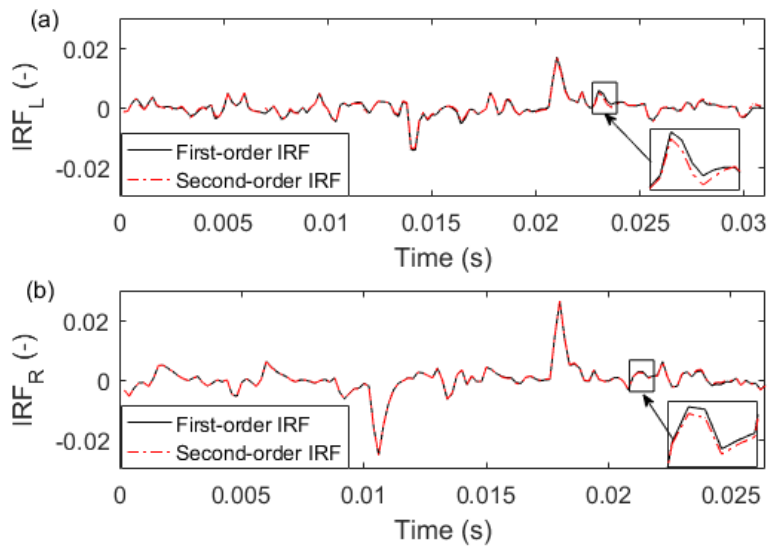


Figure 8.18 IRFs with a first-order and a second-order accuracy for (a) the pipe section on the left side of P_2 ; and (b) the pipe section on the right side of P_2 (Experiment).

8.6.2 Reconstruction of the pipe impedance

The pipeline was reconstructed following the two-step strategy using the layer-peeling algorithm with the first-order IRFs and second-order IRFs, respectively. As shown in Figure 8.19, clear features in the reconstructed wall thickness and

wave speed distributions can be observed in both the first and second reconstructions. The results of the second reconstruction (dashed line) match better with the theoretical values (for both the wall thickness and wave speed) than the results of the first reconstruction (dash-dotted line) for the deteriorated section closer to the in-line valve (the Class B pipe section in Figure 8.1). Slight differences can be observed in other places between the results of the first and the second reconstructions. The second reconstruction has improved the accuracy of the assessment and both deteriorated pipe sections (the Class B and C pipe sections in Figure 8.1) can be identified successfully. However, the results from the second reconstruction still include perturbations. One of the sources of the perturbations is from the signal separation process, in which the transfer function of the pipe section between P_2 and P_3 is not accurately known. Other factors such as the joints on the pipeline, natural variations in the pipeline parameters, fluid-structure interactions with persistent excitations and other uncertainties associated with the experiments can also cause uncertainties in the reconstructed results.

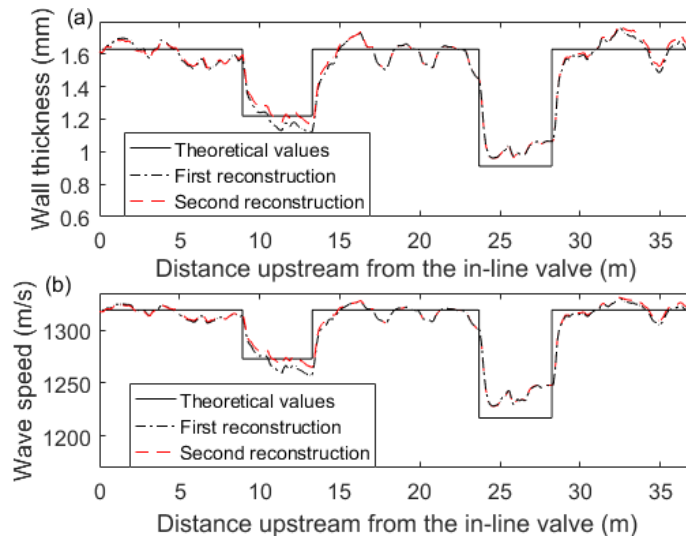


Figure 8.19 First and second reconstruction using the extracted IRFs: (a) reconstructed wall thickness distribution compared with the theoretical values; and (b) reconstructed wave speed distribution compared with the theoretical values.

8.7 Conclusions

This research proposes a new transient-based pipeline condition assessment technique using a persistent PRBS excitation, a three-pressure sensor measurement strategy, and a two-step layer-peeling-based analysis approach. The new technique enables robust and spatially continuous reconstruction of the pipeline impedance, which is then used to determine the distribution of the wall thickness and wave speed.

A significant contribution of the research is the derivation of the analytical expression of the IRFs of various pipe sections with respect to the pressure responses collected by the pressure sensors at three locations. This has advanced the knowledge of how pipeline transient pressure responses relate to pipeline physical properties. Built on this knowledge, a two-step strategy has been developed for the robust and accurate reconstruction of the pipeline properties (impedance, wall thickness and wave speed). In the first step, by neglecting the high-order terms in the IRF equations, IRFs with only the first-order terms are obtained and used to reconstruct the pipeline wall thickness and wave speed distributions with a first-order accuracy using the layer-peeling method. In the second step, the second-order terms in the IRF equations are estimated using the results of the first reconstruction. Using the IRFs with a second-order accuracy, a second pipeline reconstruction is conducted, the results of which have an enhanced accuracy.

A numerical case study has been conducted based on the information of a laboratory pipeline with two thinner-walled sections (simulating deteriorated pipe sections due to extended corrosion). The wall thickness and wave speed results obtained from the first pipeline reconstruction show discrepancies from the theoretical values in the numerical model. The results of second reconstruction show improvement and are highly consistent with the theoretical values, which demonstrates that the proposed two-step strategy can enhance the accuracy of pipe condition assessment.

Experimental verifications have been conducted on the aforementioned laboratory pipeline system. The distribution of the pipeline wall thickness and the wave speed have been successfully reconstructed, from which the two thinner-walled sections can be clearly identified. Compared to the results from the first reconstruction, the second reconstruction has resulted in improvements in the accuracy.

8.8 Appendix

8.8.1 Derivation of equation (8-15)

Equation (8-15) is derived from Eqs. (8-9) and (8-11) as follows:

Taking the ratio of (8-11) and (8-9) yields:

$$P_{2_1}^+ = H_L \frac{1+r_v R+R_R \overline{R_L}+r_v R R_R \overline{R_L}+R_H}{1+R+r_v R} \quad (8-29)$$

Manipulating Eq. (8-29) to extract 1 from the fraction yields

$$P_{2_1}^+ = H_L \left(1 + \frac{-R+R_R \overline{R_L}+R_H+r_v R R_R \overline{R_L}}{1+R+r_v R} \right) \quad (8-30)$$

Manipulating this to extract the first-order term from the fraction yields

$$P_{2_1}^+ = H_L (1 - R) + H_L \left(\frac{R^2+r_v R^2+R_R \overline{R_L}+R_H+r_v R R_R \overline{R_L}}{1+R+r_v R} \right) \quad (8-31)$$

Manipulating this to extract the second-order term from the fraction yields Eq. (8-15).

8.8.2 Derivation of equation (8-17)

Equation (8-17) is derived from Eqs. (8-9) and (8-12) as follows:

Taking the ratio of (8-12) and (8-9) yields:

$$P_{2_1}^- = H_L R_R \frac{1+r_v R}{1+R+r_v \cdot R} \quad (8-32)$$

Manipulating this to extract the first-order term from the fraction yields

$$P_{2_1}^- = H_L R_R - H_L R_R \frac{R}{1+R+r_v R} \quad (8-33)$$

Manipulating this to extract the second-order term from the fraction yields Eq. (8-17).

Acknowledgements

The research presented in this paper has been supported by the Australian Research Council through the Discovery Project Grant DP170103715.

Chapter 9

Leak Detection for Pipelines using In-Pipe Optical Fiber Pressure Sensors and a Paired-IRF Technique (Journal Publication 7)

Wei Zeng¹, Jinzhe Gong¹, Peter R. Cook², John W. Arkwright², Angus. R. Simpson¹, Benjamin S. Cazzolato³, Aaron C. Zecchin¹, and Martin F. Lambert¹

¹School of Civil, Environmental and Mining Engineering, the University of Adelaide, Adelaide, SA 5005 Australia

²School of Computer Science, Engineering and Mathematics, Flinders University, Clovelly Park, SA 5042, Australia

³School of Mechanical Engineering, University of Adelaide, SA 5005, Australia

Citation: Zeng, W., Gong, J., Cook, P. R., Arkwright, J. W., Simpson, A. R., Cazzolato, B. S., Zecchin, A. C., Lambert, M. F. (2019). "Leak detection for pipelines using in-pipe optical fiber pressure sensors and a paired-IRF technique." *IEEE Sensors Journal* (Submitted).

Statement of Authorship

Title of Paper	Leak Detection for Pipelines with Limited Access using In-Pipe Optical Fiber Pressure Sensors and a Paired-IRF Technique
Publication Status	<input type="checkbox"/> Published <input type="checkbox"/> Accepted for Publication <input checked="" type="checkbox"/> Submitted for Publication <input type="checkbox"/> Unpublished and Unsubmitted work written in manuscript style
Publication Details	Zeng, W., Gong, J., Cook, P., Arkwright, J., Simpson, A., Cazzolato, B., Zecchin, A., Lambert, M. Leak Detection for Pipelines with Limited Access using In-Pipe Optical Fiber Pressure Sensors and a Paired-IRF Technique. IEEE Sensor (Submitted)

Principal Author

Name of Principal Author (Candidate)	Wei Zeng		
Contribution to the Paper	Conception and design of the project Analysis and interpretation of research data Draft the paper		
Overall percentage (%)	65 %		
Certification:	This paper reports on original research I conducted during the period of my Higher Degree by Research candidature and is not subject to any obligations or contractual agreements with a third party that would constrain its inclusion in this thesis. I am the primary author of this paper.		
Signature		Date	8/11/2019

Co-Author Contributions

By signing the Statement of Authorship, each author certifies that:

- i. the candidate's stated contribution to the publication is accurate (as detailed above);
- ii. permission is granted for the candidate to include the publication in the thesis; and
- iii. the sum of all co-author contributions is equal to 100% less the candidate's stated contribution.

Name of Co-Author	Jinzhe Gong		
Contribution to the Paper	Conception and design of the project Analysis and interpretation of research data Critically revising the paper		
Signature		Date	24/11/19

Name of Co-Author	Peter Cook		
Contribution to the Paper	Conception and design of the project Analysis and interpretation of research data Critically revising the paper		
Signature		Date	

Please cut and paste additional co-author panels here as required.

Name of Co-Author	John Arkwright		
Contribution to the Paper	Conception and design of the project Analysis and interpretation of research data Critically revising the paper		
Signature		Date	17/10/19

Name of Co-Author	Angus Simpson		
Contribution to the Paper	Conception and design of the project Analysis and interpretation of research data Critically revising the paper		
Signature		Date	4 Nov. 2019

Name of Co-Author	Benjamin Cazzolato		
Contribution to the Paper	Conception and design of the project Analysis and interpretation of research data Critically revising the paper		
Signature		Date	8 Nov 2019

Name of Co-Author	Aaron Zecchin		
Contribution to the Paper	Conception and design of the project Analysis and interpretation of research data Critically revising the paper		
Signature		Date	15/11/19

Name of Co-Author	Martin Lambert		
Contribution to the Paper	Conception and design of the project Analysis and interpretation of research data Critically revising the paper		
Signature		Date	22/11/19

Abstract

Leak detection in water distribution systems is crucial in reducing water loss and improving the efficiency of water transmission. A hydraulic transient-based paired-IRF (impulse response function) technique has been previously developed and demonstrated as an effective method for leak detection in pipelines. However, the technique requires transient pressure measurements at two locations in close proximity in the pipe, which is often very difficult to achieve for buried pipelines using conventional flush-mounted pressure transducers. The current paper reports on the use of a customized in-pipe optical fiber sensor array for transient pressure measurement and the implementation of the paired-IRF technique for leak detection for a laboratory copper pipeline. The in-pipe optical fiber sensor array contains two fiber-Bragg-grating (FBG)-based pressure sensors contained in a protective cable. It is inserted into the laboratory pipeline through a tapping point to measure the pressure responses induced by a voice-coil-based pressure wave generator, which generates a persistent excitation following a pseudo-random binary sequence (PRBS). The paired-IRF technique is then applied to the measurements to obtain the paired-IRF response of the pipe system. The paired-IRF response is determined and it clearly indicates the existence of the simulated leak (through a side-discharge on the pipe). In addition, a pipe joint is also detected using the paired-IRF trace, which confirms the detection system and method have the ability to achieve high detectability. The successful experimental application illustrates that the in-pipe optical fiber sensor array has the ability to be applied in pipes with limited access points and leak detection can be achieved by combining with the paired-IRF technique.

9.1 Introduction

Large amounts of water are lost during transmission in ageing water distribution systems (WDSs) due to the existence of leaks. According to an estimate by the World Bank, the worldwide water-loss volume amounts to 48.6 billion m³ per year (Cataldo et al. 2012). The leakage of WDSs contributes to a significant economic cost along with increased energy consumption (Nixon and Ghidaoui 2006; Colombo et al. 2009). The transported water can also be contaminated due to backflow through the leak openings along the pipe during low pressure events (Fox et al. 2016). As a result, reliable and robust leak detection is significant for controlling water loss and to enable predictive repair and strategically targeted pipe maintenance of WDSs.

A number of leak detection techniques have been developed based on passive “listening” and analyzing the leak-induced features on the signals collected. Different types of sensors can be used for the “listening”, such as accelerometers (Stephens et al. 2018), pressure transducers (Zan et al. 2014), hydrophones and optical fiber sensors (Wong et al. 2018a; Wong et al. 2018b). Typically, the existence of a leak will induce high-frequency components (relative to the background acoustic noise) in the spectra and enhance the magnitude of the signal collected by acoustic sensors (Stephens et al. 2018). A leak signal collected by acoustic sensors can be characterized and identified by its mean value, standard deviation, peak value and waveforms, etc. (Wang et al. 2017). Transient pressure fluctuations collected by high-speed pressure transducers can also be used to identify the occurrence of a pipe break/burst in a pipe network (Zan et al. 2014). The existence of a leak or a crack can lead to strain changes of the pipe wall, which can be detected by distributed external optical fiber sensors for detection and localization purposes (Wong et al. 2018b). These leak detection techniques based on passive “listening” typically can usually only cover a very limited length of pipe due to the fact that leak-induced signals are weak and quickly attenuate. The application is very challenging in noisy city environments or in pipe systems with high background acoustic interference (e.g. pump noise).

Hydraulic transient-based leak detection techniques have been studied over the past three decades. These techniques use controlled hydraulic transient pressure waves as a tool for active leak detection: an incident pressure wave is introduced into the pipeline, and the propagating incident wave will be reflected by any physical anomalies, such as a leak or a deteriorated pipe section (e.g. with extended corrosion). The pressure traces collected by pressure transducers contain the incident wave and reflected waves, and can be analyzed using inverse transient analysis (Liggett and Chen 1994; Capponi et al. 2017), frequency response function (FRF)-based techniques (Lee et al. 2006; Gong et al. 2013a), impulse response function (IRF)-based techniques (Vítkovský et al. 2003b; Nguyen et al. 2018) or the recently developed paired-IRF technique (Zeng et al. Forthcoming). Such hydraulic transient-based methods are non-invasive and the devices for detection are portable, which can enable cost-effective leak detection. However, the connection ports to install pressure wave generators and pressure transducers are usually quite limited in buried pipe networks. To avoid excavation, typically single pressure transducers are connected to existing access points (such as fire hydrants or air valves) that are often long distances apart (Butterfield et al. 2018). The pressure measurement at a single transducer is always the superposition of waves travelling upstream and downstream along the pipe, resulting in complex waveforms that are difficult to interpret in most real pipe systems.

A wave separation technique has recently been developed using a dual-sensor (two pressure transducers in close proximity) which resolves the complexity induced by wave supposition through extracting the two directional traveling pressure waves along a pipe (Shi et al. 2017). Building on this dual-sensor concept, a paired-IRF technique has been developed for robust leak detection in complex pipe systems (Zeng et al. Forthcoming). However, as mentioned above, the implementation of a dual-sensor measurement configuration is difficult for buried pipes, where access points are usually sparsely located.

The authors have been working on an in-pipe optical fiber sensor array technology to achieve distributed transient pressure measurement through a single measurement station. Sensor arrays fabricated from Draw Tower Grating

(DTG) arrays (FBGS International, Geel, Belgium) consisting of multiple fiber Bragg grating (FBG)-based pressure transducers have been developed for a range of applications including monitoring muscular activity in the human gut (Arkwright et al. 2012), and monitoring the horizontal and vertical pressures in water tanks (Arkwright et al. 2014). A prototype in-pipe optical fiber sensor array was developed and tested for transient wave separation (Shi et al. 2019). It was also tested for measuring leak reflections induced by a transient pressure step wave (Gong et al. 2018b). The early work has validated the concept of the in-pipe optical fiber sensor array; however, it has also revealed a relatively high noise floor in the measurement.

The current paper reports a new generation of in-pipe optical fiber sensor array with an improved signal-to-noise ratio better suited to transient pressure measurement. The sensor cable can be placed in a pressurized pipe for an extended time period, and persistent but small-amplitude transient pressure waves can be used as the excitation instead of the conventional discrete step waves (which are usually large in amplitude and have the potential risk of damaging the pipe system). Combining the in-pipe optical fiber sensor array, a customized voice-coil-controlled transient wave generator that produces a persistent excitation, and the paired-IRF technique, a complete system is formed for robust leak detection in pipelines with limited access (e.g. buried water pipelines). The new system has been tested on a single pipeline in the laboratory, where a leak was simulated using a side-discharge valve on the pipe. The paired-IRF response has been successfully obtained from the pressure measurements and the leak has been successfully detected and localized. A joint of the pipeline has also been detected using the paired-IRF trace, which demonstrates the ability of the technique to achieve high detectability.

9.2 Experimental Setup

Laboratory experiments have been designed and conducted by the candidate on a single copper pipeline system in the Robin Hydraulics Laboratory at the University of Adelaide. This section presents the experimental apparatus,

including the new in-pipe optical fiber sensor array for pressure measurement, the customized voice-coil-controlled side-discharge valve for transient pressure generation, and the layout of the pipeline system.

9.2.1 In-pipe optical fiber pressure sensor array

A photograph of the new-generation in-pipe optical fiber pressure sensor array used in this research is shown in Figure 9.1. The protective cable carrying the FBG sensors has an overall length of 2.15 m with two FBG sensors located on the cable at a distance of 0.8 m. The protective cable is made of two-layer square-lock casing tubes. The internal layer consists of a hollow, interlocking spiral-wound tube made from stainless steel which structurally reinforces the cable. The outer layer is a polyvinyl chloride (PVC) coating that inhibits water ingress and aids sealing at the insertion point. The new design of the protective cable enables the in-pipe sensors to be applied in water with a high pressure.

The working mechanism of the FBG pressure sensor is illustrated in in Figure 9.2. At each FBG sensor, a flexible elastomeric sleeve is used to cover the FBG. The FBG is designed to have a downward arc under atmospheric pressure and the flexible sleeve is in contact with the optical fiber in the region of the FBG. As the pressure increases from one atmosphere, the sleeve presses the FBG further inwards, which causes a change in the strain and in turn a shift in the reflected wavelength of the FBG. The shift in reflected wavelength was monitored using a high speed optical spectrometer (I-MON HS, Ibsen photonics, Denmark).

The cable configuration enables a high sensitivity to pressure variations under high background pressure conditions (as is the case in pressurized water pipes). While the mechanism is similar to that of the previous version reported in (Shi et al. 2019), in this new-generation sensor cable, improvements have been made to the seals to prevent water leakage for high pressure conditions.

In order to enhance the signal-to-noise ratio, especially for high frequencies, the signal strength is of primary concern. Optical splice losses between the DTG

arrays and the fiber pigtails using thermally expanded core splices and the optical interrogator settings were adjusted to maximize the dynamic range of the internal analog to digital converter in the I-MON spectrometer.

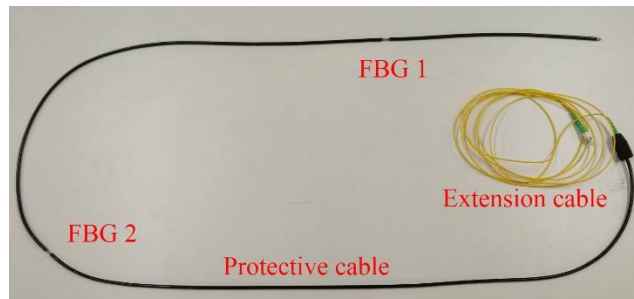


Figure 9.1 Photograph of the new generation in-pipe optical fiber sensor array.

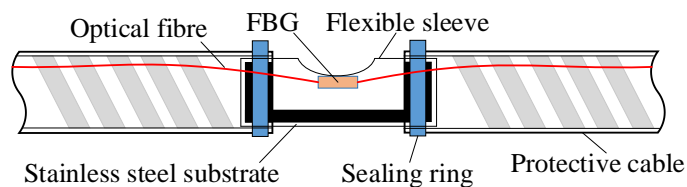


Figure 9.2 Schematic of the FBG pressure sensors.

9.2.2 Voice-coil-based transient pressure wave generation system

A schematic of the voice-coil-based transient generation system is shown in Figure 9.3. A voice-coil actuator is fixed on a brass block using a customized housing. The brass block has a clear aperture of reduced diameter running along the axis of the brass block to allow for water discharge. The piston of the actuator can travel perpendicularly through the brass block and adjust the opening of the aperture. The transient generator is connected to a side-tap in the laboratory pipe to provide a controlled discharge of water from the pipe. Signal generation software has been developed in the LabVIEW platform (National Instruments) to generate digital signals with designed waveforms. The digital signal is then sent into the power amplifier to be transferred to an analog electrical signal, which controls the movement of the piston in the voice-coil

actuator. With the piston moving, the opening area of the conduit will change accordingly. If the piston oscillates persistently, a continuous flow perturbation can be excited and it in turn induces persistent transient pressure waves inside the pipe.

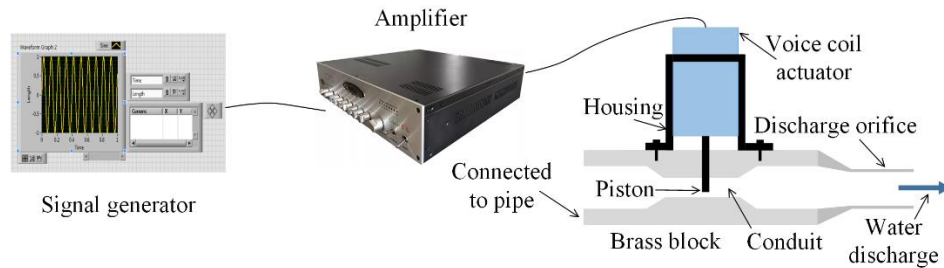


Figure 9.3 Schematic of the voice-coil based transient generation system.

When the laboratory pipe system has a steady-state pressure of 3 bar, the maximum flow rate through the generator is measured as 0.029 L/s when the piston is moved out of the conduit to maximize the discharge area. The minimum flow rate is measured as 0.009 L/s when the piston touches the bottom surface of the conduit. The generator cannot be fully sealed since the piston tip does not fully match the bottom surface of the aperture.

9.2.3 Experimental pipeline system

Figure 9.4 shows the layout of the experimental pipeline system. The pipeline was connected with a pressurized tank at the upstream end and a closed in-line valve at the downstream end. The pipeline was 37.46 m in length with an internal diameter, D_0 , of 22.14 mm throughout the pipe. The wave speed of the pressure wave in the pipe was $a_0 = 1319$ m/s (Gong et al. 2018b). A discharge orifice connected with a T-junction was used to simulate a leak (L_1 in Figure 9.4). A voice-coil based transient generator (G_1) which can generate customer-designed signals was installed at an interior point of the pipe. A solenoid-controlled side-discharge valve (G_2) was used for generating step pressure waves and was installed on the upstream face of the closed in-line valve. A conventional flush-mounted pressure transducer (T_1 , Model Druck PDCR 810, Leicester, UK) was installed next to the side-discharge valve (G_2). All the joints

(Swagelok pipe joint fittings) of the pipeline and the access point of the in-pipe optical fiber sensors are shown in the schematic. The cable that carries the optical fiber sensors was inserted into the pipe at the access point A_1 . The two FGB sensors within the optical fiber cable are denoted as F_1 and F_2 .

A pseudo random binary sequence (PRBS) signal commonly used in the electrical and electronics field for system identification was generated by the voice-coil based transient generator (G_1). Details about the characteristics of the PRBS and the method to formulate it can be found in Godfrey (1993). The PRBS signal is generated from a 10-stage shift register with a clock frequency of 100 Hz.

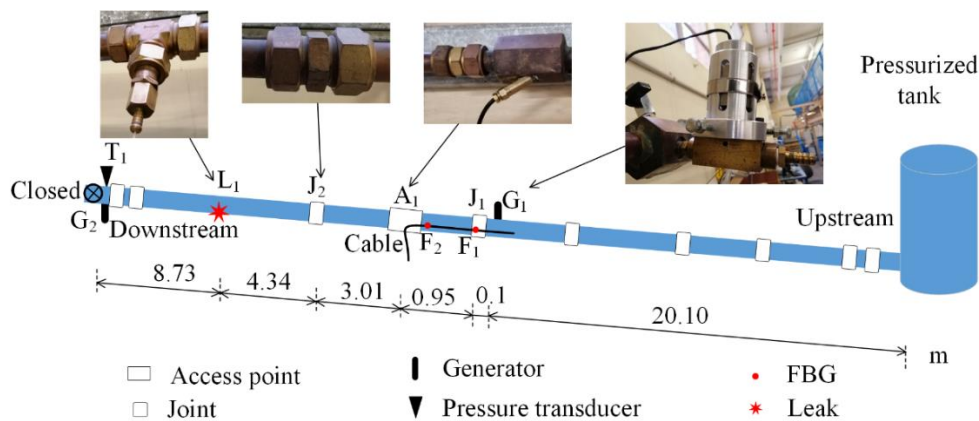


Figure 9.4 Schematic of the experimental pipeline system.

9.3 Transient Tests using Step Waves and a Conventional Pressure Transducer

Preliminary tests were conducted by using the solenoid-controlled generator (G_2) to illustrate the effect of the leak and the optical fiber sensor cable on the hydraulic transient pressure wave. The pipeline was pressurized to 3 bar in the steady state and the solenoid-controlled side-discharge valve was closed sharply to generate a step wave. The sampling rate of the pressure transducer was 10 kHz. The first test was conducted without the leak or the sensor cable, and the pressure measured by T_1 is shown as the solid line in Figure 9.5. Note

that the pressure is normalized by the magnitude of the incident step wave. Another test was conducted with the leak but without the sensor cable inside the pipe. According to the pipeline configuration shown in Figure 9.4, the pressure drop at $t = 0.024$ s, as shown in the dash-dotted line in Figure 9.5, was induced by the simulated leak on the pipeline. After deploying the sensor cable into the pipe, a third test was conducted and the result is shown as the dashed line in Figure 9.5. According to the occurrence time of the noticeable perturbations as highlighted within the oval in Figure 9.5, the perturbations are wave reflections from the sensor cable. This is because the in-pipe sensor cable introduced a change in the cross-sectional hydraulic impedance of the local pipe section. Analysis in the following section will show that this does not impede the determination of the paired-IRF or the leak detection.

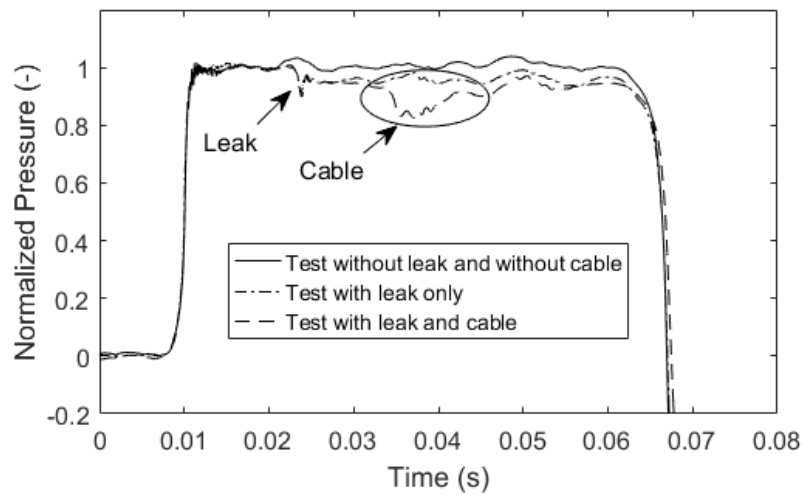


Figure 9.5 Pressure traces measured by the flush-mounted pressure transducer T_1 .

9.4 Leak Detection using the In-Pipe Optical fiber Sensors

9.4.1 Detection method

The paired-IRF method proposed in (Zeng et al. Forthcoming) is applied here to detect a leak in the laboratory pipeline. The frequency-domain representation of the pressure measured by the FBG sensors F_1 and F_2 are denoted as P_1 and P_2 , respectively. By assuming that the pipe section between F_1 and F_2 is uniform and with a transfer function of H , the relationship between P_2 and P_1 can be described by Eq. (9-1) (Zeng et al. Forthcoming) .

$$\frac{P_2}{P_1} = H + \left(\frac{1}{H} - H \right) R_L \quad (9-1)$$

where $R_L(j\omega)$ is the frequency response function [frequency-domain counterpart of the impulse response function (IRF)] of the pipeline section on the downstream side of F_1 (towards the closed in-line valve). By transferring P_2/P_1 into the time domain, the result obtained is defined as the paired-IRF trace since it consists of a superimposed pair of IRFs. By setting Δt as the one-way travel time of a transient pressure wave in section F_1 - F_2 , according to the linear systems theory (Oppenheim et al. 1997), the term $1/H$ in the brackets in Eq. (9-1) means transferring the IRF forward by Δt , while $-H$ in the brackets means reversing the sign of the IRF after delaying it by Δt . As a result, a leak (or other discrete anomalies such as a blockage) in the pipeline will induce a pair of spikes with opposite directions and with a time interval of $2\Delta t$ in the paired-IRF trace. This unique feature can be used to identify leaks with confidence.

The round-trip travel time t_{leak} of the pressure wave from F_1 to the leak and back to F_1 can be obtained by averaging the travel times between the pair of spikes. Thus, the location of the leak can be determined by

$$L_{leak} = \frac{a_0 \times t_{leak}}{2} \quad (9-2)$$

where L_{leak} is the distance from the leak to F_1 and a_0 is the wave speed.

9.4.2 Data analysis and results

The pressure perturbations measured using the FBG sensors were normalized to the range [-1,1] and the results over a 2 s period are plotted in Figure 9.6. Note that only the relative pressure perturbations are needed in the following analysis and the absolute pressure values are not needed. The paired-IRF was then extracted from the pressure traces and the results are shown in Figure 9.7. In addition to the tank-induced pulses at the end of the trace shown in Figure 9.7, two pairs of spikes, as highlighted in the boxes in the figure, can be found in the paired-IRF trace. The occurrence times of the spikes in each pair are averaged and the results are 6.03 ms and 12.65 ms. By using Eq. (9-2), the corresponding distances to F_1 of the anomalies that induced these spike-pairs are calculated to be 3.98 m and 8.34 m, respectively. According to the configuration of the pipeline system shown in Figure 9.4, the two spike-pairs are induced by the joint J_2 and the simulated leak L_1 , respectively. The predicted distances (3.98 m and 8.34 m) to P_1 are very close to the measured values (4.01 m and 8.35 m) with a relative error of 0.75% and 0.12%, respectively. Such a high accuracy of the detection has verified the usefulness of the in-pipe optical fiber sensor array for leak detection using the paired-IRF technique.

An issue that introduces some inaccuracies is that the spikes induced by the leak are contaminated with some fluctuations. This is caused by the wave oscillations in the T-junction that is used to simulate the leak. Apart from the two pairs of spikes highlighted in Figure 9.7, another small spike is also observed at $t = 0.016$ s. Conventional IRF-based detection techniques would consider this single spike as induced by a physical anomaly in the pipe. However, using the paired-IRF technique, it will be correctly categorized as an interference or numerical error since the spike is isolated and cannot be paired with another spike with a $2\Delta t$ time interval. Some relatively smooth fluctuations can be also found in the trace. They can be ascribed to the

disturbance of the transient waves caused by the sensor cable, hydraulic noise induced by the leak itself, small pressure fluctuations in the pressurized tank, fluid-structure interaction with persistent mechanical valve excitations and other uncertainties associated with the experiment.

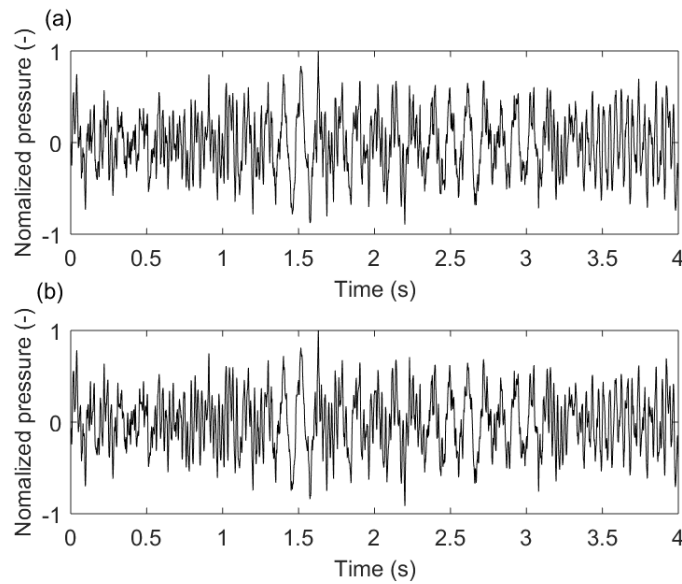


Figure 9.6 Measured pressure waves with a PRBS valve excitation for the experimental case at (a) P_1 and (b) P_2 .

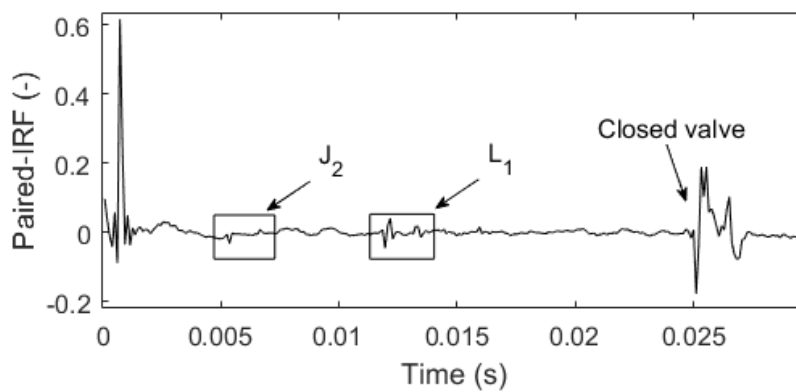


Figure 9.7 Paired-IRF extracted for the experimental case with a PRBS valve excitation.

9.5 Conclusions

A customized in-pipe optical fiber sensor array has been developed. It consists of two FBG pressure sensors carried by a two-layer square-lock protective cable. The sensor cable can be inserted into a pressurized pipeline through a single ingress, enabling pressure measurement at multiple locations in close proximity for pipelines with limited access. The composite protective sheath ensures the sensor array can withstand high pressures for an extended time period. The FBG sensors and the associated software in the data acquisition system are especially designed to enable accurate measurement of small-amplitude transient pressure waves.

Combining the in-pipe optical fiber sensor array with a voice-coil-controlled side-discharge valve that produces persistent excitation (e.g. PRBS) and the paired-IRF technique, a complete system is formed for robust leak detection in pipelines with limited access (e.g. buried water pipelines). The usefulness of the leak detection system has been validated for a single pipeline with a simulated leak in the laboratory. The paired-IRF response has been accurately determined, from which the simulated leak has been successfully detected and accurately localized. In addition to the leak, a joint on the pipe has also been detected from the paired-IRF trace, which demonstrates the high detectability of the detection system.

Acknowledgements

The research presented in this paper has been supported by the Australian Research Council through the Discovery Project Grant DP190102484. The authors thank technicians Simon Golding and Brenton Howie for their support in the experimental work, and Anthony Papageorgiou for assistance with designing the fiber optic cable.

This page is intentionally blank

Chapter 10

Conclusions

Two novel hydraulic transient-based techniques have been proposed in this thesis for the purpose of anomaly detection and condition assessment in pressurized pipelines. In addition, a voice-coil based transient generator has been developed with a new generation in-pipe optical fiber sensor array tested in the laboratory. They enable reliable transient tests for the proposed techniques. The specific contributions of this thesis are summarised below with the scope of future work presented.

10.1 Research Contributions

A novel paired-IRF technique has been developed for non-invasive anomaly detection in pressurised pipelines (Chapter 3). This is the first time that a transient-based method has been experimentally validated to be able to fully eliminate the effects from background pressure fluctuations and noise. The technique is validated to have a high detectability with the use of a continuous signal. It can be applied in pipe networks with arbitrary configurations. The advantages listed above allow for the potential of field applications.

With further development of the paired-IRF technique in Chapter 4, the technique is able to distinguish between different kinds of anomalies in pipeline systems. The detection range of the method is extended to multiple pipes in a network system. The tolerance to background pressure fluctuations and noise is further improved by using an averaging process. These improvements of the

paired-IRF technique make the technique even more suitable for field applications.

A layer-peeling method has been developed for non-invasive condition assessment in pressurised pipelines (Chapters 5). The original layer-peeling method was applied by others to solve different discrete inverse problems, such as reconstructing a tubular music instrument to check its quality. This is the first time that the layer-peeling method has been applied to water pipelines with the purpose of assessing their condition. Unsteady friction of the transient flow, pipe wall viscoelasticity and frequency-dependent wave reflections and transmissions are all incorporated into the reconstruction algorithm, which largely improves the accuracy of the reconstruction.

With further development of the layer-peeling method in Chapter 6, the method enables a bi-directional reconstruction of the pipeline. Pipelines with branches can be properly analyzed with the model of a bifurcation point incorporated. These improvements of the layer-peeling method provide the potential to apply the method to pipes in water distribution systems that contain numerous junctions.

A fast inverse transient method has been developed for non-invasive condition assessment in pressurised pipelines (Chapter 7). The layer peeling method was reversed to simulate the transient behaviour with inputting the pipeline impedance distribution. The proposed method has a high efficiency since the reversed layer peeling method has a much higher efficiency than the conventional method of characteristics. It concentrates on the major wave reflections and thus can compensate for the cumulative errors which may occur in the forward layer-peeling methods if the pipeline is long.

The layer-peeling method and the paired-IRF technique have been successfully combined (Chapter 8). The paired-IRFs of a pipeline were further manipulated to get the IRFs of the pipeline which are the input of the layer-peeling algorithm. The combination of these two methods yields a more accurate IRF since the effects from background pressure fluctuations and noise can be reduced by

using the paired-IRF technique. The detailed condition of the pipeline can be obtained with the application of the layer-peeling method.

A voice-coil-based transient generation system was developed in this research and it can send controlled (discrete or continuous) transient waves into pipelines (Chapter 9). A new generation of in-pipe optical fiber sensor array was designed and fabricated for transient pressure measurement (Chapter 9). The protective cable carries two fiber-Bragg-grating based pressure sensors and can be inserted into pressurized pipelines through the place where the transient generator is installed. Such transient generation and measurement systems enable practical transient tests for the paired-IRF and layer-peeling pipe condition assessment techniques.

The new techniques and testing devices developed in this thesis enable reliable and practical anomaly detection and condition assessment in water pipelines. The detection and assessment process involves two stages in which the paired-IRF and layer-peeling methods can be applied. The first stage (the paired-IRF method) is to identify and localize anomalies in the pipeline system and generally understand their properties, such as whether the anomaly is discrete or spatially distributed along the pipe. The results obtained at this stage can be used to guide the maintenance and rehabilitation of the pipelines. If the anomalies identified are found to be spatially distributed along the pipe in the first stage, which is common in aged water pipelines, the layer-peeling method can then be used in the second stage to reconstruct the properties of the anomalies which enables a strategic replacement of pipe sections. For example, only deteriorated sections with the wall thickness less than a threshold need to be replaced, while other sections which are only slightly deteriorated but otherwise in an acceptable condition can be still retained.

10.2 Scope of Future Work

Smart water technologies involving a large number of sensors have been emerging in recent years, and they can result in availability of large amounts of big data containing different types of information of a water network available,

such as the pressure information in the pipes. The techniques developed in this thesis provide an active detection approach with the use of pressure information measured by sensors and excited by a transient generator. Thus, the smart water technologies will provide the techniques developed in this thesis with new opportunities to be applied in the field, as well as new challenges to take advantage of the big data which contain large information of the water network.

With continuous pressure traces to be collected in a smart water network, the new challenge faced in the future is how to achieve continuous anomaly monitoring and regular pipe condition assessment. The current techniques developed in this thesis use a mobile hydraulic transient generator and mobile sensors that can be connected with the pipe or inserted into the pipe. These techniques enable targeted anomaly detection and condition assessment of a specific pipe section or sub-network. To make these techniques applicable to the future smart water networks, new methods that use the background transient signals, instead of signals excited by a transient generator, can be explored for detection purposes. Another strategy to achieve continuous monitoring of a water network is to develop permanent transient generation stations which do not need to discharge water and can be installed in the water network.

With continuous monitoring of the background pressures in a smart water network, a better understanding of the background noise can be achieved, leading to a better way to pre-process the collected pressure traces. The current techniques developed in this thesis use the raw data as the input to the developed algorithms. With the characteristics of the background noise being more fully understood, some signal processing strategies can be applied to the raw data to cancel out the effects from the background noise and thus improve the reliability of the detection results.

Long term monitoring of a water network can also provide the chance to better understand the characteristics of the transient wave propagation in pipe networks, such as the wave dissipation and dispersion characteristics. An accurate representation of the pipeline condition using the techniques developed in the thesis relies on accurate modelling of the transient wave

propagation. Thus, future work can be done to investigate the wave propagation characteristics in pipe networks with the data measured by sensors in the smart water network.

With big data of a smart water network available, computer-aided algorithms may have the potential to be combined with the techniques developed in this thesis to further improve the reliability of the results. One example is the potential to combine the paired-IRF technique with some artificial intelligence (AI) techniques. The anomaly-induced features are much clearer in the paired-IRF trace than those in the raw pressure traces. With the assistance of AI techniques and a large amount of pressure data which can be transferred to paired-IRFs, anomalies in a pipe network may have the potential to be identified automatically at a very early stage by computers in the future.

With different types of signals to be collected in a smart water network, the other challenge faced in the future is how to take full advantages of these signals. The current techniques developed in the thesis only use the pressure information measured by pressure transducers or fibre optical sensors, while accelerometers, hydrophones and many other transducers in a smart water network are becoming more commonly used. Thus, future work can focus on developing new strategies to combine the strength of different sensors in the detection process using the techniques developed in this thesis.

Overall, with the emerging smart water technologies which enable long term and large range monitoring of a water network, the anomaly detection and condition assessment techniques developed in this thesis can be further developed by taking full advantage of the data available.

This page is intentionally blank.

References

- Agulló, J., Cardona, S., and Keefe, D. H. (1995). "Time-domain deconvolution to measure reflection functions for discontinuities in waveguides." *The Journal of the Acoustical Society of America*, 97(3), 1950-1957.
- Amir, N., and Shimony, U. (1995a). "A discrete model for tubular acoustic systems with varying cross section - the direct and inverse problems. Part 1 theory." *Acustica*, 1995(81), 450-462.
- Amir, N., and Shimony, U. (1995b). "A discrete model for tubular acoustic systems with varying cross section - the direct and inverse problems. Part 2 experiments." *Acustica*, 1995(81), 463-474.
- Arkwright, J. W., Blenman, N. G., Underhill, I. D., Maunder, S. A., Spencer, N. J., Costa, M., Brookes, S. J., Szczesniak, M. M., and Dinning, P. G. (2012). "Measurement of muscular activity associated with peristalsis in the human gut using fiber bragg grating arrays." *IEEE Sensors Journal*, 12(1), 113-117.
- Arkwright, J. W., Underhill, I. D., Maunder, S. A., Jafari, A., Cartwright, N., and Lemckert, C. (2014). "Fiber optic pressure sensing arrays for monitoring horizontal and vertical pressures generated by traveling water waves." *IEEE Sensors Journal*, 14(8), 2739-2742.
- Atherton, D. L., Morton, K., and Mergelas, B. J. (2000). "Detecting breaks in prestressing pipe wire." *Journal of the American Water Works Association*, 92(7), 50-56.
- AWWA. (2012). "Buried no longer: Confronting America's water infrastructure challenge." American Water Works Association, Denver, CO.

- Bilotta, A., Morassi, A., and Turco, E. (2016). "Reconstructing blockages in a symmetric duct via quasi-isospectral horn operators." *Journal of Sound and Vibration*, 366(3), 149-172.
- Brunone, B. (1999). "Transient test-based technique for leak detection in outfall pipes." *Journal of Water Resources Planning and Management*, 125(5), 302-306.
- Brunone, B., and Ferrante, M. (2001). "Detecting leaks in pressurised pipes by means of transients." *Journal of Hydraulic Research*, 39(5), 539-547.
- Brunone, B., Ferrante, M., and Meniconi, S. (2008). "Portable pressure wave-maker for leak detection and pipe system characterization." *Journal AWWA*, 100(4), 108-116.
- Butterfield, J. D., Collins, R. P., and Beck, S. B. M. (2018). "Influence of pipe material on the transmission of vibroacoustic leak signals in real complex water distribution systems: Case study." *Journal of Pipeline Systems Engineering and Practice*, 9(3), 05018003.
- Capponi, C., Ferrante, M., Zecchin, A. C., and Gong, J. (2017). "Leak detection in a branched system by inverse transient analysis with the admittance matrix method." *Water Resources Management*, 31(13), 4075-4089.
- Cataldo, A., Cannazza, G., Benedetto, E. D., and Giaquinto, N. (2012). "A new method for detecting leaks in underground water pipelines." *IEEE Sensors Journal*, 12(6), 1660-1667.
- Chaudhry, M. H. (2014). *Applied hydraulic transients*, Springer, New York, NY.
- Chung, J. Y., and Blaser, D. A. (1980). "Transfer function method of measuring in-duct acoustic properties. I. Theory." *The Journal of the Acoustical Society of America*, 68(3), 907-913.

- Clark, R. M., and Haught, R. C. (2005). "Characterizing pipe wall demand: Implications for water quality modeling." *Journal of Water Resources Planning and Management*, 131(3), 208-217.
- Colombo, A. F., Lee, P., and Karney, B. W. (2009). "A selective literature review of transient-based leak detection methods." *Journal of Hydro-environment Research*, 2(4), 212-227.
- Covas, D., and Ramos, H. (1999). "Leakage detection in single pipelines using pressure wave behaviour." *Water industry systems: Modelling and optimisation applications*, D. A. Savic and G. A. Walters, eds., Research Studies Press Ltd., Baldock, Hertfordshire, England.
- Covas, D., and Ramos, H. (2001). "Hydraulic transients used for leakage detection in water distribution systems." *Proceedings of the 4th International Conference on Water Pipeline Systems*, BHR Group, Cranfield, UK, 227-241.
- Covas, D., and Ramos, H. (2010). "Case studies of leak detection and location in water pipe systems by inverse transient analysis." *Journal of Water Resources Planning and Management*, 136(2), 248-257.
- Covas, D., Stoianov, I., Butler, D., Maksimovic, C., Graham, N., and Ramos, H. (2001). "Leak detection in pipeline systems by inverse transient analysis - from theory to practice." *Water software systems: Theory and applications*, B. Ulanicki, B. Coulback, and J. P. Rance, eds., Research Studies Press Ltd., Baldock, Hertfordshire, England, 3-16.
- Covas, D., Stoianov, I., Mano, J. F., Ramos, H., Graham, N., and Maksimovic, C. (2005). "The dynamic effect of pipe-wall viscoelasticity in hydraulic transients. Part ii - model development, calibration and verification." *Journal of Hydraulic Research*, 43(1), 56-70.
- De Salis, M. H. F., and Oldham, D. J. (1999). "Determination of the blockage area function of a finite duct from a single pressure response measurement." *Journal of Sound and Vibration*, 221(1), 180-186.

- De Salis, M. H. F., and Oldham, D. J. (2001). "The development of a rapid single spectrum method for determining the blockage characteristics of a finite length duct." *Journal of Sound and Vibration*, 243(4), 625-640.
- Donazzolo, V., and Yelf, R. (2010). "Determination of wall thickness and condition of asbestos cement pipes in sewer rising mains using surface penetrating radar." *Proceedings of the 13th International Conference on Ground Penetrating Radar*, IEEE Computer Society, Washington, DC, 1-5.
- Duan, H. F. (2016). "Sensitivity analysis of a transient-based frequency domain method for extended blockage detection in water pipeline systems." *Journal of Water Resources Planning and Management*, 142(4), 04015073.
- Duan, H. F., Ghidaoui, M., Lee, P. J., and Tung, Y. K. (2010). "Unsteady friction and visco-elasticity in pipe fluid transients." *Journal of Hydraulic Research*, 48(3), 354-362.
- Duan, H. F., Lee, P. J., Ghidaoui, M. S., and Tuck, J. (2014). "Transient wave-blockage interaction and extended blockage detection in elastic water pipelines." *Journal of Fluids and Structures*, 46(4), 2-16.
- Duan, H. F., Lee, P. J., Ghidaoui, M. S., and Tung, Y. K. (2011). "Leak detection in complex series pipelines by using the system frequency response method." *Journal of Hydraulic Research*, 49(2), 213-221.
- Duan, H. F., Lee, P. J., Ghidaoui, M. S., and Tung, Y. K. (2012). "Extended blockage detection in pipelines by using the system frequency response analysis." *Journal of Water Resources Planning and Management*, 138(1), 55-62.
- Duan, H. F., Lee, P. J., Kashima, A., Lu, J., Ghidaoui, M. S., and Tung, Y. K. (2013). "Extended blockage detection in pipes using the system frequency response: Analytical analysis and experimental verification." *Journal of Hydraulic Engineering*, 139(7), 763-771.

- Eiswirth, M., and Burn, L. S. (2001). "New methods for defect diagnosis of water pipelines." *Proceedings of the 4th International Conference on Water Pipeline Systems*, BHR Group, Cranfield, UK, 137-150.
- Ferrante, M., and Brunone, B. (2004). "Pressure waves as a tool for leak detection in closed conduits." *Urban Water Journal*, 1(2), 145-156.
- Ferrante, M., Brunone, B., and Meniconi, S. (2009). "Leak detection in branched pipe systems coupling wavelet analysis and a Lagrangian model." *Journal of Water Supply: Research and Technology - Aqua*, 58(2), 95-106.
- Ferrante, M., Brunone, B., Meniconi, S., Karney, B. W., and Massari, C. (2014). "Leak size, detectability and test conditions in pressurized pipe systems." *Water Resources Management*, 28(13), 4583–4598.
- Forbes, B. J., Sharp, D. B., Kemp, J. A., and Li, A. (2003). "Singular system methods in acoustic pulse reflectometry." *Acta Acustica united with Acustica*, 89(5), 11.
- Fox, S., Shepherd, W., Collins, R., and Boxall, J. (2016). "Experimental quantification of contaminant ingress into a buried leaking pipe during transient events." *Journal of Hydraulic Engineering*, 142(1), 04015036.
- Fuchs, H. V., and Riehle, R. (1991). "Ten years of experience with leak detection by acoustic signal analysis." *Applied Acoustics*, 33(1), 1-19.
- Gao, Y., Brennan, M. J., Joseph, P. F., Muggleton, J. M., and Hunaidi, O. (2004). "A model of the correlation function of leak noise in buried plastic pipes." *Journal of Sound and Vibration*, 277(1), 133-148.
- Gao, Y., Brennan, M. J., Liu, Y., Almeida, F. C. L., and Joseph, P. F. (2017). "Improving the shape of the cross-correlation function for leak detection in a plastic water distribution pipe using acoustic signals." *Applied Acoustics*, 127, 24-33.

- Ghazali, M. F., Beck, S. B. M., Shucksmith, J. D., Boxall, J. B., and Staszewski, W. J. (2012). "Comparative study of instantaneous frequency based methods for leak detection in pipeline networks." *Mechanical Systems and Signal Processing*, 29(5), 187-200.
- Godfrey, K. (1993). *Perturbation signals for system identification*, Prentice Hall Inc., New York.
- Gong, J., Lambert, M. F., Nguyen, S. T. N., Zecchin, A. C., and Simpson, A. R. (2018a). "Detecting thinner-walled pipe sections using a spark transient pressure wave generator." *Journal of Hydraulic Engineering*, 144(2), 06017027.
- Gong, J., Lambert, M. F., Simpson, A. R., and Zecchin, A. C. (2012). "Distributed deterioration detection in single pipes using the impulse response function." *Proceedings of the 14th International Conference on Water Distribution Systems Analysis (WDSA 2012)*, Engineers Australia, Barton, ACT, Australia, 702-719.
- Gong, J., Lambert, M. F., Simpson, A. R., and Zecchin, A. C. (2013a). "Single-event leak detection in pipeline using first three resonant responses." *Journal of Hydraulic Engineering*, 139(6), 645-655.
- Gong, J., Lambert, M. F., Simpson, A. R., and Zecchin, A. C. (2014a). "Detection of localized deterioration distributed along single pipelines by reconstructive moc analysis." *Journal of Hydraulic Engineering*, 140(2), 190-198.
- Gong, J., Lambert, M. F., Zecchin, A. C., and Simpson, A. R. (2016a). "Experimental verification of pipeline frequency response extraction and leak detection using the inverse repeat signal." *Journal of Hydraulic Research*, 54(2), 210-219.
- Gong, J., Lambert, M. F., Zecchin, A. C., Simpson, A. R., Arbon, N. S., and Kim, Y. I. (2016b). "Field study on non-invasive and non-destructive

- condition assessment for asbestos cement pipelines by time-domain fluid transient analysis." *Structural Health Monitoring*, 15(1), 113-124.
- Gong, J., Png, G. M., Arkwright, J. W., Papageorgiou, A. W., Cook, P. R., Lambert, M. F., Simpson, A. R., and Zecchin, A. C. (2018b). "In-pipe fibre optic pressure sensor array for hydraulic transient measurement with application to leak detection." *Measurement*, 126(10), 309-317.
- Gong, J., Simpson, A. R., Lambert, M. F., and Zecchin, A. C. (2013b). "Determination of the linear frequency response of single pipelines using persistent transient excitation: A numerical investigation." *Journal of Hydraulic Research*, 51(6), 728-734.
- Gong, J., Simpson, A. R., Lambert, M. F., Zecchin, A. C., Kim, Y. I., and Tijsseling, A. S. (2013c). "Detection of distributed deterioration in single pipes using transient reflections." *Journal of Pipeline Systems Engineering and Practice*, 4(1), 32-40.
- Gong, J., Stephens, M. L., Arbon, N. S., Zecchin, A. C., Lambert, M. F., and Simpson, A. R. (2015). "On-site non-invasive condition assessment for cement mortar-lined metallic pipelines by time-domain fluid transient analysis." *Structural Health Monitoring*, 14(5), 426-438.
- Gong, J., Zecchin, A. C., Lambert, M. F., and Simpson, A. R. (2016c). "Determination of the creep function of viscoelastic pipelines using system resonant frequencies with hydraulic transient analysis." *Journal of Hydraulic Engineering*, 10.1061/(ASCE)HY.1943-7900.0001149, 04016023.
- Gong, J., Zecchin, A. C., Simpson, A. R., and Lambert, M. F. (2014b). "Frequency response diagram for pipeline leak detection: Comparing the odd and the even harmonics." *Journal of Water Resources Planning and Management*, 140(1), 65-74.
- Hao, T., Rogers, C. D. F., Metje, N., Chapman, D. N., Muggleton, J. M., Foo, K. Y., Wang, P., Pennock, S. R., Atkins, P. R., Swingler, S. G., Parker,

- J., Costello, S. B., Burrow, M. P. N., Anspach, J. H., Armitage, R. J., Cohn, A. G., Goddard, K., Lewin, P. L., Orlando, G., Redfern, M. A., Royal, A. C. D., and Saul, A. J. (2012). "Condition assessment of the buried utility service infrastructure." *Tunnelling and Underground Space Technology*, 28(1), 331-344.
- Hendrie, D. A. (2007). "Development of bore reconstruction techniques applied to the study of brass wind instruments," Ph.D. Thesis, University of Edinburgh.
- Jing, L., Li, Z., Wang, W., Dubey, A., Lee, P., Meniconi, S., Brunone, B., and Murch, R. D. (2018). "An approximate inverse scattering technique for reconstructing blockage profiles in water pipelines using acoustic transients." *The Journal of the Acoustical Society of America*, 143(5), EL322-EL327.
- Kapelan, Z. S., Savic, D. A., and Walters, G. A. (2003). "A hybrid inverse transient model for leakage detection and roughness calibration in pipe networks." *Journal of Hydraulic Research, IAHR*, 41(5), 481-492.
- Lambert, A. O. (2002). "International report: Water losses management and techniques." *Water Science and Technology: Water Supply*, 2(4), 1-20.
- Lee, P. J., Lambert, M. F., Simpson, A. R., Vítkovský, J. P., and Liggett, J. A. (2006). "Experimental verification of the frequency response method for pipeline leak detection." *Journal of Hydraulic Research*, 44(5), 693–707.
- Lee, P. J., Lambert, M. F., Simpson, A. R., Vítkovský, J. P., and Misiunas, D. (2007a). "Leak location in single pipelines using transient reflections." *Australian Journal of Water Resources*, 11(1), 53-65.
- Lee, P. J., Tuck, J., Davidson, M., and May, R. (2017). "Piezoelectric wave generation system for condition assessment of field water pipelines." *Journal of Hydraulic Research*, 55(5), 721-730.

- Lee, P. J., Vítkovský, J. P., Lambert, M. F., and Simpson, A. R. (2008a). "Valve design for extracting response functions from hydraulic systems using pseudorandom binary signals." *Journal of Hydraulic Engineering*, 136(4), 858-864.
- Lee, P. J., Vítkovský, J. P., Lambert, M. F., Simpson, A. R., and Liggett, J. A. (2005a). "Frequency domain analysis for detecting pipeline leaks." *Journal of Hydraulic Engineering*, 131(7), 596-604.
- Lee, P. J., Vítkovský, J. P., Lambert, M. F., Simpson, A. R., and Liggett, J. A. (2005b). "Leak location using the pattern of the frequency response diagram in pipelines: A numerical study." *Journal of Sound and Vibration*, 284(3-5), 1051–1073.
- Lee, P. J., Vítkovský, J. P., Lambert, M. F., Simpson, A. R., and Liggett, J. A. (2007b). "Leak location in pipelines using the impulse response function." *Journal of Hydraulic Research*, 45(5), 643-652.
- Lee, P. J., Vítkovský, J. P., Lambert, M. F., Simpson, A. R., and Liggett, J. A. (2008b). "Discrete blockage detection in pipelines using the frequency response diagram: Numerical study." *Journal of Hydraulic Engineering*, 134(5), 658-663.
- Li, A., Sharp, D. B., and Forbes, B. J. (2005). "Increasing the axial resolution of bore profile measurements made using acoustic pulse reflectometry." *Measurement Science and Technology*, 16(10), 2011-2019.
- Liggett, J. A., and Chen, L. C. (1994). "Inverse transient analysis in pipe networks." *Journal of Hydraulic Engineering*, 120(8), 934-955.
- Lin, J., Wang, X., and Ghidaoui, M. S. (2019). "Theoretical investigation of leak's impact on normal modes of a water filled pipe: Small to large leak impedance." *Journal of Hydraulic Engineering*, 145(6), 04019017.
- Liou, C. P. (1996). "Pipeline integrity monitoring using system impulse response." *1st International Pipeline Conference*, ASME, 1137-1142.

- Liou, C. P. (1998). "Pipeline leak detection by impulse response extraction." *Journal of Fluids Engineering*, 120(4), 833-838.
- Liu, Z., and Kleiner, Y. (2013). "State of the art review of inspection technologies for condition assessment of water pipes." *Measurement*, 46(1), 1-15.
- Liu, Z., and Simpson, A. R. (2018). "Influence of connection stub parameters and valve closure time on transient measurement accuracy of a pressure transducer." *Water Supply*, 18(6), 1984-1995.
- Louati, M., and Ghidaoui, M. S. (2018). "Eigenfrequency shift mechanism due to an interior blockage in a pipe." *Journal of Hydraulic Engineering*, 144(1), 04017055.
- Louati, M., Meniconi, S., Ghidaoui Mohamed, S., and Brunone, B. (2017). "Experimental study of the eigenfrequency shift mechanism in a blocked pipe system." *Journal of Hydraulic Engineering*, 143(10), 04017044.
- Mamou-Mani, A., Sharp, D. B., Meurisse, T., and Ring, W. (2012). "Investigating the consistency of woodwind instrument manufacturing by comparing five nominally identical oboes." *The Journal of the Acoustical Society of America*, 131(1), 728-736.
- McIntosh, A. C., and Yniguez, C. E. (1997). *Second water utilities data book : Asian and Pacific region*, Asian Development Bank, Manila, Philippines.
- Meniconi, S., Brunone, B., and Ferrante, M. (2011a). "In-line pipe device checking by short-period analysis of transient tests." *Journal of Hydraulic Engineering*, 137(7), 713-722.
- Meniconi, S., Brunone, B., and Ferrante, M. (2012a). "Water-hammer pressure waves interaction at cross-section changes in series in viscoelastic pipes." *Journal of Fluids and Structures*, 33(8), 44-58.

- Meniconi, S., Brunone, B., Ferrante, M., and Capponi, C. (2016). "Mechanism of interaction of pressure waves at a discrete partial blockage." *Journal of Fluids and Structures*, 62(4), 33-45.
- Meniconi, S., Brunone, B., Ferrante, M., Capponi, C., Carrettini, C. A., Chiesa, C., Segalini, D., and Lanfranchi, E. A. (2015). "Anomaly pre-localization in distribution–transmission mains by pump trip: Preliminary field tests in the milan pipe system." *Journal of Hydroinformatics*, 17(3), 377-389.
- Meniconi, S., Brunone, B., Ferrante, M., and Massari, C. (2010). "Small amplitude sharp pressure waves to diagnose pipe systems." *Water Resources Management*, 25(1), 79-96.
- Meniconi, S., Brunone, B., Ferrante, M., and Massari, C. (2011b). "Potential of transient tests to diagnose real supply pipe systems: What can be done with a single extemporary test." *Journal of Water Resources Planning and Management*, 137(2), 238-241.
- Meniconi, S., Brunone, B., Ferrante, M., and Massari, C. (2012b). "Transient hydrodynamics of in-line valves in viscoelastic pressurized pipes: Long-period analysis." *Experiments in Fluids*, 53(1), 265-275.
- Meniconi, S., Duan, H. F., Lee, P. J., Brunone, B., Ghidaoui, M. S., and Ferrante, M. (2013). "Experimental investigation of coupled frequency and time-domain transient test-based techniques for partial blockage detection in pipelines." *Journal of Hydraulic Engineering*, 139(10), 1033-1044.
- Mohapatra, P. K., Chaudhry, M. H., Kassem, A., and Moloo, J. (2006a). "Detection of partial blockages in a branched piping system by the frequency response method." *Journal of Fluids Engineering*, 128(5), 1106-1114.
- Mohapatra, P. K., Chaudhry, M. H., Kassem, A. A., and Moloo, J. (2006b). "Detection of partial blockage in single pipelines." *Journal of Hydraulic Engineering*, 132(2), 200-206.

- Mounce, S. R., Boxall, J. B., and Machell, J. (2010). "Development and verification of an online artificial intelligence system for detection of bursts and other abnormal flows." *Journal of Water Resources Planning and Management*, 136(3), 309-318.
- Mpesha, W., Gassman, S. L., and Chaudhry, M. H. (2001). "Leak detection in pipes by frequency response method." *Journal of Hydraulic Engineering*, 127(2), 134-147.
- Mutikanga, H. E., Sharma, S., and Vairavamoorthy, K. (2009). "Water loss management in developing countries: Challenges and prospects." *Journal of American Water Works Association*, 101(12), 57-68.
- Nash, G. A., and Karney, B. W. (1999). "Efficient inverse transient analysis in series pipe systems." *Journal of Hydraulic Engineering, ASCE*, 125(7), 761-764.
- Nguyen, S. T. N., Gong, J., Lambert, M. F., Zecchin, A. C., and Simpson, A. R. (2018). "Least squares deconvolution for leak detection with a pseudo random binary sequence excitation." *Mechanical Systems and Signal Processing*, 99(1), 846-858.
- Nguyen, S. T. N., Lambert, M. F., Gong, J., Zecchin, A. C., and Simpson, A. R. (2019). "Pipeline condition assessment using pseudo random binary sequence excitation and linear approximation approach." *Mechanical Systems and Signal Processing*, Under review.
- Nixon, W., and Ghidaoui, M. S. (2006). "Range of validity of the transient damping leakage detection method." *Journal of Hydraulic Engineering*, 132(9), 944-957.
- Oppenheim, A. V., Willsky, A. S., and Nawab, S. H. (1997). *Signals and systems*, Prentice Hall, Upper Saddle River, N.J.
- Puust, R., Kapelan, Z., Savic, D. A., and Koppel, T. (2010). "A review of methods for leakage management in pipe networks." *Urban Water Journal*, 7(1), 25 - 45.

- Romano, M., Kapelan, Z., and Savić, D. A. (2014). "Automated detection of pipe bursts and other events in water distribution systems." *Journal of Water Resources Planning and Management*, 140(4), 457-467.
- Roubal, M. (2002). "Condition assessment of pipeline networks." *Pipelines 2002 - Beneath Our Feet: Challenges and Solutions - Pipeline Division Specialty Conference*, American Society of Civil Engineers.
- Sanz, G., Pérez, R., Kapelan, Z., and Savic, D. (2016). "Leak detection and localization through demand components calibration." *Journal of Water Resources Planning and Management*, 142(2), 04015057.
- Sattar, A. M., and Chaudhry, M. H. (2008). "Leak detection in pipelines by frequency response method." *Journal of Hydraulic Research*, 46(1), 138-151.
- Sattar, A. M., Chaudhry, M. H., and Kassem, A. A. (2008). "Partial blockage detection in pipelines by frequency response method." *Journal of Hydraulic Engineering*, 134(1), 76-89.
- Seybert, A. F., and Ross, D. F. (1977). "Experimental determination of acoustic properties using a two-microphone random-excitation technique." *The Journal of the Acoustical Society of America*, 61(5), 1362-1370.
- Shamloo, H., and Haghghi, A. (2009). "Leak detection in pipelines by inverse backward transient analysis." *Journal of Hydraulic Research*, 47(3), 311-318.
- Sharp, D. B. (1996). "Acoustic pulse reflectometry for the measurement of musical wind instruments," Ph.D. Thesis, University of Edinburgh, Edinburgh, UK.
- Sharp, D. B. (1998). "Increasing the length of tubular objects that can be measured using acoustic pulse reflectometry." *Measurement Science and Technology*, 9(9), 1469-1479.

- Sharp, D. B., and Campbell, D. M. (1997). "Leak detection in pipes using acoustic pulse reflectometry." *Acta Acustica (Stuttgart)*, 83(3), 560-566.
- Shi, H., Gong, J., Cook, P. R., Arkwright, J. W., Png, G. M., Lambert, M. F., Zecchin, A. C., and Simpson, A. R. (2019). "Wave separation and pipeline condition assessment using in-pipe fibre optic pressure sensors." *Journal of Hydroinformatics*, 21(2), 371-379.
- Shi, H., Gong, J., Zecchin, A. C., Lambert, M. F., and Simpson, A. R. (2017). "Hydraulic transient wave separation algorithm using a dual-sensor with applications to pipeline condition assessment." *Journal of Hydroinformatics*, 10.2166/hydro.2017.146.
- Shucksmith, J. D., Boxall, J. B., Staszewski, W. J., Seth, A., and Beck, S. B. M. (2012). "Onsite leak location in a pipe network by cepstrum analysis of pressure transients." *Journal AWWA*, 104(8), E457-E465.
- Smith, S. W. (1999). *The scientist and engineer's guide to digital signal processing*, California Technical Publishing.
- Stephens, M. L. (2008). "Transient response analysis for fault detection and pipeline wall condition assessment in field water transmission and distribution pipelines and networks," Ph.D. Thesis, University of Adelaide, Adelaide, Australia.
- Stephens, M. L., Gong, J., Marchi, A., Dix, L., Wilson, A., and Lambert, M. F. (2018). "Leak detection in the adelaide CBD water network using permanent acoustic monitoring." *Ozwater Proceedings*, Brisbane, Australia.
- Stephens, M. L., Lambert, M. F., and Simpson, A. R. (2013). "Determining the internal wall condition of a water pipeline in the field using an inverse transient model." *Journal of Hydraulic Engineering*, 139(3), 310–324.
- Stephens, M. L., Simpson, A. R., and Lambert, M. F. (2008). "Internal wall condition assessment for water pipelines using inverse transient

analysis." *Proceedings of the 10th Annual Symposium on Water Distribution Systems Analysis*, ASCE, Reston, VA.

Stephens, M. L., Vítkovský, J. P., Lambert, M. F., Simpson, A. R., Karney, B. W., and Nixon, J. B. (2004). "Transient analysis to assess valve status and topology in pipe networks." *Proceedings of the 9th International Conference on Pressure Surges*, BHR Group Ltd, Cranfield, UK, 211-224.

Storn, R., and Price, K. (1997). "Differential evolution – a simple and efficient heuristic for global optimization over continuous spaces." *Journal of Global Optimization*, 11(4), 341-359.

Suo, L., and Wylie, E. B. (1990). "Complex wavespeed and hydraulic transients in viscoelastic pipes." *Journal of Fluids Engineering*, 112(4), 496-500.

Swietlik, J., Raczyk-Stanisawiak, U., Piszora, P., and Nawrocki, J. (2012). "Corrosion in drinking water pipes: The importance of green rusts." *Water Research*, 46(1), 1-10.

Tafari, A. N. (2000). "Locating leaks with acoustic technology." *Journal of American Water Works Association*, 92(7), 57-66.

Taghvaei, M., Beck, S. B. M., and Staszewski, W. J. (2006). "Leak detection in pipelines using cepstrum analysis." *Measurement Science and Technology*, 17, 367-372.

Tran, D. H., Perera, B. J. C., and Ng, A. W. M. (2009). "Predicting structural deterioration condition of individual storm-water pipes using probabilistic neural networks and multiple logistic regression models." *Journal of Water Resources Planning and Management*, 135(6), 553-557.

Tran, D. H., Perera, B. J. C., and Ng, A. W. M. (2010). "Hydraulic deterioration models for storm-water drainage pipes: Ordered probit versus probabilistic neural network." *Journal of Computing in Civil Engineering*, 24(2), 140-150.

- Vardy, A. E., and Brown, J. M. B. (1995). "Transient, turbulent, smooth pipe friction." *Journal of Hydraulic Research*, 33(4), 435-456.
- Vardy, A. E., and Brown, J. M. B. (2003). "Transient turbulent friction in smooth pipe flows." *Journal of Sound and Vibration*, 259(5), 1011-1036.
- Vítkovský, J. P., Bergant, A., Simpson, A. R., and Lambert, M. F. (2003a). "Frequency-domain transient pipe flow solution including unsteady friction." *Pumps, Electromechanical Devices and Systems Applied to Urban Water Management: Proceedings of the International Conference*, A. A. Balkema Publishers, Lisse, The Netherlands, 773-780.
- Vítkovský, J. P., Lambert, M. F., Simpson, A. R., and Liggett, J. A. (2007). "Experimental observation and analysis of inverse transients for pipeline leak detection." *Journal of Water Resources Planning and Management*, 133(6), 519-530.
- Vítkovský, J. P., Lee, P. J., Stephens, M. L., Lambert, M. F., Simpson, A. R., and Liggett, J. A. (2003b). "Leak and blockage detection in pipelines via an impulse response method." *Pumps, Electromechanical Devices and Systems Applied to Urban Water Management: Proceedings of the International Conference*, A. A. Balkema Publishers, Lisse, The Netherlands, 423-430.
- Vítkovský, J. P., Simpson, A. R., and Lambert, M. F. (2000). "Leak detection and calibration using transients and genetic algorithms." *Journal of Water Resources Planning and Management*, 126(4), 262-265.
- Vreeburg, I. J. H. G., and Boxall, D. J. B. (2007). "Discolouration in potable water distribution systems: A review." *Water Research*, 41(3), 519-529.
- Wang, F., Lin, W., Liu, Z., Wu, S., and Qiu, X. (2017). "Pipeline leak detection by using time-domain statistical features." *IEEE Sensors Journal*, 17(19), 6431-6442.

- Wang, L., and Erdogan, T. (2001). "Layer peeling algorithm for reconstruction of long-period fibre gratings." *Electronics Letters*, 37(3), 154-156.
- Wang, X., and Ghidaoui, M. S. (2018a). "Identification of multiple leaks in pipeline: Linearized model, maximum likelihood, and super-resolution localization." *Mechanical Systems and Signal Processing*, 107(7), 529-548.
- Wang, X., and Ghidaoui, M. S. (2018b). "Pipeline leak detection using the matched-field processing method." *Journal of Hydraulic Engineering*, 144(6), 04018030.
- Wang, X., Ghidaoui, M. S., and Lee, P. J. (2018). "Regularization for pipeline impulse response extraction with least square deconvolution." *13th International Conference on Pressure Surges*, BHR Group, Bordeaux, France.
- Wang, X., Lin, J., Keramat, A., Ghidaoui, M. S., Meniconi, S., and Brunone, B. (2019). "Matched-field processing for leak localization in a viscoelastic pipe: An experimental study." *Mechanical Systems and Signal Processing*, 124(6), 459-478.
- Wang, X. J., Lambert, M. F., and Simpson, A. R. (2005). "Detection and location of a partial blockage in a pipeline using damping of fluid transients." *Journal of Water Resources Planning and Management*, 131(3), 244-249.
- Wang, X. J., Lambert, M. F., Simpson, A. R., Liggett, J. A., and Vítkovský, J. P. (2002). "Leak detection in pipelines using the damping of fluid transients." *Journal of Hydraulic Engineering*, 128(7), 697-711.
- Ware, J. A., and Aki, K. (1969). "Continuous and discrete inverse-scattering problems in a stratified elastic medium. 1 plane waves at normal incidence." *The Journal of the Acoustical Society of America*, 45(4), 911-921

- Wong, L., Chiu, W. K., and Kodikara, J. (2018a). "Using distributed optical fibre sensor to enhance structural health monitoring of a pipeline subjected to hydraulic transient excitation." *Structural Health Monitoring*, 17(2), 298-312.
- Wong, L., Rathnayaka, S., Chiu, W. K., and Kodikara, J. (2018b). "Utilising hydraulic transient excitation for fatigue crack monitoring of a cast iron pipeline using optical distributed sensing." *Structural Control and Health Monitoring*, 25(4), e2141.
- Wu, Q., and Fricke, F. (1989). "Estimation of blockage dimensions in a duct using measured eigenfrequency shifts." *Journal of Sound and Vibration*, 133(2), 289-301.
- Wu, Q., and Fricke, F. (1990). "Determination of blocking locations and cross-sectional area in a duct by eigenfrequency shifts." *The Journal of the Acoustical Society of America*, 87(1), 67-75.
- Wylie, E. B., and Streeter, V. L. (1993). *Fluid transients in systems*, Prentice Hall Inc., Englewood Cliffs, New Jersey, USA.
- Xu, X., and Karney, B. W. (2017). "An overview of transient fault detection techniques." *Modeling and Monitoring of Pipelines and Networks*, Springer, Cham.
- Zamanzadeh, M., Kirkwood, G. C., Scheinman, S., and Bayer, G. T. (2007). "Corrosion sensors for detecting graphitization of cast iron in water mains." *Proceedings of Corrosion Conference and Expo 2007*, Curran Associates, Inc., Red Hook, NY.
- Zan, T. T. T., Lim, H. B., Wong, K. J., Whittle, A. J., and Lee, B. S. (2014). "Event detection and localization in urban water distribution network." *IEEE Sensors Journal*, 14(12), 4134-4142.
- Zecchin, A. C., Gong, J., Simpson, A. R., and Lambert, M. F. (2014). "Condition assessment in hydraulically noisy pipeline systems using a pressure wave splitting method." *Procedia Engineering*, 89, 1336-1342.

- Zeng, W., Gong, J., Cazzolato, B. S., Zecchin, A. C., Lambert, M. F., and Simpson, A. R. (2019a). "Condition assessment of pipelines using a bi-directional layer-peeling method and a dual-sensor configuration." *Journal of Sound and Vibration*, 457(9), 181-196.
- Zeng, W., Gong, J., Lambert, M. F., Simpson, A. R., Cazzolato, B. S., and Zecchin, A. C. (2019b). "Detection of extended blockages in pressurised pipelines using hydraulic transients with a layer-peeling method." *IOP Conference Series: Earth and Environmental Science*, 240, 052019.
- Zeng, W., Gong, J., Simpson, A. R., Cazzolato, B. S., Zecchin, A. C., and Lambert, M. F. (Forthcoming). "Paired-IRF method for leakage detection of pipes in a network." *Journal of Water Resources Planning and Management*, 10.1061/(ASCE)WR.1943-5452.0001193.
- Zeng, W., Gong, J., Zecchin, A. C., Lambert, M. F., Simpson, A. R., and Cazzolato, B. S. (2018). "Condition assessment of water pipelines using a modified layer-peeling method." *Journal of Hydraulic Engineering*, 144(12), 04018076.
- Zeng, W., Yang, J., and Hu, J. (2017). "Pumped storage system model and experimental investigations on s-induced issues during transients." *Mechanical Systems and Signal Processing*, 90(6), 350-364.
- Zhang, C., Gong, J., Simpson, A. R., Zecchin, A. C., and Lambert, M. F. (2019). "Impedance estimation along pipelines by generalized reconstructive method of characteristics for pipeline condition assessment." *Journal of Hydraulic Engineering*, 145(4), 04019010.
- Zhang, C., Gong, J., Zecchin, A. C., Lambert, M. F., and Simpson, A. R. (2018a). "Faster inverse transient analysis with a head-based method of characteristics and a flexible computational grid for pipeline condition assessment." *Journal of Hydraulic Engineering*, 144(4), 04018007.
- Zhang, C., Zecchin, A. C., Lambert, M. F., Gong, J., and Simpson, A. R. (2018b). "Multi-stage parameter-constraining inverse transient analysis

for pipeline condition assessment." *Journal of Hydroinformatics*, 10.2166/hydro.2018.154.

Zheng, F., Simpson, A. R., and Zecchin, A. C. (2011). "A combined NLP-differential evolution algorithm approach for the optimization of looped water distribution systems." *Water Resources Research*, 47(8).

Zheng, F., Zecchin, A. C., and Simpson, A. R. (2013). "Self-adaptive differential evolution algorithm applied to water distribution system optimization." *Journal of Computing in Civil Engineering*, 27(2), 148-158.